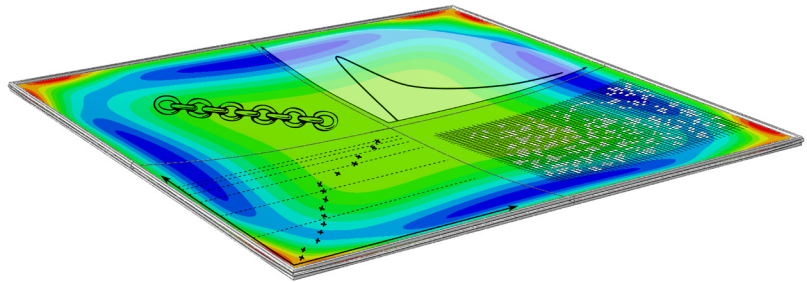




LUND
UNIVERSITY



MODELLING OF ANNEALED GLASS FRACTURE

DAVID KINSELLA

Structural
Mechanics

Licentiate Dissertation

DEPARTMENT OF CONSTRUCTION SCIENCES
DIVISION OF STRUCTURAL MECHANICS

ISRN LUTVDG/TVSM--18/3079--SE (1-227) | ISSN 0281-6679

ISBN 978-91-7753-760-1 (Print) | 978-91-7753-761-8 (Pdf)

LICENTIATE DISSERTATION

MODELLING OF ANNEALED GLASS FRACTURE

DAVID KINSELLA

Copyright © 2018 Division of Structural Mechanics,
Faculty of Engineering LTH, Lund University, Sweden.

Printed by V-huset tryckeri LTH, Lund, Sweden, August 2018 (*Pf*).

For information, address:

Div. of Structural Mechanics,
Faculty of Engineering LTH, Lund University, Box 118, SE-221 00 Lund, Sweden.

Homepage: www.byggmek.lth.se

Acknowledgements

The work presented in this thesis was carried out at the Division of Structural Mechanics at the Faculty of Engineering LTH, Lund University. Prof Kent Persson was the main supervisor and Dr Susanne Heyden and Prof Erik Serrano were the co-supervisors. Financial support was provided by the Swedish glass associations, Glasbranschföreningen, Svensk Planglasförening, Balkongföreningen.

I would like to thank Kent Persson for his guidance and support which led to this work being finalized. Thanks also to Susanne Heyden and Erik Serrano for valuable encouragement and advice.

I would furthermore like to acknowledge the support of Anders Sjöström in how to use the Lunarc computing facilities.

I am grateful towards the rest of the staff at the Division of Structural Mechanics who contribute to an inspiring workplace.

Thanks to Dr Johan Lindström at the Division of Mathematical Statistics for his guidance in how to perform statistical analysis.

The excellent service provided by the librarians at Lund University was essential to the proper information structuring of the research field. Andreas Karman at the Faculty of Engineering library is in particular recognized for his service.

Lund, 10th August 2018
David Kinsella

Abstract

A survey was performed of the experiments on glass tested in an ambient environment and which were conducted in the last 40 years. The experiments which comprise some 3100 tests of individual specimens in nearly 200 samples, recorded the fracture stress of new and monolithic annealed float glass panes. Four different testing devices were employed in the experiments, viz. the three-point and four-point bending devices, the double ring bending device, and the setup that allows for laterally supported plates to be subjected to uniform out-of-plane pressure. It was found that the strength ranges from about 20 MPa to over 200 MPa. The strength of annealed glass is a complex entity that is dependent on a number of factors including the load-duration and environmental conditions.

A review of strength models for use with glass was carried out. The models can be separated into three categories. First, there are models that assume no particular representation of the surface condition in glass. To these phenomenological or macroscopic models we reckon e.g. the application of some standard statistical distribution. Second, there are models which are based on a flaw size approach towards brittle failure. The surface flaws are represented rigorously with stochastic cracks that have shape, a size distribution, and an orientation of the crack plane. Third, there are models which are based on an elemental strength approach which is not dependent on an explicit representation of the surface condition in terms of flaw shape and crack plane orientation.

The performance of various standard statistical distributions for modelling the strength was examined. In the case of edge failures in glass, it was found that the Weibull distribution provides a basic model that performs better than the normal and the lognormal distributions, and at least as good as the extreme value Gumbel distribution. However, when surface failures are considered, the strength modelling is complicated and no standard statistical distribution was found to be capable of modelling the strength. It is likely that multiple flaw populations govern the pristine surface condition in glass such that the extreme value Weibull and Gumbel distributions are unsuited to model the surface strength.

A development was made of a type of strength model which depends on a flaw size approach towards brittle failure. The surface condition in glass was represented rigorously with stochastic cracks that have shape, a size distribution and an orientation in the plane. This approach was used to model the fracture stress and failure origins in small plates subjected to double ring bending. Both a single and a dual flaw population concept was explored and the implication of using a

mode I as well as a mixed mode fracture criterion was investigated. The dual population flaw size approach was found to better reflect the apparent bimodality in the empirical data set that was selected as a benchmark than the ordinary Weibull model, however at the expense of two additional degrees of freedom. The flaw size approach was further studied in simulations of the fracture origins in laterally supported plates subjected to uniform out-of-plane pressure. The boundary conditions were governed by either soft neoprene gasket supports or continuous strips of thick nylon. It was found that the support conditions had a profound impact on the fracture statistics while the incorporation of shear stress into the fracture criterion had little or no impact on the distribution of failure origins. Furthermore, the flaw size approach was used to model the fracture stress and failure origins in a tall slender panel with a complex structural geometry that was subjected to a soft body impact. The complex geometry was due to the existence of an array of ventilation holes near the bottom of the tall panel.

Although it is feasible to model glass fracture with a flaw size approach, there is a need for more research on the surface condition in glass of which little is currently known with any significant degree of confidence. This is a major drawback with the flaw size approach modelling of fracture in glass. Nevertheless, it is clear that the standard statistical distributions are insufficient for the modelling of the surface strength of glass and hence more sophisticated approaches are warranted. It is indicated that the extreme value Weibull distribution can be used as a basic model for the edge strength although further investigation is needed. As an interesting alternative to either the application of a standard distribution or to the modelling based on a flaw size approach, there emerges the models that are based on an elemental strength approach. These models are more sophisticated than the mere application of a standard distribution but are somewhat less stringent than the models that are based on a flaw size approach. Hence, this type of fracture model might be examined further in future research.

Populärvetenskaplig sammanfattning

Glas används allt mer i byggnader. Vanligt planglas är genomsiktligt vilket gör det möjligt att utforma miljöer som är både ljusa och som upplevs som öppna. Den ökande användningen av byggnadsglas förstärks av samtida trender i modern arkitektur. Ett traditionellt fönsterglas har som huvudsyfte att utestänga vind, väta och kyla samt att möjliggöra för ljusinsläpp och utblickar. I moderna tillämpningar ingår glaset i konstruktioner som exempelvis bär upp permanent last från intilliggande bärverksdelar såsom blir fallet när glaset används som ett balk- eller pelarelement. I andra fall ingår glaset i konstruktioner som på grund av sin belägenhet utsätts för snölast såsom blir fallet när glaset utgör ett takparti. När en vägghpanel eller balustrad utformas i glas måste det beaktas att det kan komma att utsättas för en mjuk stöt på grund av en person som av en olyckshändelse faller in mot det. Således finner vi glas i en mängd tillämpningar där det traditionellt sett inte har använts. Detta medför nya krav på dimensioneringen vid utförandet av dessa konstruktioner.

I dimensioneringen beaktas vanligtvis att hållfastheten uppvisar en viss spridning i sitt värde som i princip betraktas som en materialparameter. Hållfastheten kan mätas i försök med provuppställningar som är standardiserade. Ett hållfasthetsvärde som är betryggande med hänsyn till konstruktionens säkerhet kan identifieras med hjälp av den statistiska fördelning som bäst passar provresultaten. Experiment på vanligt planglas som provats i ett inomhusklimat avslöjar att hållfastheten varierar inom vida gränser och att variationen är mycket svår att förutsäga. Det visar sig också att brottläget varierar till synes slumpmässigt. Gångse metoder för att bestämma hållfasthetsvärdet fungerar därför inte. Tolkningen av mätresultaten försvåras av att glasmaterialet uppvisar ett utmattningsbeteende som innebär att brotlasten är starkt beroende av belastningstiden.

Spridningen i uppmätt hållfasthet och variationen i brottläge kan förklaras genom att anta att glasytan är bemängd med en mångfald mikroskopiska sprickor som fungerar som brottanvisningar. Utmattningsbeteendet kan förklaras genom att anta långsam tillväxt av de befintliga sprickorna på grund av en kemisk process som äger rum vid sprickspetsen och som aktiveras av påkänning, temperatur och luftfuktighet. En spricka som tillväxer tillräckligt mycket blir kritisk och föranleder brott som kännetecknas av ett sprött verknings sätt. Det betyder att brottet sker plötsligt, utan förvarning eller andra tecken på upphällning.

Detta medför i praktiken att stora säkerhetsmarginaler måste tillgripas i dimensioneringen av glaskonstruktioner. Det innebär att materialåtgången ofta blir onödigt stor vilket medför extra produktionskostnader och större energiåtgång under transporten från glasverket till byggarbetsplatsen. Det innebär också att konstruktionerna ofta blir onödigt stora och tunga. Med anledning av detta har ett forskningsprojekt genomförts med syfte att bättre kunna förutsäga hållfastheten i glas.

Det visar sig att det finns ett flertal hållfasthetsmodeller för glas som kan indelas i tre kategorier baserat på hur glasytans beskaffenhet beaktas. En första kategori av modeller är i grund och botten frikopplade från ett begrepp om glasytans särskilda beskaffenhet. Hit hör vanliga statistiska standardfördelningar som anpassas till provresultat. De för glasmaterialet relevanta standardfördelningarna har granskats och jämförts med avseende på deras anpassningsgrad till provresultat som finns tillgängliga. För det ändamålet har en genomgång gjorts av experiment från de senaste 40 åren och närmare 200 stickprov har insamlats vilka omfattar över 3100 mätresultat för hållfastheten i vanligt planglas som är ohärdat och som provats i ett inomhusklimat. Slutsatsen kan dras att den såkallade Weibullfördelningen motsvarar den modell som överlag bäst anpassar sig till provresultaten jämfört med andra standardfördelningar när kanthållfastheten studeras. När istället ythållfastheten studeras visar det sig att ingen av standardfördelningarna har potential för att vara modell. Det föreligger således en grundläggande skillnad i karaktär mellan kantbrott i glas och brott som börjar från ytan. De statistiska standardfördelningarna är relativt enkla att använda eftersom det finns standardiserade metoder för att anpassa dem till mätresultat.

En andra kategori av hållfasthetsmodeller baseras på en rigorös gestaltning av glasytans beskaffenhet genom antagande om ytsprickors form och storlek, såväl som orientering och läge. Dessa modeller beforskas i skrivande stund av ett antal forskarlag i Europa och Nordamerika såväl som i Asien och Australien. I avhandlingsarbetet har en modell inom denna kategori utvecklats och anpassats för att tolka mätresultat från ett experiment med en vanlig form av provuppställning. En modell har också tagits fram för att förutsäga brottläget i firsidigt infästa plattor som är utsatta för jämnt utbredd last. Ytterligare en modell har utvecklats för att förutsäga hållfasthet och brottläge i konstruktioner med komplex geometri vilka utsätts för dynamisk belastning av sådant slag som kan förväntas på grund av en mjuk stöt. Tyvärr råder det brist på tillförlitliga upplysningar om glasytans beskaffenhet som kan ligga till grund för en stringent gestaltning av ytsprickorna. Det saknas även effektiva metoder för att verifiera glasytans beskaffenhet. Således är denna sortens modellskapande förenat med betydande svårigheter, åtminstone för tillfället.

En tredje kategori av hållfasthetsmodeller bygger på ett antagande om en fundamental hållfasthetsfördelning som gäller lokalt på mikroskopisk nivå och som är direkt knuten till förekomsten av en viss spricka. Här görs inget antagande

om sprickans särskilda gestaltning med hänsyn till form, storlek eller orientering. Hållfastheten för konstruktionen som helhet erhålls genom en sammanvägning där det tas hänsyn dels till den fundamentala hållfasthetsfördelningen och dels till det aktuella spänningsläget orsakat av någon viss belastning. Dessa modeller är mera sofistikerade än de som resulterar från en anpassning av en vanlig statistisk standardfördelning. Men dessa modeller är mindre stringenta än de som är baserade på en rigorös gestaltning av glasytans beskaffenhet. Denna tredje kategori av hållfasthetsmodeller framstår därför som ett intressant alternativ för vidare beforskning.

En vidare slutsats som kan dras är att insamlad mätdata behöver analyseras mera för att kunna dra robusta slutsatser om hållfasthetens beroende av ett flertal faktorer inbegripet kantbearbetningen och betydelsen av var glaset kommer ifrån, det vill säga effekten av tillverkningen och leverantören.

Contents

I	Introduction and overview	1
1	Introduction	3
1.1	Background	3
1.2	Aim and objectives	7
1.3	Limitations	9
2	Glass material	11
2.1	Material properties	11
2.2	Manufacture	12
2.3	Types of product	15
2.3.1	Edge treatments	15
2.3.2	Tempering	15
2.3.3	Laminated glass	17
2.3.4	Insulated glass units	17
2.4	Glass fatigue	17
2.5	Fracture mechanics	18
2.5.1	Background	18
2.5.2	Surface flaws	20
2.5.3	Subcritical crack growth	26
3	Calculating the strength	33
3.1	Defining the strength	33
3.1.1	Time-dependent strength	34
3.2	Test devices	35
3.3	Calculation methods	35
3.3.1	Analytical methods	36
3.3.2	Numerical solutions	37
3.3.3	Combination of methods	42
4	Measuring and portraying the strength	43
4.1	Introduction	43
4.2	Probability theory and methods of statistical inference	44
4.3	Statistical outliers	47
4.4	Analysis	48
5	Strength prediction models and design rules	53

5.1	Strength models	54
5.1.1	Normal and lognormal distributions	54
5.1.2	Gumbel distribution	55
5.1.3	Weibull (1939)	55
5.1.4	Matthews et al. (1976)	59
5.1.5	Batdorf and Crose (1974)	60
5.1.6	De Jayatilaka and Trustrum (1977)	61
5.1.7	The GFPM	62
5.1.8	Haldimann (2006)	63
5.1.9	Yankelevsky (2014)	64
5.1.10	Kinsella and Persson (2018b)	65
5.2	Design rules	66
5.2.1	prEN 16612:2017	66
6	Discussion of strength models	69
6.1	The Weibull model	70
6.2	Macroscopic/phenomenological approaches	75
6.3	Microscopic/ flaw-based failure approaches	77
6.3.1	Elemental strength approach	77
6.3.2	Flaw size approach	79
6.4	Edge and surface failure origins	83
6.5	Stress corrosion	83
6.6	Error sources	85
7	Summary of appended publications	89
7.1	Paper A	89
7.2	Paper B	90
7.3	Paper C	91
7.4	Paper D	92
8	Conclusions and further research needs	93
	References	97
II	Appended publications	107

Paper A

Performance of standard statistical distributions for modelling glass fracture.

David Kinsella, Johan Lindström, Kent Persson.

Accepted for publication in the International Journal of Structural Glass and Advanced Materials Research.

Paper B

A numerical method for analysis of fracture statistics of glass and simulations of a double ring bending test.

David Kinsella, Kent Persson.

Published in the Glass Structures & Engineering journal.

Paper C

An analysis of glass fracture statistics.

David Kinsella, Kent Persson.

Published in the proceedings of the Challenging Glass Conference 6.

Paper D

Survey of experimental data on the strength of annealed float glass panes in the as-received condition tested in an ambient environment.

David Kinsella

Published on the website of the Division of Structural Mechanics, Lund University.

Part I

Introduction and overview

1

Introduction

1.1 BACKGROUND

Glass is increasingly used in structures such as large windows, doors, rooflights, stair-cases, walls, floors, and balustrades. The demand for glass in structures is magnified by the qualities inherent in the material which allow for making the most of natural daylight while satisfying modern architectural trends for style and design. With glass it is also possible to control heat, light, and sound transmission while meeting requirements for safety, security, and energy efficiency.

The role of glass in a building can be decorative, functional, structural, or any combination of these. Fig. 1.1 exemplifies this with photographs of various glazed units. The role of a traditional window glass pane is mainly functional, i.e. to shut out the weather, cold, and wind while allowing for light transmission. With modern use of glass in buildings, however, the structural role as a beam, pillar, plate or panel element is significant. The glass unit can be a primary or secondary member of the load-bearing structure. The strength design has to consider static load cases due to e.g. snow load and secondary structural members. The design also has to take into account dynamic load cases due to e.g. accidental impacting from a soft body. Fig. 1.1a illustrates an infill wall panel inside the Mathematics Annex at the Faculty of Engineering, LTH. The infill panel consists of laminated glass units with an artwork interlayer. The role of this panel is decorative. It is also structural because the glass unit has to be able to withstand significant load from e.g. an accidental human impact. Fig. 1.1b illustrates the Tornet building at Helsingkrona Nation in Lund. The thirteen story building was constructed in

the year 2015 and contains a conference room on the top floor with large windows that provide a view over Lund, Malmö, and Copenhagen. The balcony on the top floor has a glazed balustrade. The role of this balustrade is structural because it was designed to resist static and dynamic loads. It is moreover functional because it allows for a stunning view of the surroundings. It also allows for the light to reach further onto the balcony floor. Fig. 1.1c illustrates the Orkanen building at Malmö University, the facade of which comprises some 3000 monolithic and tempered glass panes with a decorated surface consisting of many small grooves that run from the top to the bottom on the outward facing side. The visual impact is magnified by the location at the waterfront. The main role of this glazed unit is decorative. It is moreover structural because it has to be able to withstand significant climatic loads induced by the wind as well as the rising and setting sun that is capable of producing thermal gradients over the thickness of the pane.

Research into the structural use of glass in buildings is an emerging field. This is reflected e.g. in the increased number of dedicated scientific journals and conferences as well as in the overall number of peer-reviewed publications which deal with this topic. As an indication of the increasing research activity, we may consider the statistics generated by the following two search strings in the Scopus database (www.scopus.com) which is an abstract and citation database of scientific journals, books, and conference proceedings. Both search phrase (1.1) and (1.2) are limited to the title, abstract and keywords fields. The second search phrase is in addition limited to the subject area “engineering”. The search phrases are:

$$\text{”glass in buildings”} \tag{1.1}$$

and

$$\{\text{structural glass}\} \text{ OR } \{\text{glass structures}\} \tag{1.2}$$

The number of retrieved records per year with the respective search phrases are illustrated in the graphs in Fig. 1.2 and it is evident that structural glass engineering is being researched at an accelerated pace. The reason for this increased activity is mainly due to glass being used more in load-bearing situations.

The strength of glass is a complex entity. To begin with, it can only be revealed by destroying the glass. And yet, the strength thus revealed is not the strength at the onset of testing, for it is significantly altered during the course of loading. As a matter of fact, the strength depends on the load history, environment, and temperature, as well as the size of the structure and the state of the surface, the condition of which might be new as-received or aged and weathered. The simultaneous action of stress and environmental conditions promote a fatigue phenomenon in glass. The combined effect of load-history and climate on the strength can be accounted for by implementing the stress corrosion rate theory or some empirical formula.

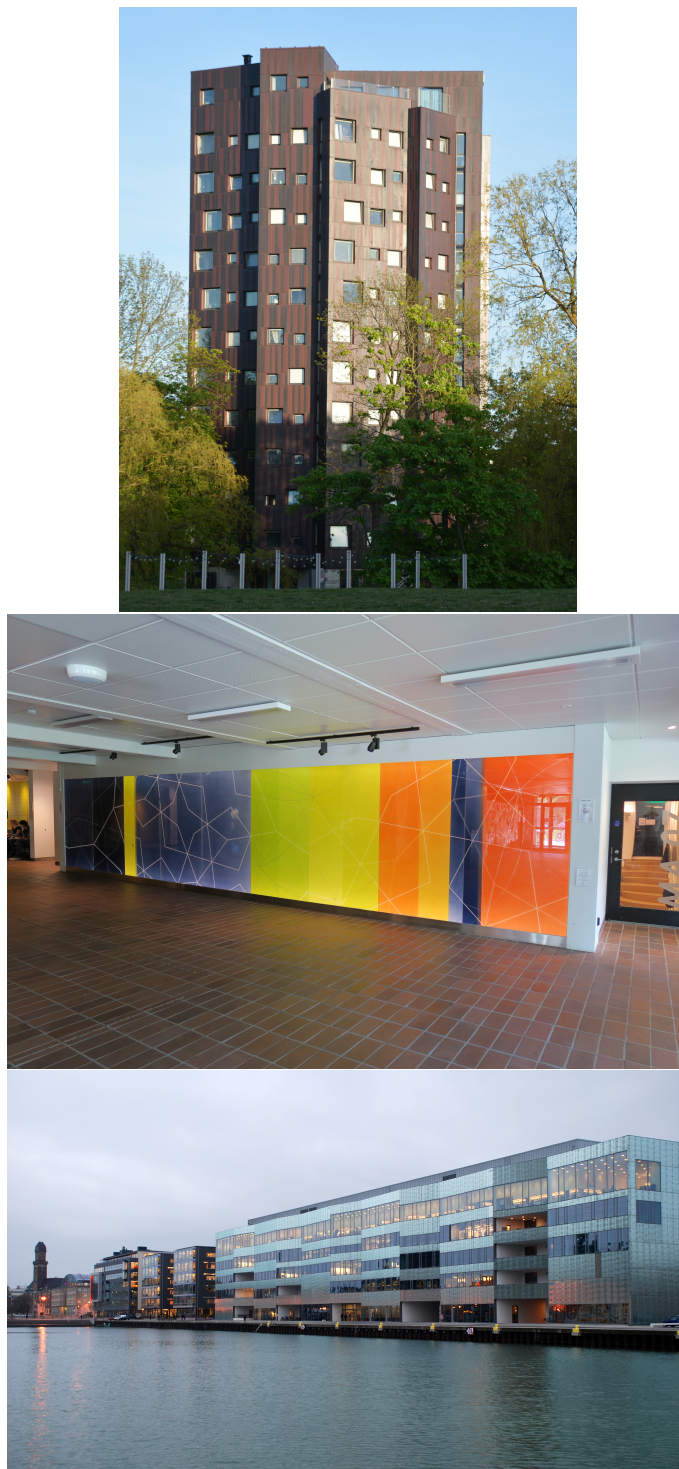


Figure 1.1: The Tornet building at Helsingkrona Nation in Lund. Artwork infill panel in the Mathematics annex at the Faculty of Engineering, LTH. The Orkanen building at Malmö University. Photographs of Tornet and Orkanen were obtained from Wikimedia Commons.

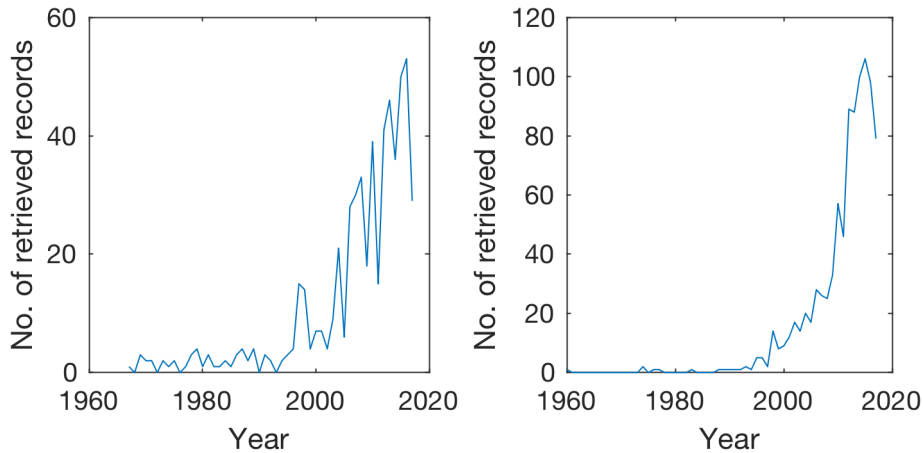


Figure 1.2: Number of retrieved records per year in Scopus (www.scopus.com) from search phrase (1.1) on left-hand side and search phrase (1.2) on right-hand side. The data shown is until the year 2017.

A relatively large number of experiments on annealed glass have been conducted over the past four decades, many of which were carried out in recent years. These tests provide statistics about the strength and the location of fracture origins. The results from these experiments demonstrate that the strength exhibits a large variation which spans about one order of magnitude. In spite of efforts to create probabilistic strength models which are fitted with methods of statistical inference, it remains a great challenge to try to model and predict the strength value for some structural glass unit.

Present techniques for modelling and predicting the strength are based either on a fracture mechanical approach or on some phenomenological method which takes into consideration only the macroscopic behaviour. As an example of the latter we may take the adoption of a standard statistical distribution to model the fracture stress. Current failure prediction models, however, are limited in scope. At best, they are suited to particular test arrangements and environmental conditions. In fact, the failure prediction remains a formidable challenge in the general case of a structural unit with boundary conditions that can vary from very rigid to fairly flexible with continuous support or point fixings, where the load is either distributed or concentrated, and with the geometrical properties of the glass depending on e.g. aspect ratio and the existence of boreholes. Additionally, although the failure prediction generally refers to the strength value, it can also be useful to make predictions about the failure origin. There is need for further development of a failure prediction model that can be conducive to the improvement of structural standards and building codes.

The failure prediction and strength design of a glass structure is dependent on a

range of theories and methods at the material as well as the structural level as illustrated in Fig. 1.3. Fracture mechanical theories consider the microscopic behaviour of solids and form the basis of failure prediction models for use with brittle materials. At the structural level, mechanical models allow for the determination of the stresses and strains in plates and beams due to bending under various forms of loading and support conditions. In combination, fracture mechanical and structural mechanical models provide a powerful tool for the analysis of brittle specimens subjected to bending loads. However, glass fatigue complicates the prediction-making. Experimental test results can be used to validate the models at the structural level, to make investigations into the surface condition at the material level e.g. through the estimation of a surface flaw size density function, and to quantify the rate of subcritical crack growth. Ultimately, it is necessary to employ probability theory and methods of statistical inference at both the material and the structural level to account for the various aspects of glass failure. Some of the methods thus employed are made feasible by the use of numerical techniques such as the finite element method. Finally, the failure prediction model has to be put to practical use by carefully considering the requirements and directives of modern building codes and structural standards.

Monolithic panes of annealed float glass are an important object for modelling because according to the structural standards, e.g. prEN 16612:2017 and DIN 18008-1:2010, the strength of a glass pane is based on the so-called characteristic value for the strength of annealed glass. In practice, a glass structure may comprise a monolithic pane of heat-strengthened or fully tempered glass. Or it may involve a laminated set of annealed, heat-strengthened, or fully tempered plies of glass. In either case, knowledge of the strength of a monolithic pane of annealed glass is a basis. Hence, it can be said that a key to making predictions about the strength of some heat-strengthened or tempered pane of glass, or some laminated component, lies in modelling the strength of ordinary annealed glass.

1.2 AIM AND OBJECTIVES

The main aim of the research is to develop models that can be used in engineering practice for failure prediction of glass structures, e.g. as a basis for design rules. Failure prediction is dependent on a range of theories and methods at the material as well as the structural level as illustrated in Fig. 1.3. This includes

- fracture mechanics
- the phenomenon of glass fatigue
- structural mechanical models that determine the behaviour of plates and beams subjected to various forms of bending

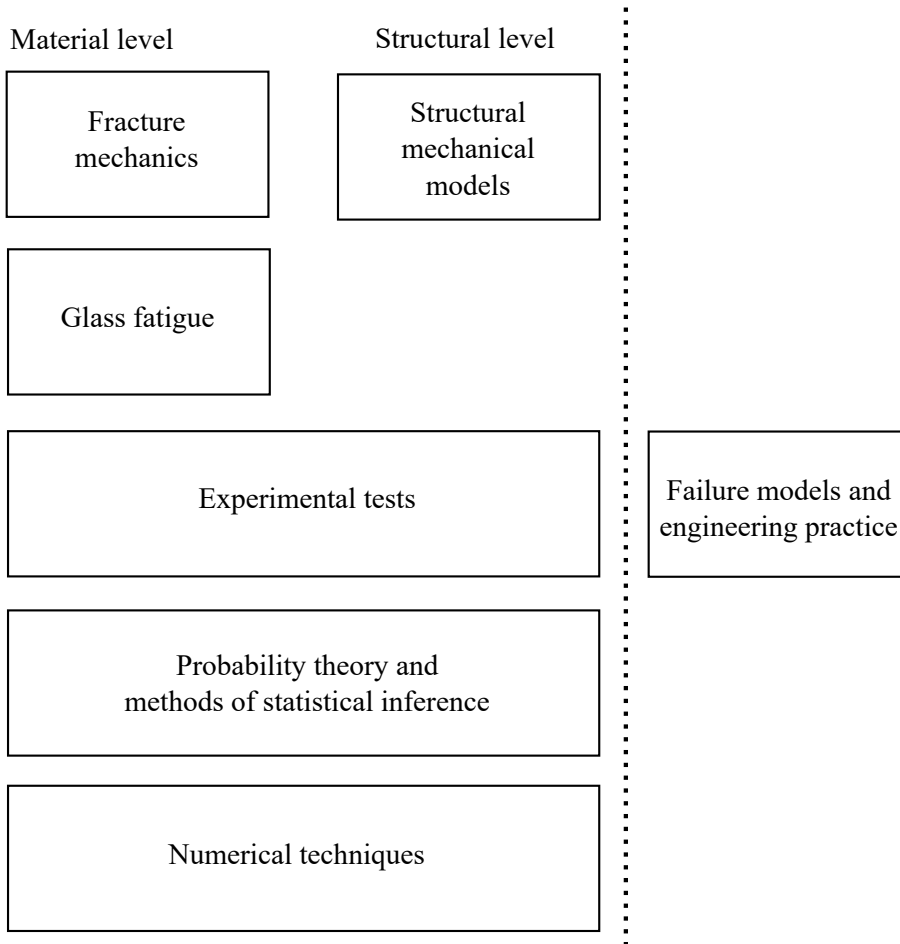


Figure 1.3: Engineering practice dependencies.

- various models in probability theory which are used to e.g. represent surface microcrack concepts
- various numerical techniques including the finite element method which is key to calculating the stresses and strains in solids
- and more recently, certain numerical schemes used to implement stochastic flaws in Monte Carlo simulations of the strength

Statistical methods which are used to draw inference about model parameters and performance is a fundamental part of a prediction model. Strength models for potential use with glass should be mapped out with respect to the basic characteristics and assumptions. This would permit a careful analysis which comprehensively considers the utilities and drawbacks of each model and which may provide guidance and direction for the benefit of future research efforts. In order to appraise

the potential in performance of any strength model, there is a need for empirical data on the fracture stress to be collected and organized.

As a first objective, a glass strength model for use with plates tested in the double ring bending device is developed based on Monte Carlo simulations of Griffith flaws. Secondly, the empirical data on the strength of new monolithic annealed glass when it is tested in ambient conditions is collected from the available literature, i.e. scientific journals, conference proceedings, and academic dissertations, and organized in a summarized form that permits an overview. The performance of the most pertinent standard statistical distributions for modelling glass strength with is evaluated based on the empirical data set. Moreover, a model is developed which allows for analyzing the fracture origins in laterally supported glass plates subjected to uniform pressure. Also, a dynamic load case involving a glass structure with a complex geometry is modelled with respect to both fracture stress and failure location. Finally, various strength models for potential use with glass are reviewed.

1.3 LIMITATIONS

Only monolithic panes of float glass are considered. It is generally assumed that the glass is stressed in an ambient environment meaning that the temperature and relative humidity are similar to indoor conditions. Flaws in the bulk are generally disregarded from and it is assumed that failure is governed by surface flaws. It is assumed that the shape of flaws can be represented by planar cracks. Mode III crack displacement is not considered. Crack healing effects are not taken into account in the strength modelling. The analysis and discussion of structural standards is limited mainly to the draft for a European standard for strength of glass in building, viz. prEN 16612:2017.

2

Glass material

The facts in sec. 2.1 to 2.4 are mostly from Le Bourhis (2008). When no reference is given, it is implicit that Le Bourhis (2008) is cited.

2.1 MATERIAL PROPERTIES

Soda-lime silicate glass is an amorphous and inorganic ceramic material with a typical composition according to Tab. 2.1. Glass can be considered a supercooled liquid which has solidified from a melt without crystallizing. However, at room temperature, the viscosity is so high that no flow can be observed. The glass material is formed by a network of Si–O which have covalent bonds. The network is modified by Na^+ and Ca_2^+ ions through ionic bonds. The glass network is characterized by a short-range order which means that after about five interatomic distances, order almost vanishes. This conclusion can be drawn from investigations carried out with X-ray or neutron diffraction techniques. In three dimensions, the Si and O atoms arrange to form tetrahedral elements with a Si atom at the centre. The elemental tetrahedrons are connected by the sharing of corners. This is illustrated in Fig. 2.1 which contains a two-dimensional projection of the glassy form of SiO_2 . The addition of Na^+ causes the rupture of O–O bonds. Although the bond is broken, the pair of tetrahedra still interact electrostatically. The modification of the network induces a decrease in viscosity. This is of great practical importance because it lowers the melting temperature of glass significantly. In pure silica the melting temperature is about 1700 °C while in soda glass it is only about 790

Table 2.1: Typical composition of soda-lime silicate glass in weight percent (Le Bourhis 2008).

SiO ₂	Na ₂ O	K ₂ O	CaO	MgO	Al ₂ O ₃	Fe ₂ O ₃
71-73	13-15.5	0-1	6.5-12	2-4.5	0-2	0-1

Table 2.2: Typical values for a range of glass material properties (Le Bourhis 2008)

Density (kg m ⁻³)	2500
Thermal conductivity (W (mK) ⁻¹)	1.00
Thermal expansion coeff. (10 ⁻⁶ K ⁻¹)	8.5
Young's modulus (GPa)	74
Poisson's ratio	0.22
Surface energy (J m ⁻²)	0.6
Fracture toughness (MPa m ^{1/2})	0.75
Stress corrosion threshold limit (MPa m ^{1/2})	0.25

°C after addition of 25% soda to silica. Values for a range of material properties including the elastic properties are given in Tab. 2.2.

2.2 MANUFACTURE

The manufacturing involves a long process line with the following operations, viz. batching, melting, fining, forming, and annealing, see also Fig. 2.2. Glass for use

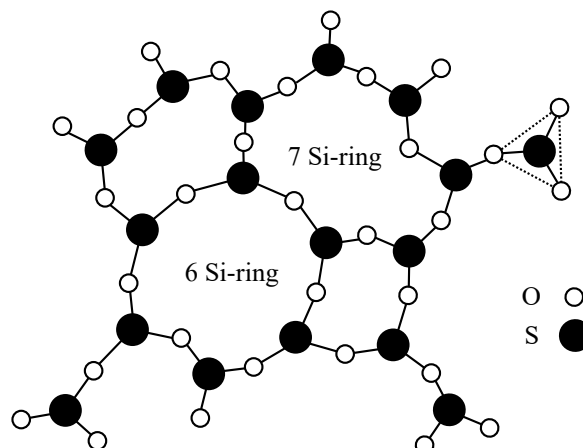


Figure 2.1: Glassy state of SiO₂ with an elemental tetrahedron indicated by dashed lines. Adapted from Le Bourhis (2008).

in structures is composed of the following raw materials which are selected in the batching operation, viz. sand, sodium carbonate, calcium carbonate, and various metal oxides. Grain size distribution and purity are important considerations in the batching operation (McLellan & Shand 1984). The composition of raw material is indicated in Tab. 2.3. The material composition is further standardized in EN 572-1:2004. The role of sodium in the batch is to soften the glass network and reduce the melting temperature to a practical regime while the addition of calcium stabilizes the network (McLellan & Shand 1984). Various metal oxides are added, among other reasons, to facilitate in the fining operation. The melting is done in a furnace which is usually combustion heated. In the fining operation, the glass composition and temperature is made uniform through convection and bubbles are eliminated. In the float process which was introduced in the late 1950's, the glass melt is floated on a bed of molten tin at a temperature of about 1100 °C under a nitrogen atmosphere. As the glass exits the float, it has a temperature of about 600 °C. Then, it enters the annealinglehr where it is cooled down to room temperature. The thermal history is carefully controlled to design the residual stresses. The glass is usually cut into standard size panes with the dimensions 6x3.21 m² (EN 572-1:2004).

When the sheet is cut it is first scribed in a lateral movement under a sharp tip of high hardness using an automated cutting machine. Cutting oil is applied in front of the cutting head to protect the mark from the environment. The scribing generates median cracks. The scribing tool is carefully controlled to limit the introduction of lateral cracks which degrade the edge quality. In Fig. 2.3, the median and lateral cracks are illustrated for the case of a sharp indentation fracture. While flexuring the scribed glass, the median cracks are driven through the thickness of the plate breaking it in two, cf. Fig. 2.4. The cut edge is characterized by 1) a mechanically scribed and damaged edge on one side and 2) a sharp edge on the other. The raw-cut edge was studied in a project related to this thesis for three different thicknesses, viz. 4, 6, and 8 mm, of new annealed glass using an optical microscope model WILD Makroskop M420 together with an integrated Leica system DMC 2900. Fig. 2.5a illustrates the opposite side of the mechanically scribed edge of the 4 mm glass while Fig. 2.5b and 2.5c demonstrate the scoring edge of the 6 and 8 mm glass, respectively. The raw-cut edge is sharp and can cause injury.

In the manufacturing process line, the glass is like a continuous ribbon that is pulled upstream. The standard thicknesses are 2, 3, 4, 5, 6, 8, 10, 12, 15, 19, and 25 mm according to EN 572-1:2004. American standard thicknesses are given in ASTM C1036-01:2011.

Table 2.3: Raw material composition in a batch of soda-lime silicate float glass (Le Bourhis 2008).

Raw material	Sand	Sodium carbonate	Calcium carbonate	Metal oxides
Concentration (%)	54	24	16	2

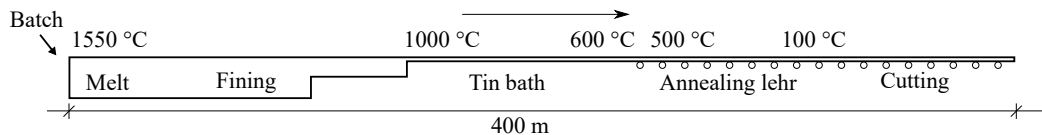


Figure 2.2: Flat glass production line with the float process. Adapted from Haldimann (2006) and Le Bourhis (2008).

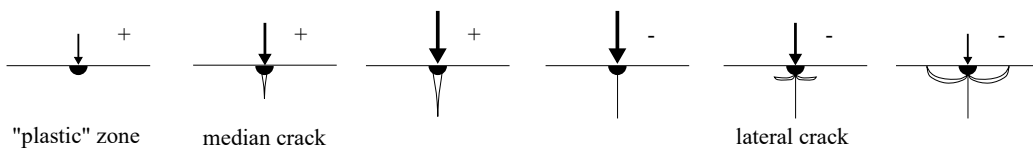


Figure 2.3: Median crack forming and extending upon loading under a sharp indenter. Lateral cracks form during unloading. If the load is large enough the lateral cracks extend to the surface. Adapted from Le Bourhis (2008).

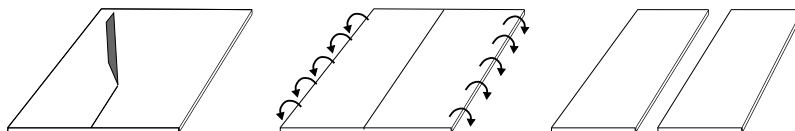


Figure 2.4: Glass is cut in the process of scribing, flexuring and breaking. Adapted from Lindqvist (2013).



Figure 2.5: The cut edge as seen on (left) 4 mm thick glass at opposite side of the scribed edge, (middle) 6 mm thick glass at scribed edge, (right) 8 mm glass at scribed edge. The photographs were acquired with the support of Smart Housing Småland.

2.3 TYPES OF PRODUCT

The flat glass that exits the annealing lehr in the float glass production line can be further processed in several ways to produce various products with added value. Here follows a description of the operations that are most pertinent to glass products for structural use. The processing can be done on the manufacturing site or off-site, e.g. with a supplier. The basic, un-processed product is in this context understood to be the monolithic pane of annealed float glass with an as-cut edge, see Fig. 2.6a.

2.3.1 Edge treatments

The arrised edge has got small bevels introduced at an angle of about 45 degrees to the surface of the glass, see Fig. 2.6b. The arrising is performed in a grinding operation. Grinding is to cause irregular-shaped grains of abrasive to wedge between the surface of a moving body and the glass so that glass material breaks down into small fragments (McLellan & Shand 1984). Water is used to increase the grinding rate and to prevent overheating. A so-called ground edge, see Fig. 2.6c, is an arrised edge that has been subjected to further grinding cycles. The ground surface is characterized by its roughness. The roughness depends on the grinding wheel's properties and settings as well as its total age and usage. Instead of a grinding wheel, a belt can be used. The direction of grinding has a bearing on the quality of the ground edge (Kleuderlein et al. 2014). The appearance of a ground edge is rough with fine abrasion marks. Sometimes, smooth spots of raw-cut glass may be visible on the surface edge depending on the amount of grinding that took place, see Fig. 2.6d. A polished edge, see Fig. 2.6e, has been subjected to both grinding and polishing operations. The action of polishing is carried out in a similar manner to grinding, however, very little material is removed in the process (McLellan & Shand 1984). A polished edge is characterized by a shiny and reflective appearance. A water-jet cut edge, see Fig. 2.6f, is created by a water jet that carries with it fine sand particles which pierce the glass. The water-jet cut edge is characterized by a matt appearance (Veer & Rodichev 2012).

2.3.2 Tempering

Tempering produces a glass sheet with all surfaces subjected to compressive stresses which are counter-balanced by tensile stresses in the interior. The compressive surface stresses have to first be overcome before the tempered glass can be broken, unless the fracture is initiated from the interior (Tooley 1984). Thermal tempering is performed by heating up the glass article close to the transition temperature at about 650 °C and rapidly quenching it by chilling the surface with blasts of

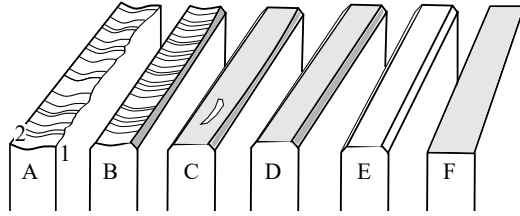


Figure 2.6: Edge finishings. (A) As-cut. (B) Arrised. (C) Ground with smooth spots. (D) Ground. (E) Polished. (F) Water-jet cut.

air (McLellan & Shand 1984). The rapidly cooled glass material is subjected to a thermal gradient while it passes through the viscous-elastic domain which results in the build-up of compressive residual stresses at the surface. The compressive stresses are balanced by tensile stresses in the core. The thermal and structural histories during tempering are complex and include unknown thermal transfer coefficients. However, a simple model for the through-the-thickness stress distribution can be achieved by assuming a constant rate of cooling and supposing that no structural relaxation takes place. Then, the temperature variation through-the-thickness is parabolic and the temperature difference between the surface and the centre is

$$\Delta T = \frac{b^2 c_R c_P}{8k} \quad (2.1)$$

where b is the thickness of the pane, c_R is the cooling rate, c_P is the specific heat, and k is the thermal conductivity.

A fully tempered glass pane usually has a breaking stress that is increased by a factor of 2.5 to 3.5 compared to annealed glass (McLellan & Shand 1984). According to prEN 16612:2017, the strength of properly toughened safety glass is about 2.5 times as great as that of ordinary annealed glass while the strength of heat strengthened glass is about 1.5 times as great. Upon failure, a fully tempered pane shatters into small cubes and this is referred to as dicing. The dice are unlikely to cause serious injury. Heat-strengthened glass is produced similarly to fully tempered glass but with a lower rate of quenching which produces smaller compressive surface stresses. On failure, heat-strengthened glass does not dice into small fragments like fully tempered glass. Instead, it retains a large fracture pattern similar to annealed glass.

Chemical tempering is performed by immersing the glass in a molten salt bath. The outer surface of the glass is strengthened through an ion exchange process. It is possible to achieve much higher surface compression with chemical tempering than with thermal tempering. However, the ion exchange depth is limited which results in a much smaller compression depth compared to thermally tempered articles. Moreover, the ion diffusion rates are very slow for ordinary soda-lime-silica glass which is widely used in building applications (Tooley 1984).

2.3.3 Laminated glass

Laminated glass is formed by bonding together two panes by a tough polymer in an autoclave. Polyvinyl butyral (PVB) is the most common choice of interlayer material and normally two foils are used, each foil having a thickness of 0.38 mm. However, there exist a whole range of alternative interlayer materials that offer higher stiffness, greater temperature resistance, etc. Laminated glass units achieve a greatly improved post-fracture behaviour compared to monolithic units due to the way in which the polymer interlayer absorbs energy from impacting objects, retains the fractured pieces of glass providing structural redundancy, and limits the risk of flying shards (McLellan & Shand 1984).

2.3.4 Insulated glass units

An insulated glass unit is composed of two or more glass panes with closed cavities which reduce heat transfer due to radiation, conduction, and convection. A low-conductivity gas fill is normally used between the panes. Radiative heat transfer can be further limited by tinted or coated glazing.

2.4 GLASS FATIGUE

Material fatigue means that the strength deteriorates over time. The earliest record of fatigue in glass is found in Grenet (1899) who subjected rectangular plates and small rods of glass to three-point bending at various rates of loading. He observed a decrease in strength as the load-duration was increased. Since then, many experiments have manifested fatigue in glass. For instance, Baker & Preston (1946*a*) observed in experiments that the fracture stress in glass was about three times as great for load durations only a fraction of a second in length compared to load durations 24 hours in length. The effect of fatigue was found to decrease when moisture was removed from the environment (Baker & Preston 1946*b*, Culf 1957, Mould & Southwick 1959). In fact, the strength of glass depends on the duration and magnitude of load as well as on the environment and temperature. The environment comprises agents such as water, usually in the form of humidity. Glass fatigue is not observed at temperatures below -196°C . It has been demonstrated that fatigue in glass is not aggravated by cyclic loading as is otherwise the case with e.g. steel (Lü 1997). Fatigue in glass is conventionally termed static fatigue, perhaps to distinguish it from cyclic fatigue which is common in the steel engineering literature, see e.g. Haldimann (2006). However, fatigue in glass is present whether the loading is static or dynamic. Present theories that explain glass fatigue are based on the assumption of pre-existing surface flaws, see Sec. 2.5.3.

2.5 FRACTURE MECHANICS

2.5.1 Background

Suppose that the strength is determined by the work necessary to separate the atoms in a given plane which slices the material in two. From a purely theoretical point of view then, the inert strength can be estimated at (Le Bourhis 2008, Orowan 1949)

$$\sigma_f = \sqrt{\frac{E\zeta}{\rho_0}} \quad (2.2)$$

where E is Young's modulus, ζ is the surface energy of the cleavage surface, and ρ_0 is the Si–O distance. Taking $E = 70$ GPa, $\zeta = 0.6$ J m⁻², and $r_0 = 0.15$ nm, the strength is found to be about 16 GPa (Le Bourhis 2008). However, experiments on annealed float glass panes demonstrate that this value is incorrect by more than two orders of magnitude, see Chap. 4. It is well-known that a scratch can reduce the strength of a glass sheet. In fact, glass is cut into the desired dimensions by flexuring a pane that has been scored on the surface with the use of a cutting wheel. The sharp indenter used in scoring produces median cracks that are driven through the thickness by the action of bending (Le Bourhis 2008).

In this section, we consider explanations for how some material flaw might prompt the onset of fracture in a solid based on a representation of the flaw as a crack. A crack is a flat separation bounded within the material by a leading edge which is approximated by a simple curve (Mencik 1992). A flaw can refer to many sorts of defects in general, for a discussion see Mencik (1992). On a submicroscopic scale it might refer to a dislocation array, an interstitial atom, etc. Flaws include bonded precipitate particles, surface grains, inhomogeneities, etc. Possibly visible to the naked eye are bubbles, pores, “cracks”, voids, impurities, etc. In the following, a crack refers to an idealization. It is a concept that represents the type of flaw that is thought to prompt failure in glass.

Based on linear elasticity theory, Inglis (1913) offered a logical explanation for the weakening effect of a material flaw. Inglis (1913) considered the elastic stresses near the edge of an elliptical through-the-thickness hole in an infinite plate of isotropic material subjected to uniform uniaxial tension. It was found that the crack warps the stress field. The maximum stress at the tip of the elliptical hole was calculated to be

$$\hat{\sigma} = \sigma \left(1 + 2\frac{a}{b}\right) \quad (2.3)$$

where $\hat{\sigma}$ denotes the crack tip stress, a is the half major axis, b is the half minor axis, and σ is the farfield stress. A sharp crack tip is obtained by letting the radius of curvature tend to zero. However, then the crack tip stress is magnified indefinitely. Nevertheless, supposing that an elliptical crack represents a real material flaw,

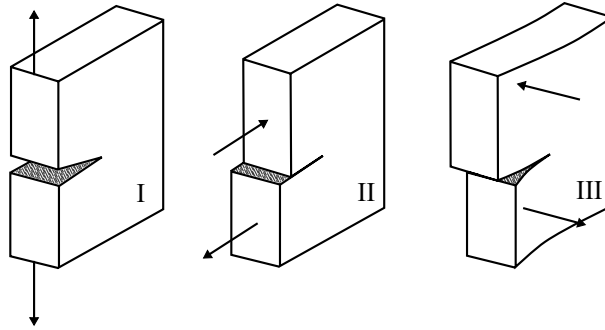


Figure 2.7: Crack displacement modes: mode I opening, mode II sliding, and mode III tearing. Adapted from Broek (1983).

Inglis' (1913) model explains how a flaw is capable to prompt failure for farfield stresses well below the theoretical bond strength.

The three modes of cracking denoted by mode I, II, and III, respectively, are illustrated in Fig. 2.7 (Irwin 1958). Mode I refers to crack opening due to displacements normal to the crack plane surfaces. Mode II and III describe in-plane and out-of-plane shearing displacement cracking (Broek 1983). The Inglis solution pertains to pure mode I crack opening.

Griffith (1920) adopted Inglis' (1913) solution and developed a fracture condition based on a consideration of the elastic energy released upon crack growth. The condition for crack growth is expressed in terms of a reversible thermodynamic process. The rate of elastic energy release, typically denoted by G in most literature, is balanced by the energy consumed during crack propagation. The critical energy release rate which can be determined experimentally, is a measure of material toughness. In the case of the elliptical crack subjected to uniform uniaxial stress that was studied by Inglis (1913) and further adopted by Griffith (1920), a fracture criterion is

$$G \geq G_{Ic} \quad (2.4)$$

where G_{Ic} denotes the mode I critical energy release rate.

Another way of representing the fracture condition, and in fact an equivalent one, is provided by a characterization of the elastic stress field near the crack tip (Broek 1983). A solution in rectangular coordinates was found by Westergaard (1939) for a sharp through-the-thickness crack in an infinite plate subjected to uniform biaxial tension. By use of the Euler identity, Irwin (1957) showed that the following expressions for the stress field near the crack tip approximate those of Westergaard (1939). Expressed in polar coordinates, the stresses near the crack tip were

calculated to be

$$\sigma_x = \sigma \sqrt{\frac{a}{2r}} \cos \frac{\theta}{2} \left(1 - \sin \frac{\theta}{2}\right) \sin \frac{3\theta}{2} \quad (2.5)$$

$$\sigma_y = \sigma \sqrt{\frac{a}{2r}} \cos \frac{\theta}{2} \left(1 + \sin \frac{\theta}{2}\right) \sin \frac{3\theta}{2} \quad (2.6)$$

$$\tau = \sigma \sqrt{\frac{a}{2r}} \sin \frac{\theta}{2} \cos \frac{\theta}{2} \cos \frac{3\theta}{2} \quad (2.7)$$

where a is the semi-crack length. Irwin (1957) introduced the stress intensity factor (SIF) which is denoted by K_I in the case of mode I opening displacements, based on the fact that from Eq. (2.5), (2.6), and (2.7), we have

$$\sigma_{ij} = \frac{K_I}{\sqrt{2\pi r}} f_{ij}(\theta) \quad (2.8)$$

where $K_I = \sigma \sqrt{\pi a}$. The SIF completely determines and characterizes the stress field at the crack tip (Broek 1983). A pure mode I fracture condition is given by

$$K_I \geq K_{Ic} \quad (2.9)$$

where K_{Ic} denotes the critical SIF, i.e. the fracture toughness. It can be shown (Broek 1983) that in the case of plane stress

$$\frac{K_I^2}{E} = G_I \quad (2.10)$$

while in the case of plane strain

$$(1 - \nu^2) \frac{K_I^2}{E} = G_I \quad (2.11)$$

2.5.2 Surface flaws

As a more realistic representation of surface flaws in glass, we consider mainly two types of part-through flat edge cracks, viz. the long straight-fronted plane edge crack and the semi-circular edge crack. In addition, the quarter circle corner crack was used in a strength model by Porter (2001). The semi-circular edge crack is also known as the half-penny crack. It is assumed that the crack is contained in a semi-infinite specimen. The mode I SIF for a straight-fronted edge crack is (Tada et al. 2000)

$$K_I = 1.12\sigma\sqrt{\pi a} \quad (2.12)$$

The SIF at the deepest point on the crack contour of a semi-circular edge crack can be approximated as (Newman & Raju 1981)

$$K_I = 1.14\sigma \frac{2}{\pi} \sqrt{\pi a} \quad (2.13)$$

For other crack shapes, however, it is possible to define a geometry factor Y associated with the crack shape such that

$$K_I = Y\sigma\sqrt{\pi a} \quad (2.14)$$

Suppose that the edge crack is subjected to a biaxial stress field with the crack plane inclined at an angle θ in the coordinate system of the principal stresses σ_1 and σ_2 . Then, the stress acting normal to the crack plane is

$$\sigma_n = \sigma_1 \cos^2 \theta + \sigma_2 \sin^2 \theta \quad (2.15)$$

and the shear stress is

$$\tau = \frac{1}{2}|\sigma_1 - \sigma_2|\sin 2\theta \quad (2.16)$$

The mode II SIF for the straight-fronted edge crack is (Tada et al. 2000)

$$K_{II} = 1.12\sqrt{\pi a}\tau \quad (2.17)$$

while the mode II SIF for the semi-circular edge crack can be approximated as (Thiemeier et al. 1991)

$$K_{II} = 1.14\frac{4}{\pi}\frac{1}{2-\nu}\sqrt{\pi a}\tau \quad (2.18)$$

There exist a range of mixed mode fracture criteria and a number of them were compared in Thiemeier et al. (1991). We consider a mixed mode fracture criterion based on the maximum noncoplanar energy release rate (Hellen & Blackburn 1975) which was found to be relatively shear sensitive compared to criteria based on e.g. the coplanar energy release rate, the maximum hoop stress factor, and the minimum strain-energy density (Thiemeier et al. 1991). The fracture condition based on the maximum noncoplanar energy release rate is

$$\sqrt{K_I^4 + 6K_I^2 K_{II}^2 + K_{II}^4} \geq K_{Ic}^2 \quad (2.19)$$

In Eq. (2.19), the right-hand side means that it is assumed that the mode I fracture toughness characterizes the material resistance against unstable crack propagation even though it is a mixed mode condition.

Flaw location distribution is generally assumed to be uniform in the plane of the surface. In Wereszczak et al. (2014), an empirical flaw location distribution is indicated in the measurement results using optical scanning techniques. Wereszczak et al. (2014) has already been cited extensively by those who recently have attempted to model glass strength with a flaw size approach in Monte Carlo simulations, see further Chap. 6. However, due to the low resolution of the diagram in the journal article print (Wereszczak et al. 2014), it is hardly possible to extract a spatial distribution. Nevertheless, the investigation in Wereszczak et al. (2014) was limited to an examination of two panes of glass comprising four surface sides.

Hence, the conclusions drawn from this study are suggestive but require further experimentation to be corroborated.

Regarding the representation of the surface flaws condition in glass, the following can be noted. A single population concept was used by a number of researchers. Freudenthal (1968) assumed a Cauchy distributed flaw size distribution. Poloniecki & Wilshaw (1971) and Poloniecki (1974) proposed a flaw size density function in the form of Eq. (5.44) which was based on empirical results and which was subsequently adopted in the strength model by De Jayatilaka & Trustrum (1977). Yankelevsky (2014) assumed a flaw size distribution function that can be interpreted as a truncated exponential distribution. Osnes, Hopperstad & Børvik (2018) discretized the Yankelevsky (2014) flaw size distribution in the following way

$$a_i = a_{\max} \left(1 - \frac{\ln N_i}{\ln N_0} \right) \quad (2.20)$$

where N_0 is the total number of flaws, a_{\max} is the upper boundary on flaw size, and N_i is the number of flaws with a depth larger than a_i with

$$N_i = R_1(N_0 - 1) + 1 \quad (2.21)$$

where R_1 is a uniformly distributed random variable on $[0, 1]$. Haldimann (2006) adopted a Pareto flaw size distribution which by the way is implicit in an adoption of the Weibull distribution if it is assumed that the stress state is uniform uniaxial and the flaws are oriented perpendicular to the stress. A number of researchers implement into their strength models a right-truncated flaw size distribution. Pisano & Royer-Carfagni (2017), e.g., assume the following argument: Due to optical and aesthetic performance requirements on commercial glass, strict production controls “usually assure that glass with large defects are discarded and not placed on the market.” (Pisano & Royer-Carfagni 2017) In fact, this was the same kind of argument adopted by Yankelevsky (2014) for a right-truncated flaw size distribution. However, does this assumption agree with what happens in reality, i.e. can it really be assured that glass with large defects are simply discarded in the production? And are there test results available that corroborate such an assumption? As a matter of fact there is a need for greater insight into the surface condition in glass. At present, however, there is a lack of methods and technology available by which to probe the surface flaws.

Several authors have considered dual flaw populations concepts. In fact, the empirical data suggests that flaw size in glass is bimodal. Consider e.g. Krohn et al. (2002) who performed fractographic analyses of broken glass plates which had been subjected to double ring bending tests. It was concluded that “there is some evidence for a second flaw population to be contributing to the low strength of the float glass specimens.” A statistical model for characterizing glass strength when two flaw populations are superimposed due to abrasive phenomena was proposed by Pisano & Royer-Carfagni (2017) and Bonati et al. (2018). Pathirana et al. (2017)

implemented a dual population of lognormally distributed flaw sizes in Monte Carlo simulations of Griffith flaws. Kinsella & Persson (2018*b*), see Paper B, implemented a dual flaws population concept consisting of a Pareto flaw size distribution corresponding to large, “rogue” flaws of which there were assumed to be only a small number on a given plate, and a Fréchet flaw size distribution corresponding to numerous small flaws according to an argument based on extreme value theory.

Mencik (1992) distinguishes between four surface flaw populations according to their supposed origin. There are large cracks caused by contact damage which limits the strength to 20-60 MPa. Then, there are microscopic and submicroscopic cracks smaller than 100 microns in size whose origin lie in the glass formation process as well as in contact damage. The small flaws are numerous. On a given square centimeter there may be hundreds or even tens of thousands. Then, there are flaws that arise due to foreign microscopic particles that adhere firmly to the surface at higher temperatures during manufacturing in the glassworks. Such flaws act as fracture initiators for failure at several hundred or thousands of MPa of tensile stress. Their effect is generally overlapped by flaws of the first two categories of origin. Finally, there are flaws occurring during manufacture and subsequent heat-treatment due to changes in the surface resulting from reactions with the environment, e.g. in the form of volatilization. Again, their effect is generally overlapped by the more severe flaws in the first two categories of origin.

When it comes to the representation of flaws in glass, it can be said in general that it is assumed that the effect of bulk flaws, if they are present at all, is overlapped by the effect of surface flaws. By the same token, this is an argument for neglecting bulk flaws in the strength modelling. Glass is mostly loaded in bending which results in the surface stresses being larger than the stresses in the bulk.

When you consider the recorded values for the fracture stress from a given experiment, you cannot know exactly what shape of flaw that prompted the observed fracture, nor are you able to tell what orientation the hypothetical crack plane had with respect to the stress field. A thorough fractographical investigation may provide some insight into the fracture process but such detailed investigation is rare. Lindqvist (2013) attempted to measure the critical flaw size by performing fractographical studies of the failure origin before and after destructive testing but was ultimately unable to establish a relationship between the observed strength and the measured flaw depth. What you sometimes encounter in the literature are measurements of the so-called mirror zone radius which are obtained in fractographic studies. It is usually possible to identify a smooth mirror-like zone around the flaw that prompted failure using an optical microscope, see e.g. Calderone (1999), Johar (1981), Lindqvist (2013), Yankelevsky et al. (2017). The mirror zone is surrounded by the so-called mist and hackle regions, cf. Fig. 2.8 for an illustration. There exist empirical relations between the critical stress and the mirror zone radius, although such formulae do not always produce reliable results when

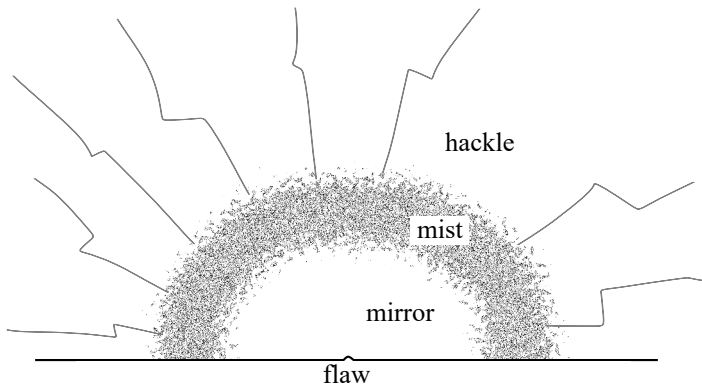


Figure 2.8: Mirror, mist, and hackle zones which surround the failed flaw. Adapted from Lawn (1993).

comparisons are made with the calculated fracture stress (Johar 1981).

Edge vs surface condition

When glass is tested using the double ring bending device, then due to the emergent stress field, edge fractures are extremely unlikely to occur. For practical purposes therefore, it can be assumed that only surface failures are produced. So is not the case for other commonly employed testing devices. When the testing is performed using a three or four-point bending device and the bending takes place in-plane, then one edge is positioned in the tension zone which makes the fracture prone to occur along this edge. However, from a theoretical point of view of course, a pure surface failure is still possible during this kind of bending. See Fig. 2.9 for an illustration of the possible failure origins near the edge in the case of a beam tested in four-point bending with in-plane loading. With reference to Fig. 2.9, we next consider the case when the failure origin is located at points S1 or S5, i.e. one of the main surfaces of the glass specimen. Vandebroek et al. (2014) appear to be the only ones who have stringently examined the rate of surface failures in the case of glass beam tests with in-plane bending. According to their research, on average 13% of ground and 20% of cut specimen failures occurred from either of the main surfaces of the glass. This was according to fractographic analysis of the failed specimens. Hence, even in practice, some of the failures during in-plane beam bending can occur away from the edge itself. However, it may be the case that these fracture sites are located very close to the edge. We do not know this from the source, viz. Vandebroek et al. (2014). Nonetheless, the majority of failures clearly occur at the edge when the beam is subjected to in-plane bending and it is assumed that the error involved in taking all such failures to be edge failures is small. In other words, we assume that the bending type itself is a proxy for the edge type

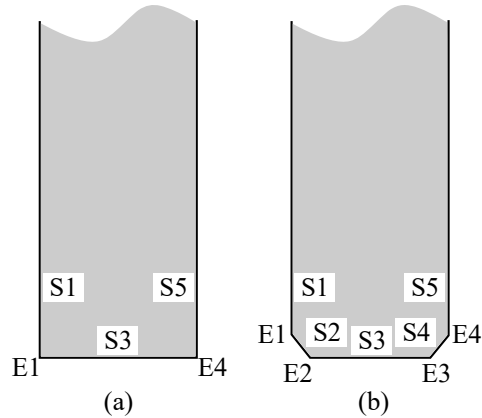


Figure 2.9: Possible fracture sites for the edge in the tension zone when a beam is tested in four-point bending with in-plane loading of the specimen. (a) cut edge, (b) ground edge.

of failure in this case. Without this assumption, it would generally not be possible to analyse the difference in condition between edge failures and surface failures in glass. This is so because the bulk of experiments that produce the results on the edge condition were performed using the four-point bending device with in-plane loading, cf. Chap. 4. Generally speaking, there was no researcher who provided a fractographic analysis of the kind that would allow us to differentiate between these types of failure origin. In fact, Vandebroek et al. (2014) proceed to examine the edge strength and to draw conclusions about e.g. edge size effects while including data results from failures that were determined as originating from the surface as per fractographic analysis. Based on this data they write that “the test results demonstrate that there is a considerable size effect for the *edge strength* of glass” (this author’s emphasis), (Vandebroek et al. 2014). Hence, the test results are considered to be edge failures whether the failure originates from one of the edge corners or from the surface near the edge in the case of in-plane loading of beams in four-point bending.

In the case of glass beams subjected to out-of-plane bending, the research shows that on average half of the failures occurred from the edge, although the results on this vary a lot between the individual experiments. In some cases over 90% of failures were from the edge while in other cases the majority were from the surface. See also Paper D.

In the case of laterally supported plates subjected to uniform out-of-plane pressure, the research shows that on average 30% of failures occur from the edge. These results are much more consistent across the experiments in spite of the fact that the boundary conditions vary significantly. In some cases the support conditions were very flexible, the glass being more or less simply supported on neoprene gaskets

(Kanabolo & Norville 1985). In other cases the glass was fixed between neoprene gaskets (Johar 1981, 1982). In yet another case the glass was firmly fixed between continuous strips of 20 mm thick nylon (Calderone 1999).

Based on the findings from experiments on glass as well as numerical studies, it can be concluded that the edge condition cannot be neglected for any real structure under practical circumstances. This is so because in practice, the structure is never supported and loaded under such extraordinary conditions like those that are produced with the double ring bending device. In practice, the glass is usually like a linearly supported plate subject to out-of-plane loading or like a slender beam or pillar element. If it is the latter, i.e. a slender beam or pillar, then it follows directly that some part of the edge is subject to significant tensile stress in the design state. If it is the former, i.e. a laterally supported plate, then the edge parts are evidently prone to fail for two reasons. First, because the experiments on laterally supported plates which comprise the results from hundreds of tests demonstrate that this is the case. Second, because finite element analyses of square plates, see e.g. Kinsella & Persson (2018a), Paper C, demonstrate that the tension near the edges can reach significant magnitudes even when the support conditions are relatively flexible, i.e. the glass is fixed between soft neoprene gaskets. When the supports are rigid, the maximum principal tensile stress on the compression side near the edges was found to be comparable to the maximum principal tensile stress at the centre point on the tension side, at moderate to high magnitudes of lateral pressure.

The production method which includes scribing, cutting and grinding operations alters the condition of the edge in glass. According to Veer & Rodichev (2011), even when the grinding is done to produce an edge that appears to be free from defects, there may still remain hidden damage. This is so because the lateral cracks that are introduced by scribing can extend so far that they are not removed entirely by grinding operations.

2.5.3 Subcritical crack growth

As was noted early on by researchers, glass subjected to stress in normal atmospheres, i.e. in environments containing water vapour, is prone to fatigue at ordinary temperatures, see Sec. 2.4. Present theories that explain glass fatigue are based on the concept of preexisting cracks that grow subcritically, i.e. at a rate much smaller than at catastrophic failure. Subcritical crack growth can be characterized by velocities of the order $\mu\text{m s}^{-1}$ to mm s^{-1} while crack velocity at rupture is of the order km s^{-1} (Lawn 1993).

Stress corrosion

Charles (1958*a*) proposed an explanation for glass fatigue based on the assumption of a pre-existing flaw that propagates subcritically until fracture. The subcritical crack growth is due to a corrosive mechanism, like a chemical attack by water vapour that is activated by crack tip stress and temperature. The chemical process was termed stress corrosion. There has been much debate over the chemical reaction that supposedly takes place at the crack tip. A brief discussion of a chemical reaction model is given in the next subsection. Charles (1958*b*) supposed that the corrosion rate conforms to an arbitrary power function of the crack tip stress, i.e.

$$v \propto \hat{\sigma}^n \quad (2.22)$$

where v denotes the corrosion rate, $\hat{\sigma}$ denotes the crack tip stress, and n is the stress corrosion parameter. The crack tip stress $\hat{\sigma}$ was estimated by Charles (1958*b*) through adoption of the Inglis (1913) solution of the stress at the tip of an elliptical flaw, Eq. (2.3). Charles (1958*b*) obtained the value $n = 16$ through analysis of experimental data results from four-point bending tests carried out on 3000 glass rods, 100 mm long and 2.5 mm in diameter, while using a dead-weight loading system. The tests were performed at various temperatures between -170 °C and 242 °C in an atmosphere at 100% relative humidity. Moreover, Charles (1958*b*) assumed the temperature dependence to be a simple Arrhenius one (Arrhenius 1889), i.e.

$$v \propto e^{\left(-\frac{1}{T}\right)} \quad (2.23)$$

where T denotes the absolute temperature.

Wiederhorn (1967) found that the corrosion rate in soda-lime-silicate glass is approximately proportional to the relative humidity, i.e.

$$v \propto \text{RH} \quad (2.24)$$

The validity of Eq. (2.24) was demonstrated using the double-cantilever cleavage arrangement in tests on microscope slide specimens into which cracks with a pre-determined length were introduced (Wiederhorn 1967).

Brown (1972) developed an equation which states that the cumulative effect of an arbitrary stress history on a given crack is constant. This equation was integrated into a theory sometimes referred to as Brown's Load Duration Theory. The works by Charles (1958*a,b*) and Wiederhorn (1967) form a basis for the understanding of the theory. Brown (1972) assumed that

$$v \propto \text{RH} e^{\left(-\frac{\hat{\sigma}}{T}\right)} \quad (2.25)$$

The dependence on stress in Eq. (2.25) was approximated by a power term. After carrying out an integration and substituting the crack tip stress for the farfield

stress, Brown (1972) obtained the following formula which is given below in original notation

$$\int_0^{t_f} \text{RH} \cdot \exp\left(-\frac{\gamma_0}{RT}\right) \left(\frac{\sigma}{T}\right)^n dt = \text{constant} \quad (2.26)$$

where γ_0 and R are constants, t_f is the time until failure, and n is the stress corrosion parameter. The right-hand side of Eq. (2.26) contains various constants including the distance traversed by the subcritically propagated crack. However, when the stress intensity is below a certain threshold limit, no stress corrosion can be observed in experiments (Wiederhorn & Tornsens 1970). With Eq. (2.26), the threshold limit value for the stress corrosion is neglected.

Consider now a given crack which has been subjected to a certain amount of stress corrosion, the corrosion being measured in terms of the distance traversed by the growing crack. If the environmental conditions are assumed to be the same, we find with Eq. (2.26) that it provides for an equivalence class of stress histories. Specifically, we derive from Eq. (2.26) that

$$\int_0^{t_{1,f}} \sigma_1^n(\tau) d\tau = \int_0^{t_{2,f}} \sigma_2^n(\tau) d\tau \quad (2.27)$$

where $(\sigma_1, t_{1,f})$ and $(\sigma_2, t_{2,f})$ correspond to a pair of stress histories and load-durations until fracture.

Eq. (2.27) has been employed by various researchers to calculate 3 s and 60 s constant stress-equivalent strength values, see e.g. Beason (1980), Mencik (1992) and Calderone (1999). It is the constant stress that when applied during 3 s or 60 s, respectively, would produce the same amount of stress corrosion assuming the environmental conditions are identical. More specifically, the t -sec constant stress-equivalent strength is

$$\sigma_{t,\text{const}} = \left(\frac{\int_0^{t_f} \sigma^n(\tau) d\tau}{t} \right)^{\frac{1}{n}} \quad (2.28)$$

For a linear stress rate $\dot{\sigma}$ at the crack tip, the stress history is given by

$$\sigma(t) = \dot{\sigma}t \quad (2.29)$$

from which it follows that the fracture stress at time t_f is

$$\sigma_f = \dot{\sigma}t_f \quad (2.30)$$

Hence,

$$\int_0^{t_f} \sigma^n(\tau) d\tau = \int_0^{t_f} (\dot{\sigma}\tau)^n d\tau = \frac{\dot{\sigma}^n t_f^{n+1}}{n+1} = \frac{\sigma_f^{n+1}}{\dot{\sigma}(n+1)} \quad (2.31)$$

where Eq. (2.30) was used in the last step. For two constant rate stress histories, $\sigma_1(t)$ and $\sigma_2(t)$, Eq. (2.31) can be rewritten

$$\frac{\sigma_{1,f}^{n+1}}{\dot{\sigma}_1} = \frac{\sigma_{2,f}^{n+1}}{\dot{\sigma}_2} \quad (2.32)$$

As a matter of fact, many experiments on glass are conducted using a load rate that produces a constant rate of stress at the location where fracture subsequently occurs. A 2 MPa s^{-1} stress rate is frequently adopted, probably because this rate is given in various standards, see e.g. EN 1288-2:2000 to EN 1288-5:2000. A convenient characterization of the strength is thus provided by the 2 MPa s^{-1} constant stress rate-equivalent strength, i.e. the strength that would have been, were the crack subjected to a constant stress rate of 2 MPa s^{-1} until failure. This choice of metric is convenient because in the case of much experimental data, 1) a test arrangement that produces a constant rate of stress is adopted and 2) it enables one to operate directly on the nominal or received values in many cases. Suppose an experiment is conducted while subjecting a glass specimen to a loading that produces a constant stress rate of $\dot{\sigma}$ at the fracture location until failure at the stress σ_f . From Eq. (2.32), we find the 2 MPa s^{-1} constant stress rate-equivalent strength to be

$$\sigma_{2,f} = \left(\frac{2}{\dot{\sigma}} \right)^{\frac{1}{1+n}} \sigma_f \quad (2.33)$$

with the stress and rate values given in units of MPa and MPa s^{-1} , respectively, and where σ_f and $\dot{\sigma}$ are the recorded fracture stress and stress rate, respectively.

Stress corrosion can be divided into four regions according to the rate of crack propagation. We consider now the logarithm of crack growth velocity as function of mode I SIF, see Fig. 2.10 for an illustration of this in the form of a graph (Freiman et al. 1985, Wiederhorn 1967, Wiederhorn & Tornsens 1970). In region I, the crack growth velocity is generally modelled with Eq. (2.22) as a basis. Region 0 denotes the domain in which no stress corrosion is observable. The threshold limit value for detectable stress corrosion is about $0.25 \text{ MPa m}^{-\frac{1}{2}}$, however, the estimates for this parameter value vary somewhat, see e.g. Freiman et al. (1985), Gehrke et al. (1991), Wiederhorn & Tornsens (1970). Regions II and III are generally not relevant for the strength design of glass structures because once the mode I SIF enters these regions, the time scale is very short and catastrophic failure is imminent (Fischer-Cripps & Collins 1995).

Based on the test results which produced the general appearance of the crack growth velocity curve as function of the mode I SIF in region I, cf. Fig. 2.10, Evans (1974) proposed the following expression for the crack growth velocity.

$$v = AK_1^n \quad (2.34)$$

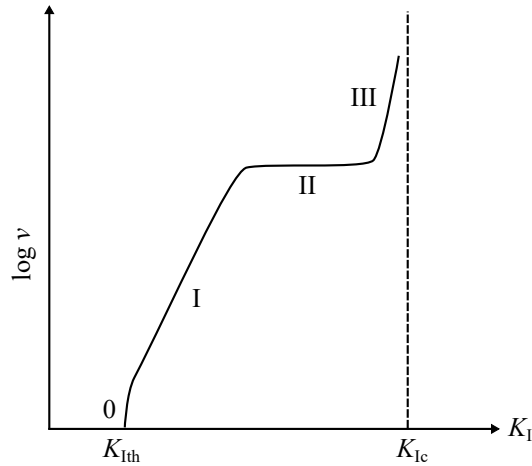


Figure 2.10: General shape of the subcritical crack growth velocity as function of mode I SIF. Adapted from Evans (1974).

Eq. (2.34) represents an empirically based approximation of the crack growth velocity which is valid for region I. In Eq. (2.34), A and n are crack growth velocity parameters and n is moreover identical to the stress corrosion parameter in Charles (1958*b*) stress corrosion theory. Eq. (2.34) can be reformulated as

$$v = v_0 \left(\frac{K_I}{K_{Ic}} \right)^n \quad (2.35)$$

The benefit of Eq. (2.35) is that the crack growth velocity parameter v_0 has the same unit as the velocity v .

Chemical reaction model

A classical explanation for the chemical reaction that takes place during stress corrosion is given by Charles & Hillig (1962). It is supposed that stress enhanced hydrolysis happens at the crack tip according to the following formula



and this represents stress corrosion in region I, cf. Fig. 2.10. Fig. 2.11 illustrates the hydrolysis near the crack tip. In region II, it is believed that the rate of stress corrosion depends strongly on the environment since it is limited by the transport of reactants to the crack tip (Le Bourhis 2008). However, no general consensus exists so far about the exact reaction that happens during stress corrosion, see e.g. Haldimann (2006) for a discussion of this.

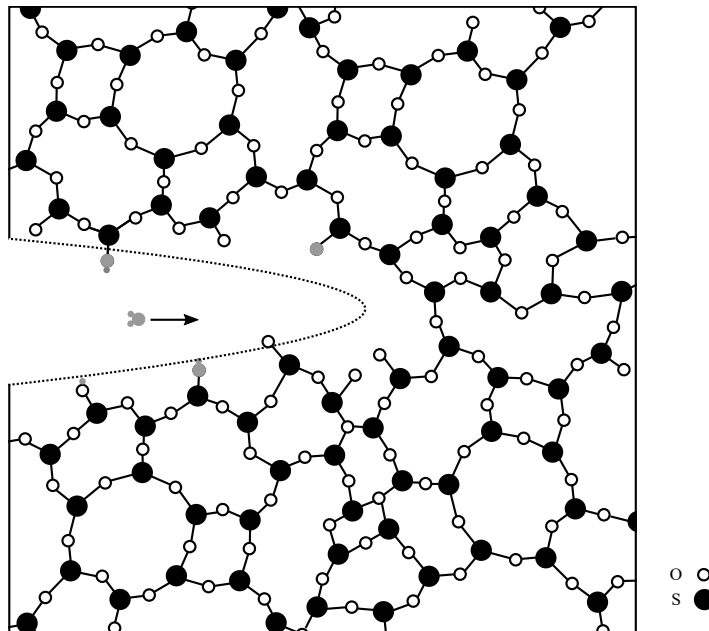


Figure 2.11: Representation of water-induced bond rupture in silica glass. Dashed line corresponds to the elliptical crack contour. Environmental water species are shown in grey colour. Adapted from Lawn (1993).

3

Calculating the strength

3.1 DEFINING THE STRENGTH

The strength of glass is a property that can only be revealed by destroying the sample specimen. Glass is much stronger in compression than in tension so that in practice, only the tensile strength is considered. One way to evaluate the strength would be to grip the specimen at two ends and pull it thus subjecting the surface to uniform stress. However, for practical reasons, this arrangement is usually avoided because of the risk that the specimen would either slip or else fail at the grips. In practice, glass plates are usually put to the test in a bending device that subjects part of the specimen to significant tensile stress. The four most common bending arrangements are detailed in Sec. 3.2 and comprise the following setups, viz. the three-point bending device, the four-point bending device, the co-axial double ring bending device, and the device that allows for four-sided laterally supported panes to be subjected to uniform pressure.

The strength is defined as the maximum principal tensile stress at the fracture location. The strength determined from a bending test is sometimes defined as the maximum tensile stress that is reached within some predefined area of the specimen, e.g. within the load span in the case of four-point bending, irrespective of whether the fracture site was contained in the same area or not. For convenience, we refer to this as the apparent strength.

For instance, in a three-point bending setup, the apparent strength is determined by the stress at the midpoint where the load is introduced, cf. Sec. 3.2. Hence, the

strength is generally smaller than the apparent strength because it is not unusual for the fracture origin to be located some distance away from the midpoint. Furthermore, there are reports in the literature of a substantial proportion of fractures occurring from outside the loading ring area in some double ring bending tests (Reid 2007). In a four-point bending test it is not unusual for fracture to occur outside the load span. In fact, not every experimenter records the fracture location. Others simply discard the data point when the fracture origin was located outside the predefined loading area. However, simply discarding observations like that is not necessarily sound practice. Speaking of the double ring bending device, Reid (2007) notes that “failure outside the loading ring is a real physical phenomenon that cannot be eliminated by any experimental technique, because it is an inescapable consequence of the spatial variability of glass strength.” In the case of laterally supported plates subjected to uniform pressure, the stress distribution is nonlinear and very much dependent on the boundary conditions, cf. e.g. Kinsella & Persson (2018a) which can also be found in Paper C. According to a recent review of the test results from hundreds of large laterally supported panes subjected to uniform pressure, it was found that none failed at the location of maximum principal tensile stress (Natividad et al. 2016).

3.1.1 Time-dependent strength

In an ordinary environment with a normal atmosphere, the strength cannot be revealed without intervening with the glass so as to alter the strength significantly. Hence, what might have been the strength at the onset of testing, the so-called inert strength, is reduced while putting the specimen to the test. Ultimately, delayed fracture might happen, e.g. when the specimen breaks under a static load that was sustained to begin with. Measurements of the strength carried out at different load rates and in different environments produce results that can differ substantially even when the test setup, specimen dimensions, and fracture location are exactly the same.

In order for the strength to be well defined in the time domain, there exist alternative routes. One way is to employ a purely empirical model for the effect of glass fatigue to enable a comparison of strength measurements made at different load-histories. As an example of this we have the universal static fatigue curve of Mould & Southwick (1959) who carried out experiments on glass rods subjected to static loads, see also Varshneya (1994)

$$\frac{\sigma}{\sigma_N} = -A \log \left(\frac{t}{t_{0.5}} \right) + B \quad (3.1)$$

In Eq. (3.1) which is valid in the linear portion in the plot of the time to fracture, σ_N is the strength of pristine glass rods immersed in liquid nitrogen, B is a term dependent on the manner of abrasion of the rod while using different grits, $\log t_{0.5}$

is the time corresponding to $\sigma/\sigma_N = 0.5$ and A is the slope in the plots, the slopes of which were found to be approximately the same according to the experiment in Mould & Southwick (1959).

Another way to account for glass fatigue is to adopt the theory of stress corrosion and employ the logical model that follows, i.e. a crack growth velocity described by an Arrhenius process that is stress and temperature-activated. This is frequently done by various researchers at present. As a consequence, the following technique is established. The measured strength is transformed into the 3 second or 60 second-equivalent constant stress. This transformation enables the comparison of test results carried out at different load-rates and with different load-durations, as was shown in Sec. 2.5.3. In the remainder of this section however, it is explained how to calculate the strength without consideration of glass fatigue.

3.2 TEST DEVICES

In the following, four bending devices are considered, viz. the three-point bending device, the four-point bending device, the co-axial double ring bending device, and the device that allows for four-sided laterally supported panes to be subjected to uniform lateral pressure. These are the most common devices employed to measure the strength of float glass panes for use in structures. A schematic view of the three-point bending arrangement is given in Fig. 3.1 where l denotes the distance between the supports. A schematic of the four-point bending arrangement is shown in Fig. 3.2 where l_1 denotes the distance between the inner loads and outer supports. Fig. 3.3 shows a schematic of the double ring bending arrangement which uses two opposing coaxial rings of unequal diameters, one loading ring and one reaction ring. The test specimen is positioned between the rings and a load is transmitted through the smaller concentric loading ring. r_0 and r_1 denote the radii of the inner and outer rings, respectively. Fig. 3.4 illustrates the general test arrangement for the application of uniform pressure to laterally supported plates. The boundary conditions vary substantially between experiments with laterally supported plates subjected to uniform pressure. The rigidity in the supports varies depending on the gasket material in use and the clamping force applied along the edges as well as the stiffness of the surrounding frame.

3.3 CALCULATION METHODS

The methods employed by various researchers and experimenters to calculate the strength comprise the following, viz. analytical formulae, the finite element method, and interpolations and extrapolations from strain gauge measurements. Sometimes, these methods are used in combination.

3.3.1 Analytical methods

The bending strength can be determined according to the Bernoulli beam bending theory

$$\sigma_f = \frac{M}{W} \quad (3.2)$$

where M is the maximum bending moment and W is the section modulus of the specimen, see e.g. Mencik (1992). The contribution of self-weight is neglected. While using Eq. (3.2), it is assumed that the cross-sections remain even and perpendicular to the deflected axis of the bent beam. For a rectangular cross-section

$$W = \frac{bh^2}{6} \quad (3.3)$$

where b denotes the cross-sectional width and h the height. In Eq. (3.3), it is assumed that bending takes place around an axis parallel to the cross-sectional width. The largest bending moment in three-point bending is $Fl/4$ with F the fracture load, cf. Fig. 3.1. With Eq. (3.2) and (3.3) the bending strength is determined as

$$\sigma_f = \frac{3Fl}{2bh^2} \quad (3.4)$$

The largest bending moment in four-point bending is $Fl_1/2$, cf. Fig 3.2. The bending strength in four-point bending is similarly found to be

$$\sigma_f = 3\frac{Fl_1}{bh^2} \quad (3.5)$$

In the double ring bending setup, a uniform biaxial tensile stress is produced in the surface of the sample plate within the loading ring area. The stresses on the tensile surface of the specimen have radial and circumferential components, σ_r and σ_θ , and are given by a set of approximate analytical solutions (Kirstein & Woolley 1967). The uniform biaxial stress within the loading ring area is

$$\sigma_r = \sigma_\theta = \frac{3F}{2\pi b^2} \left((1 + \nu) \ln \frac{r_1}{r_0} + (1 - \nu) \frac{r_1^2 - r_0^2}{2r_2^2} \right), \quad r \leq r_0 \quad (3.6)$$

where r_2 is the equivalent outer radius used for a square shaped specimen with side length $2L$, viz.

$$r_2 = L(1 + \sqrt{2}) \quad (3.7)$$

The radial stress outside the loading ring area at the distance r from the centre point is

$$\sigma_r = \frac{3F}{2\pi b^2} \left((1 + \nu) \ln \frac{r_1}{r} + (1 - \nu) \frac{r_0^2(r_1^2 - r^2)}{2r^2 r_2^2} \right), \quad r > r_0 \quad (3.8)$$

while the circumferential stress is

$$\sigma_\theta = \frac{3F}{2\pi b^2} \left((1 + \nu) \ln \frac{r_1}{r} - (1 - \nu) \frac{r_0^2(r_1^2 + r^2)}{2r^2 r_2^2} + 2(1 - \nu) \frac{r_1^2}{r_2^2} \right), \quad r > r_0 \quad (3.9)$$

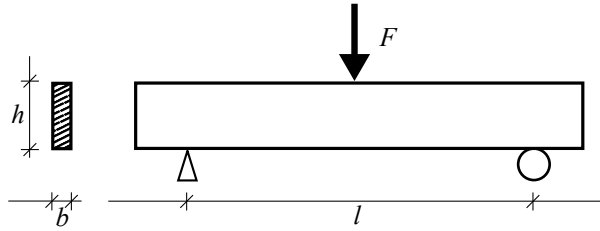


Figure 3.1: Three-point bending test setup.

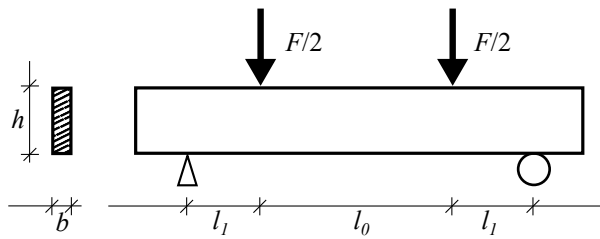


Figure 3.2: Four-point bending test setup.

In the case of laterally supported plates subjected to uniform pressure, cf. Fig. 3.4, analytical formulae based on plate equations are not generally used. The reason for this is the difficulty to accurately determine the stresses at some arbitrary point on the plate surface while employing approximate solutions due to nonlinearities and elastic boundary conditions. However, simplified formulae for the determination of the maximum principal tensile stress at the plate centre point are sometimes given in standards, see e.g. the prEN 16612:2017.

3.3.2 Numerical solutions

In Blank et al. (1994), the stress distribution in slender glass beams subjected to out-of-plane four-point bending was analyzed using the finite element method with nonlinear shell theory and comparisons were made with the Bernoulli beam theory. In practice, deviations from the Bernoulli beam theory can be expected due to the emergence of shear forces and membrane stresses as the deflections exceed about half the specimen thickness. In such case, the cross-sections initially perpendicular to the longitudinal axis start to curve and the stresses get biaxial, see Fig. 3.5. There no longer exists a linear relationship between bending force, stress, strain and deflection. The conclusion from Blank et al. (1994) who investigated thicknesses of 3, 4, 5, 6, 8, 10, 12, 15, and 19 mm, was that the Bernoulli beam bending theory is sufficient for practical requirements. However, the beam theory

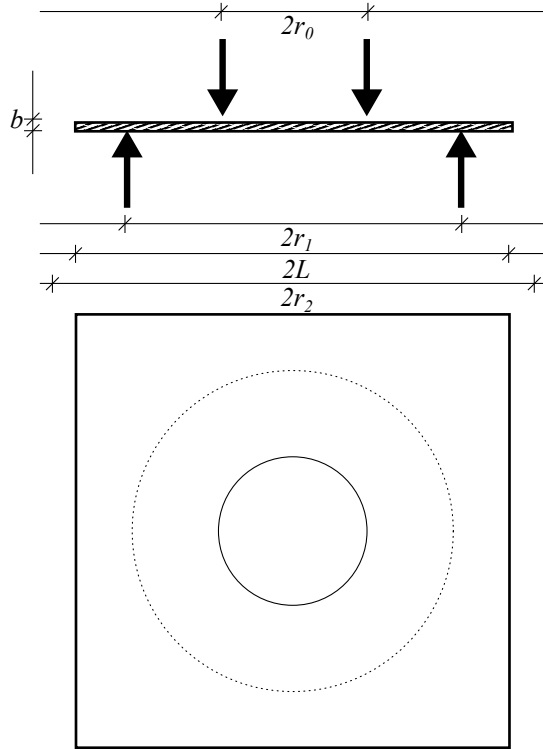


Figure 3.3: Co-axial double ring bending test setup.

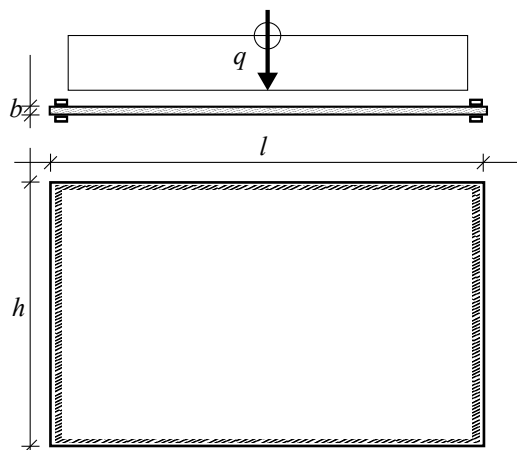


Figure 3.4: Laterally supported plate subjected to uniform lateral pressure.

underestimates the true edge stress, the deviation of which can amount to 11% depending on the centre deflection and plate thickness.

The stresses in laterally supported plates subjected to double ring bending or uniform pressure can be accurately calculated with the finite element (FE) method, see e.g. Haldimann (2006). The general problem of determining the stresses at an arbitrary location on the surface of a laterally supported plate which is subjected to uniform loading does not have a tractable solution when using analytical formulae except for some elementary cases with special boundary conditions. With the finite element method, approximate solutions are obtained to partial differential equations that arise in the modelling of structures. However, the solutions are highly dependent on the boundary conditions.

Equations of motion

Here follows an outline of the differential equations of motion with respect to the current or spatial configuration. The presentation follows the format found in Holzapfel (2000). A continuum body in Euclidian space is considered. The body contains a set of particles that occupy an arbitrary region Ω with boundary surface $\partial\Omega$ at time t . The spatial mass density is ρ . Suppose a motion that generates a spatial displacement field \mathbf{u} . We adopt the balance of linear momentum according to the generalized form of Newton's principles of motion, i.e.

$$\frac{D}{Dt} \int_{\Omega} \rho \dot{\mathbf{u}} dv = \mathbf{F}(t) \quad (3.10)$$

where we assume that the structure of forces, $\mathbf{F}(t)$, acting on the body are such that they can be separated into traction and body forces, respectively, i.e.

$$\mathbf{F}(t) = \int_{\partial\Omega} \mathbf{t} ds + \int_{\Omega} \mathbf{b} dv \quad (3.11)$$

where \mathbf{t} is the Cauchy traction vector and $\mathbf{b} = \rho \mathbf{g}$ with \mathbf{g} the constant gravitational acceleration. It is supposed that there exists a spatial tensor field $\boldsymbol{\sigma}$ with the property that $\mathbf{t} = \boldsymbol{\sigma} \mathbf{n}$ where \mathbf{n} is an outward normal vector of unit length to the surface. It can be shown that $\boldsymbol{\sigma}$ is symmetric. Cauchy's first equation of motion is derived from Eq. (3.10) and (3.11) while applying Cauchy's stress theorem and Gauss' divergence theorem, i.e.

$$\int_{\Omega} (\text{div} \boldsymbol{\sigma} + \mathbf{b} - \rho \ddot{\mathbf{u}}) dv = \mathbf{0} \quad (3.12)$$

Since Eq. (3.12) holds for any volume v , we deduce

$$\text{div} \boldsymbol{\sigma} + \mathbf{b} = \rho \ddot{\mathbf{u}} \quad (3.13)$$

which is the strong form of the equation of motion. Providing that the problem is static, we have the boundary conditions

$$\begin{cases} \mathbf{u} = \bar{\mathbf{u}} & \text{on } \partial\Omega_u \\ \mathbf{t} = \bar{\mathbf{t}} & \text{on } \partial\Omega_\sigma \end{cases} \quad (3.14)$$

where displacement $\bar{\mathbf{u}}$ and load $\bar{\mathbf{t}}$ are prescribed functions on the boundary.

The strong form, Eq. (3.13), contains functions whose derivatives might not be defined. We develop the weak form while noting that functions have well-defined integrals even when the derivative is undefined thus allowing for us to access the underlying solution. An arbitrary test function \mathbf{v} is introduced with the property that $\mathbf{v} = \mathbf{0}$ on the boundary surface $\partial\Omega$. The test function represents a virtual displacement field on the current configuration. After multiplication by \mathbf{v} , integration over Ω , and application of Gauss' divergence theorem, it can be shown that

$$\int_{\Omega} (\boldsymbol{\sigma} : \text{grad} \mathbf{v} + \rho \ddot{\mathbf{u}} \cdot \mathbf{v}) dv = \int_{\Omega} \mathbf{b} \cdot \mathbf{v} dv + \int_{\partial\Omega} \mathbf{t} \cdot \mathbf{v} ds \quad (3.15)$$

Eq. (3.15) is the weak form with the natural and essential boundary conditions, respectively, which for the case of a static problem are the same as in Eq. (3.14). Henceforth, a quasi-static condition is assumed which implies that the second term vanishes in Eq. (3.15).

Finite Element Method

The finite element formulation is based on the weak form of the equation of motion, Eq. (3.15), and Galerkin's method (Ottosen & Petersson 1992). In the following, we use matrix notation so that the stress tensor in Sec. 3.3.2 is understood to be

$$\boldsymbol{\sigma} = \begin{bmatrix} \sigma_{xx} \\ \sigma_{yy} \\ \sigma_{zz} \\ \tau_{xy} \\ \tau_{xz} \\ \tau_{yz} \end{bmatrix} \quad (3.16)$$

and the vector differential operator is

$$\nabla = \begin{bmatrix} \frac{\partial}{\partial x} & 0 & 0 \\ 0 & \frac{\partial}{\partial y} & 0 \\ 0 & 0 & \frac{\partial}{\partial z} \\ \frac{\partial}{\partial y} & \frac{\partial}{\partial x} & 0 \\ \frac{\partial}{\partial z} & 0 & \frac{\partial}{\partial x} \\ 0 & \frac{\partial}{\partial z} & \frac{\partial}{\partial y} \end{bmatrix} \quad (3.17)$$

The independent displacement vector field \mathbf{u} is discretized at the nodes in a finite element mesh and a shape function is associated with each unique node. The displacement field is approximated throughout the body by

$$\mathbf{u} = \mathbf{N}\mathbf{a} \quad (3.18)$$

where \mathbf{N} is a matrix that represents a global shape function. The vector \mathbf{a} represents the nodal displacements and is a vector of size equal to the total number of degrees of freedom. Following Galerkin's method, test functions are selected according to

$$\mathbf{v} = \mathbf{N}\mathbf{c} \quad (3.19)$$

where \mathbf{c} is an arbitrary constant vector. Combining Eq. (3.18) and (3.19) with Eq. (3.15) yields

$$\int_{\Omega} \mathbf{c}^{\top} (\nabla \mathbf{N})^{\top} \boldsymbol{\sigma} dv = \int_{\partial\Omega} \mathbf{c}^{\top} \mathbf{N}^{\top} \mathbf{t} ds + \int_{\Omega} \mathbf{c}^{\top} \mathbf{N}^{\top} \mathbf{b} dv \quad (3.20)$$

which can be simplified to

$$\int_{\Omega} (\nabla \mathbf{N})^{\top} \boldsymbol{\sigma} dv = \int_{\partial\Omega} \mathbf{N}^{\top} \mathbf{t} ds + \int_{\Omega} \mathbf{N}^{\top} \mathbf{b} dv \quad (3.21)$$

since \mathbf{c} is arbitrary and constant. In the special case of a linear elastic material we derive from Eq. (3.18) while assuming $\boldsymbol{\sigma} = \mathbf{D}\nabla\mathbf{u}$ that

$$\int_{\Omega} (\nabla \mathbf{N})^{\top} \mathbf{D}(\nabla \mathbf{N})\mathbf{a} dv = \int_{\partial\Omega} \mathbf{N}^{\top} \mathbf{t} ds + \int_{\Omega} \mathbf{N}^{\top} \mathbf{b} dv \quad (3.22)$$

Eq. (3.22) can be rewritten in a compact form as

$$\mathbf{K}\mathbf{a} = \mathbf{f}_l + \mathbf{f}_b \quad (3.23)$$

with

$$\mathbf{K} = \int_{\Omega} (\nabla \mathbf{N})^{\top} \mathbf{D}(\nabla \mathbf{N}) dv \quad (3.24)$$

$$\mathbf{f}_l = \int_{\Omega} \mathbf{N}^{\top} \mathbf{b} dv \quad (3.25)$$

$$\mathbf{f}_b = \int_{\partial\Omega} \mathbf{N}^{\top} \mathbf{t} ds \quad (3.26)$$

where \mathbf{K} represents the stiffness matrix, \mathbf{f}_l is the body force vector, and \mathbf{f}_b is the boundary force vector. Also, the essential boundary conditions must be specified in the nodes.

The assumption of material linear elasticity is insufficient for the modelling of non-linearly elastic and viscoelastic materials such as are present in e.g. the interlayers in laminated glass and in certain types of gasket in laterally supported plates. For a further treatment of hyperelastic material modelling the reader is referred to Holzapfel (2000).

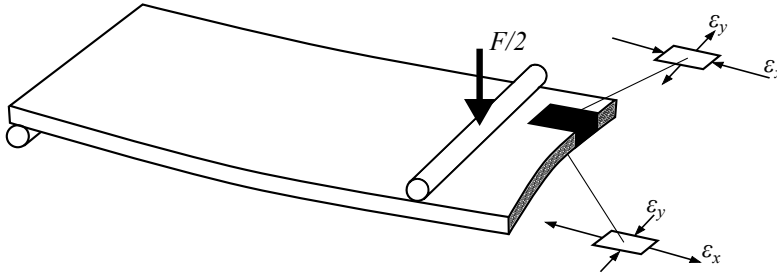


Figure 3.5: Cross-section of a specimen under four-point bending where the double curvature is indicated. Adapted from Blank et al. (1994).

3.3.3 Combination of methods

In practice a combination of calculation methods is sometimes employed. As an example of this we take Vandebroek et al. (2014) who calculates the stress due to four-point bending based on Eq. (3.5). The beam is subdivided into 10 equal bins along the longitudinal axis. The stress values in the bins closest to the load introduction points are corrected based on calculations with the FEM. This is done in order to obtain a more accurate measure of the stress concentration that occurs due to nonlinearities at the load introduction points. Blank et al. (1994) recommends to use a weighted mean value to take into account the variations in stress in the transversal direction due to double curvature of the bent beam, cf. Fig. 3.5.

4

Measuring and portraying the strength

4.1 INTRODUCTION

In the year 1990, Dalglish & Taylor (1990) wrote that “[t]est results available from around the world refer to about 5000 panes broken in total.” The tests in reference were not exclusively performed on the float type of glass. Moreover, some experiments involved glass panes which were submerged in water while testing. About 500 of the tests in reference were on weathered glass, i.e. glass exposed to service conditions in buildings. Additionally, all test results were not such that a value for the fracture stress could be given. In many cases, only a fracture load or fracture pressure was available. In the case of laterally supported plates subjected to lateral loading, a fracture load does not easily translate into a value for the fracture stress, even when the precise fracture origin is known. For all these reasons, most of the tests mentioned by Dalglish & Taylor (1990) are not directly useful for an estimation of the fracture stress of new annealed float glass tested in ambient conditions.

There is no up-to-date record of the test results available for the strength of glass panes. However, a survey (Kinsella 2018) was carried out of the experimental data on the strength of annealed float glass panes in the as-received condition which were tested in an ambient environment, see also Paper D. Tab. 4.1 contains a list of references for tests that record the bending strength of new annealed float glass

tested in ambient conditions which were carried out over the past four decades. The sources consist of journal articles, dissertations, and conference proceedings. The list of references in Tab. 4.1 is not exhaustive, however. The tests involve either the three-point or four-point bending device, or the co-axial double ring bending device, or the setup that allows for a uniform pressure to be applied to a laterally supported plate.

Many of the tests were conducted using a loading device that generated a constant stress rate at the fracture location. These tests which are interesting for the sake of performing a normalization of the fracture stress using Brown's (1972) Load Duration Theory, are further identified in Tab. 4.1.

The fracture stress may depend on a range of factors. With the data recorded in the experiments which are cited in Tab. 4.1, it is possible to analyze the strength as function of the edge processing, the edge thickness, the surface area under tension, the glass supplier, the stress rate, the bending mode, and the individual experimenter. It is moreover possible to consider potential interaction effects between certain factors.

4.2 PROBABILITY THEORY AND METHODS OF STATISTICAL INFERENCE

This section provides some of the background to the theories of probability and statistical inference and it is based on the textbook presentations by Gut (1995) and Young & Smith (2005). In probability theory, one assumes a sample space, Ω , which contains the set of elementary events ω . For any collection of such events, A , its probability is defined, $P(A)$, so that it satisfies the three Kolmogorov axioms. The first axiom states that $P(A) \geq 0$ while the second axiom states that $P(\Omega) = 1$. The third axiom states that for any countable collection of pairwise disjoint events

$$P\left(\bigcup_{i=1}^{\infty} A_i\right) = \sum_{i=1}^{\infty} P(A_i) \quad (4.1)$$

where A_i are the events.

A random variable X is a function from the probability space to the real numbers

$$X : \Omega \rightarrow \mathbb{R} \quad (4.2)$$

The collection of events in the sample space are induced by the random variable in the sense that

$$P(X = x) = P(\{x : X(w) = x\}) \quad (4.3)$$

Table 4.1: List of references that contain the strength of new monolithic annealed float glass tested in ambient conditions. ULP=Plate bending due to uniform lateral pressure, CDR=Co-axial double ring bending, 4PB=Four-point bending, 3PB=Three-point bending.

Reference	No. of samples	No. of observations	Bending mode	Const. stress rate
Johar (1981)	9	78	ULP	No
Johar (1982)	5	106	ULP	No
Simiu et al. (1984)	2	85	CDR	Yes
Carre (1996)	5	81	4PB	Yes
Calderone (1999)	32	195	ULP	No
Hess (2000)	3	15	4PB	No
Fink (2000)	2	127	CDR	Yes
Haldimann (2006)	2	20	CDR	Yes
Veer et al. (2006)	3	32	4PB	Yes
Sglavo et al. (2007)	8	115	3PB	Yes
Veer et al. (2009)	2	54	4PB	Yes
Postigo (2010)*	1	41	CDR	Yes
Veer & Rodichev (2011)	2	177	4PB	Yes
Veer & Rodichev (2012)	2	60	4PB	Yes
Vandebroek et al. (2012)	4	77	4PB	Yes
Lindqvist (2013)	32	478	4PB	Yes
Vandebroek et al. (2014)	8	202	4PB	Yes
Kozłowski (2014)	1	6	4PB	Yes
Kleuderlein et al. (2014)	33	830	4PB	Yes
Schula (2015)	1	15	CDR	Yes
Kinsella & Persson (2016)	2	58	4PB	Yes
Muniz-Calvente et al. (2016)	2	73	CDR 4PB	Yes
Navarrete et al. (2016)	8	69	CDR	Yes
Yankelevsky et al. (2017)	1	56	4PB	Yes
Osnes, Hopperstad & Børvik (2018)	3	93	4PB	Yes
Total:	173	3143		

* Obtained from Huerta et al. (2011)

The cumulative distribution function (CDF) F_X provides a complete description of a random variable and it is defined by

$$F_X(x) = P(X \leq x) \quad \text{for } x \in \mathbb{R} \quad (4.4)$$

For a discrete distribution the probability function, p_X , is defined by

$$p_X(x) = P(X = x) \quad \text{for } x \in \mathbb{Z} \quad (4.5)$$

For a continuous distribution the density function, f_X , has the property that

$$F_X(x) = \int_{-\infty}^x f(y)dy \quad \text{for } x \in \mathbb{R} \quad (4.6)$$

A random variable can be characterized by its moments. The k th moment, m_k , is defined by

$$m_k = \begin{cases} \sum x_i^k p_X(x_i) & \text{if } X \text{ is discrete} \\ \int_{\mathbb{R}} x^k f_X(x) dx & \text{if } X \text{ is continuous} \end{cases} \quad (4.7)$$

provided that the sum or integral is absolutely convergent. The first moment is the mean denoted by $E(X)$, i.e. the expected value. The variance, $Var(X)$, is a measure of dispersion

$$Var(X) = \begin{cases} \sum (x_k - E(X))^2 p_X(x_k) & \text{if } X \text{ is discrete} \\ \int_{\mathbb{R}} (x - E(X))^2 f_X(x) dx & \text{if } X \text{ is continuous} \end{cases} \quad (4.8)$$

In statistical inference, the objective is to draw conclusions of the underlying distribution of a random variable X on the basis of its observed value x . Typically, we have a number of n observations so that the data has the form $\mathbf{x} = (x_1, \dots, x_n) \in \mathbb{R}^n$. In a parametric model, the distribution of X is of known analytic form, but involves a finite number, d , of real unknown parameters $\boldsymbol{\theta} = (\theta_1, \theta_2, \dots, \theta_d)$. The parameter space is defined by the region $\Theta \subseteq \mathbb{R}^d$ of possible values of $\boldsymbol{\theta}$.

In a hypothesis test, we consider

$$H_0 : \boldsymbol{\theta} \in \Theta_0 \quad \text{versus} \quad H_1 : \boldsymbol{\theta} \in \Theta_1 \quad (4.9)$$

where Θ_0 and Θ_1 are two disjoint subsets of Θ that possibly, but not necessarily, satisfy the condition that $\Theta_0 \cup \Theta_1 = \Theta$. The unknown parameter value $\boldsymbol{\theta}$ is the quantity we wish to make inference about. According to the likelihood principle, the general problem of inference for $\boldsymbol{\theta}$ is solved by examining the likelihood function, $L(\boldsymbol{\theta})$. In the case when $\mathbf{X} = (X_1, X_2, \dots, X_n)$ is an independent identically distributed sample, and after observing \mathbf{x} , the likelihood function is defined by

$$L(\boldsymbol{\theta}) = \prod_i f(x_i, \boldsymbol{\theta}) \quad (4.10)$$

In Eq. (4.10), $L(\boldsymbol{\theta})$ is viewed as a function of $\boldsymbol{\theta}$ for the fixed value \mathbf{x} . The maximum likelihood estimate, $\hat{\boldsymbol{\theta}}(\mathbf{x})$, is defined to be the value of $\boldsymbol{\theta}$ that maximizes the likelihood function.

When parametric models are applied to find solutions to real-world problems, the question arises if this distribution adequately fits the sampled data. It is a matter of determining the potential of a statistical model. A goodness-of-fit test is one way of measuring the potential. The general test of fit is a test of the null-hypothesis

$$H_0 : \text{A random sample of } n \text{ observations of } X \text{ comes from } F_0(x, \boldsymbol{\theta}) \quad (4.11)$$

where $F_0(x, \boldsymbol{\theta})$ is the hypothetical distribution under consideration.

Next, we consider tests based on the empirical cumulative density function. The empirical cumulative density function (EDF) is a step function that estimates the CDF that generated the observed data points. Suppose we have a random sample X_1, \dots, X_n drawn from a distribution with CDF F_X . The EDF is defined by

$$\hat{F}_n(x) = \begin{cases} 0 & \text{for } x < X_{(1)} \\ \frac{i}{n} & \text{for } X_{(i)} \leq x < X_{(i+1)}, i = 1, \dots, n-1 \\ 1 & \text{for } x \geq X_{(n)} \end{cases} \quad (4.12)$$

where $X_{(i)}$ denotes the i th order statistic. An EDF statistic measures the discrepancy between the EDF and a hypothetical distribution. A classic EDF statistic is the Kolmogorov-Smirnov statistic defined by

$$D = \sup_x \left\{ |\hat{F}_n(x) - F_0(x, \boldsymbol{\theta})| \right\} \quad (4.13)$$

and it measures the largest vertical difference between $\hat{F}_n(x)$ and $F_0(x, \boldsymbol{\theta})$. A generally superior set of EDF statistics are based on the class of quadratic statistics of the form (D'Agostino & Stephens 1986)

$$Q = n \int_{\mathbb{R}} \left(\hat{F}_n(x) - F_0(x, \boldsymbol{\theta}) \right)^2 \omega(x) dF_0(x, \boldsymbol{\theta}) \quad (4.14)$$

where $\omega(x)$ is a weight function. The Anderson-Darling (Anderson & Darling 1952) statistic is obtained by choosing

$$\omega(x) = (F_0(x, \boldsymbol{\theta})(1 - F_0(x, \boldsymbol{\theta})))^{-1} \quad (4.15)$$

For a further description of some of the ways to visualize statistics, see Paper D.

4.3 STATISTICAL OUTLIERS

While analyzing the individual sources that were listed in Tab. 4.1 and after making comparisons, three data samples emerged which may be considered as statistical outliers for reasons as follow. The three samples provided by Overend (2002) give exceptionally high values for the bending strength of annealed glass. The tests were carried out using the co-axial double ring bending device. A comparison of all experiments using the same bending device is given in Fig. 4.1 in the form of a boxplot. For an explanation of the boxplot including the meaning of the box, whiskers, and symbols, see Paper D. The specimen thickness and test rig setup in Overend (2002) is very similar to e.g. Simiu et al. (1984) and more or less identical to Haldimann (2006). Both Overend (2002) and Haldimann (2006) conducted a

series of 10 tests on 6 mm thick plates with loading and reaction ring diameters of 51 mm and 127 mm. The failure loads reported in both references are similar in range (about 2-10 kN) except for a single outlier at 17 kN in Overend (2002). However, the recorded values for the deflection at fracture at the centre point differ significantly between the sources, as though the specimens in Overend (2002) were much less stiff for some reason. This might indicate an error in the measurements by Overend (2002) since the recorded stiffness of glass is low. Seeing as the data in Haldimann (2006) appears to agree generally with the rest of the available data, cf. Fig. 4.1, it was decided to exclude from the analysis the data in Overend (2002).

4.4 ANALYSIS

The strength of monolithic panes of annealed float glass which are tested in ambient conditions scatters much. The overall strength ranges from a little under 20 MPa to well over 200 MPa. The strength may be separated according to the type of bending device employed, cf. Fig. 4.2a. The strength in co-axial double ring bending appears to be higher than in other types of bending. However, this effect may not be statistically significant because it depends on a range of factors as was already mentioned in Sec. 4.1. The value for the fracture stress may be further analyzed with respect to the fracture origin type, i.e. edge or surface, cf. Fig. 4.2b. The values included in Fig. 4.2b correspond to results that could be determined uniquely as edge failures or surface failures, respectively. In the case of laterally supported plates subjected to out-of-plane pressure, this means that there was no ambiguity involved in the detection of the fracture origin mode. Sometimes, there was a potential fracture origin at the edge and another one on the surface simultaneously (Calderone 1999, Johar 1981, 1982). In the case of three and four-point bending tests subjected to out-of-plane bending, this means that the edge and surface failure origins were determined by the author who recorded these by fractographic analysis. If no such fractographic analysis was performed, then the test results were not included in Fig. 4.2b. In the case of three and four-point bending tests subjected to in-plane bending, this means that it was assumed that all failures originated from the edge. In the latter case, this is a simplifying assumption because according to one study (Vandebroek et al. 2014), the fractographic analyses of the beam specimens that failed due to in-plane loading revealed that in some cases the fracture origin was located at one of the main surfaces. See Sec. 2.5.2 for a further discussion of this including details from the experiment conducted by Vandebroek et al. (2014). In summary then, the extreme values do not necessarily agree between the two boxplots in Fig. 4.2. It appears at first sight as though the surface strength is greater than the edge strength. Again, however, this effect may not be statistically significant due to the potentially confounding effect of the various factors that are known to influence the recorded strength.

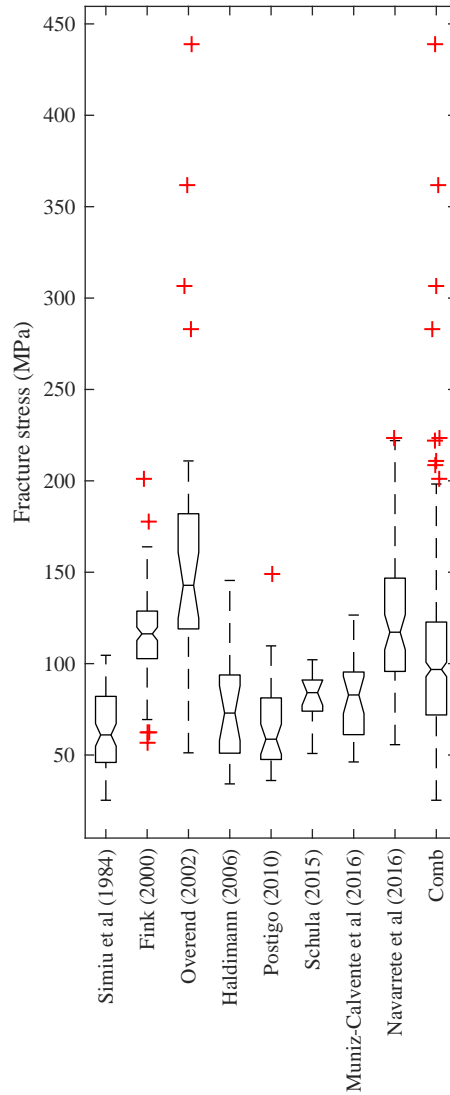


Figure 4.1: Boxplot of the strength of annealed float glass in tests using the CDR bending device. The data in Postigo (2010) was obtained from Huerta et al. (2011). Comb=Combined data set.

Detailed information about each experiment in Tab. 4.1 including an overview of each sample is given in Kinsella (2018) which can be found in Paper D. In those cases where the stress rate was constant, the fracture stress was normalized using Brown's (1972) Load Duration Theory. Most data samples were fitted by this author to a normal, lognormal, and Weibull distribution and the probability plots are available in Paper D. In these plots, the data points that correspond to edge failures are identified with solid marks. In some cases, however, it was not recorded if the failure occurred at the edge or on the surface. Moreover, some data samples were too small to admit a fitting to a standard distribution.

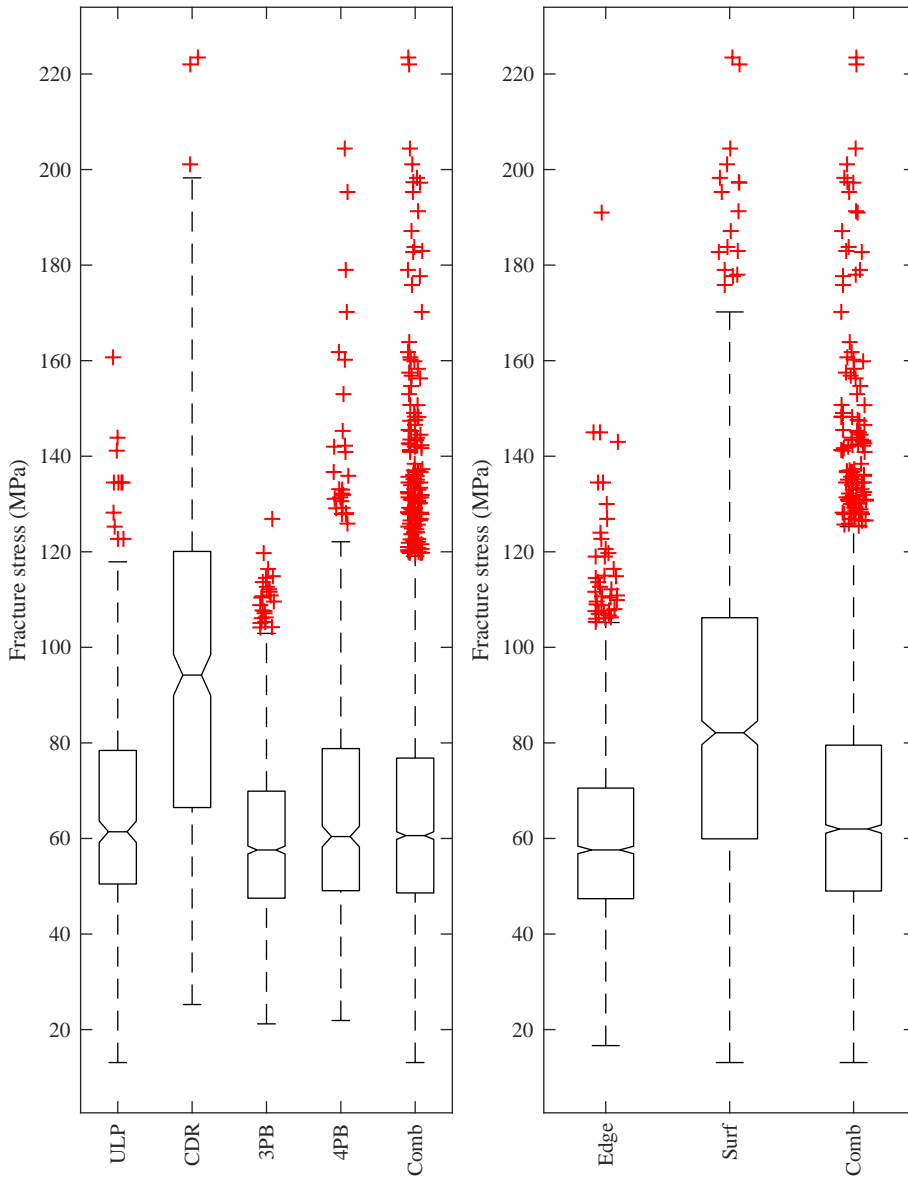


Figure 4.2: On the left: Boxplot of the strength of annealed float glass in tests divided according to the type of bending device employed. To the right: Boxplot of the strength of annealed float glass in tests separated according to the recorded type of fracture origin. Comb=Combined data set.

5

Strength prediction models and design rules

Glass strength prediction models are numerous. A subset of the models are selected and reviewed in the following. Tab. 5.1 provides a summary of the selection. The models were selected either because 1) they were specifically devised with structural glass engineering in mind, or 2) because they are representative of a range of similar models, the similarity having to do with fundamental assumptions such as the way of representing individual flaws, or 3) they were influential and became well-established. However, the review does not claim to be comprehensive. In fact, there is no exhaustive and comprehensive overview of glass failure prediction models that is up to date. Nevertheless, the following references do provide a useful background, viz. Haldimann (2006), Lamon (2016), Rinne (2009). Haldimann (2006) provides some of the references to the strength models and moreover performs a comparative analysis of the European and North American structural standards. Lamon (2016) examines strength models for application on brittle materials in general and considers statistical-probabilistic theories based on flaw size density as well as flaw strength density. Following Lamon (2016), a distinction can be made between models that are fundamentally based on the existence of flaws which determine the strength in glass on one hand, and on the other hand models that take a macroscopic or phenomenological approach to glass strength. Rinne (2009) provides an in-depth treatment of the Weibull distribution.

In the sections that follow, the original notation is adopted so far as possible for the sake of transparency and simplicity. In structural standards generally, the strength

Table 5.1: Overview of glass strength prediction models selected for the review. GFPM=Glass Failure Prediction Model of Beason (1980) and Beason & Morgan (1984)

Flaw-based approach (microscopic)	Phenomenological (macroscopic)
Matthews et al. (1976)	Normal distribution
Batdorf & Crose (1974)	Lognormal distribution
Weibull distribution	(Weibull distribution)
De Jayatilaka & Trustrum (1977)	GFPM
Gumbel distribution	
Haldimann (2006)	
Yankelevsky (2014)	
Kinsella & Persson (2018b)	

model is implemented and applied according to some design philosophy to come up with a set of design rules.

5.1 STRENGTH MODELS

5.1.1 Normal and lognormal distributions

The normal distribution was employed early in e.g. Pilkington design charts assuming a coefficient of variation of 0.20 (Calderone 1999). A number of researchers have recently either recommended to base failure predictions for glass on the normal or lognormal distributions or else called into question the superiority of the Weibull distribution over the normal and lognormal distributions (Calderone et al. 2001, Huerta et al. 2011, Kinsella & Persson 2016, Lü 1997, Veer et al. 2009). The normal distribution has the probability density function (Forbes et al. 2011)

$$f(x) = \frac{1}{\sqrt{2\pi\sigma^2}} e^{-\frac{(x-\mu)^2}{2\sigma^2}} \quad (5.1)$$

where μ and σ^2 refer to the mean and variance, respectively. If Y denotes a normally distributed random variable, then

$$X = e^Y \quad (5.2)$$

is lognormally distributed with the probability density function

$$f(x) = \frac{1}{x\sqrt{2\pi\sigma^2}} e^{-\frac{(\ln x - \mu)^2}{2\sigma^2}} \quad (5.3)$$

In Eq. (5.3), μ and σ^2 refer to the mean and variance of the corresponding normal distribution, Eq. (5.1).

The use of a normal distribution as a standard model for data is due to the Central Limit Theorem (Beirlant et al. 2004) which states that averages of many samples will tend to follow a normal distribution. By the same token, the lognormal distribution would be a natural model for geometric means.

5.1.2 Gumbel distribution

The Gumbel extreme value distribution in the form of Eq. (5.4) is associated with the minimum value among a large set of independent and identically distributed random variables. The Gumbel distribution is the limiting distribution in the case of sampling distributions which decay exponentially (Forbes et al. 2011). The density function is

$$f(x) = \frac{1}{b} \exp\left(\frac{x-a}{b}\right) \exp\left(-\exp\left(\frac{x-a}{b}\right)\right) \quad (5.4)$$

where a and b signify the location and scale parameters, respectively.

5.1.3 Weibull (1939)

The Weibull distribution can be expressed in the following way

$$P_f = 1 - e^{-\left(\frac{\sigma}{k}\right)^m} \quad (5.5)$$

where k and m are the scale and shape parameters, respectively. This is the functional form that is adopted elsewhere, e.g. in Forbes et al. (2011), Rinne (2009). However, note that in Weibull (1939), the distribution was introduced in the following format, viz.

$$S = 1 - e^{-V\left(\frac{\sigma}{\sigma_0}\right)^m} \quad (5.6)$$

where S denotes the failure probability, V denotes the volume of material, and σ_0 and m represent two parameters. Note also that Weibull used the letter k in the following way, viz.

$$S = 1 - e^{-Vk\sigma^m} \quad (5.7)$$

where k represents a parameter. In this thesis, we adopt the format in Eq. (5.5).

Weibull distribution from a phenomenological/macroscopic point of view

Weibull (1939) derived a fundamental equation for the failure probability of a brittle isotropic material of volume V subject to uniaxial stress σ . The fundamental form is expressed in

$$S = 1 - e^{-B} \quad (5.8)$$

where B denotes the risk function. The risk function is supposed to depend on the uniaxial stress and the volume according to

$$B = \int n(\sigma) dv \quad (5.9)$$

for some function $n(\sigma)$. For a uniform stress field this amounts to

$$P_f = 1 - e^{-Vn(\sigma)} \quad (5.10)$$

where the frequently encountered notation P_f is used to signify the failure probability. A convenient derivation of Eq. (5.10) which is mainly due to Freudenthal (1968) is as follows. Let P_S denote the survival probability. Supposing that the events of survival of the non-overlapping volumes V and ΔV at stress σ are independent, it follows that the joint survival probability is

$$P_S(V + \Delta V, \sigma) = P_S(V, \sigma) \cdot P_S(\Delta V, \sigma) \quad (5.11)$$

Taking the logarithms and dividing throughout by ΔV yields, after some rearrangement

$$\frac{\ln P_S(V + \Delta V, \sigma) - \ln P_S(V, \sigma)}{\Delta V} = \frac{P_S(\Delta V, \sigma)}{\Delta V} \quad (5.12)$$

In Eq. (5.12), the right-hand side is independent of V and hence may be rewritten as $-n(\sigma)$ where it is understood that $n(\sigma) = |n(\sigma)|$. As $\Delta V \rightarrow 0$, the left-hand side of Eq. (5.12) tends to $\frac{d}{dV} \ln P_S(V, \sigma)$. Hence, after integration we obtain

$$\ln P_S(V, \sigma) = -Vn(\sigma) \quad (5.13)$$

which can be rewritten as

$$P_S(V, \sigma) = e^{-Vn(\sigma)} \quad (5.14)$$

Finally, the failure probability is given by Eq. (5.10). Weibull (Weibull 1939, ?) postulated that $n(\sigma)$ is a simple function such as

$$n(\sigma) = k\sigma^m \quad (5.15)$$

which inserted into Eq. (5.14) yields Eq. (5.7). Alternatively, $n(\sigma)$ can be expressed as in

$$n(\sigma) = \left(\frac{\sigma}{\sigma_0} \right)^m \quad (5.16)$$

which inserted into Eq. (5.14) yields Eq. (5.6). The standard two-parameter Weibull distribution function, Eq. (5.5), with scale and shape parameters k and m , is obtained e.g. from Eq. (5.6) by combining the volume factor V and the scale factor σ_0 into a single scale parameter.

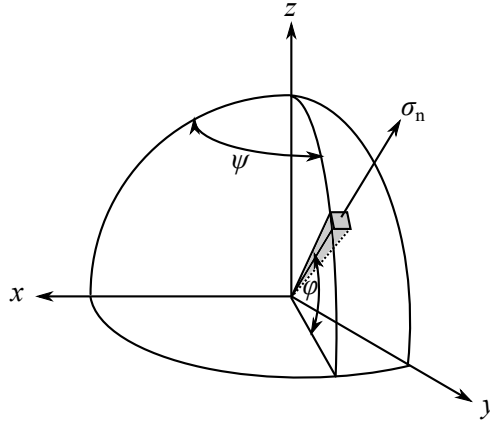


Figure 5.1: Solid angle in the unit sphere. One half-quadrant shown. Adapted from Weibull (1939).

Weibull offered an expression for a polyaxial stress state if it is assumed that only the normal component of stress contributes to failure. The normal stress component in 3D is determined by the principal stresses σ_1 , σ_2 , and σ_3 , and is given by

$$\sigma_n = \cos^2 \varphi (\sigma_1 \cos^2 \psi + \sigma_2 \sin^2 \psi) + \sigma_3 \sin^2 \varphi \quad (5.17)$$

where φ and ψ are angles in the unit sphere according to Fig. 5.1. The differential solid angle, do , indicated in the figure is

$$do = \cos \varphi d\varphi d\psi \quad (5.18)$$

Hence, the failure probability is

$$P_f(\sigma) = 1 - e^{-\int_V \int_{\Omega} n(\sigma(x, y, z)) \cos \varphi d\varphi d\psi dV} \quad (5.19)$$

where the integration domain Ω is over the part of surface of the unit sphere where σ contributes to failure, i.e. where σ is tensile (Lamon 2016).

Weibull distribution from a flaw-based approach/microscopic point of view

The following derivation can be found in Lamon (2016) although it exists elsewhere too. Suppose there is a flaw density function $f(a)$ where a denotes the flaw size and let a_c denote the critical flaw size that prompts catastrophic failure in a differential

volume element ΔV containing the flaw. The probability that the volume element contains the critical flaw is

$$P_f(\Delta V, a_c) = \Delta V \int_{a_c}^{\infty} f(a) da \quad (5.20)$$

Assuming that the material of volume V is subdivided into a number N of non-overlapping volumes ΔV , each of which fail independently of another, the weakest-link principle gives that the global survival probability is

$$1 - P_f(V, a_c) = \left(1 - \Delta V \int_{a_c}^{\infty} f(a) da\right)^N \quad (5.21)$$

Substituting ΔV for V/N in Eq. (5.21) while comparing with the standard expression

$$\lim_{N \rightarrow \infty} \left(1 - \frac{x}{N}\right)^N = e^{-x} \quad (5.22)$$

leads to the following expression for the survival probability

$$1 - P_f(V, a_c) = e^{-V \int_{a_c}^{\infty} f(a) da} \quad (5.23)$$

It follows that the global failure probability is (Lamon 2016)

$$P_f(V, a_c) = 1 - e^{-V \int_{a_c}^{\infty} f(a) da} \quad (5.24)$$

Let $f(a)$ be the density of a Pareto distributed random variable. Then, (Forbes et al. 2011)

$$f(a) = ca_0^c a^{-(c+1)} \quad (5.25)$$

where a_0 and c denote the scale and shape parameters, respectively. Substitution of Eq. (5.25) into Eq. (5.24) and integration yields

$$P_f(V, a_c) = 1 - e^{-V \left(\frac{a_0}{a_c}\right)^c} \quad (5.26)$$

In the case of a uniform uniaxial tensile stress, linear elastic fracture mechanics dictates that the remote stress is inversely proportional to the square of the critical crack size, cf. Eq. (2.5) to (2.7). By substituting for this in Eq. (5.26), an expression emerges that is of identical form as the ordinary Weibull distribution, Eq. (5.5). It is readily verified that

$$m = 2c \quad (5.27)$$

and

$$k = \frac{K_{Ic}}{Y \sqrt{\pi a_0} V^{\frac{1}{c}}} \quad (5.28)$$

5.1.4 Matthews et al. (1976)

Suppose there exists a flaw strength density function $g(S)$ where S denotes the strength such that $g(S)dS$ is the number of flaws per unit area with a strength in the range S to $S + dS$. Then, by application of the postulates for a spatial Poisson process, $\int_0^{S_1} g(S) dS$ represents the average number of flaws per unit area that give a strength smaller than S_1 . See further about the Poisson process in Sec. 6.3.2. Moreover, the probability that a flaw with strength smaller than S_1 occurs in δA is

$$\delta\phi(S_1) = \delta A \int_0^{S_1} g(S) dS \quad (5.29)$$

where $\delta\phi$ denotes the failure probability. By application of the weakest-link principle and while assuming independence of flaws' action, it is seen that the differential survival probability is

$$1 - \delta\phi(S_1) = 1 - \delta A \int_0^{S_1} g(S) dS \quad (5.30)$$

which can be approximated by

$$1 - \delta\phi(S_1) = e^{-\delta A \int_0^{S_1} g(S) dS} (1 + \mathcal{O}(\delta A^2)) \quad (5.31)$$

where \mathcal{O} is the big-O Landau symbol (LeVeque 1977). Assuming that the total area is divided into many small regions, i.e.

$$A = n\delta A \quad (5.32)$$

it is found that the probability of global survival at stress S_m is

$$1 - \Phi(S_m) = e^{-n\delta A \int_0^{S_m} g(S) dS} (1 + n\mathcal{O}(\delta A^2)) \quad (5.33)$$

which can be rearranged, while noting Eq. (5.32), into

$$1 - \Phi(S_m) = e^{-A \int_0^{S_m} g(S) dS} (1 + \mathcal{O}(\delta A)) \quad (5.34)$$

Hence,

$$\lim_{\delta A \rightarrow 0} 1 - \Phi(S_m) = e^{-A \int_0^{S_m} g(S) dS} \quad (5.35)$$

and the global failure probability is

$$P_f(A, S_m) = 1 - e^{-A \int_0^{S_m} g(S) dS} \quad (5.36)$$

Matthews et al. (1976) attempt to estimate the density function $g(S)$ based on experiments on plate and window glass, as well as other materials.

5.1.5 Batdorf and Crose (1974)

It is assumed that there exists a flaw strength density function $N(\sigma_{\text{cr}})$ where the subscript signifies the critical stress. The number of cracks in volume ΔV with a strength between σ_{cr} and $\sigma_{\text{cr}} + d\sigma_{\text{cr}}$ is

$$dN = \Delta V \frac{dN(\sigma_{\text{cr}})}{d\sigma_{\text{cr}}} d\sigma_{\text{cr}} \quad (5.37)$$

Let Ω represent the solid angle containing the normals to all orientations of the applied stress for which the component of stress normal to the crack plane, i.e. σ_n , would prompt failure, i.e. all orientations for which $\sigma_n > \sigma_{\text{cr}}$. For a single crack then, the probability of failure is

$$P_f = \frac{\Omega(\Sigma, \sigma_{\text{cr}})}{4\pi} \quad (5.38)$$

where Σ denotes the applied stress state. Hence, the probability of failure in volume ΔV for stresses in the range σ_{cr} to $\sigma_{\text{cr}} + d\sigma_{\text{cr}}$ is

$$P_f(\Delta V, d\sigma_{\text{cr}}) = \Delta V \frac{dN(\sigma_{\text{cr}})}{d\sigma_{\text{cr}}} d\sigma_{\text{cr}} \frac{\Omega(\Sigma, \sigma_{\text{cr}})}{4\pi} \quad (5.39)$$

It is noted that the survival probability of a volume V in the same stress state is the product of the probabilities of survival of each element ΔV . Then from Eq. (5.39), after integrating over critical stresses and operating on the survival probability instead of failure probability, we arrive at

$$P_S(V, \Sigma) = \left(1 - \Delta V \int_0^\infty \frac{\Omega(\Sigma, \sigma_{\text{cr}})}{4\pi} \frac{dN(\sigma_{\text{cr}})}{d\sigma_{\text{cr}}} d\sigma_{\text{cr}} \right)^{\frac{V}{\Delta V}} \quad (5.40)$$

Eq. (5.40) can be rewritten in the limit by observing the standard relation

$$\lim_{h \rightarrow 0} (1 + xh)^{\frac{1}{h}} = e^x \quad (5.41)$$

so

$$P_S(V, \Sigma) = e^{-V \int_0^\infty \frac{\Omega(\Sigma, \sigma_{\text{cr}})}{4\pi} \frac{dN(\sigma_{\text{cr}})}{d\sigma_{\text{cr}}} d\sigma_{\text{cr}}} \quad (5.42)$$

from which the failure probability valid for a uniform state of stress, is

$$P_f = 1 - e^{-V \int_0^\infty \frac{\Omega(\Sigma, \sigma_{\text{cr}})}{4\pi} \frac{dN(\sigma_{\text{cr}})}{d\sigma_{\text{cr}}} d\sigma_{\text{cr}}} \quad (5.43)$$

In the case of uniaxial tension, the solid angle Ω is given by two cones as illustrated in Fig. 5.2. In Fig. 5.2, θ_{cr} denotes the critical angle within which failure is prompted.

Batdorf & Crose (1974) assumed that the flaw strength density function had a lower bound σ_u . They approximated the density function by carrying out a Taylor series expansion about the boundary value while maintaining only the first order terms in the series.

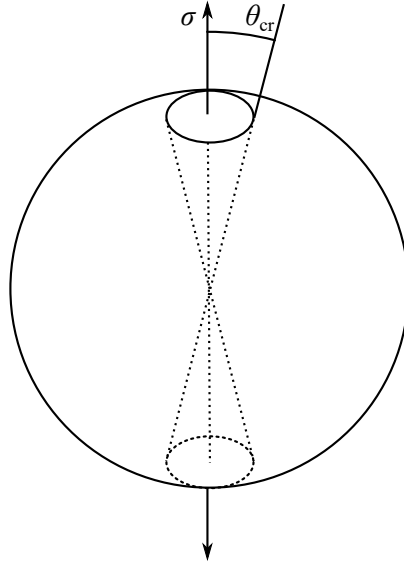


Figure 5.2: Solid angle represented by two cones in the case of uniaxial tension. Adapted from Batdorf & Crose (1974).

5.1.6 De Jayatilaka and Trustrum (1977)

It is assumed that there exists a flaw size density function $f(a)$. Through Hertzian indentation fracture tests, it was proposed by Poloniecki & Wilshaw (1971) and Poloniecki (1974) that $f(a)$ can be closely fitted by an inverse gamma distribution

$$f(a) = \frac{c^{n-1}}{(n-2)!} a^{-n} e^{-\frac{c}{a}} \quad (5.44)$$

where c and n denote a pair of scale and shape parameters. De Jayatilaka & Trustrum (1977) considered an inclined crack in a uniform uniaxial tensile stress field and applied strain energy concepts to derive the critical crack size as function of fracture toughness and applied stress. It was assumed that any crack angle is equally likely. Then, the failure probability associated with a single crack at stress σ is

$$F(\sigma) = \int_{\frac{K_{Ic}^2}{\pi\sigma^2}}^{\infty} \left(1 - \frac{K_{Ic}^2}{\pi a \sigma^2}\right) f(a) da \quad (5.45)$$

Supposing that there are N cracks, the probability of global failure is

$$P_f = 1 - (1 - F(\sigma))^N \quad (5.46)$$

which in the case of large N and small σ , i.e.

$$\frac{\sigma\sqrt{\pi c}}{K_{Ic}} \ll 1 \quad (5.47)$$

leads to the following approximation

$$P_f \approx 1 - e^{-NF(\sigma)} \quad (5.48)$$

Based on Eq. (5.45) and Eq. (5.48), it can be shown that

$$P_f \approx 1 - e^{-N \frac{c^{n-1}}{n!} \left(\frac{\pi \sigma^2}{K_{Ic}^2} \right)^{n-1}} \quad (5.49)$$

Since the number of cracks is proportional to the volume of material, Eq. (5.49) can be reformulated as Eq. (5.6) with

$$m = 2n - 2 \quad (5.50)$$

In such case, σ_0 in Eq. (5.6) is a parameter dependent on n .

5.1.7 The GFPM

The so-called Glass Failure Prediction Model (GFPM) was first developed by Beason (1980). It takes as its starting point the fundamental equation of Weibull (1939), i.e. Eq. (5.8). It is proposed that the risk function B in Eq. (5.8) be taken as

$$B = k \int_0^a \int_0^b (c(x, y) \tilde{\sigma}_{\max}(x, y))^m dx dy \quad (5.51)$$

which is valid for a rectangular plate of dimensions a and b . In Eq. (5.51), k and m are the so-called surface flaw parameters, c is a correction factor for the case of biaxial stresses, and $\tilde{\sigma}_{\max}$ is the so-called maximum equivalent principal tensile (MEPT) stress. In principle, the equivalent stress, $\tilde{\sigma}$, is obtained through application of Brown's (1972) Load Duration Theory in the form of Eq. (5.52), viz.

$$\tilde{\sigma} = \left(\frac{\int_0^{t_f} \text{RH} \left(\frac{\sigma(t)}{T} \right)^n e^{-\frac{\gamma_0}{RT}} dt}{t_r \text{RH}_r e^{-\frac{\gamma_0}{RT_r}} T_r^{-n}} \right)^{\frac{1}{n}} \quad (5.52)$$

In Eq. (5.52), t_r , RH_r , and T_r are the reference load duration, relative humidity, and temperature. Moreover, n is Charles' (1958b) stress corrosion parameter, the value of which is supposed to equal 16. However, the special choice of equivalent stress made in Beason (1980), is the constant stress of 60 second duration which would have the same effect on a surface flaw as an arbitrary time-dependent stress $\sigma(t)$, i.e.

$$\tilde{\sigma}_{60} = \left(\frac{\int_0^{60} \sigma(t)^n dt}{60} \right)^{\frac{1}{n}} \quad (5.53)$$

The risk function B is integrated numerically in a particular procedure based on a nonlinear plate analysis solution. The surface flaw parameters are subsequently determined in a number of steps. In Beason & Morgan (1984), the method was modified in significant ways. It incorporates the Vallabhan & Wang (1981) finite difference plate solution to the von Karman nonlinear plate equations. The failure probability of a laterally supported plate subject to out-of-plane loading is expressed in terms of the surface flaw parameters, k and m , and the load, q , in a procedure as follows. The magnitudes of surface tensile stresses are calculated, given the load q , and the maximum principal tensile stress is converted to equivalent stress. The risk function is evaluated and the failure probability is determined. For the estimation of the surface flaw parameters, an original method was developed. It involves an iterative procedure in which the following property of the exponential distribution is exploited, viz. that the coefficient of variation equals to 1. The iterative process involves calculating a set of so-called risk factors for a wide range of assumed values of m . The optimal pair of surface flaw parameter values are determined by choosing the value of m such that the coefficient of variation of the risk factor is closest to 1, thus obeying the governing property of the underlying exponential distribution. The value of k is subsequently calculated for it depends on the value of m .

5.1.8 Haldimann (2006)

Haldimann (2006) presents the so-called Lifetime Prediction Model. It is assumed that there exists a flaw size density function $f_a(a)$ which is supposed to be Pareto distributed, i.e.

$$f_a(a) = (r - 1)a_0^{r-1}a^{-r} \quad (5.54)$$

where a_0 and r denote the scale and shape parameters, respectively. Hence, the probability of failure for a single crack is

$$P_{f,\text{inert}}^{(1)} = 1 - \int_0^{a_c} f_a(a) da \quad (5.55)$$

where a_c denotes the critical crack depth that prompts failure. Assuming the existence of k flaws, the survival probability in inert conditions is

$$P_{s,\text{inert}}^{(k)} = (1 - P_{f,\text{inert}}^{(1)})^k \quad (5.56)$$

In Eq. (5.57), the global failure probability is expressed. It can be derived from Eq. (5.56) by applying the Poisson postulates and by expressing the exponential function as an infinite series.

$$P_{f,\text{inert}} = 1 - e^{-M \cdot P_{f,\text{inert}}^{(1)}} \quad (5.57)$$

In Eq. (5.57), M denotes the total number of flaws. Assume next that the critical crack depth a_c is related to applied stress normal to the crack plane through Eq. (5.58),

$$a_c = \left(\frac{K_{Ic}}{\sigma_n Y \sqrt{\pi}} \right)^2 \quad (5.58)$$

where Y is the crack geometry factor. After substituting for Eq. (5.58) in Eq. (5.57), it can be shown that

$$P_{f,\text{inert}}(\sigma_n) = 1 - e^{-\left(\frac{\sigma}{\theta}\right)^{m_0}} \quad (5.59)$$

which is valid for a uniform and uniaxial state of tensile stress. In Eq. (5.59),

$$m_0 = 2r - 2 \quad (5.60)$$

and

$$\theta = \frac{K_{Ic}}{M^{\frac{1}{m_0}} Y \sqrt{\pi a_0}} \quad (5.61)$$

The so-called lifetime prediction model is obtained through extension to account for subcritical crack growth. In this case, subcritical crack growth is modelled by the ordinary differential equation

$$v = \frac{da}{dt} \quad (5.62)$$

where v is given by Eq. (2.35). Assuming Eq. (5.62) to be valid over the whole range of K_I and that n in Eq. (2.35) is time-independent, it can be shown that the initial depth of a crack that fails at time τ , i.e. $\tilde{a}_c(\tau)$, when exposed to stress history $\sigma_n(\tau)$ acting normal to the crack plane, is

$$\tilde{a}_c(\tau) = \left(\left(\frac{\sigma_n(\tau) Y \sqrt{\pi}}{K_{Ic}} \right)^{n-2} + \frac{n-2}{2} v_0 K_{Ic}^{-n} (Y \sqrt{\pi})^n \int_0^\tau \sigma_n^n(\tilde{\tau}) d\tilde{\tau} \right)^{\frac{2}{2-n}} \quad (5.63)$$

The time-dependent failure probability of a single crack can then be shown to be

$$P_f^{(1)}(t) = \left(\frac{a_0}{\min_\tau \tilde{a}_c(\tau)} \right)^{\frac{m_0}{2}} \quad (5.64)$$

which substituted into Eq. (5.57) gives the time-dependent failure probability while taking subcritical crack growth into account. The model can be extended to non-uniform polyaxial stress states.

5.1.9 Yankelevsky (2014)

Yankelevsky (2014) assumes the existence of a flaw size distribution function of exponential shape that can be expressed analogous to Mott's law, i.e.

$$\frac{N_f}{N_0} = e^{-\frac{\delta}{\mu}} \quad (5.65)$$

where δ is the flaw size and N_f is the number of flaws that are larger than or equal in size to δ . In Eq. (5.65), μ is a scaling parameter and N_0 is the total number of flaws. The parameter μ can be derived as

$$\mu = \frac{\delta_{\max}}{|\ln N_0|} \quad (5.66)$$

because at $\delta = 0$, $N_f = N_0$, and at $\delta = \delta_{\max}$, $N_f = 1$. Hence, it is assumed that there exists an upper bound on the flaw size. It is assumed that flaw size δ relates to critical stress σ_c according to

$$K_{Ic} = 1.12\sigma_c\sqrt{\pi\delta} \quad (5.67)$$

A base sheet of glass of standard size is considered over which a population of flaws are uniformly distributed in unit cells of 1 cm^2 each. The flaw size in each cell is sampled from the flaw size distribution which is similar to a truncated exponential distribution, cf. Eq. (5.65). A plate is cut out from the base sheet and subjected to loading. The resulting stress distribution is compared with the critical stresses on the plate. A search method is conducted to detect the location and stress magnitude at which the applied stress first reaches the critical stress. The procedure is repeated in Monte Carlo simulations to obtain a large sample of fracture stress and failure location.

5.1.10 Kinsella and Persson (2018b)

Based on the numerical method in Yankelevsky (2014), Kinsella & Persson (2018b) develops a failure model for glass plates in co-axial double ring bending. Kinsella & Persson (2018b) can also be found in Paper B. The plate surface area is subdivided into 1 mm^2 unit cells. Two types of representations for the surface flaw condition are implemented based on a single population and a dual population of half-penny shaped cracks which have a uniformly distributed crack plane orientation. The single population was given a Pareto distributed flaw size. The dual population comprised one Pareto and one Fréchet distribution of flaw sizes, each corresponding to a large and a small flaws population concept, respectively. The relative frequency of large flaws on a specimen were estimated based on the results from investigations to reveal the flaw size density using image scanning techniques on a pair of soda-lime silicate glass panes (Wereszczak et al. 2014). The Pareto flaws assumption was based on the Hertzian fracture indentation tests by Poloniecki & Wilshaw (1971) and Poloniecki (1974). The number of small flaws in any unit cell was assumed to be numerous thus motivating the Fréchet flaws assumption as follows. It is supposed that the fracture mechanical behaviour in a unit cell due to the small flaws population is governed by the largest small flaw. Assuming that the small flaws population has a Pareto size distribution, the limiting distribution for the largest small flaw would be Fréchet according to extreme value theory.

Three different fracture criteria were employed and compared based on the simulated strength and fracture location distributions. The model was calibrated to data from an experiment with the double ring bending device conducted by Simiu et al. (1984).

5.2 DESIGN RULES

5.2.1 prEN 16612:2017

The prEN 16612:2017 gives a method for determining the strength of linearly supported glass elements due to lateral loading. The method given is a draft in compliance with EN 1990: Basis of structural design. The design value of bending strength for annealed glass is

$$f_{g;d} = \frac{k_e k_{\text{mod}} k_{sp} f_{g;k}}{\gamma_{M;A}} \quad (5.68)$$

where $f_{g;k}$ is the characteristic, i.e. 5%-fractile, value in the distribution of bending strength, viz. 45 MPa. This value was determined by fitting a two-parameter Weibull distribution to co-axial double ring bending test results of 741 panes of 6 mm float glass. The tests were carried out according to EN 1288-2. In Eq. (5.68), $\gamma_{M;A}$ is the material partial factor and for annealed glass in the ultimate limit state it equals to 1.8. With $\gamma_{M;A} = 1.8$, the characteristic bending strength is reduced from 45 MPa to 25 MPa which agrees with the 0.0005%-fractile in the strength distribution of predamaged glass according to experiments with the co-axial double ring bending device carried out by Blank. prEN 16612:2017 does not provide a more detailed reference to Blank except for the following document: CEN/TC129/WG8-N88E. This author was unable to obtain a copy of the said document. In Eq. (5.68), k_{sp} is the factor for the glass surface profile and it depends on the surface condition. For as-produced float glass its value equals to 1.0 while for sandblasted glass, e.g., it is 0.6. In Eq. (5.68), k_{mod} is the factor for load duration according to

$$k_{\text{mod}} = 0.663t^{-\frac{1}{16}} \quad (5.69)$$

where t is the load duration in hours. However, $0.25 \leq k_{\text{mod}} \leq 1.0$ for normal building loads and $0.25 \leq k_{\text{mod}} \leq 1.1$ for exceptional loads of very short duration, e.g. explosions. The factor for the load duration is based on the formula

$$\sigma^n T = \text{constant} \quad (5.70)$$

where T is the duration of stress and $n = 16$. Hence, in applying Eq. (5.69) it is assumed that the long-term strength is no smaller than 25% of the short-term strength where “short-term” is 83 ms. Moreover, Eq. (5.69) is assumed to be valid

for load durations down to 20 ms. However, according to a list of pre-calculated values of k_{mod} provided in a table, the word “short-term” can be assumed to apply to load durations of 5 sec or less which would be representative of wind gust actions. Furthermore, seeing as the long-term strength is no smaller than 25% of the short-term strength, it is implied that the threshold limit value for stress corrosion is 25% of the short-term strength. However, the threshold limit value for stress corrosion, cf. Sec. 2.5.3, is otherwise usually represented in terms of the stress intensity factor.

In Eq. (5.68), k_e is the reduction factor for edge bending strength which considers that the edge strength is less than the surface strength. For float glass, the value of k_e ranges between 0.8-1.0 and depends on the edge processing method, viz. as-cut, arrised, ground, polished, and on the abrasive action, viz. across the edge or along the length of the edge. Notably, the polished edge corresponds to $k_e = 1.0$. Finally, the maximum bending stress calculated for the design load shall not exceed the design value for the bending strength, i.e.

$$\sigma_{max} \leq f_{g;d} \tag{5.71}$$

6

Discussion of strength models

The strength prediction of a glass structure is a complex task which may depend on a range of theories and techniques. Fig. 6.1 presents an overview of the models involved in this discussion including some references. The shaded gray box in Fig. 6.1 corresponds to models that implement stress corrosion theory. This chapter contains a comparative discussion of the benefits and drawbacks of various strength models some of which were covered in Chap. 5. The strength models are generally divided into those that take a phenomenological approach towards failure at the macroscopic level, and those that assume the preexistence of material flaws at the microscopic level from which failure is derived. In the latter case the models can be separated into those with a flaw size approach and those with an elemental strength approach. The flaw size approach depends on a more or less rigorous representation of the surface flaws in terms of a flaw size distribution, a flaw shape, and an orientation of the flaw in the plane. The elemental strength approach does not depend on a direct representation of the flaw geometry. Instead, it is based on the isotropic material resistance to uniaxial tension. As indicated in Fig. 6.1, there are also flaw-based models that position themselves in between the flaw size approach and the elemental strength approach. Sec. 6.2 contains a discussion of the models with a macroscopic/phenomenological approach towards failure while Sec. 6.3 contains a discussion of the models with a microscopic/flaw-based approach. In Sec. 6.1, the Weibull distribution is given a separate treatment due to the central position it takes in glass strength modelling at present. Strictly speaking, the Weibull distribution can be associated with both a macroscopic and a microscopic approach towards failure. Much of what is said about the Weibull distribution in Sec. 6.1 would however fit into Sec. 6.3. There is a vast amount of

literature that considers the Weibull distribution for application on glass. Sec. 6.4 and 6.5 consider aspects of the treatment of edge and surface failure origins in the strength modelling, and the dealing with stress corrosion. Sec. 6.6 contains a discussion of the sources of error that may be involved when glass strength data is considered.

6.1 THE WEIBULL MODEL

In the literature on glass, the Weibull distribution is the most commonly employed model for the fracture stress obtained in test results. The Weibull distribution has descriptive virtue (Weibull 1959). According to a recent survey (Rinne 2009), there are a great number of papers and monographs that demonstrate the successful application of the Weibull model in some 180 distinct topics that encompass nearly all scientific disciplines. However, the descriptive virtue can become a liability when the sample sizes are small because the Weibull model maintains its flexibility all the same; in such case, the better fitting means nothing (Danzer et al. 2001). There are multiple explanations for this. According to Danzer (1994), the size difference between the smallest and the largest critical defect is expected to be small for a data set of limited size, e.g. 30 specimens. Fig. 6.2 illustrates the part of the flaw size distribution that is probed with a small sample. In Fig. 6.2, $g(a)$ denotes the flaw size density function whose graph corresponds to a multimodal distribution. Considering this multimodal shape and the limited range of flaw size that is probed, Danzer (1994) makes the following remark: “Over a small interval, $g(a)$ can always be approximated by a power law. This explains the good description of small sets of data by the Weibull distribution.” This may be related to the findings in Kinsella et al. (2018) where the standard distributions including the Weibull distribution were fitted to samples of varying minimum size. Kinsella et al. (2018) can be found in Paper A. It was found that when the minimum sample size was small, then it was impossible to properly judge the performance of the Weibull distribution.

Errors can emerge when making extrapolations from a limited data set with the Weibull model. This poses a challenge to the way that design rules are set up. In the case of prEN 16612:2017, the value of the factor for the load duration, k_{mod} , depends on extrapolating data results into a smaller probability domain. However, as the authors of the draft standard admit: “Attempts to analyse the distribution of results as a two-parameter Weibull distribution to obtain an estimate of the stress at a probability level around 1×10^{-4} lead to values much lower than are viable for glass design.” This is a testimony to the fact that even though the Weibull model has descriptive virtue, it is not a model with great enough potential to be used while setting up design rules. This conclusion is emphasized by the fact that the data sample analysed by the authors of the draft comprised some 741 specimens which represents a particularly large data sample in this research field. It can therefore be

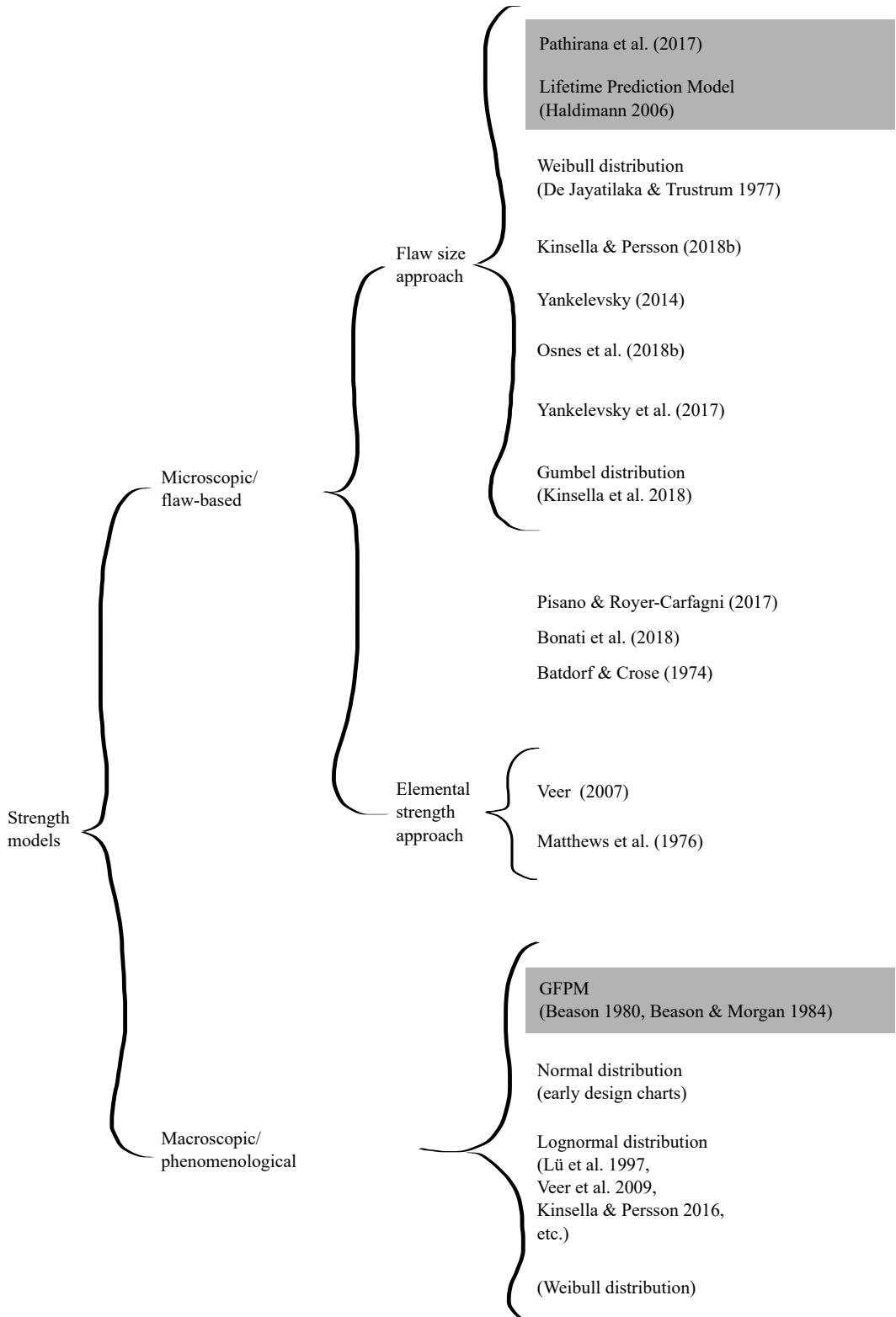


Figure 6.1: Overview of strength models.

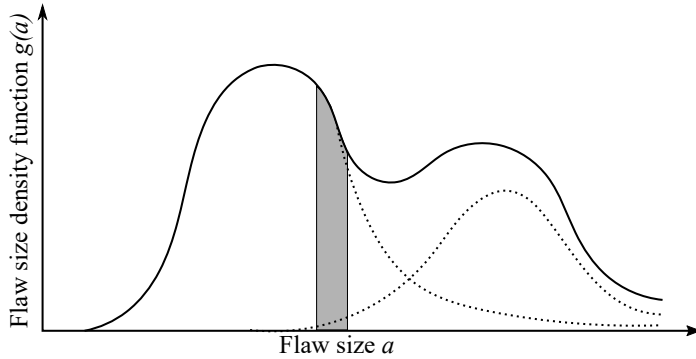


Figure 6.2: Sketch of a bimodal flaw size density function (solid curve) superposed by two different flaw population densities (dashed lines). The shaded area represents the probability range probed by a small sample of measurements. Adapted from Danzer (1994).

said, that the Weibull distribution has limited predictive capacity for glass strength. The multimodal behaviour of the strength distribution is clearly indicated when the draft authors conclude that extrapolations are not viable. In an effort to remedy this, some researchers have attempted to employ another Weibull distribution in the high reliability domain, i.e. low probabilities of failure, the distribution of which was fitted to glass specimens with artificially induced flaws. The artificial damage was performed by e.g. dropping sand particles onto the glass surface from a predefined height (Blank 1993). However, it remains to be demonstrated that such artificially treated glass properly represents the condition of the surface in the low probability domain. If the low probability domain is thought of as corresponding to the state of the surface when it is used and weathered, then there is definitely a need for more empirical data on the strength of glass which has been subjected to in-service conditions. The importance of this has been emphasized before, e.g. in Dalglish & Taylor (1990). The practical issues involved in gaining access to used glass in buildings can be an obstacle towards acquiring specimens of glass from in-service conditions.

Given a data set of N observations of the strength, the estimate of the failure probability for a specimen can be based on its rank n as follows, see also Paper D.

$$P = 1 - \frac{n - \frac{1}{2}}{N} \quad (6.1)$$

The value of P in Eq. (6.1) ranges from $(2N - 1)/2N$ for the specimen with the smallest defect, to $1/2N$ for the specimen with the largest defect (Danzer 1992). These values are located along the ordinate in a probability plot. Hence, the number of specimens required to probe the strength value at the probability level $1 \cdot 10^{-4}$ amounts to 5000. This is obviously not a practicable number of tests to be performed.

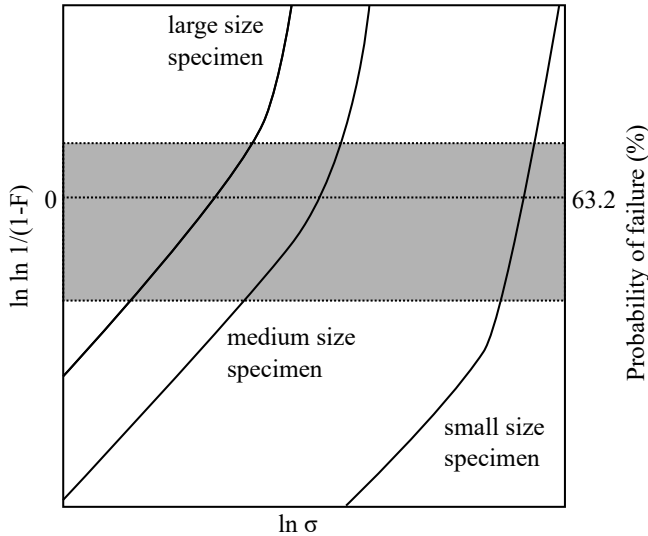


Figure 6.3: Sketch of the probability plot for three sets of specimens with different size. The shaded area corresponds to the probability range probed with a given number of specimens. Adapted from Danzer et al. (2001).

Rather than to increase the sample size, Danzer et al. (2007) proposes to test specimens of varying sizes as a means for appraising the nonlinearity in the strength distribution. In this way, it may be feasible to probe a greater range of the underlying flaw size distribution. See also Fig. 6.3 which contains a sketch of three bimodal strength distributions. Suppose that you probe the probability range with N specimens corresponding to the shaded region in the figure. By employing three different sizes of surface area, it would be possible to detect a greater portion of the total curve. This could offer a more economical way of appraising the strength distribution than to carry out large sample experiments. According to Danzer et al. (2001), there is a “great chance to discover multimodal structure in the distribution by choosing at least five samples of 30 specimens or more which cover a volume range of several orders of magnitude.” Danzer et al. (2001) speaks here in terms of volume of material, however, the line of reasoning is applicable to surface area as well.

What is the minimum sample size necessary to obtain reliable information on the distribution of strength in glass? And furthermore, under which conditions can extrapolations be made safely? Danzer et al. (2001) sample artificial Weibull distributions in Monte Carlo simulations in an attempt to answer these questions. To begin with, it is found that statistical artefacts arise in the probability plots, the artefacts of which can be misinterpreted as e.g. bimodalities. In fact, when the sample size is small, e.g. 30 specimens, it is hardly possible to distinguish real

structures in the distribution from artefacts. This pertains to e.g. “bends” in the tails of the probability plot. The origin of artefacts involves the frequent grouping or “lumping” together of some ranked observations while other data points consequently become more separated. All of this further complicates the analysis of the fracture data. It means, for instance, that if a researcher claims to have detected a nonlinearity in the strength distribution based on the Weibull probability plot, and the sample size is limited, then it cannot be ruled out that it is simply a statistical artefact. This insight might cast into doubt a range of analyses of glass fracture data made by various researchers. The strength distribution is most surely nonlinear, so making a claim to that end is not controversial. It is the evidence put forward in support of such a claim that may be suspicious when the sample size comprises only some 30-50 specimens.

What attitude should we adopt towards the Weibull model? There are multiple reasons to be sceptical of its potential as a strength model for glass as has been mentioned already, e.g. due to its limited capacity for prediction-making. If one suspects that glass failure is influenced by the presence of shear stress such as Reid (2007) suggests, then one has another reason to object to the Weibull model because with this model it is assumed that fracture is independent of shear stress. Objections to the Weibull model from the point of view of other subject areas exist too, e.g. a critique in terms of reliability analysis can be found in Robins (1962). The most blunt critique of the application of the ordinary Weibull model was probably delivered by Gorski (1969) who had to say the following under the heading “Beware of the Weibull Euphoria”: “The unpretentious freehand curve fitting exceeds the usefulness of the Weibull function if only because the freehand curve is taken at its face value.” Gorski (1969) may be correct about the ultimate lack of utility of the Weibull model in some cases, however, he is unaware of the logical basis for the application of the Weibull distribution to model brittle material fracture in general and glass fracture in particular. For the sake of this logical basis which we shall now consider, it is not easy to dismiss the Weibull model.

There have been experiments conducted to detect the surface flaw size density in glass using methods of Hertzian indentation fracture. The empirical density function is given in Eq. (5.44) and is furthermore similar to a Pareto distribution in the tail. In fact, the Weibull functional form was derived by De Jayatilaka & Trustrum (1977) based on Eq. (5.44). Hence, a strong case can be made for applying the Weibull distribution to model glass strength, at least when the stress state is uniform and uniaxial at each flaw. Compared to the normal and lognormal distributions, there is no similar failure-based logic in favour. The normal distribution is associated with the average of a large set of identically and independently distributed random variables as expressed in the Central Limit Theorem. By the same token, the lognormal distribution can be associated with the geometrical mean value.

6.2 MACROSCOPIC/PHENOMENOLOGICAL APPROACHES

Strength prediction models are generally of the macroscopic/phenomenological type, or the microscopic/flaw-based failure type. The first category includes the application of various standard statistical distributions such as the normal and Weibull distributions. As a matter of fact, the Weibull distribution as it was conceived by Weibull (1939), is phenomenological because it depends on a heuristical argument for the functional form of the so-called “risk function”, see Eq. (5.8) (Gumbel 1954). Eq. (5.8), however, is logical and depends solely on statistical arguments, viz. the subdivision of a material body into non-interacting regions with independent probabilities of failure and the application of a weakest-link principle. Alternatively, there is a complete analogy here with a homogeneous spatial Poisson process with random sized events, see further Sec. 6.3.2. Nevertheless, the benefit with the macroscopic/phenomenological approach is the simplicity in the model fitting, for which there is usually a standard procedure, e.g. using the maximum likelihood method, cf. Sec. 4.2.

In the literature on glass, there emerges mainly three standard statistical distributions for use with glass, viz. the normal, the lognormal, and the Weibull distributions. These models were analyzed and compared with respect to their performance based on a survey of the empirical data for the strength which is available in the open literature, cf. Kinsella et al. (2018) and Kinsella (2018) which can also be found in Paper A and D. According to the survey, most of the data on the strength of glass pertains to the edge type of fracture origin. This is so because the most common type of testing device employed was the four-point bending device with in-plane loading. This testing device naturally promotes edge fractures. It was found that when the failure is restricted to the edge, then the Weibull distribution outperforms the normal and lognormal distributions as a model for the strength. When the failure is restricted to the surface of the glass, however, there was no standard distribution that was capable of modelling the strength.

In the course of analysis by Kinsella et al. (2018), the Gumbel distribution emerged as an interesting object to study because it is the extreme value distribution associated with a whole range of standard-type distributions which lie in its domain of attraction, including the exponential, normal and lognormal distributions. If Yankelevsky (2014), Pathirana et al. (2017), and Osnes, Børvik & Hopperstad (2018*a*), Osnes, Hopperstad & Børvik (2018), who model glass failure, are essentially correct in their respective approaches towards the underlying flaw size distribution, with it having a density that decays exponentially, then it may indeed be warranted to consider the Gumbel distribution as a model for glass strength, at least for a uniform uniaxial state of stress at each flaw with a unimodal flaw population. However, the data does not favour with a Gumbel distribution for the

surface strength. Hence, there is an empirically based objection raised against the aforementioned authors' assumptions about flaw size distribution in glass when a unimodal flaw population is considered. Nevertheless, when the edge strength of glass is examined, the empirical data shows that both the extreme value Weibull and Gumbel distributions perform better than the normal and lognormal models, although it is indicated that the Weibull model is the best of them all (Kinsella et al. 2018), see Paper A.

In spite of the convenience of the standard distributions, there are serious objections that can be raised against their application to model glass fracture. Bearing in mind that these distributions generally do not perform satisfactory, one might agree with Lamon (2016) who says that they focus on the symptoms instead of the causes of fracture. In fact, the physical processes underlying fracture as we know it, including the presence of microcracks of stochastic nature which prompt failure (Griffith 1920), become masked and concealed when applying a standard statistical distribution. For instance, there can be no notion of size effects in glass with the normal and lognormal distributions. But, should the failure phenomenon not be represented in a rigorous strength prediction model? The mere simplicity and convenience of standard models of the macroscopic/phenomenological type should not be exploited as an argument for their utility, when the performance is poor; and testimony to the latter may be found in multiple references, among them Veer et al. (2009) and prEN 16612:2017. Hence, we should abandon the standard statistical distributions as potential models for use with glass and focus our efforts instead on more rigorous kinds of approach.

The Glass Failure Prediction Model (GFPM)

The GFPM can be located among the macroscopic/phenomenological models. While the adoption of the fundamental Eq. (5.8) is stringent, the particular selection and further treatment of the so-called risk function is heuristical. Fracture in glass is said to depend on the existence of surface microcracks and it is assumed that a biaxial stress correction factor can be applied to account for random crack plane orientations. More specifically, an equivalent stress is calculated “which acts normal to the axis of a flaw” (Beason 1980). But as a matter of fact, the GFPM does not directly deploy a flaw size density function nor an elemental strength distribution. The GFPM relies on a sophisticated procedure for the estimation of the so-called surface flaw parameters which unfortunately cannot be measured directly at present. In what sense then, do the surface flaw parameters represent the surface flaws? The relationship between surface flaws and surface flaw parameters is obscured by the complexity inherent in the method. The unit of the surface flaw parameter which is denoted by k depends on the value for m and hence varies from one model fit to another. For instance, with the Dallas glass plates that were extracted from the Johnson Chevrolet Building and subsequently analyzed

by Beason (1980), the value of k including its unit was estimated at $3.01 \cdot 10^{-15} \text{ mm}^{10} \text{ N}^{-6}$ (Beason & Morgan 1984). The surface flaw parameters appear to be intricate and the question is whether the sophisticated procedure involved in their estimation is warranted? Another question is whether the biaxial correction factor used by Beason (1980) is suitable? See Haldimann (2006) for a discussion of this. Haldimann (2006) also performs a thorough comparison of the ASTM E-1300 with the various European counterparts including the prEN 13474 which is an early version of prEN 16612. Note that the GFPM was implemented in the ASTM E-1300. Further points of critique include the following: It might not seem consistent to adopt an equivalent load level for an entire plate and the surface flaw parameter which is usually denoted by m is assumed to be time-independent which is hardly realistic (Reid 1991).

6.3 MICROSCOPIC/FLAW-BASED FAILURE APPROACHES

What remain to be considered are various types of models that are based on some concept which takes into account the microscopic aspect of brittle material failure, by assuming the existence of flaws which are understood to be real physical entities that are operated upon by stresses. We are able to distinguish between two approaches that have been termed the elemental strength approach, and the flaw size approach, respectively (Lamon 2016). In between, we find the Batdorf & Crose (1974) model that incorporates parts of both approaches. In Pisano & Royer-Carfagni (2017) and Bonati et al. (2018), the Batdorf & Crose (1974) model was adapted to incorporate a left-truncated flaw size distribution and a dual flaw population concept.

6.3.1 Elemental strength approach

The elemental strength approach supposes that fracture is governed by the existence of microscopic flaws in the material. However, no specific representation of the flaws' geometry is necessary, nor is it needed to directly represent crack plane orientations. The material strength is based on the elemental strength distribution which represents the isotropic material resistance to uniaxial tension (Lamon 2016), see Fig. 6.4 for an illustration. As a representative of this class of model, we have the Matthews et al. (1976) model. The main issue with this class of model is how to properly deal with failure when it is supposed that the elemental strength is dependent on a multiaxial state of stress. The elemental strength corresponds to a density function $g(S)$, where S denotes the elemental strength. But, S is a scalar and hence the orientation of S with respect to the stress field is ignored. A usual way to deal with this is to calculate an equivalent normal stress which is then

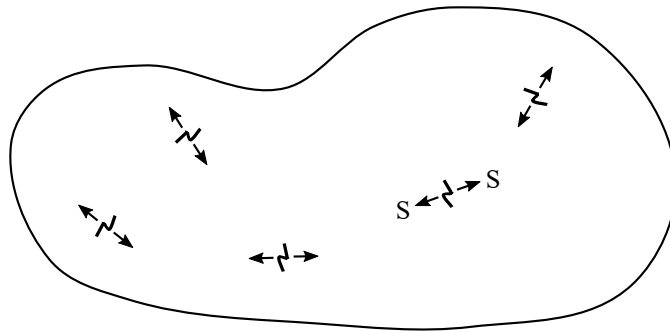


Figure 6.4: Material flaws with corresponding uniaxial elemental strengths. Adapted from Lamon (2016).

compared with the uniform uniaxial resistance. This is, for instance, done in the principle of independent action of stresses, which by the way is a rough approximation, see Lamon (2016) and Rufin et al. (1984). However, there are different ideas for how to properly represent the equivalent normal stress which lead to different results. There appears to be no consensus on this, see e.g. Lamon (2016) for a recent discussion.

Can the stress state be neglected for glass? It is sometimes assumed that flaws in glass are always oriented perpendicular to the maximum in-plane principal tensile stress on the grounds that this is conservative for design purposes. So far, the literature says that glass is stronger in uniaxial tension than in biaxial stress, see Haldimann (2006) for a discussion of this. This result is logical if it is assumed that the flaws are oriented randomly in the plane. In a future project, the data that was surveyed as part of this research project might be used to further investigate the strength dependence on the stress state, cf. Sec. 4 and Paper D.

The advantage of the elemental strength approach compared to the flaw size approach is that the former more readily conforms to the kind of information that is acquired from experimental tests on glass which measure the fracture stress. In other words, when the strength is measured experimentally, it is actually the strength due to some stress state that is measured. Hypothetical cracks with a size and crack plane orientation are not directly measured with common test setups, although these entities may be inferred from the fracture stress data based on fracture mechanical concepts.

Veer (2007) developed a rudimentary model for the edge strength of glass based on two superposed flaw strength distributions with normally distributed elemental strengths. The concept was based on test results from plates which were machine cut and ground, measuring $1000 \times 125 \times 10 \text{ mm}^3$, and subjected to in-plane four-point bending tests. Veer (2007) selected a subset of the data sample which he associated with one type of defect denoted Q and which was supposed to occur once in every

two meters of edge length with a mean failure stress of 30 MPa and a coefficient of variation of 7 %. The other type of defect denoted N, had a frequency of once in every millimeter with a mean failure stress of 60 MPa and a coefficient of variation of 12%.

6.3.2 Flaw size approach

The flaw size approach assumes an explicit representation of the flaws so that they are given a shape as well as an orientation of the crack plane with respect to the stress field. Hence, if the flaws have different orientations with respect to a given uniaxial stress state, then some flaws will be severe, while others are innocuous and yet others are intermediate, cf. Fig. 6.5. Interestingly, the Weibull distribution is an example of a strength model that can be deductively derived based on the flaw size approach as was demonstrated by e.g. Freudenthal (1968), see Sec. 5.1.3. However, such closed form expressions as Eq. (5.5) are available only for uniform uniaxial stress states over the cracks where it is assumed that the crack plane orientations are normal to the stress. Recently, the flaw size approach has gained in popularity as numerical techniques have been employed to model brittle fracture in Monte Carlo simulations with Griffith flaws, see e.g. Kinsella & Persson (2018*a,b*), Osnes, Børvik & Hopperstad (2018*b*), Pathirana et al. (2017), Yankelevsky (2014), Yankelevsky et al. (2017). A major objection to this approach is the limited information which is available today on the surface condition in glass. The glass surface condition has been probed by means of Hertzian indentation fracture methods in the past (Poloniecki 1974, Poloniecki & Wilshaw 1971) and recently by using image scanning techniques (Wereszczak et al. 2014). In the case of the Hertzian indentation fracture method, it is destructive and requires a large number of tests and involves much time and effort. With the image scanning techniques on the other hand and to this date, it has not been demonstrated that these are capable of detecting all pertinent flaws. There is for instance the issue of optically closed crack surfaces (Mencik 1992). With regards the image scanning techniques, the question emerges as how to define the flaw size (Lamon 2016)? In fact, flaws can appear to have curved shapes and the diameter was used as a simple metric in one experimental investigation (Wereszczak et al. 2014). However, it is not self-evident that this is the proper metric. And what would the hypothetical crack plane orientation be? These are some of the issues facing the flaw size approach. Hence, methods for measuring the surface flaws would be beneficial for the flaw size theory approach.

De Jayatilaka & Trustrum (1977)

The model proposed in De Jayatilaka & Trustrum (1977) and which is based on strain energy considerations for the fracture criterion, gives some justification for the Weibull distribution as a model for glass strength because it is derived from an

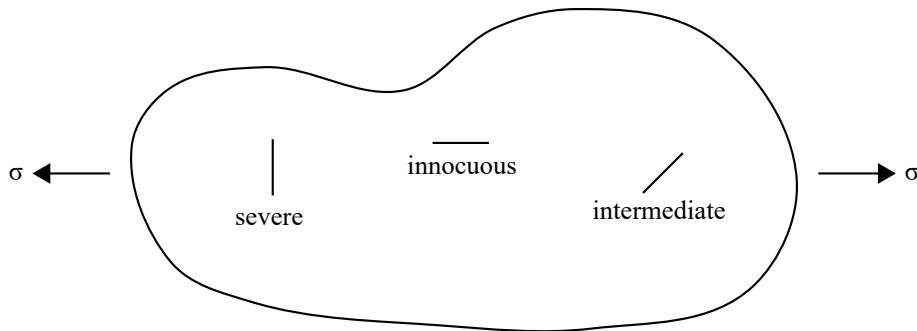


Figure 6.5: Inclined cracks in a uniaxial stress field. Due to the variation in crack plane orientation, some cracks become severe while others remain innocuous. Adapted from Lamon (2016).

empirical flaw size density function, Eq. (5.44). It also provides physical meaning to the Weibull shape parameter which is directly related to the shape of the flaw size distribution according to Eq. (5.50). However, flaw size may not in general be distributed according to Eq. (5.44). In a subsequent paper, Trustrum & De Jayatilaka (1983) investigated the ramifications of assuming flaw size distributions other than the empirical one in Eq. (5.44). It was shown that the Pareto, Cauchy, t , and F distributions, result in a Weibull distribution for the strength. The resulting shape parameter is given by Eq. (5.50) when the flaw size density $f(a) \propto \kappa a^{-n}$ where n is the shape parameter in the flaw size distribution and κ is a constant. However, assuming that the flaw size distribution is governed by a normal, lognormal, exponential, gamma, or χ^2 distribution results instead in a Gumbel distribution for the strength. The results in Trustrum & De Jayatilaka (1983) are based on a theorem that contains the sufficient conditions for the convergence of the minimum of a set of identically and independently distributed random variables to a given limit distribution. The results can also be found in standard textbooks on extreme value theory, see e.g. Beirlant et al. (2004). The conclusion is that if the flaw size distribution decays like a^{-n} for large a , then the Weibull distribution is justified. This is what is meant when Trustrum & De Jayatilaka (1983) write that “the distribution of failure stress is insensitive to the flaw size distribution.”

The Lifetime Prediction Model

The Lifetime Prediction model that was advanced in Haldimann (2006), incorporates subcritical crack growth but neglects the crack growth threshold limit, cf. Sec. 2.5.3. The model is extended to multiaxial states of stress, however, this extension suffers from the same drawbacks as the Weibull multiaxial model, Eq. (5.19). The derivation of the Lifetime Prediction Model is based on the Poisson postulates which are also referenced as a basis in Matthews et al. (1976). However,

Table 6.1: Analogy between the fundamental form, Eq. (5.8), and a spatial Poisson process. Adapted from Mesarovic et al. (1992).

Homogeneous spatial Poisson process with random sized events	Derivation of Eq. (5.8)
Homogeneous increments with mean occurrence rate λ	A constant flaw density
Independent increments	Subdivision of material into linked regions with independent strengths
No simultaneous occurrences	Each subdivided region contains one flaw only
For small volume increment ΔV , the probability of an occurrence is λV	No flaw interaction
The distribution of random sized events is the same for all events	All subdivided regions have the same strength distribution

neither Haldimann (2006) nor Matthews et al. (1976) explain the background to or motivation for involving a Poisson process. According to Mesarovic et al. (1992), there is a complete analogy between the assumptions that result in the fundamental Eq. (5.8), and the assumptions of a homogeneous spatial Poisson process for flaw occurrence with random sized events. Given the relationship between a crack in terms of its shape, and the mode I SIF, see e.g. Eq. (2.12), the spatial Poisson process of crack occurrences induces a Poisson process of K_I -occurrences. The complete analogy was laid out by Mesarovic et al. (1992) and is summarized in Tab. 6.1. For its implementation, the Lifetime Prediction Model is dependent on the determination of two so-called surface condition parameters, as well as two crack growth velocity parameters, and the geometry factor that corresponds to the supposed crack shape. Compared to the GFPM, the latter does not depend on an explicit representation of flaw shapes, as is the case with the Lifetime prediction model. Moreover, to determine the surface condition parameters stringently is a challenge. The estimates for the crack velocity parameter that is usually denoted v_0 vary a lot, see Sec. 6.5. Compared with the GFPM, the latter has the benefit of not depending directly on the value for v_0 because the GFPM treats the effect of stress corrosion differently. In the GFPM, the stress is normalized with respect to an equivalent constant stress of standard duration, e.g. 3 s or 60 s, the equivalent stress of which would have produced the same amount of corrosion as the actual stress. In the Lifetime Prediction Model, the subcritical crack growth is implemented rigorously through employment of the crack growth velocity parameter v_0 . So far, the Lifetime Prediction Model has not been implemented in any structural standards. Finally, notice that the definition of the Pareto distribution which was employed in Sec. 5.1.8 is different from the definition introduced in Sec. 5.1.3 insofar as $r = c + 1$.

Is the flaw size approach viable?

The question is whether the attempt to represent the surface flaws condition is too demanding? Given the lack of methods and techniques by which to effectively probe the surface condition, it is hardly possible to represent the flaws with the sort of realism that is involved in the flaw size approach, i.e. representing the crack size and shape, the crack location on the surface, and the crack plane orientation. What can be done is of course to attempt to find a representation that performs well in a strength model. But which representation would that be? There are already a multitude of representations proposed for use with glass. Just consider the flaw size representations in various strength models. Yankelevsky (2014) proposes to use a sort of truncated exponential distribution for the flaw size. Pathirana et al. (2017) assumes lognormally distributed flaw sizes. Kinsella & Persson (2018*b*), see Paper B, assumes both Pareto and Fréchet distributed flaw sizes. There is an element of speculation involved in this type of modelling and it is the flaw size approach in combination with the lack of knowledge of the surface condition that is conducive to this.

Perhaps then, it is best to abandon the flaw size approach? At least the Pareto distribution has the merit of being supported by experiments that detect flaw size distribution in glass (Tandon et al. 2013). Nevertheless, a Pareto-type distribution may be easy to fit to a limited range of the flaw size domain, as was demonstrated by Danzer et al. (2001). It may then be naive to employ a Pareto distribution for the whole range of flaw size. As a matter of fact, the fitting of a Weibull distribution to glass fracture data on the grounds that there is thus a logical failure-mechanical basis, logically implies a Pareto distribution for the whole tail in the flaw size range. Moreover, with the ordinary Weibull distribution, a uniform uniaxial stress state over the cracks with mode I crack opening is implicit. In this case then, the models in Kinsella & Persson (2018*a,b*), Paper B and C, although assuming Pareto flaw sizes, are at least not so simplistic in the treatment of the stress state and crack plane orientations as would be the case with the casual fitting of an ordinary Weibull distribution. In Kinsella & Persson (2018*a,b*), Paper B and C, the proper stress state is accounted for and random crack plane orientations are considered. But how should crack plane orientation be distributed? Again, there may be an element of speculation involved in the models. Assuming that there is no tendency for the flaws to be oriented in any particular direction, it is reasonable to assume a uniform spatial distribution. However, for various reasons flaws may tend to be oriented in certain directions. For instance, the production method which involves transportation on rollers and edge processing may promote flaws with a certain orientation.

6.4 EDGE AND SURFACE FAILURE ORIGINS

The structural standards, e.g. the draft prEN 16612:2017 which de facto is used by structural engineers today, see e.g. Vasilchenko-Malishev & Chesnokov (2018), and DIN 18008-1:2010, apply different representations for the strength depending on whether the strength design considers the surface or the edge. The question is whether data from edge failures can be safely combined with data from surface failure origins? Or is a special treatment warranted when mixed failure origins are present in the data sample? According to the study that was performed on the performance of standard statistical distributions for modelling the strength of glass, cf. Kinsella et al. (2018) which can also be found in Paper A, there is a fundamental difference between the surface condition and edge condition in glass. The study was based on a large collection of experimental test results. The results showed that none of the standard statistical distributions in consideration were able to properly model the surface strength. Hence, it is not self-evident that edge and surface failure data can be combined in an analysis of the strength. Moreover, the edge length and surface area of a given specimen do not scale uniformly, indicating that size effects might not be treated properly when combining edge and surface failure data. In fact, size effects have generally not been examined in this thesis although this is an important topic. Moreover, the distribution of edge strength may depend significantly on the edge treatment in question. This was not directly considered in the comparison of model performance of standard statistical distributions that was conducted in Kinsella et al. (2018), see Paper A.

6.5 STRESS CORROSION

Regarding the implementation of stress corrosion into the strength models, there are only three of the reviewed models that account for it, viz. the GFPM (Beason 1980, Beason & Morgan 1984), the Lifetime Prediction Model (Haldimann 2006), and the numerical model in Pathirana et al. (2017). In the case of the GFPM, the account for stress corrosion is based on Eq. (2.28) which is due to Brown (1972). In the case of the Lifetime Prediction Model and the numerical model in Pathirana et al. (2017), the account is based on Eq. (2.35) which is an empirically based approximation that was proposed in Evans (1974). In either case, the threshold limit for subcritical crack growth is neglected which means that predictions based on these models become conservative, i.e. they underestimate the strength. On the other hand, non-conservative results will be obtained for calibration purposes. A problem with the implementation of Brown's (1972) Load Duration Theory involves the inconsistencies that emerge when the failure time is either very long or very short. For very long time periods, the equivalent strength, Eq. (5.53), tends towards zero which is not realistic due to crack arrest at the threshold limit. For very short

time periods, the equivalent strength tends to infinity which is unrealistic. As a consequence, the implementation of Brown's (1972) Load Duration Theory is not valid at near-inert conditions. Nevertheless, the way in which Beason (1980) implements Brown's (1972) Load Duration Theory by application of an equivalent stress is very useful because compared to the implementation with the empirical formulation, Eq. (2.35), we have one less parameter to be concerned with, viz. the crack growth velocity parameter v_0 . While the literature is generally in agreement that the stress corrosion parameter value can be estimated at about $n = 16$ for soda-lime-silicate glass in ambient conditions, there is no consensus on the value of the crack growth velocity parameter v_0 . As a matter of fact, even if we restrict ourselves to an atmosphere of 50% RH, the various estimates for the velocity parameter span more than two orders of magnitude. This conclusion is based on a range of experiments which were reviewed in Schula (2015). Haldimann (2006) claims that $v_0 = 6 \text{ mm s}^{-1}$ is a conservative estimate for design purposes. The argument for this is based on an enveloping curve that was fitted to a set of empirical results for the crack growth velocity curve. There are two problems with this estimate. To begin with, it is not useful for calibration purposes. Secondly, it is probably overly conservative. Nevertheless, the value $v_0 = 6 \text{ mm s}^{-1}$ was adopted by Pathirana et al. (2017).

Reid (1991) compared two different implementations of stress corrosion, viz. the one in the GFPM and the one in the so-called Crack Growth Model which is essentially a precursor to the Lifetime Prediction Model. For the simple ramp loading case, it was found that the failure probability of flaw strengths

$$F_{S(t)}(\sigma) \propto \sigma^{m + \frac{3m}{n-2}} \quad (6.2)$$

when the loading rate is slow to moderate, while

$$F_{S(t)}(\sigma) \propto \sigma^m \quad (6.3)$$

when the loading rate is very fast. Here, m and n refer to the corresponding Pareto flaw size distribution shape parameter and the stress corrosion parameter, respectively. It was found that the GFPM "grossly underestimates" the probability of failure compared to the Crack Growth Model. Hence, different implementations of Charles' (1958*b*) Stress Corrosion Rate Theory do not produce comparable results. This highlights the complexity involved in the modelling of subcritical crack growth.

In Reid (2006), the performance of the GFPM when applied to sinusoidal load cases was investigated. The conclusion was drawn that the GFPM "does not provide a dependable basis for assessing the effects of dynamic wind loading." This result is directly connected to the methodology by which stress corrosion is implemented in the GFPM. Hence, it can be said that the GFPM "can give dependable results only for standardized load conditions." (Reid 2007)

6.6 ERROR SOURCES

Concerning the measurements of strength, there can be a range of error sources that impact the results recorded in the various experiments other than errors in the measurement devices and setups, cf. Chap. 4. In a three-point bending setup, the fracture stress at the failure origin is generally smaller than the maximum bending stress. This is so because generally speaking, the fracture origin is located at some distance away from the midpoint where the load is introduced and the bending stress is the greatest. The results from three-point bending tests do therefore not record the strength in a way that is directly comparable to other common testing devices. The utility of the three-point bending device as a tool for appraising the strength of glass is questioned.

In the case of four-point bending, the stress concentration that occurs under the load introduction points was sometimes taken into account (Vandebroek et al. 2014), but most often not. When the stress concentration was not taken into account in the in-plane bending mode, an error at about 5% can be assumed for the recorded value. There can be an error of up to 11% in the out-of-plane bending mode, depending on the thickness, when the fracture origin is located along the edge and the Bernoulli beam theory is employed, Eq. (3.5), according to Blank et al. (1994). Moreover, when the deflections become large in four-point bending, the inner rollers that transmit the loading shift outwards and the outer rollers shift inwards, supposing that rollers are used at the supports. This produces an error of less than 1% (Munz & Fett 1999).

The float process allows for the production of flat glass panes with a very smooth and flat surface. The value of the section modulus is proportional to the width and to the square of the thickness of the rectangular cross section. When the thickness was recorded by the experimenter, it was usually determined by taking the average of several measurements along the length and width of the specimen. In doing so, the error was minimized. In the case of tempered glass, however, there can be small warping of the sheet and unevenness to the thickness. In this work only annealed float glass was considered. The error involved in estimating the section modulus is assumed to be negligible.

When the fracture stress is calculated based on strain gauge measurements or with the finite element method, knowledge is required of the material properties, viz. the Young's modulus E and the Poisson's ratio ν . There are uncertainties in the value of the elastic constants, mainly of the Young's modulus. In some experiments, the elastic constants were estimated based on dedicated measurements of the compliance of glass plates obtained from the same supplier. In this way, e.g. Carre (1996) arrived at the mean value of $E = 70.7$ GPa for the test specimens. However, in other experiments, the elastic constants were not measured directly but were assumed based on values obtained from the literature. According to the

various sources in the literature that were surveyed by this author, the value for the Young's modulus ranges from 68.9 GPa to 75 GPa (Le Bourhis 2008, Simiu et al. 1984). The value of ν is either 0.22 or 0.23.

It is assumed that there exists a small error due to uncertainties in the applied load and in the dimensions of the bending rig fixture, e.g. in the dimensions of the loading rings in the case of the ring-on-ring device. It is assumed that these errors amount to no more than 5%.

The calculation method governs, to some extent, which strength value is produced. Compared to the analytical formulae, Eqs. (3.4) to (3.9), the finite element method is able to better model the geometrically nonlinear effects that can occur especially due to plate bending when membrane stresses are activated. It can be assumed that membrane stress activation becomes significant when the deflection exceeds half the specimen thickness. Sometimes, a mixture of methods were used, such as when the stress concentrations under the load introduction points in four-point bending were estimated with the finite element method while in general, the bending stress was calculated with the analytical formula, Eq. (3.5).

In practice, deviations from the assumption of a ramp stress history can occur. For instance, it was reported in several references (Calderone 1999, Johar 1982) that the electronics of the hydraulically controlled loading device that was designed to apply a linearly increasing load in fact caused harmonic oscillation toward the load history. This could have a bearing on the calculation to adjust for static fatigue, Eq. (2.28). The possible deviations, however, are minor and are assumed to have only a negligible effect on the calculated "equivalent" strength.

In most of the reviewed experiments, bending was applied with deformation control. However, in a few cases, the bending was produced using force control. It is not believed that this difference in setup would cause any significant error since the nonlinear effects are small.

There could be variations to the strength depending on the manufacturing site including variations in surface precompression from one batch to another. This effect is hard to quantify a priori, but it might be substantial. Even in float glass which has been annealed there can be small amounts of compressive residual stresses on the surface. This could have an impact on the measured fracture stress. When compressive residual stresses are present on the surface, the strength increases.

Some experiments (Krohn et al. 2002, Tummala & Foster 1975) indicate that the tin side of the float glass contains more severe flaws than the air side. This could have an impact on the measured strength. It may be that data recorded from fractures originating on the tin side are not directly comparable to the air side. However, it may be that this effect is limited and moreover overlapped by other uncertainties. The float process production method causes the diffusion of tin into

the surface that was in contact with the molten tin bath. The depth of the tin penetration layer is generally accepted to range from 10 to 40 microns (Krohn et al. 2002). However, whether it is the tin diffusion or the contact damage caused by the rollers as the glass exits the float that is responsible for the difference in strength that is sometimes observed between the air and tin sides is an unresolved question.

7

Summary of appended publications

7.1 PAPER A

Performance of standard statistical distributions for modelling glass fracture

David Kinsella, Johan Lindström, Kent Persson.

Accepted for publication in the International Journal of Structural Glass and Advanced Materials Research.

Summary

A comparison was made between four standard distributions, the normal, lognormal, Gumbel and Weibull, with respect to the performance in modelling the strength of new annealed float glass. The performance was evaluated based on experimental data on the strength of glass plates tested in an ambient environment. The Weibull distribution outperforms the normal and lognormal distributions and is at least as good as the Gumbel distribution as a model for glass strength when the fracture data is selected to comprise edge only failure origins. In the case of surface only failure origins, it is indicated that the extreme value distributions perform worse than the normal and lognormal distributions. However, the surface strength is complicated to model and none of the standard distributions which were examined are capable of producing a proper model. The sample size also has a profound

impact on the performance of the surface strength models.

Contributions by David Kinsella

David Kinsella was the main author of the paper and he planned the research tasks, surveyed the literature for experimental data, performed the statistical analysis, and drew the conclusions that were presented.

7.2 PAPER B

A numerical method for analysis of fracture statistics of glass and simulations of a double ring bending test.

David Kinsella, Kent Persson.

In: Glass Structures & Engineering, Vol. 3(2): 139-152. Springer, 2018.

Summary

The fracture stress and failure locations of small glass plates subjected to double ring bending are calculated with a numerical method that considers the stochastic properties of surface microcracks. The method involves the weakest-link principle and a fracture mechanics approach to brittle failure. The results are compared with experimental data from a double ring bending test. The numerical method is dependent on a representation of the surface flaws condition in glass. Two types of flaw distribution are considered in this paper. First, a Pareto distributed flaw size distribution is implemented. Second, two populations of flaws are implemented as a combination of a Pareto flaw size distribution and a Fréchet size distribution. The logical basis for the selected flaw size distributions depend on empirical results as well as extreme value theoretical arguments. However, depending on the chosen representation of the surface flaws condition, a number of parameter values have to be estimated in order for the model to work. There is a need for more data on the surface condition in glass. A distribution for the strength that is indistinguishable from a Weibull distribution is obtained when a single population of Pareto distributed crack sizes are implemented. This distribution, however, makes a poor fit with the experimental data that was compared with. With the dual populations concept a model for the strength is obtained that better fits the apparent bimodality in the empirical data set. The effect of using different fracture criteria is investigated. However, the incorporation of mode II shearing displacement into the fracture criterion has only a minor impact on the simulated strength distribution when the glass is subjected to double ring bending. When new and improved

techniques become available for examining the surface characteristics of glass, this type of numerical simulation tool can lead to improved strength models.

Contributions by David Kinsella

David Kinsella was the main author of the paper and he planned the research tasks, performed the finite element modelling and analyses, implemented the numerical procedure for the statistical evaluation, and drew the conclusions that were presented.

7.3 PAPER C

An analysis of glass fracture statistics

David Kinsella, Kent Persson.

In: The proceedings of the Challenging Glass Conference 6, Delft. 2018.

Summary

A numerical method is applied to model the fracture stress and failure location in glass panes subjected to various forms of loading. The method is based on a stochastic approach to brittle failure in glass assuming the weakest-link principle and a Pareto distributed flaw size distribution. The fracture stress and failure origin are revealed through a search algorithm. The stresses in large laterally supported plates which are subjected to uniform pressure are modelled and the distribution of fracture location is determined. Two types of gasket support materials are considered, neoprene and nylon. The softer gasket material produces a greater number of fractures nearer the corners of the plate. A comparison is made with the recorded fracture locations according to various experiments. In addition, a tall vertical panel of laminated glass subjected to dynamic impact loading is modelled and the distribution of fracture location is determined.

Contributions by David Kinsella

David Kinsella was the main author of the paper and he planned the research tasks, performed the finite element modelling and analyses, implemented the numerical procedure for the statistical evaluation, and drew the conclusions that were presented.

7.4 PAPER D

Survey of experimental data on the strength of annealed float glass panes in the as-received condition tested in an ambient atmosphere

David Kinsella.

In: Report TVSM-7166, published on the website of the Division of Structural Mechanics in July 2018.

Summary

A survey of the literature was performed in order to collect and organize the experimental data that is available on the strength of ordinary annealed float glass that is in the as-received condition and which was tested in an ambient environment. A detailed overview is provided which comprises experiments conducted in the past four decades. The experiments were conducted with the coaxial double ring bending device, the three-point bending device, the four-point bending device, and the arrangement that allows for laterally supported plates to be subjected to uniform pressure. When the stress history was linear, the 2 MPa s^{-1} stress rate-equivalent strength was calculated and compared with the nominal value of the strength. The strength is visualized in the form of boxplots and probability plots. The following three types of probability plots were considered, viz. the Weibull, the normal, and the lognormal. The goodness-of-fit was tested numerically with the Anderson-Darling statistic.

Contributions by David Kinsella

David Kinsella was the author of the report and he planned the research tasks, collected the data and organized the results.

8

Conclusions and further research needs

The following conclusions can be drawn.

- The edge strength warrants special consideration because in most practical situations, the boundary conditions cause significant tensile stresses to act along the edges.
- The experimental data from laterally supported plates subjected to uniform pressure demonstrate that on average about one in every third fracture occurred along one of the edges.
- The Weibull distribution provides a basic model for the edge strength that performs better than the normal and lognormal distributions and at least as well as the extreme-value Gumbel distribution.
- In the case of surface fractures in glass, neither the extreme-value Weibull and Gumbel distributions nor the normal and lognormal distributions are able to model the strength.
- In the case of monolithic annealed float glass in the as-received condition that was tested in an ambient environment, a record for the strength could be obtained from the scientific literature published over that past 40 years for nearly 200 samples comprising some 3100 individual test specimens.

- There exist a multitude of strength models which have been used on glass and these can be divided into 1) models with a phenomenological approach towards failure where failure is considered at the macroscopic level and no particular representation of the surface condition is assumed, and 2) models which consider fracture at the microscopic level by supposing the preexistence of material flaws from which failure is derived.
- Flaws in glass can be represented more or less rigorously with stochastic cracks of a certain shape, size and orientation, or flaws can be represented by an elemental strength distribution.
- The flaw size approach is currently an emerging trend magnified by the computational power that is available and which makes it feasible to determine the strength in Monte Carlo simulations with stochastic Griffith flaws.
- The models based on a flaw size approach are challenged by the fact that the knowledge about the surface condition in glass is very limited and moreover, there is a lack of methods by which to investigate the flaws.
- The flaw size approach can be used to model the strength of small plates in double ring bending with a dual flaw population concept.
- With a numerical method based on the flaw size approach, it is possible to model the fracture stress and failure origins in glass articles with complex geometries and which are subject to static loads as well as dynamic impact loads.

The following should be considered in future research.

- An in-depth investigation and analysis of the edge strength and its dependencies. This involves studying the effect of factors such as the thickness, the type of edge processing, the load rate and duration, and the edge support span.
- It is relevant to further consider size effects in glass, both how the various models that were investigated in this work relate to size effects and what the combined set of empirical data on the strength of glass has to tell about size effects.
- The elemental strength approach emerges as an interesting approach for further investigation. The flaw size approach is more stringent when it comes to representing the surface condition rigorously. This turns into a liability due to the lack of techniques by which to probe the surface flaws. The elemental strength approach is more stringent than the application of standard statistical distributions, but it is somewhat less stringent in terms of realism in the representation of flaws than the flaw size approach.

- There is a need for greater insight into the surface condition in glass. This would involve new methods and improved technology by which to probe the surface flaws.
- None of the strength models covered in this work have so far been applied to model glass edge and surface strength simultaneously while considering the potential differences in condition between edge and surface. This is a topic for future research.

References

- Anderson, T. W. & Darling, D. A. (1952), ‘Asymptotic Theory of Certain ”Goodness of Fit” Criteria Based on Stochastic Processes’, *Ann. Math. Statist.* (2), 193–212.
- Arrhenius, S. A. (1889), ‘Über die Reaktionsgeschwindigkeit bei der Inversion von Rohrzucker durch Säuren’, *Z. Physik. Chem.* **4**, 226–248.
- ASTM C 1036-01 (2011), ‘Standard Specification for Flat Glass’, American Society for Testing Materials.
- Baker, T. C. & Preston, F. W. (1946*a*), ‘Fatigue of Glass under Static Loads’, *J Appl Phys* **17**, 170–178.
- Baker, T. C. & Preston, F. W. (1946*b*), ‘The Effect of Water on the Strength of Glass’, *J Appl Phys* **17**, 179–188.
- Batdorf, S. & Crose, J. (1974), ‘A statistical theory for the fracture of brittle structures subjected to nonuniform polyaxial stresses’, *J Appl Mech* **41**(2), 459–464.
- Beason, W. L. (1980), *A Failure Prediction Model for Window Glass*, NTIS Accession no. PB81-148421, Texas Tech University, Institute for Disaster Research.
- Beason, W. L. & Morgan, J. R. (1984), ‘Glass Failure Prediction Model’, *J Struct Eng* **110**, 197–212.
- Beirlant, J., Goegebeur, Y., Teugels, J., Segers, J., De Waal, D. & Ferro, C. (2004), *Statistics of Extremes – Theory and Applications*, John Wiley & Sons, Ltd.
- Blank, K. (1993), *Dickenbemessung von vierseitig gelagerten rechteckigen Glasscheiben unter gleichförmiger Flächenlast*, Vol. 3, 2 edn, Institut für Konstruktiven Glasbau, Gelsenkirchen.
- Blank, K., Duerkop, D., Durchholz, M., Grueters, H., Helmich, G. & Senger, W. (1994), ‘Strength tests of flat glass by means of four-point bending’, *Glastechnische Berichte* **67**, 9–15.

- Bonati, A., Occhiuzzi, A., Pisano, G. & Royer-Carfagni, G. (2018), ‘A micro-mechanically motivated model for the strength of heat-treated glass’, *Glass Struct Eng* **3**, 153–166.
- Broek, D. (1983), *Elementary Engineering Fracture Mechanics*, 3 edn, Martinus Nijhoff Publishers, The Hague.
- Brown, W. G. (1972), A load duration theory for glass design, Technical Report NRCC 12354, National Research Council of Canada.
- Calderone, I. (1999), The equivalent wind loading for window glass design, PhD thesis, Monash University.
- Calderone, I., MacDonald, C., Jacob, L. & Jacob and Associates Pty Ltd (2001), The Fallacy of the Weibull Distribution for Window Glass Design, in ‘Glass Performance Days 2001’, pp. 293–297.
- Carre, H. (1996), Etude du comportement à la rupture d’un matériau fragile précontraint : le verre trempé, Phd thesis, Ecole Nationale des Ponts et Chaussées.
- Charles, R. J. (1958*a*), ‘Static Fatigue of Glass I’, *J Appl Phys* **29**, 1549–1553.
- Charles, R. J. (1958*b*), ‘Static Fatigue of Glass II’, *J Appl Phys* **29**, 1554–1560.
- Charles, R. J. & Hillig, W. B. (1962), The kinetics of glass failure by stress corrosion, in ‘Symposium on Mechanical Strength of Glass and Ways of Improving it’, pp. 511–527.
- Culf, C. J. (1957), ‘Fracture of Glass under Various Liquids and Gases’, *J. Soc. Glass Tech.* **41**, 157.
- D’Agostino, R. B. & Stephens, M. A., eds (1986), *Goodness-of-fit Techniques*, Marcel Dekker, Inc., New York, NY, USA.
- Dalgliesh, W. A. & Taylor, D. A. (1990), ‘The strength and testing of window glass’, *Can J Civ Eng* **17**, 752–762.
- Danzer, R. (1992), ‘A General Strength Distribution Function for Brittle Materials’, *J Eur Ceram Soc* **10**, 461–472.
- Danzer, R. (1994), ‘Ceramics: Mechanical Performance and Lifetime Prediction’, *The Encyclopedia of Advanced Materials* **1**, 385–398.
- Danzer, R., Lube, T. & Supancic, P. (2001), ‘Monte Carlo Simulations of Strength Distributions of Brittle Materials - Type of Distribution, Specimen and Sample Size’, *Z. Metallkd.* **92**, 773–783.

- Danzer, R., Supancic, P., Pascual Herrero, J. & Lube, T. (2007), 'Fracture Statistics of Ceramics - Weibull Statistics and Deviations from Weibull Statistics', *Eng Fract Mech* **74**, 2919–2932.
- De Jayatilaka, A. & Trustrum, K. (1977), 'Statistical approach to brittle fracture', *J Mater Sci* **12**, 1426–1430.
- DIN 18008-1 (2010), 'Glas im Bauwesen - Bemessungs- und Konstruktionsregeln - Teil 1: Begriffe und allgemeine Grundlagen.', CEN.
- EN 1288-2 (2000), 'Glass in building - Determination of the bending strength of glass - Part 2: Coaxial double ring test on flat specimens with large test surface areas', CEN.
- EN 1288-5 (2000), 'Glass in building - Determination of the bending strength of glass - Part 5: Coaxial double ring test on flat specimens with small test surface areas', CEN.
- EN 572-1 (2004), 'Glass in building - Basic soda lime silicate glass products - Part 1: Definitions and general physical and mechanical properties.', CEN.
- Evans, A. G. (1974), 'Slow crack growth in brittle materials under dynamic loading conditions', *Int J Fracture* **10**, 251–259.
- Fink, A. (2000), Ein Beitrag zum Einsatz von Floatglas als dauerhaft tragender Konstruktionswerkstoff im Bauwesen, Phd thesis, TU-Darmstadt.
- Fischer-Cripps, A. C. & Collins, R. E. (1995), 'Architectural glazings: Design standards and failure models', *Building and environment* **30**, 29–40.
- Forbes, C., Evans, M., Hastings, N. & Peacock, B. (2011), *Statistical distributions*, 4 edn, John Wiley and sons, Inc.
- Freiman, S. W., White, G. S. & Fuller, E. R. (1985), 'Environmentally Enhanced Crack Growth in Soda-Lime Glass', *J Am Ceram Soc* **68**(3), 108–112.
- Freudenthal, A. M. (1968), *Statistical Approach to Brittle Fracture*, Vol. II of *Fracture*, Academic Press, New York.
- Gehrke, E., Ullner, C. & Hähner, M. (1991), 'Fatigue limit and crack arrest in alkali-containing silicate glasses', *J. Mater. Sc.* **26**, 5445–5455.
- Gorski, A. (1969), 'Beware of the Weibull Euphoria', *Reliability, IEEE Transactions on* **17**, 202–203.
- Grenet, L. (1899), 'Mechanical Strength of Glass', *Bull. Soc. Enc. Industr. Nat. Paris* **4**, 838–48.

- Griffith, A. (1920), 'The Phenomena of Rupture and Flow in Solids', *Phil. Trans. R. Soc.* **A221**, 163.
- Gumbel, E. J. (1954), *Statistical theory of extreme values and some practical applications: a series of lectures*, Applied mathematics series, U. S. Govt. Print. Office.
- Gut, A. (1995), *An intermediate course in probability*, Springer.
- Haldimann, M. (2006), Fracture strength of structural glass elements – analytical and numerical modelling, testing and design, Phd thesis, Ecole Polytechnique Fédérale de Lausanne EPFL.
- Hellen, T. K. & Blackburn, W. S. (1975), 'The Calculation of Stress Intensity Factors for Combined Tensile and Shear Loading', *Int J Fract* **11**, 605.
- Hess, R. (2000), *Glasträger*, Forschungsbericht 20, ETH Zürich. Institut für Hochbautechnik, Zürich, Switzerland.
- Holzapfel, G. (2000), *Nonlinear solid mechanics*, Wiley.
- Huerta, M. C., Pacios-Alvarez, A., Lamela-Rey, M. J. & Fernandez-Canteli, A. (2011), Influence of experimental test type on the determination of probabilistic stress distribution, in 'Glass Performance Days 2011'.
- Inglis, C. E. (1913), 'Stresses in a Plate due to the Presence of Cracks and Sharp Corners', *Trans. Inst. Naval. Archit.* **55**, 219.
- Irwin, G. (1958), Fracture, in 'Handbuch der Physik', Vol. 6, Springer, p. 551.
- Irwin, G. R. (1957), 'Analysis of Stresses and Strains Near the End of a Crack Traversing a Plate', *J. Appl. Mech.* **24**, 361.
- Johar, S. (1981), Dynamic fatigue of flat glass - Phase II, Technical report, Ontario Research Foundation, Department of Metals, Glass and Ceramics.
- Johar, S. (1982), Dynamic fatigue of flat glass - Phase III, Technical report, Ontario Research Foundation, Department of Metals, Glass and Ceramics.
- Kanabolo, D. C. & Norville, H. S. (1985), The strength of new window glass using surface characteristics, Master's thesis, Texas Tech University.
- Kinsella, D. (2018), Survey of experimental data on the strength of annealed float glass panes in the as-received condition tested in an ambient atmosphere, Technical Report TVSM-7166, Division of Structural Mechanics, Lund University.
- Kinsella, D., Lindström, J. & Persson, K. (2018), 'Performance of standard statistical distributions to model glass fracture', *Submitted for review*.

- Kinsella, D. & Persson, K. (2016), On the applicability of the Weibull distribution to model annealed glass strength and future research needs, *in* ‘Challenging Glass Conference 5’, Ghent, Belgium.
- Kinsella, D. & Persson, K. (2018*a*), An Analysis of Glass Fracture Statistics, *in* ‘Challenging Glass Conference 6’, Delft, The Netherlands.
- Kinsella, D. T. & Persson, K. (2018*b*), ‘A numerical method for analysis of fracture statistics of glass and simulations of a double ring bending test’, *Glass Structures & Engineering* **3**(2), 139–152.
- Kirstein, A. & Woolley, R. (1967), ‘Symmetrical bending of thin circular elastic plates of equally spaced point supports’, *J Res Natl Bur Stds* **71C**, 1–10.
- Kleuderlein, J., Ensslen, F. & Schneider, J. (2014), Investigation of edge strength dependent on different types of edge processing, *in* ‘Engineered Transparency. International Conference at Glasstec’, Düsseldorf, Germany.
- Kozłowski, M. (2014), Experimental and numerical analysis of hybrid timber-glass beams, Phd thesis, Silesian University of Technology.
- Krohn, M. H., Hellmann, J. R., Shelleman, D. L. & Pantano, C. D. (2002), ‘Biaxial flexure strength and dynamic fatigue of soda-lime-silica float glass’, *J. Am. Ceram. Soc.* **85**(7), 1777–1782.
- Lamon, J. (2016), *Brittle Fracture and Damage for Brittle Materials and Composites*, Elsevier.
- Lawn, B. (1993), *Fracture of Brittle Solids*, Cambridge Solid State Science Series, 2nd edn, Cambridge University Press, Cambridge, UK.
- Le Bourhis, E. (2008), *Glass*, Wiley-VCH Verlag GmbH & Co KGaA, Weinheim.
- LeVeque, W. J. (1977), *Fundamentals of Number Theory*, Dover Publications, Inc.
- Lindqvist, M. (2013), Structural Glass Strength Prediction Based on Edge Flaw Characterization, Phd thesis, Ecole Polytechnique Fédérale de Lausanne EPFL.
- Lü, B.-T. (1997), ‘Fatigue strength prediction of soda-lime glass’, *Theor Appl Fract Mec* **27**, 107–114.
- Matthews, J. R., McClintock, F. A. & Shack, W. J. (1976), ‘Statistical determination of surface flaw density in brittle materials’, *J. Am. Ceram. Soc.* **59**, 304–308.
- McLellan, G. W. & Shand, E. B. (1984), *Glass engineering handbook*, McGraw-Hill.
- Mencik, J. (1992), *Strength and Fracture of Glass and Ceramics*, Vol. 12 of *Glass Science and Technology*, Elsevier.

- Mesarovic, S., Gasparini, D., Muju, S. & McNelis, M. (1992), ‘Probability of crack growth in Poisson field of penny cracks’, *J Eng Mech* **118**(5), 961–978.
- Mould, R. E. & Southwick, R. D. (1959), ‘Strength and Static Fatigue of Abraded Glass Under Controlled Ambient Conditions: II, Effect of Various Abrasions and the Universal Fatigue Curve’, *J Am Ceram Soc* **42**(12), 582–592.
- Muniz-Calvente, M., Ramos, A., Pelayo, F., Lamela, M. J. & Fernández-Canteli, A. (2016), ‘Statistical joint evaluation of fracture results from distinct experimental programs: An application to annealed glass’, *Theor Appl Fract Mec* **85**(Part A), 149–157.
- Munz, D. & Fett, T. (1999), *Ceramics. Mechanical Properties, Failure Behaviour, Materials Selection*, Materials Science, Springer.
- Natividad, K., Morse, S. M. & Norville, H. S. (2016), ‘Fracture Origins and Maximum Principal Stresses in Rectangular Glass Lites’, *J Archit Eng* **22**(2), –1—-1.
- Navarrete, B., Juarez, H., Olmos, L., Guerrero, J. & Garnica, P. (2016), ‘Failure behavior of annealed glass for building windows’, *Eng Struct* **141**, 417–426.
- Newman, J. C. & Raju, I. S. (1981), ‘An empirical stress intensity factor equation for the surface crack’, *Eng. Fract. Mech.* **15**, 185–192.
- Orowan, E. (1949), ‘Fracture and strength of solids’, *Rep Prog Phys* **12**(1), 185.
- Osnes, K., Børvik, T. & Hopperstad, O. (2018a), Shock Tube Testing and Modelling of Annealed Float Glass, in ‘12th International DYMAT Conference’, Archon, France.
- Osnes, K., Børvik, T. & Hopperstad, O. (2018b), ‘Testing and modelling of annealed float glass under quasi-static and dynamic loading’, *Eng Fract Mech* .
- Osnes, K., Hopperstad, O. & Børvik, T. (2018), Quasi-static and Dynamic Testing of Annealed Float Glass, in ‘18th International Conference on Experimental Mechanics (ICEM18)’, Brussels, Belgium.
- Ottosen, N. & Petersson, H. (1992), *Introduction to the finite element method*, Prentice Hall.
- Overend, M. (2002), The appraisal of structural glass assemblies, PhD thesis, University of Surrey.
- Pathirana, M., Lam, N., Perera, S., Zhang, L., Ruan, D. & Gad, E. (2017), ‘Risks of failure of annealed glass panels subject to point contact actions’, *Int J Solids Struct* **129**, 177–194.

- Pisano, G. & Royer-Carfagni, G. (2017), ‘A micromechanical derivation of the macroscopic strength statistics for pristine or corroded/abraded float glass’, *J Eur Ceram Soc* **37**, 4197–4206.
- Poloniecki, J. (1974), Statistical investigation of surface flaws, Phd thesis, The University of Sussex.
- Poloniecki, J. D. & Wilshaw, T. R. (1971), ‘Determination of Surface Crack Size Densities in Glass’, *Nature Physical Science* **229**, 226–227.
- Porter, M. (2001), Aspects of Structural Design with Glass, Phd thesis, University of Oxford.
- Postigo, S. (2010), Estudio teorico experimental de impactos humanos contra vidrios de acristalamientos de edificacion, PhD thesis, Universidad de Politecnica de Madrid.
- prEN 16612 (2017), ‘Glass in building - Determination of the lateral load resistance of glass panes by calculation’, CEN.
- Reid, S. (1991), Flaws in the Failure Prediction Model of Glass Strength, in ‘Sixth International Conference on Applications of Statistics and Probability in Civil Engineering’, pp. 111–117.
- Reid, S. (2006), Effect of spatial distribution of flaws on glass ring-on-ring test strengths, in ‘International Forum on Engineering Decision Making’, Lake Louise, Canada.
- Reid, S. G. (2007), ‘Effects of spatial variability of glass strength in ring-on-ring tests’, *Civ Eng Environ Syst* **24**, 139–148.
- Rinne, H. (2009), *The Weibull Distribution – A Handbook*, Taylor & Francis Group.
- Robins, R. (1962), ‘On models for reliability prediction’, *IRE Transactions on reliability and quality control* **11**(1), 33–43.
- Rufin, A., Samos, D. & Bollard, R. (1984), ‘Statistical prediction models for brittle materials’, *AIAA Journal* **22**(0.1), 135–140.
- Schula, S. (2015), *Charakterisierung der Kratzanfälligkeit von Gläsern im Bauwesen*, Springer.
- Sglavo, V. M., Muller, C. & Righetti, F. (2007), Influence of edge finishing on the resistance to thermal stresses of float glass, in ‘Glass Performance Days 2007’.
- Simiu, E., Reed, D., Yancey, C., Martin, J., Hendrickson, E., Gonzalez, A., Koike, M., Lechner, J. & Batts, M. (1984), Ring-on-ring tests and load capacity of cladding glass, Technical report, NBS Building Series 162, U.S. Department of Commerce – National Bureau of Standards.

- Tada, H., Paris, P. C. & Irwin, G. R. (2000), *The stress analysis of cracks handbook*, The American Society of Mechanical Engineers.
- Tandon, R., Paliwal, B. & Gibson, C. (2013), ‘Practical aspects of using Hertzian ring crack initiation to measure surface flaw densities in glasses: influence of humidity, friction and searched areas’, *Philos Mag* **93**, 2847–2863.
- Thiemeier, T., Brückner-Foit, A. & Kölker, H. (1991), ‘Influence of the fracture criterion on the failure prediction of ceramics loaded in biaxial flexure’, *J. Am. Ceram. Soc.* **74**(1), 48–52.
- Tooley, F. V. (1984), *The handbook of glass manufacture*, 3 edn, Books for the glass industry division Ashlee Publishing Co., Inc.
- Trustrum, K. & De Jayatilaka, A. (1983), ‘Applicability of Weibull analysis for brittle materials’, *J Mater Sci* **18**, 2765–2770.
- Tummula, R. R. & Foster, B. J. (1975), ‘Strength and dynamic fatigue of float glass surfaces’, *J. Am. Ceram. Soc.* **58**(3–4), 156–157.
- Vallabhan, C. & Wang, B.-T. (1981), Nonlinear analysis of rectangular glass plates by finite difference method, Technical report, Institute for disaster research, Texas Tech University, Lubbock, Tex.
- Vandebroek, M., Belis, J., Louter, C. & Tendeloo, G. V. (2012), ‘Experimental validation of edge strength model for glass with polished and cut edge finishing’, *Eng Fract Mech* **96**, 480–489.
- Vandebroek, M., Louter, C., Caspeelee, R., Ensslen, F. & Belis, J. (2014), ‘Size effect model for the edge strength of glass with cut and ground edge finishing’, *Eng Struct* **79**, 96–105.
- Varshneya, A. (1994), *Fundamentals of Inorganic Glasses*, Academic Press.
- Vasilchenko-Malishev, G. & Chesnokov, S. (2018), Zaryadye Park, Glass Grid Shell Roof, in ‘Challenging Glass Conference 6’, Delft, The Netherlands, pp. 671–680.
- Veer, F. A. (2007), ‘The strength of glass, a nontransparent value’, *HERON* **52**, 87–104.
- Veer, F. A., Louter, C. & Bos, F. P. (2009), ‘The strength of annealed, heat-strengthened and fully tempered float glass’, *Fatigue Fract Eng M* **32**, 18–25.
- Veer, F. A., Louter, P. C. & Romein, T. (2006), Quality control and the strength of glass, in ‘ECF 16 conference’.
- Veer, F. A. & Rodichev, Y. M. (2011), ‘The structural strength of glass: Hidden damage’, *Strength Mater+* **43**, 302–315.

- Veer, F. A. & Rodichev, Y. M. (2012), The strength of water jet cut glass, *in* 'Glass Performance Days 2011', pp. 434–438.
- Weibull, W. (1939), 'A Statistical Theory of the Strength of Materials', *Ingenjörsvetenskapsakademiens handlingar* **151**.
- Weibull, W. (1959), 'A Statistical Distribution Function of Wide Applicability', *ASME Journal of Applied Mechanics* pp. 293–297.
- Wereszczak, A., Ferber, M. & Musselwhite, W. (2014), 'Method for Identifying and Mapping Flaw Size Distributions on Glass Surfaces for Predicting Mechanical Response', *Int J Appl Glass Sci* **5**, 16–21.
- Westergaard, H. (1939), 'Bearing Pressures and Cracks', *J Appl Mech* **6**, A49–53.
- Wiederhorn, S. M. (1967), 'Influence of Water Vapor on Crack Propagation in Soda-Lime Glass', *J. Am. Ceram. Soc.* **50**, 407–417.
- Wiederhorn, S. M. & Tornsand, P. (1970), 'Crack healing in glass', *J. Am. Cer. Soc.* **53**, 486–489.
- Yankelevsky, D. (2014), 'Strength prediction of annealed glass plates – A new model', *Eng Struct* **79**, 244–255.
- Yankelevsky, D., Spiller, K., Packer, J. & Seica, M. (2017), 'Fracture characteristics of laboratory-tested soda lime glass specimens', *Can J Civ Eng* **44**, 151–160.
- Young, G. A. & Smith, R. L. (2005), *Essentials of Statistical Inference*, Cambridge Series in Statistical and Probabilistic Mathematics, Cambridge University Press.

Part II

Appended publications

Paper A



Performance of Standard Statistical Distributions for Modeling Glass Fracture

¹David Kinsella, ²Johan Lindström and ¹Kent Persson

¹Construction Sciences, Lund University, Sweden

²Centre for Mathematical Sciences, Lund University, Sweden

Article history

Received: 07-06-2018

Revised: 13-07-2017

Accepted: 2-08-2018

Corresponding Author:

David Kinsella

Construction Sciences,
Lund University, Sweden

Email:

david.kinsella@construction.lth.se

Abstract: Experimental data on the strength of new annealed float glass tested in an ambient environment was collected. A comparison was made between four standard distributions, the normal, lognormal, Gumbel and Weibull, with respect to the performance in modelling the strength. The Weibull distribution outperformed the normal and lognormal distributions when the data contained edge only failure origins. When the data was selected to contain surface only failure origins it is indicated that the extreme value distributions performed poorly. The Weibull model is known to have a basis in a failure-mechanism concept based on the weakest-link principle. The Gumbel distribution can also be derived from failure-based mechanics and be associated with certain types of flaw size distribution. The Weibull model, however, is a better choice for a failure model of glass edge strength compared to the normal and lognormal distributions and at least as good as a Gumbel distribution. The surface strength is complicated to model and none of the standard distributions which were examined are capable of producing a proper model. The sample size also has a profound impact on the performance of the surface strength models.

Keywords: Glass, Strength, Fracture statistics, Weibull distribution

Introduction

The normal distribution was previously used by glass manufacturers to model the fracture stress. In e.g., the early Pilkington design charts, the design stress was based on the 1%-fractile of a normal distribution with a coefficient of variation of 0.20 (Calderone, 1999). Today, the Weibull distribution is commonly used to model the fracture stress data from experiments on glass. However, a number of researchers have questioned whether the Weibull distribution is in fact superior to an ordinary normal or lognormal distribution as a model of the fracture stress in glass. Based on the test results of a large set of full-size rectangular plates of both new and old annealed float glass, Calderone (1999) found that the lognormal distribution provided a better fit with the experimental data than the Weibull distribution. The lognormal distribution has support on the right half axis only and that gives it a logical advantage over the normal distribution because the strength is a positive number. Later studies by Calderone *et al.* (2001) and Calderone *et al.* (2005)

recommended that the Weibull distribution should in fact not be used to predict the strength of window glass panels. However, the 32 samples of data in Calderone (1999) were of limited size ranging from 5 to 9 specimens each. Lü (1997) carried out tests on glass in three-point and four-point bending and concluded, based on the correlation coefficient of the fitted line in the probability plots, that all three standard distributions, i.e., the normal, lognormal and Weibull, were applicable as failure models. Veer *et al.* (2009) carried out tests on glass beams in four-point bending and concluded that on the one hand, the lognormal distribution provided a fit that was at least as good as the Weibull model. On the other hand, it was concluded that none of the standard distributions properly modelled the data on annealed glass.

So far and to the best of our knowledge, no one has made a comparison of the standard distributions based on a comprehensive survey of the published data results that are available in the open literature. In fact, a substantial portion of the total number of experiments that have been reported were conducted only recently within the last decade.

Moreover, it is sometimes believed that the edge strength in glass differs from the surface strength. This is reflected in the structural standards in different ways. For example, DIN 18008:2010 gives a reduction factor to be applied when calculating the edge strength, the factor of which is 0.8. Hence, the edge condition is always considered to be inferior to the surface condition. On the other hand, prEN 16612:2017 provides a different set of reduction factors for the edge strength depending on the edge treatment, i.e., cut, arised, ground, or polished. In the case of the polished edge, the edge reduction factor is unity which amounts to no reduction at all. This implies that the polished edge condition is considered to be equal to the pristine surface. In summary it is possible then, but not self-evident perhaps, that different models should be used for the edge and surface fractures in glass.

The question of which standard distribution that provides the best fit has important implications. Currently, there is a draft for a European standard for strength of glass in building, prEN 16612:2017, that bases its estimate of the characteristic value of the strength of glass on test results that were fitted with a Weibull distribution. The characteristic value of the bending strength is defined from the 5% fractile in the distribution for monolithic panes of annealed float glass.

In this study, the performance of the following four standard statistical distributions is examined, viz. the normal, lognormal, Gumbel and Weibull distributions.

Standard Distributions

A Weibull distribution with the parameter values $m = 6$ and $k = 74$ MPa was fitted to test results on annealed float glass specimens that were performed as a basis for the DIN 1249-10:1990 (Haldimann, 2006). The tests were carried out using the R400 double ring bending device at a stress rate of approximately 2 MPa s^{-1} . The characteristic value of the bending strength was estimated at 45 MPa which was the 5% fractile in the distribution. This value was subsequently adopted in the draft standard which currently is referred to as prEN 16612:2017.

The Weibull distribution (Weibull, 1939) has the cumulative distribution function:

$$F(\sigma) = 1 - \exp\left(-\left(\frac{\sigma}{k}\right)^m\right) \quad (1)$$

where, k and $m > 0$ denote the scale and shape parameters, respectively. Glass strength is governed by the existence of surface flaws which magnify the stresses locally (Griffith, 1920). The stress-raising property of a given flaw can be determined from the associated crack size and shape using fracture mechanics (Mencik, 1992). Let

$f(a)$ denote the flaw size density function with a signifying the flaw size. Suppose a_c denotes the critical crack size that prompts failure of the crack. In the case of a plane crack with geometry factor Y that is subjected to a uniform uniaxial stress σ , it can be shown that:

$$a_c = \frac{K_{Ic}^2}{Y^2 \sigma^2 \pi} \quad (2)$$

where, K_{Ic} represents the fracture toughness (Mencik, 1992). Let $P_f(\Delta A, a_c)$ denote the failure probability in the small region ΔA at the critical crack depth a_c . It can be shown that (Lamon, 2016):

$$P_f(\Delta A, a_c) = \Delta A \int_{a_c}^{\infty} f(a) da \quad (3)$$

Suppose the total area is:

$$A = N \Delta A \quad (4)$$

for some number N . By application of the weakest link principle while assuming that the regions are non-interacting it is found that the survival probability is:

$$1 - P_f(A, a_c) = \left(1 - P_f(\Delta A, a_c)\right)^N \quad (5)$$

Substituting for Equation 3 and 4 in Equation 5 while observing the standard limit:

$$\lim_{N \rightarrow \infty} \left(1 + \frac{x}{N}\right)^N = e^x \quad (6)$$

it follows after some rearrangement that:

$$P_f(A, a_c) = 1 - \exp\left(-A \int_{a_c}^{\infty} f(a) da\right) \quad (7)$$

Suppose $f(a)$ is a Pareto density function, i.e.:

$$f(a) = c a_0^c a^{-(c+1)} \quad (8)$$

where, c and a_0 are scale and shape parameters (Forbes *et al.*, 2011). Inserting Equation 8 into Equation 7 while substituting for Equation 2 yields the Weibull distribution, Equation 1, with:

$$m = 2c \quad (9)$$

and:

$$k = \frac{K_{Ic}}{Y \sqrt{\pi a_0 A^{1/c}}} \quad (10)$$

In fact, for reasons of extreme value theory (Beirlant *et al.*, 2004), the Weibull distribution is the limiting distribution when the flaw size distribution decays like a power-law in the tail. This means that the Weibull distribution emerges for the strength model when the flaw size distribution is e.g., Pareto, Cauchy, t , or F . Another common extreme value distribution is the Gumbel distribution which has the density function:

$$f(\sigma) = \frac{1}{s} \exp\left(\frac{\sigma - \mu}{s}\right) \exp\left(-\exp\left(\frac{\sigma - \mu}{s}\right)\right) \quad (11)$$

where, μ and s signify the location and scale parameters, respectively. It is the limiting distribution when the flaw size distribution decays exponentially in the tail. This includes flaw size distributions such as the normal, lognormal, exponential, gamma and χ^2 (Trustrum and De Jayatilaka, 1983).

The normal distribution has the probability density function (Forbes *et al.*, 2011):

$$f(\sigma) = \frac{1}{\sqrt{2\pi s^2}} \exp\left(-\frac{(\sigma - \mu)^2}{2s^2}\right) \quad (12)$$

where, μ and s^2 are the mean and variance, respectively. The use of a normal distribution as a standard model for data is due to the Central Limit Theorem (Beirlant *et al.*, 2004) which states that averages of many samples will tend to follow a normal distribution.

The lognormal distribution arises from the normal distribution through a change of variables transformation. If Y is a random variable with a normal distribution, then $X = \exp(Y)$ has a lognormal distribution with the density function (Forbes *et al.*, 2011):

$$f(\sigma) = \frac{1}{\sigma\sqrt{2\pi s^2}} \exp\left(-\frac{(\log \sigma - \mu)^2}{2s^2}\right) \quad (13)$$

In Equation 13, μ and s^2 denote the mean and variance of the related normal distribution. By token of the Central Limit Theorem, the lognormal distribution would be a natural model for geometric means.

Method

Data on the strength of annealed float glass was collected from a set of references, see Table 1 for the complete list including details on the experimental setups. The strength was the maximum principal tensile stress at the fracture origin location. Only those data samples were extracted from the references and included in the analysis which fulfilled the following conditions: the glass was monolithic annealed float glass in the as-

received condition that was tested in an ambient environment. The experiments were conducted using either the double ring bending device, the three or four-point bending device, or the setup that allows for a uniform pressure to be applied to a laterally supported plate. In the case of four-point bending tests, the recorded strength value was discarded in case the failure origin was located outside the load span. In one case of double ring bending tests, viz. Simiu *et al.* (1984), the fracture stress values that corresponded to failure origins outside the loading ring area were adjusted using Equation 14 in order to reflect the maximum principal tensile stress at the failure origin. This was possible to do because the fracture origins were recorded by Simiu *et al.* (1984). Otherwise, all the recorded strength values were taken as-received. The radial stress outside the loading ring area in a double ring bending setup at the distance r from the centre point is:

$$\sigma_r = \frac{3F}{2\pi b^2} \left[(1 + \nu) \ln \frac{r_1}{r} + (1 - \nu) \frac{r_0^2 (r_1^2 - r^2)}{2r^2 r_2^2} \right], \quad r > r_0 \quad (14)$$

where, r_2 is the equivalent outer radius used for a square shaped specimen with side length $2L$, viz:

$$r_2 = L(1 + \sqrt{2}) \quad (15)$$

In Equation 14, F is the failure load, b is the plate thickness, ν is Poisson's ratio, r_0 is the loading ring radius and r_1 is the support ring radius.

An overview of the experiments including a more detailed presentation of each data sample can be found in Kinsella (2018). All data samples that were larger in size than 5, 15, 30 and 45, respectively, were fitted with the four standard probability distributions. The parameter estimation was performed with the maximum likelihood method. The goodness-of-fit was calculated with the Anderson-Darling statistic (D'Agostino and Stephens, 1986) and a set of four p-values were derived for each sample, the p-values being associated with the normal, lognormal, Gumbel and Weibull distributions, respectively.

The float process production method causes the diffusion of tin into the surface that was in contact with the molten tin bath and this side is termed the tin side. The other side is the air side. When the statistical models were fitted to the data samples, it was not taken into account whether the fracture origin was located on the tin side of the glass or on the air side.

The method used to measure and compare the potential of various statistical models allows for the effect of different surface area size or edge length and different stress state to be taken into account by adaptation of the

two parameter values. This is done in the maximum likelihood estimation. However, the method of analysis used in this study does not take into account that the strength in e.g., uniaxial stress states is of one type of distribution, e.g., Weibull, while in biaxial stress states is of a different type of distribution, e.g., normal.

In some experiments the fracture origin mode was not recorded while the data contained a mixture of surface and edge fractures or there was an ambiguity towards the fracture origin due to multiple potential fracture locations. Hence only a mixed failure origin mode could be determined in those cases. This pertains to a number of cases with the four-point bending device with the loading taking place out-of-plane and with laterally supported plates subjected to uniform pressure. In the examination that follows, it was assumed that when a glass beam was tested in the four-point bending device with in-plane loading, then the type of fracture produced was an edge failure origin. For an illustration of the meaning of in-plane and out-of-plane loading with the four-point bending device, see Fig. 1. The model fitting was performed in the following three cases, viz. mixed failure origins, edge only failure origins and surface only failure origins.

In a first procedure, the resulting measures of performance were visualized in the form of boxplots. Subsequently, the multiple models over multiple data sets were compared in a Friedman test (Friedman, 1937; 1940) under the null-hypothesis that all models perform equally. In case the null-hypothesis was rejected, a post-hoc test was performed to determine which of the models that were significantly different. For this, the Wilcoxon signed-rank test (Wilcoxon, 1945) was used and the family-wise error was controlled with the Bonferroni-Holm method (Holm, 1979).

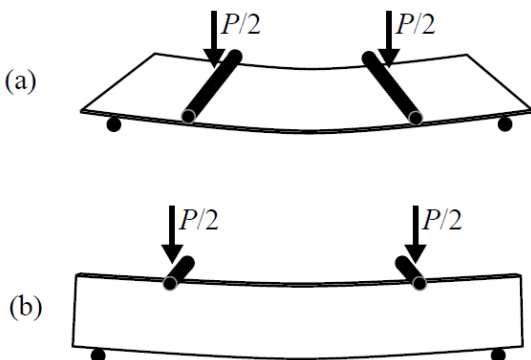


Fig. 1: Illustration of the (a) out-of-plane loading of a beam in four-point bending and the (b) in-plane loading

Friedman Test

The Friedman test is a non-parametric test for comparing models over multiple data sets. The performance of the m models is calculated for each of the n data sets and then ranked with rank 1 corresponding to the best performance. The ranks can be organized in a matrix:

$$R = \begin{bmatrix} R_{11} & R_{12} & \cdots & R_{1n} \\ R_{21} & R_{22} & \cdots & R_{2n} \\ \vdots & \vdots & \vdots & \vdots \\ R_{m1} & R_{m2} & \cdots & R_{mn} \end{bmatrix} \quad (16)$$

where, R_{ij} is the rank of model i in data set j (Benavoli *et al.*, 2016). Under the null-hypothesis, there is no difference in performance between the models, in which case the average value of each row in R is $\frac{n(m+1)}{2}$. The test statistic is:

$$T = \frac{12}{nm(m+1)} \sum_{j=1}^n \left(\sum_{k=1}^m R_{jk} - \frac{n(m+1)}{2} \right)^2 \quad (17)$$

which under the null-hypothesis is χ^2 -distributed with $m-1$ degrees of freedom.

Wilcoxon Signed-Rank Test

The Wilcoxon signed-rank test is a non-parametric test for comparing the performance of two models over multiple data sets. Under the null-hypothesis, both models perform equally and hence the distribution of the pairwise difference is symmetrical about the value 0. Let d_i denote the difference in performance between the two models for data set number i among n sets when the first model outperforms the second. In case $d_i = 0$, i.e., a tie, one has to exclude observations. Suppose there are an odd number of ties. Then one tie is excluded and half of the remaining ties are included. Suppose there are an even number of ties. Then half of the ties are included. The rank sum R is calculated:

$$R = \sum_{d_i > 0} \text{rank}(d_i) + \frac{1}{2} \sum_{d_i = 0} \text{rank}(d_i) \quad (18)$$

The test statistic is:

$$z = \frac{R - \frac{1}{4}n(n+1)}{\sqrt{\frac{1}{24}n(n+1)(2n+1)}} \quad (19)$$

which for a large number of samples is approximately normally distributed under the null-hypothesis (Demsar, 2006).

Bonferroni-Holm Method

When making multiple comparisons between pairs of models, the Bonferroni-Holm method (Holm, 1979) can be used to adjust the significance level to control the family-wise Type 1 error, i.e. the probability of making at least one Type 1 error in any of the comparisons (Densar 2006). Suppose the desired significance level is α . Then, with the Bonferroni method, the corrected significance level is simply $\frac{\alpha}{m}$. However, this is very conservative.

Holm (1979) provided a sequentially rejective version of the Bonferroni method that has larger probability of rejecting the false hypothesis. The hypotheses are ordered by their significance levels p_1, p_2, \dots with $p_1 \leq p_2 \leq \dots \leq p_m$. Starting with the most significant p -value, p_1 is compared with $\frac{\alpha}{m}$ and if it is greater than so, the procedure stops and no p -values are significant. If, however, $p_1 \leq \frac{\alpha}{m}$, the

corresponding hypothesis is rejected and the second p -value is compared with $\frac{\alpha}{m-1}$. If the corresponding hypothesis is also rejected, the third p -value is compared with $\frac{\alpha}{m-2}$, etc. Hence, p_i is compared sequentially to $\frac{\alpha}{m-i}$ in a step-down procedure that stops when there is failure to reject the hypothesis.

Limitations

The glass included in the investigation was new and in the as-received condition when it was tested. Moreover, the glass was stressed in an ambient atmosphere, typically represented by an indoor temperature of about 20°C and a relative humidity between 40-70%. Only monolithic panes of annealed float glass was considered. Static fatigue was not taken into account in the analysis of the data.

Table 1: List of references which were the basis for an investigation. ULP = Plate bending due to Uniform Lateral Pressure, CDR = Co-axial Double Ring bending, 4PB = Four-Point Bending, 3PB = Three-Point Bending

Reference	No. samples	No. observations	Bending mode
Johar (1981)	9	78	ULP
Johar (1982)	5	106	ULP
Simiu <i>et al.</i> (1984)	2	85	CDR
Carre (1996)	5	81	4PB
Calderone (1999)	32	195	ULP
Hess (2000)	3	15	4PB
Fink (2000)	2	127	CDR
Haldimann (2006)	2	20	CDR
Veer <i>et al.</i> (2006)	3	32	4PB
Sglavo <i>et al.</i> (2007)	8	115	3PB
Veer <i>et al.</i> (2009)	2	54	4PB
Postigo (2010)*	1	41	CDR
Veer and Rodichev (2011)	2	177	4PB
Veer and Rodichev (2012)	2	60	4PB
Vandebroek <i>et al.</i> (2012)	4	77	4PB
Lindqvist (2013)	32	478	4PB
Vandebroek <i>et al.</i> (2014)	8	202	4PB
Kozlowski (2014)	1	6	4PB
Kleuderlein <i>et al.</i> (2014)	33	830	4PB
Schula (2015)	1	15	CDR
Kinsella and Persson (2016)	2	58	4PB
Muniz-Calvente <i>et al.</i> (2016)	2	73	CDR 4PB
Navarrete <i>et al.</i> (2016)	8	69	CDR
Yankelevsky <i>et al.</i> (2017)	1	56	4PB
Osnes <i>et al.</i> (2018b)	3	93	4PB
Total:	173	3143	ULP CDR 3PB 4PB

*Obtained from Huerta *et al.* (2011)

Table 2: Friedman test p-values based on the samples that contained at least 15 observations of the strength

p-value	Edge fail. origins	Surf. fail. origins
	0.0000	0.0104

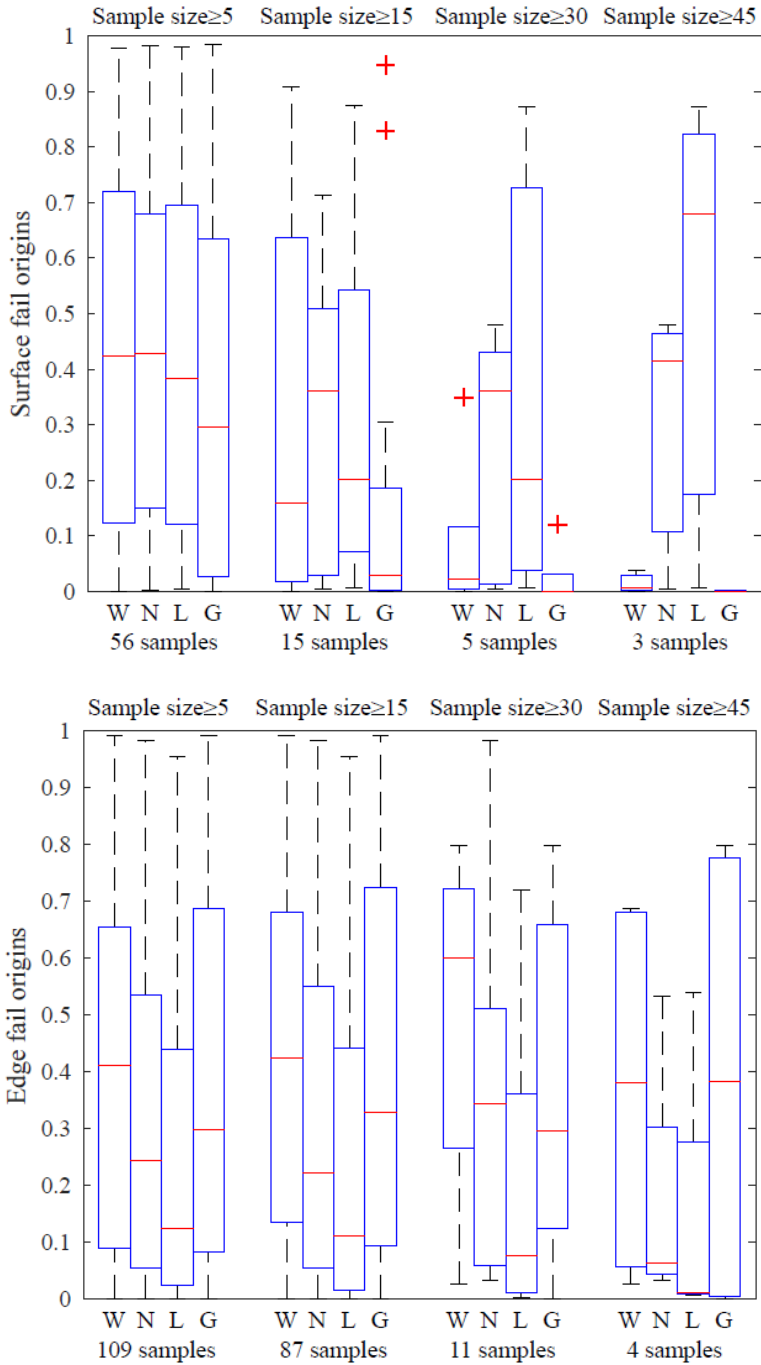


Fig. 2: Boxplots for the p-values from the Anderson-Darling tests that measured the goodness-of-fit of various standard statistical models of the fracture stress of annealed float glass. The results are separated according to the failure origin mode as well as according to the minimum number of observations per sample included in the analysis. W = Weibull, N = normal, L = lognormal and G = Gumbel distribution

Edge fails					Surface fails				
W	N	L	G		W	N	L	G	
	+0.0017 (*)	+0.0000 (*)	+0.0722	W		-0.5995	-0.8040	+0.0166	W
		+0.0000 (*)	-0.0944	N			-0.8904	+0.0256	N
			-0.0011 (*)	L				+0.1205	L
				G					G

Fig. 3: p-values for the pairwise comparison of model performance with the signed-rank test. (*) indicates that the p-value was significant while controlling for the family-wise type I error. A plus sign in front indicates that the row had a higher rank while a minus sign indicates that the column had a higher rank. Analysis comprises all samples of size 15 or greater. W = Weibull, N = Normal, L = Lognormal and G = Gumbel distribution

Results

The samples from the references in Table 1 which fulfilled the limitations, see Sec. Limitations, were modelled using the normal, lognormal, Gumbel and Weibull distributions. The goodness-of-fit was tested with the Anderson-Darling statistic. The models were fitted in the following three cases, viz. mixed failure origins, edge only failure origins and surface only failure origins. An overview of the performances is provided in Fig. 2 which contains a set of boxplots separated according to the failure origin mode as well as according to the minimum sample size in the analysis. Note that under the null-hypothesis the p-values are uniformly distributed between 0 and 1. Fig. 2 only contains the results from pure edge and surface failures, i.e., not mixed failure origins. Due to the fundamental difference that is apparent in the behaviour between edge and surface failure mode, it is not effective to combine the results in an analysis, see further the Discussion section.

A further investigation was performed based on all samples that included at least 15 observations of the strength, the results of which follow. Similar features were exhibited when the analysis was selected to comprise minimum sample sizes of 30 and 45 observations, respectively. A Friedman test was performed to make multiple comparisons over the data sets and the null-hypothesis was rejected in both cases corresponding to edge only failure origins and surface only failure origins, see further Table 2 for the p-values. Finally, pairwise comparisons were made between the models using the Wilcoxon signed-rank test and the family-wise Type I error was controlled using the Bonferroni-Holm correction method, see Fig. 3. The results show that in the case of edge failure origins, the normal and lognormal distributions did not perform as well as the Weibull distribution. In the case of surface only failure origins, however, none of the pairwise comparisons rendered a statistical significance.

Discussion

The Weibull model has been praised for its utility in a wide range of applications (Weibull, 1959). According to a recent survey (Rinne, 2009), there are a great number of papers and monographs that demonstrate the successful application of the Weibull model in some 180 distinct topics that encompass nearly all scientific disciplines. Part of the reason for the versatility may lie in the fact that the Weibull distribution is one of the three extreme value distributions. It emerges naturally as the limiting distribution of the minimum or maximum value in a sample.

The utility of the Weibull model has been called into question, however, both from within the structural glass engineering community and from outside. As was noted in the Introduction section, certain experiments on glass have indicated that the Weibull model does not perform better than a normal or lognormal distribution. These experiments have included laterally supported plates subjected to uniform loading as well as beams in three-point and four-point bending. However, the fact that the Weibull model does not appear to outperform other standard models may be due to the sample sizes being too limited. In order to illustrate this, consider Fig. 4 which illustrates the results when drawing 1000 random samples from a Weibull distribution with different sample sizes and fitting the standard distributions to the drawn samples. The Weibull parameter values were selected as $m = 6$ and $k = 74$ MPa, i.e., the same distribution as was mentioned already in Sec. Standard Distributions. The figure indicates that it may be hard or indeed impossible to distinguish properly between a Weibull model and models based on other standard distributions when the sample sizes are limited. In particular this applies to detecting a difference in performance between the Weibull model with these parameter values and the model based on a normal distribution.

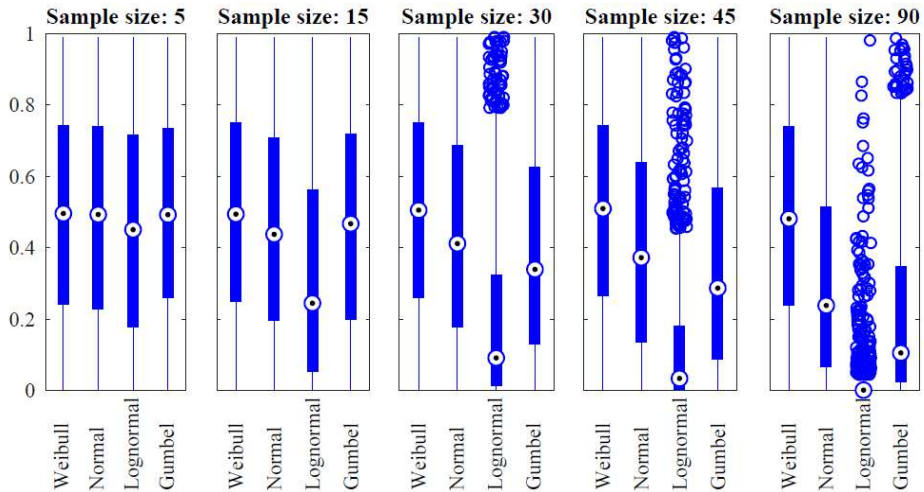


Fig. 4: Simulations of the p-values based on 1000 random samples from a Weibull distribution of varying sample size

From the point of view of structural glass engineering, however, the Weibull model has a logical basis. According to experiments with Hertzian indentation fracture (Poloniecki and Wilshaw, 1971; Poloniecki, 1974), flaw size in glass can be closely fitted by an inverse gamma distribution:

$$f(a) = \frac{r^{n-1}}{(n-2)!} a^{-n} e^{-r/a} \quad (20)$$

which is like a Pareto distribution in the tail. In Sec. Standard Distributions, it was shown that the Weibull distribution can be derived from the weakest-link principle when supposing a Pareto flaw size density function, see Equation 3 to 10. Hence, a strong case can be made for applying the Weibull distribution to model glass strength when the stress state is uniform and uniaxial over each crack (De Jayatilaka and Trustrum, 1977). Notwithstanding, a number of studies have questioned the utility of the Weibull distribution while noting that it does not perform better than a normal or lognormal distribution. In fact, some studies have recommended to abandon the Weibull model altogether and use a normal or lognormal distribution instead. However, when one is unable to distinguish between fitted distributions, preference should be given to the model that has a physical and theoretical foundation, in this case a model that is logically based on fracture mechanics.

In recent attempts to model glass surface fracture in Monte Carlo simulations with distributed Griffith flaws, it was assumed by some researchers that flaw size is governed by a density function that decays like

an exponential distribution (Yankelevsky, 2014; Pathirana *et al.*, 2017; Osnes *et al.*, 2018a; 2018b). Assuming a single population of flaws with a size distribution that decays exponentially would naturally lead to Gumbel-like distributions for the strength in the limit, assuming a uniform and uniaxial stress normal to the crack planes. However, a Gumbel-like distribution for the strength model of the surface of glass is not supported by the empirical data.

In connection with this study, a comprehensive survey of the data on annealed glass strength was performed (Kinsella, 2018). Based on the results it was noted that when taking the whole collection of empirical data into account, the Weibull distribution turns out to be a better model for the strength than the normal and lognormal distributions in the case of edge failure origins. The performance was investigated in a statistical testing procedure and found to be significant, see Fig. 3, with the following exception: The Weibull distribution was not found to be significantly better than a Gumbel distribution. Nevertheless, it is indicated in Fig. 2 and 3 that the Weibull model is at least as good as the Gumbel distribution. The test procedure was based on the Friedman non-parametric method and a post-hoc test with the Wilcoxon signed-rank test. In the case of surface only failure origins, the multiple comparisons using the Friedman test rendered a rejection of the null-hypothesis meaning that it can be concluded that there are significant differences in performance between the four standard models in this case. In fact, the boxplots in Fig. 2 clearly suggest that the extreme value Weibull and Gumbel distributions can be dismissed as a model for the surface strength of glass. However, the number of relevant data samples is limited in the case of surface failure origin data.

The analysis depends on a choice for the minimum sample size to be included. In this study, the main analysis considered samples of size 15 or greater, cf. Fig. 3. It might be argued that even greater sample sizes are needed to distinguish properly between the different models when only a limited or moderate number of samples are available, such as is typically the case in the respective experimental campaigns considered in this study. The dependence on sample size is clearly indicated in Fig. 4 which contains simulation results of the goodness-of-fit while varying the underlying sample size. However, the empirical data only provides a limited number of samples when the sample size is 30 or greater. Nonetheless, the following conclusions can be drawn from Fig. 2 while noting the effect of the minimum sample size upon the results. When all samples are included which contain at least five observations, no particular effect can be seen between the different models for the surface strength. However, as the minimum sample size increases, the Weibull distribution performs poorly while the normal and lognormal distributions appear to perform better. In order to address this phenomenon properly, an investigation was carried out into the properties of the underlying samples. Fig. 5 illustrates the results from this investigation in the form of three diagrams. The top diagram shows the size of surface area in maximum tension as a function of the minimum sample size. The y-axis scaling is logarithmic for the sake of visual clarity. The surface areas were not included in Fig. 5 in the case of laterally supported plates subjected to uniform pressure because of the difficulty associated with assigning a value to the size of surface area in maximum tension. The diagram shows that the whole range of surface sizes are present at the first two levels, i.e., sample sizes greater than or equal to 5 and 15. However, already as the sample sizes are restricted to 15 or greater, the extreme value Gumbel distribution is clearly performing poorly as can be seen in Fig. 2. The extreme value Weibull distribution seems to be performing worse than at the first level, i.e. for sample sizes restricted to 5 or greater. Furthermore, a considerable portion of the whole range of surface sizes is still present at the third level, i.e., for sample sizes restricted to 30 or greater. However, both the extreme value distributions perform poorly as can be seen in Fig. 2. Finally, at the last level, i.e., for sample sizes restricted to 45 or greater, the surface area sizes that remain are the following, viz. approx. 2000, 2400 and 3800 mm². The extreme value distributions perform poorly again. The conclusion is that the poor performance of the extreme value distributions cannot simply be explained as a consequence of the surface size converging towards a small size or a large size. In other words, it is not simply

the surface size that governs the features of Fig. 2. Next, consider the middle diagram in Fig. 5 which shows the bending modes of the underlying samples. Here, ULP refers to the setup that allows for a uniform lateral pressure to be applied to linearly supported plates, CDR refers to the coaxial double ring bending device, while 3PB and 4PB refer to the three and four-point bending devices, respectively. The diagram shows that both a uniaxial stress state from the four-point bending device and an equibiaxial stress state from the double ring bending device are present at all levels of samples sizes. Hence, the attributes of Fig. 2 cannot be explained as a consequence of the stress state converging towards one or the other configuration. Rather, there is a mixture of stress states present at each level. Next, the bottom diagram in Fig. 5 shows whether the fracture origin was located on the tin side, air side, or whether it was unknown because it was not recorded in the publication. With many of the samples, the publication did not record the configuration of the glass specimens in terms of the tin and air side being in the tension zone. This likely implies that there was a mixture of tin and air side failures. This would be so, because if the experimenter made the effort to identify the tin and air side of each specimen properly and configure them accordingly in the testing device, then this would probably have been recorded or at least mentioned in the ensuing publication. Hence, the conclusion can be drawn that a mixture of tin and air side failures are present at all levels of sample size. This demonstrates that the features of the surface origin failures in Fig. 2 probably cannot be explained as a consequence of the configuration of the test specimens in the testing device with respect to the air or tin side in tension. In other words, it is probably not the case that the fracture origins converge towards either pure tin side or pure air side failures as the sample sizes are restricted to at least 15, 30 and 45, respectively.

The following explanation for the features of the surface origin failures in Fig. 2 is suggested. When the surface condition in glass is considered, there is no single population of flaws that govern the failure because if so were the case, then the Weibull and Gumbel distributions would have performed much better. Hence it is indicated that multiple flaw populations are present on the surface. If the underlying flaw size distribution is governed by multiple unimodal populations which are superposed, it is natural to expect a more symmetrical and "rounded out" shape for the extreme value such as would correspond better with a normal distribution. By the same token, when the minimum sample sizes are small, then it would be logical that the Weibull and Gumbel models perform better because the probability decreases that you sample all the underlying flaw populations hence resulting in a better fit.

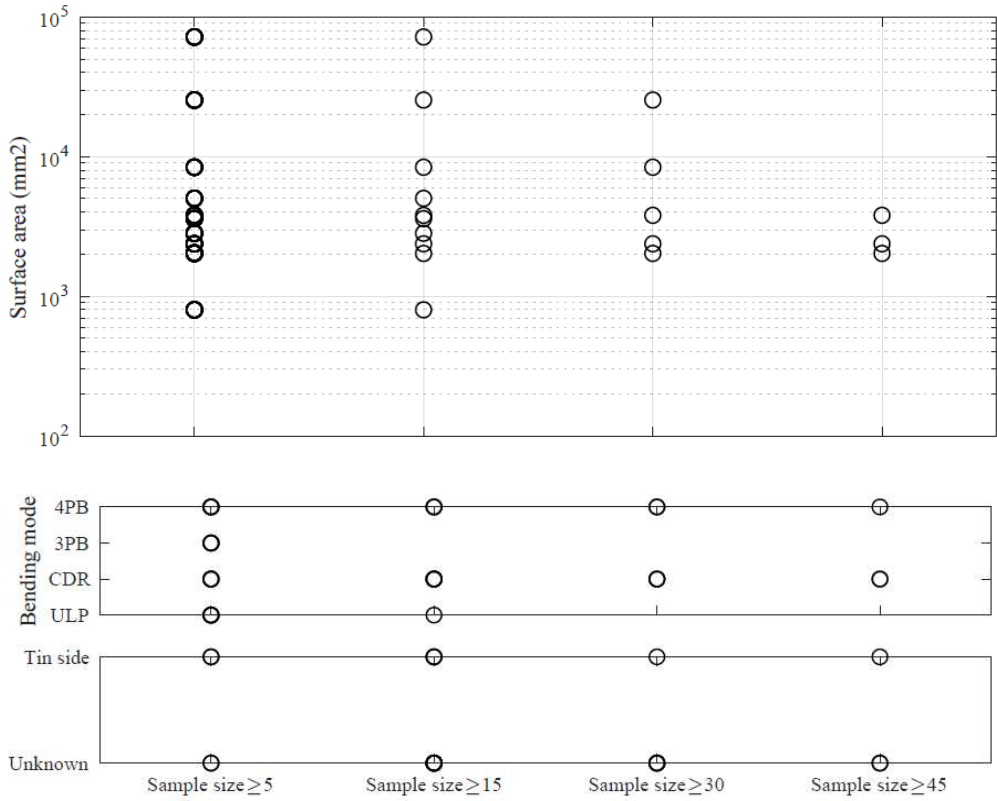


Fig. 5: Properties of the underlying samples that generated the surface origin boxplots in Fig. 2

On the other hand, the generally equal performance of the models in the case of ≤ 5 sample size may just as well be attributed to small-sample effects, i.e., the difficulty of detecting any effects when the sample sizes are small. Moreover, the fact that the normal distribution performs better when the sample sizes increase should not be taken as argument for adopting this distribution as a model for the surface strength. From a weakest-link perspective, the normal distribution is not suitable. As already mentioned, there may be a logical explanation for the better performance of the normal distribution compared to the extreme value distributions that has to do with the presence of multiple flaw populations.

However, attempts to address the presence of multiple flaw populations may lead to more or less exotic distributions for the flaw size. So far, attempts have been made by Pathirana *et al.* (2017), Kinsella and Persson (2018b) and Pisano and Royer-Carfagni (2017) to model surface failure in glass with a multimodal flaw size distribution approach.

With the edge strength data, the conclusions are different. Here, it is readily seen that the Weibull distribution overall performs better than the normal and

lognormal distributions and at least as well as the Gumbel distribution, irrespective of the minimum sample size in the analysis. This indicates that when the edge strength is considered, there is a tendency towards a unimodal flaw size distribution that governs the failure. This may be logical when you consider the mechanical treatment of the edge which undergoes various operations such as scoring and machining. As a comparison, consider when the glass surface is artificially scratched by sandblasting (Blank, 1993; Schula, 2015). Then the result is generally to produce a better Weibull fit compared with the original pristine surface.

In summary then, it can be concluded that the edge and surface condition in glass differ fundamentally. A proper analysis of the strength has then to discriminate between these failure origins. However, it may be that certain kinds of testing device can be used as a proxy for either the edge of the surface condition. In other words, when a given test device produces failures with the majority of one kind, then it may be that this data can be combined without producing significant errors. This proxy-effect has not been quantified in the present study

but it will be considered in a future investigation. In a recent paper (Yankelevsky *et al.*, 2018), it was examined whether edge failures should be excluded from the analysis of the data sample that is produced with the four-point bending device with out-of-plane loading or whether they may be included. The examination was based on a reference sample of 83 specimens that were tested in accordance with ASTM C158-02. The results from the investigation were not conclusive with regards the possible proxy-effect of the bending device, nevertheless the authors recommended to exclude edge failures.

The majority of experimental data points included in this investigation pertain to the edge strength of glass. As a matter of fact, the edge strength is of great importance for the strength design of a structural glass component. The edge is thought to contain more weaknesses than the surface, probably due to machining operations done to the edge while scoring, cutting and processing (Veer and Rodichev, 2011; Vandebroek *et al.*, 2014). When a laterally supported plate is subject to uniform pressure, significant tensile stresses occur near the edges, see e.g., Kinsella and Persson (2018a) which contains an analysis of the fracture origins in laterally supported plates subject to uniform pressure. For glass beams and pillars, the edges are always subject to significant tensile stress in the design state. Hence, in practical situations the edge strength can hardly be neglected for most types of structural units, including laterally supported plates. Also during handling, transportation and maintenance, the edge is prone to damage. The fact that the Weibull distribution outperforms the normal and lognormal distributions in the case of edge only failure origins is an argument for adopting this model rather than the others.

The lognormal distribution might seem like a better candidate than the normal distribution because the strength is a positive number and the lognormal model lacks support on the left-hand side of the real axis. Nevertheless, a better fit was indicated using the normal distribution.

In summary, the Weibull distribution is recommended as a basic model for the edge strength of glass for reasons of empirical evidence and physics. The empirical evidence is that the Weibull model is generally superior to a normal and lognormal distribution and at least as good as a Gumbel distribution in the case of edge failure origins. For physics-based reasons, the extreme value Weibull and Gumbel models are preferable because they derive from the weakest-link principle and thus harmonize with an essential brittle material concept. In fact, assuming a population of material flaws with a unimodal crack size distribution that is Pareto, F , Cauchy, or t in the tail, the Weibull distribution can be deductively derived from the weakest-link principle. This supposes that the stress state is uniform and uniaxial over each crack. In the case of the

normal and lognormal distributions, however, there is no such failure-mechanism basis. However, the Weibull and Gumbel models are unsuited to represent the strength of glass when the fracture originates from the surface.

Finally, there exist numerous strength prediction models for use with glass. For example, Monte Carlo simulations of glass fracture with stochastic Griffith flaws have recently been performed by Yankelevsky (2014), Pathirana *et al.* (2017), Yankelevsky *et al.* (2017), Osnes *et al.* (2018a; 2018b) and Kinsella and Persson (2018b). In such case, no closed form exists for the probability distribution. It could be an interesting future research project to compare the performance of a larger set of models over a comprehensive set of data samples.

Conclusion

Based on a large set of empirical data, the Weibull distribution outperforms the normal and lognormal distributions and is at least as good as a Gumbel distribution as a model for glass strength when the fracture data is selected to comprise edge only failure origins. In the case of surface only failure origins, it is indicated that the normal and lognormal distributions perform better than the extreme value distributions. The analysis of the surface strength is dependent on the sample size. A proper distinction between the tentative models is more straight-forward to make, the greater the sample sizes that are included in the analysis. It is suggested that when the minimum sample size is much smaller than 15 then no distinction is possible to make. The Weibull and Gumbel models have a logical basis in a failure-mechanism that applies to brittle glass behaviour assuming a weakest-link argument. The Weibull model is therefore recommended instead of a normal or lognormal distribution to model glass fracture when the edge strength is considered. The analysis of the surface strength distribution is complicated. This is probably due to the presence of multiple flaw populations. Neither extreme value Weibull or Gumbel nor normal or lognormal distributions are able to properly model the surface strength of glass.

Author's Contributions

David Kinsella: Is the main author of the article and the conceptual designer of the project, the main analysis and the interpretation of data.

Johan Lindström: Contributes to the analysis and interpretation of the data, and with suggestions to the revision of the manuscript.

Kent Persson: Contributes to the conception of the project and to reviewing, writing, and making changes to the manuscript.

Ethics

The corresponding author confirms that all of the other authors have read and approved the manuscript and there are no ethical issues involved.

References

- prEN 16612, 2017. Glass in building-determination of the lateral load resistance of glass panes by calculation. CEN.
- Beirlant, J., Y. Goegebeur, J. Segers and J. Teugels, 2004. *Statistics of Extremes: Theory and Applications*. 1st Edn., John Wiley and Sons, ISBN-10: 0471976474, pp: 522.
- Benavoli, A., G. Corani and F. Mangili, 2016. Should we really use post-hoc tests based on mean-ranks? *J. Mach. Learn. Res.*, 17: 152-161. <https://dl.acm.org/citation.cfm?id=2946650>
- Blank, K., 1993. *Dickenbemessung von Vierseitig Gelagerten Rechteckigen Glasscheiben unter Gleichförmiger Flächenlast*. 2nd Edn., Institut für Konstruktiven Glasbau, Gelsenkirchen.
- Calderone, I., 1999. *The equivalent wind loading for window glass design*. PhD Thesis, Monash University.
- Calderone, I., C. MacDonald and L. Jacob 2001. The Fallacy of the Weibull Distribution for Window Glass Design. In: *Glass Performance Days*, pp: 293-297.
- Calderone, I., L. Jacob, J. Ltd and A. Pty, 2005. The Dangers of Using a Probabilistic Approach for Glass Design. In: *Glass Performance Days*, Tampere, Finland.
- Carre, H., 1996. *Etude du comportement à la rupture d'un matériau fragile précontraint: Le verre trempé*. PhD Thesis, Ecole Nationale des Ponts et Chaussees.
- D'Agostino, R.B. and M.A. Stephens, 1986. *Goodness-of-Fit Techniques*. 1st Edn., CRC Press, ISBN-10: 0824774876, pp: 576.
- De Jayatilaka, A. and K. Trustrum, 1977. Statistical approach to brittle fracture. *J. Mater. Sci.*, 12: 1426-1430. DOI: 10.1007/BF00540858
- Demsar, J., 2006. Statistical comparisons of classifiers over multiple data sets. *J. Mach. Learn. Res.*, 7: 1-30. <https://dl.acm.org/citation.cfm?id=1248548>
- DIN 18008-1, 2010. *Glas im Bauwesen-Bemessungs- und Konstruktionsregeln-Teil 1: Begriffe und allgemeine Grundlagen*. CEN.
- Fink, A., 2000. *Ein Beitrag zum Einsatz von Floatglas als dauerhaft tragender Konstruktionswerkstoff im Bauwesen*. PhD Thesis, TU-Darmstadt.
- Forbes, C., M Evans, N. Hastings and B. Peacock, 2011. *Statistical Distributions*. 4th Edn., John Wiley and Sons, Hoboken, ISBN-10: 1118097823, pp: 230.
- Friedman, M., 1937. The use of ranks to avoid the assumption of normality implicit in the analysis of variance. *J. Am. Stat. Assoc.*, 32: 675-701. DOI: 10.2307/2279372
- Friedman, M., 1940. A comparison of alternative tests of significance for the problem of m rankings. *Ann. Math. Stat.*, 11: 86-92. DOI: 10.1214/aoms/1177731944
- Griffith, A., 1920. The phenomena of rupture and flow in solids. *Phil. Trans. R Soc. A*, 221: 163-198. https://www.jstor.org/stable/91192?seq=1#page_scan_tab_contents
- Haldimann, M., 2006. *Fracture strength of structural glass elements: Analytical and numerical modelling, testing and design*. PhD Thesis, Ecole Polytechnique Federale de Lausanne EPFL.
- Hess, R., 2000. *Glasträger*. Forschungsbericht 20, ETH Zurich. Institut für Hochbautechnik, Zurich, Switzerland.
- Holm, S., 1979. A simple sequentially rejective multiple test procedure. *Scandinavian J. Stat.*, 6: 65-70. https://www.jstor.org/stable/4615733?seq=1#page_scan_tab_contents
- Huerta, M.C., A. Pacios-Alvarez, M.J. Lamela-Rey and A. Fernandez-Canteli, 2011. Influence of experimental test type on the determination of probabilistic stress distribution. In: *Glass Performance Days*.
- Johar, S., 1981. *Dynamic fatigue of flat glass-Phase II*. Technical report, Ontario Research Foundation, Department of Metals, Glass and Ceramics.
- Johar, S., 1982. *Dynamic fatigue of flat glass - Phase III*. Technical Report, Ontario Research Foundation, Department of Metals, Glass and Ceramics.
- Kinsella, D., 2018. *Survey of experimental data on the strength of annealed float glass panes in the as-received condition tested in an ambient atmosphere*. Tech. Rep. TVSM-7166, Division of Structural Mechanics, Lund University.
- Kinsella, D. and K. Persson, 2016. On the applicability of the Weibull distribution to model annealed glass strength and future research needs. *Proceedings of the Challenging Glass Conference 5, (CGC' 16)*, Ghent, Belgium.
- Kinsella, D. and K. Persson, 2018a. *An Analysis of Glass Fracture Statistics*. *Proceedings of the Challenging Glass Conference 6, (CGC' 18)*, Delft, The Netherlands.
- Kinsella, D.T. and K. Persson, 2018b. A numerical method for analysis of fracture statistics of glass and simulations of a double ring bending test. *Glass Struct. Eng.*, 3: 139-152. DOI: 10.1007/s40940-018-0063-z

- Kleuderlein, J., F. Ensslen and J. Schneider, 2014. Investigation of edge strength dependent on different types of edge processing. Proceedings of the International Conference at Glasstec, (ICG' 14), Düsseldorf, Germany.
- Kozlowski, M., 2014. Experimental and numerical analysis of hybrid timber-glass beams. PhD Thesis, Silesian University of Technology.
- Lamon, J., 2016. Brittle Fracture and Damage of Brittle Materials and Composites: Statistical-Probabilistic Approaches. 1st Edn., ISTE Press, London, ISBN-10: 008101161X, pp: 296.
- Lindqvist, M., 2013. Structural glass strength prediction based on edge flaw characterization. PhD Thesis, Ecole Polytechnique Federale de Lausanne EPFL.
- Lü, B.T., 1997. Fatigue strength prediction of soda-lime glass. *Theor. Applied Fract. Mech.*, 27: 107-114. DOI: 10.1016/S0167-8442(97)00012-8
- Mencik, J., 1992. Strength and Fracture of Glass and Ceramics. 1st Edn., Elsevier, New York, ISBN-10: 0444986855, pp: 357.
- Muniz-Calvente, M., A. Ramos, F. Pelayo, M.J. Lamela and A. Fernández-Canteli, 2016. Statistical joint evaluation of fracture results from distinct experimental programs: An application to annealed glass. *Theor. Applied Fract. Mech.*, 85: 149-157. DOI: 10.1016/j.tafmec.2016.08.009
- Navarrete, B., H. Juarez, L. Olmos, J. Guerrero and P. Garnica, 2016. Failure behavior of annealed glass for building windows. *Eng. Struct.*, 141: 417-426. DOI: 10.1016/j.engstruct.2016.12.050
- Osnes, K., T. Börvik and O. Hopperstad, 2018a. Shock tube testing and modelling of annealed float glass. Proceedings of the 12th International DYMAT Conference, (IDC' 18), Arcachon, France.
- Osnes, K., O. Hopperstad, T. Börvik, 2018b. Quasi-static and dynamic testing of annealed float glass. Proceedings of the 18th International Conference on Experimental Mechanics, (CEM' 18), Brussels, Belgium.
- Pathirana, M., N. Lam, S. Perera, L. Zhang and D. Ruan *et al.*, 2017. Risks of failure of annealed glass panels subject to point contact actions. *Int. J. Solids Struct.*, 129: 177-194. DOI: 10.1016/j.ijsolstr.2017.09.001
- Pisano, G. and G. Royer-Carfagni, 2017. A micromechanical derivation of the macroscopic strength statistics for pristine or corroded/abraded float glass. *J. Eur. Ceram. Soc.*, 37: 4197-4206.
- Poloniecki, J., 1974. Statistical investigation of surface flaws. PhD Thesis, The University of Sussex.
- Poloniecki, J.D. and T.R. Wilshaw, 1971. Determination of surface crack size densities in glass. *Nat. Phys. Sci.*, 229: 226-227. DOI: 10.1038/physci229226a0
- Postigo, S., 2010. Estudio teorico experimental de impactos humanos contra vidrios de acristalamientos de edificacion. PhD Thesis, Universidad de Politecnica de Madrid.
- Rinne, H., 2009. The Weibull Distribution: A Handbook. 1st Edn., CRC Press, ISBN-10: 1420087444, pp: 808.
- Schula, S., 2015. Charakterisierung der Kratzanfälligkeit von Gläsern im Bauwesen. 1st Edn., Springer, Berlin, ISBN-10: 3662477823, pp: 406.
- Sglavo, V.M., C. Muller and F. Righetti, 2007. Influence of edge finishing on the resistance to thermal stresses of float glass. *Glass Performance Days*.
- Simiu, E., D. Reed, C. Yancey, J. Martin and E. Hendrickson *et al.*, 1984. Ring-on-ring tests and load capacity of cladding glass. *Tech. Rep.*, NBS Building Series 162, U.S. Department of Commerce: National Bureau of Standards
- Trustrum, K. and A. De Jayatilaka, 1983. Applicability of Weibull analysis for brittle materials. *J. Mater. Sci.*, 18: 2765-2770. DOI: 10.1007/BF00547593
- Vandebroek, M., J. Belis, C. Louter and G.V. Tendeloo, 2012. Experimental validation of edge strength model for glass with polished and cut edge finishing. *Eng. Fract. Mech.*, 96: 480-489. DOI: 10.1016/j.engfracmech.2012.08.019
- Vandebroek, M., C. Louter, R. Caspeepe, F. Ensslen and J. Belis, 2014. Size effect model for the edge strength of glass with cut and ground edge finishing. *Eng. Struct.*, 79: 96-105. DOI: 10.1016/j.engstruct.2014.08.004
- Veer, F.A. and Y.M. Rodichev, 2011. The structural strength of glass: Hidden damage. *Strength Mater+*, 43: 302-315. DOI: 10.1007/s11223-011-9298-5
- Veer, F.A., Y.M. Rodichev, 2012. The strength of water jet cut glass. In: *Glass Performance Days*, pp: 434-438.
- Veer, F.A., P.C. Louter and T. Romein, 2006. Quality control and the strength of glass.
- Veer, F.A., C. Louter and F.P. Bos, 2009. The strength of annealed, heat-strengthened and fully tempered float glass. *Fatigue Fract. Eng. Mater.*, 32: 18-25. DOI: 10.1111/j.1460-2695.2008.01308.x
- Weibull, W., 1939. A statistical theory of the strength of materials. *Ingenjörsvetenskapsakademiens handlingar* 151.
- Weibull, W., 1959. A Statistical distribution function of wide applicability. *ASME J. Applied Mechan.*, 18: 293-297.
- Wilcoxon, F., 1945. Individual comparisons by ranking methods. *Biometrics*, 1: 80-83.
- Yankelevsky, D., 2014. Strength prediction of annealed glass plates-a new model. *Eng. Struct.*, 79: 244-255. DOI: 10.1016/j.engstruct.2014.08.017

Yankelevsky, D., K. Spiller, J. Packer and M. Seica, 2017. Fracture characteristics of laboratory-tested soda lime glass specimens. *Can. J. Civ. Eng.*, 44: 151-160. DOI: 10.1139/cjce-2016-0374

Yankelevsky, D., K. Spiller, J. Packer and M. Seica, 2018. Standard testing of glass revisited - experimental and theoretical aspects. *J. Test. Eval.*, 46: 20170221-20170221. DOI: 10.1520/JTE20170221

Paper B



A numerical method for analysis of fracture statistics of glass and simulations of a double ring bending test

David T. Kinsella · Kent Persson

Received: 15 September 2017 / Accepted: 20 March 2018
© The Author(s) 2018

Abstract The results from a new numerical method for simulating the strength and fracture locations of small glass specimens subjected to double ring bending are compared with experimental data. The method implements the weakest-link principle while assuming the existence of Griffith flaws. A Weibull distribution for the strength is simulated based on a single population of Pareto distributed crack sizes. The effect of using different fracture criteria is investigated. An alternative distribution is simulated based on two populations of flaws. This distribution models the apparent bimodality in the empirical data set. The numerical method is dependent on a representation of the surface flaws condition in glass. As new techniques become available for examining the surface characteristics, this numerical method is promising as a means for modelling the strength better than current methods do.

Keywords Glass · Strength · Fracture statistics · Stochastic methods

1 Introduction

In order to explain and predict the strength of annealed glass a range of concepts and methods have been applied with mixed results. Typically, the strength is explained assuming the existence of Griffith flaws and supposing the weakest-link principle. Predictions are based either on some standard distribution or on tables and diagrams obtained using a modelling tool such as the Glass Failure Prediction Model (GFPM) (Beason and Morgan 1984). There is disagreement among researchers as to which prediction model is the correct one to use (Fischer-Cripps and Collins 1995). A range of experiments have shown a consistent bilinearity in the probability plots when the Weibull distribution is used for modelling the strength of annealed glass (Veer 2007; Veer et al. 2009). As regards the GFPM, it has been said that it “is best suited to representing glass strength for specific test conditions.” (Reid 2007) Neither the standard distributions nor the GFPM are able to consistently provide for an acceptable goodness-of-fit while modelling data from experiments, something that is called for in a prediction model with true potential. At the same time, structural glass is gaining in popularity among designers and units are being installed in buildings and public spaces worldwide at an increasing rate. The search for a failure prediction model is therefore as topical as ever. Moreover, a study has indicated that shear stress might affect the observed strength of glass in double ring bending tests (Reid 2007). Shear stress is generally not considered in current failure models

D. T. Kinsella (✉) · K. Persson
Division of Structural Mechanics, Faculty of Engineering
LTH, Lund University, P.O. Box 118, 221 00 Lund, Sweden
e-mail: david.kinsella@construction.lth.se

K. Persson
e-mail: kent.persson@construction.lth.se

for glass. In this article, a numerical method for predicting the failure of glass is investigated and applied to double ring bending tests. The method is general and can be applied to a range of specimen geometries, loading setups and support conditions. The results are compared with experimental data. The presented method depends on a model that is based on fracture mechanics and the weakest-link principle while assuming a preexisting population of surface cracks. Stress corrosion is not directly considered in this study. The presented method should not be taken as a complete and final strength design tool. The aim is to promote a failure model for glass that is based on a logical and tractable representation of the surface condition in glass with a suitable consideration of the fracture mechanics. With further research, this could in the end lead to an improved strength design tool for use with glass.

2 Background

Flaws in glass are capable of promoting brittle failure due to the lack in capacity for plastic flow. While assuming that the surface contains a large number of minute flaws that act like cracks, so-called Griffith flaws, it is possible to explain the scatter in fracture location observed in experiments. It also helps to explain the variation in failure stress observed and the relatively low strength attained in practice. Surface flaws arise in the production line during manufacture as well as in subsequent handling, transportation, assembly, use, and maintenance. Bulk flaws are disregarded in the following, cf. Bourhis (2008). Griffith (1920) modelled crack growth as a reversible thermodynamical process. For a crack subjected to mode I opening displacement, fracture is governed by the following criterion

$$K_I \leq K_{Ic} \quad (1)$$

where K_I is the Stress Intensity Factor (SIF) and K_{Ic} denotes the fracture toughness (Irwin 1957). The value of K_{Ic} for glass has been estimated at about $0.75 \text{ MPa m}^{1/2}$ (Mencik 1992). It is assumed that the individual cracks do not interact with each other. The shape of a surface crack in glass is typically conceived of as being either a long, straight-fronted plane crack or a semi-circular crack (Haldimann 2006). There exist several solutions to the calculation of the SIF for a semi-circular crack subjected to a uniform tensile stress field σ_n oriented perpendicular to the crack plane. Accord-

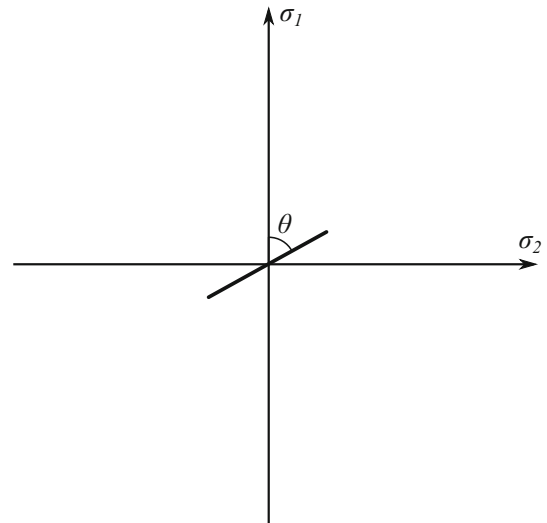


Fig. 1 A plane crack subjected to a biaxial stress field with the crack plane inclined at an angle θ in the coordinate system of the principal stresses σ_1 and σ_2

ing to one solution the SIF at the deepest point on the crack contour is (Newman and Raju 1981)

$$K_I = 1.14 \times \frac{2}{\pi} \sqrt{\pi a} \times \sigma_n \quad (2)$$

where a denotes the crack depth, see also Thiemeier et al. (1991). Figure 1 illustrates a crack subjected to a biaxial stress field with the crack plane inclined at an angle θ in the coordinate system of the principal stresses σ_1 and σ_2 . If the crack plane is oriented perpendicular to the Maximum Principal Tensile Stress (MPTS) σ_1 then

$$\sigma_n = \sigma_1 \quad (3)$$

is substituted into Eq. (2). Otherwise, the tensile stress acting normal to the crack plane can be calculated as

$$\sigma_n = \sigma_1 \cos^2 \theta + \sigma_2 \sin^2 \theta \quad (4)$$

The presence of shear stress does not have any effect in a pure mode I fracture criterion. There exists a range of fracture criteria for a crack subjected to both normal and shear stresses while assuming mode I crack opening and mode II in-plane shearing displacements. One such mixed mode fracture criterion which is based on the maximum non-coplanar energy release rate (Hellen and Blackburn 1975) is given by the following inequality

$$\sqrt[4]{K_I^4 + 6K_I^2 K_{II}^2 + K_{II}^4} \leq K_{Ic} \quad (5)$$

where the left-hand side of inequality (5) is a mode I-equivalent SIF, cf. Thiemeier et al. (1991). For a semi-circular crack K_{II} can be approximated as (Thiemeier et al. 1991)

$$K_{II} = 1.14 \times \frac{4}{\pi} \frac{1}{2 - \nu} \sqrt{\pi a} \times \tau \tag{6}$$

In Eq. (6) ν is Poisson’s ratio. τ is the shear stress in the crack plane which can be calculated from the in-plane principal stresses as

$$\tau = \frac{1}{2} |\sigma_1 - \sigma_2| \sin 2\theta \tag{7}$$

The idea that you can calculate the distribution of macroscopic strength of a stressed solid by starting from an analysis of the microscopic defects dates back at least to Peirce (1926). Peirce (1926) formulated the Weakest-Link Principle (WLP), i.e. that the strength of a chain is governed by its weakest link, and applied it in the study of the tensile strength of cotton yarn. Also using the WLP, Weibull (1939) came up with the following distribution function for the strength of a brittle solid

$$S = 1 - e^{-B}, \quad B \geq 0 \tag{8}$$

where B , denoted “the risk of rupture”, is a function of body size and tensile stress. According to Weibull (1939), a simple mathematical form that is in general accord with experimental data is

$$B = \left(\frac{\sigma}{k}\right)^m, \quad \sigma \geq 0 \tag{9}$$

where k and m denote the scale and shape parameters, respectively. Inserting Eq. (9) into Eq. (8) gives the standard two-parameter Weibull distribution function where k is also the 63rd percentile (Wachtman et al. 2009). Various derivations of the strength distribution function for a brittle solid are offered by e.g. Freudenthal (1968), Matthews et al. (1976), Batdorf and Heinisch (1978), Evans and Jones (1978) and Danzer (1992). In general, the derivation is based on a subdivision of the stressed solid into regions. It is assumed that there exists a population of non-overlapping cracks which are distributed among the regions. Each crack is associated with a critical stress. It is assumed that the stress state varies slowly so that all cracks within a subdivided region are subjected to the same nominal stress. The solution methods, which are analytical, vary. Also varying are certain assumptions, such as whether or not it is supposed that the fracture of the crack depends only on the component of stress normal to the crack plane, whether or

not there exist multiple crack populations, etc. Essentially, the analytical expression for the strength distribution is obtained through a limit operation in which the region size shrinks infinitesimally while the number of subdivided regions increases indefinitely. All these solution methods are capable of producing the fundamental Eq. (8). However, the mathematics soon become intractable when all but the simplest assumptions are made for the stress state, fracture criterion, crack size distribution, flaw density, crack plane orientation, and the existence of multiple flaw populations. Yankelevsky (2014) offers a numerical solution method to the problem of determining the strength distribution of a brittle solid while building upon the same general ideas as in the aforementioned studies except that the limit operation is not carried out. In other words, it is not necessary to assume that a crack of some finite size is contained within an infinitesimally small space, cf. Afferrante et al. (2006). Yankelevsky illustrates the method in a study of a glass square plate subjected to bending. He neglects bulk flaws and considers failures starting from the surface area only. The surface area of the plate is subdivided into unit cells measuring 1 cm². One crack is distributed into each cell. The flaw size density function proposed by Yankelevsky (2014) and which is motivated for use with glass material can be interpreted as a truncated exponential distribution. The square plate is laterally supported along two opposite edges and subjected to a line-load at midspan producing a uniaxial state of stress in the plane of the tensioned surface. A Monte Carlo simulation is carried out for a large sample of thousands of virtual specimens. This numerical method offers a tractable way of calculating the strength distribution as well as the fracture location distribution for arbitrary stress states, fracture criteria, crack plane orientations, crack size distributions, and multiple flaw populations. However, in Yankelevsky (2014), only a uniaxial tensile stress field is considered where the cracks are stressed normal to their crack planes. Subcritical crack growth is not considered. Nor is the method applied to a double ring bending test which is quite a common and relatively inexpensive method to evaluate the strength of small glass plates (Dalgliesh and Taylor 1990).

Based on Hertzian indentation tests it has been suggested that flaw size in glass can be closely fitted by a Pareto distribution (Poloniecki and Wilshaw 1971; Poloniecki 1974; Tandon et al. 2013). The Pareto distribution has the scale and shape parameters $a_0 > 0$

and $c > 0$ and the distribution function is (Forbes et al. 2010)

$$F(x) = 1 - \left(\frac{a_0}{x}\right)^c, \quad x \geq a_0 \quad (10)$$

It has moreover been shown that the Weibull distribution function is derived from the WLP if it is assumed that the surface flaws condition is represented by a single population of cracks whose size is Pareto distributed in the tail (Jayatilaka and Trustrum 1977). In this view the Weibull shape parameter is a true material parameter. Then, the relation between the shape parameters m and c of the Weibull and Pareto distributions, respectively, is found to be

$$m = 2c \quad (11)$$

When stressed in an ambient atmosphere, glass strength is reduced over time due to a process known as static fatigue which is due to subcritical crack growth, the effects of which are only observed when the mode I SIF lies above a threshold limit value at about 0.25 MPa m^{1/2} (Wiederhorn and Bolz 1970). In Charles' stress corrosion rate theory (Charles 1958a, b), subcritical crack growth is explained as a thermally activated chemical process whereby water moisture interacts with tensile stress at the crack tip. Equation (12), however, often approximates observed values of subcritical crack growth (Mencik 1992)

$$v = AK_1^n \quad (12)$$

where v is the subcritical crack growth velocity, A is a constant, and n is the stress corrosion parameter. While the value of n was repeatedly estimated at about 16 for soda-lime glass in ambient conditions, the value of A at 50% relative humidity was estimated in a range spanning more than two orders of magnitude, see Schula (2015) for an overview of those experiments. Hence, it is generally challenging to predict subcritical crack growth in ambient conditions.

3 Surface flaws concept

For the representation of the surface flaws condition, we consider two models. The first one comprises a single population of semi-circular edge cracks with a Pareto distributed crack size. The second model comprises a dual population of semi-circular edge cracks with a Pareto and Fréchet distributed crack size, respectively.

In both cases, a choice of crack density at 2 cm⁻² is made. The purpose with the dual population model presented here is to provide a logical basis for a strength distribution with a bimodality. The choice of crack density at 2 cm⁻² is guided by the following observation. Based on optical scanning techniques applied to a pair of small soda-lime silicate glass plates in the as-received condition there were 632 flaws observed and it was noted that the flaw mean density varied between 1.2 and 2.6 cm⁻² for flaw sizes greater than approximately 8 microns (Wereszczak et al. 2014).

3.1 Single population model

For the single population model, it is assumed that the cracks are uniformly distributed over the surface area of the original plate and that the crack planes are oriented between $[0, \pi)$ according to a uniform distribution.

The logical basis for the selected choice of single population model are the Hertzian indentation tests that have been carried out in the past (Poloniecki and Wilshaw 1971; Poloniecki 1974; Tandon et al. 2013) and which have provided data that could be closely fitted by a Pareto distribution, see Sect. 2.

3.2 Dual population model

For the dual population model it is assumed that it comprises two populations of semi-circular edge cracks with a Pareto and Fréchet distributed crack size, respectively. All cracks are uniformly distributed over the surface area of the original plate and the crack planes are oriented perpendicular to the MPTS. The Pareto population cracks represent large surface flaws. The Fréchet cracks represent small surface flaws. It is assumed that the number of Pareto cracks is a small fraction of the total number of cracks. It is assumed that the fraction is 0.002.

The logical basis for the dual population model is the following. First, glass fracture statistics tend to produce bimodalities in the probability plots according to e.g. Veer et al. (2009). In fact, the experiment considered in Sect. 5 is no exception because the histogram of the data appears to exhibit two modes, see also Fig. 3. Other researchers have suggested to represent the surface cracks using two populations. Mencik (1992) distinguishes between several populations of surface flaws

according to their origin. In doing so, Mencik (1992) distinguishes between a large flaws and a small flaws population of cracks with relevance for the practical engineering strength of glass. Mencik (1992) characterizes the large flaws population as being responsible for the tensile stress to decrease to 20–60 MPa. Substituting these values into Eq. (2) while assuming that the SIF equals to $0.75 \text{ MPa m}^{1/2}$, the corresponding crack depth is found to be 94–850 microns. Mencik (1992) characterizes the small flaws population as containing cracks smaller than a hundredth of a millimeter in depth. He associates this with a strength reduced to 60–200 MPa. Substituting these values into Eq. (2) yields a corresponding crack depth of 8–94 microns. A statistical model for characterizing glass strength when two flaw populations are superimposed due to abrasive phenomena has been proposed in Pisano and Carfagni (2017). Pathirana et al. (2017) implemented a dual population of cracks in a numerical model for the evaluation of the strength distribution in panels subjected to point contact actions. Second, the choice for the value of the fraction of large cracks, i.e. 0.002, is guided by the following observation. Out of the total number of flaws detected in the investigations by Wereszczak et al. (2014), the proportion of large flaws greater in size than or equal to about 200 microns was approximately 0.002. This corresponds with a crack depth of 100 microns assuming that the flaws are semi-circular surface cracks. Taking a crack depth of about 100 microns as a value that separates large flaws from small flaws is through adoption of the line of reasoning in Mencik (1992). Third, the logical basis for the Pareto distribution are the Hertzian indentation tests that have been carried out in the past and which have been mentioned earlier in this paper already. Fourth, the logical basis for the Fréchet distribution is motivated as follows. Assuming that small flaws are exceedingly numerous, one might select only the greatest small flaw in a given region and let this one determine the fracture mechanical behaviour of the small flaws population in that region (Freudenthal 1968). Because it is assumed that the cracks in the small population are abundant, it is supposed that the selected crack plane is oriented approximately normal to the maximum principal tensile stress. If the numerous small flaws have an independent Pareto size distribution then in the limit the largest flaw size is Fréchet distributed (Beirlant et al. 2004). For extreme-value theoretical reasons the greatest flaw size among a large set of flaws whose size is iden-

tically and independently distributed is approximately Fréchet distributed if the following holds (Horst 2009); the sampled distribution has a range which is unlimited from above and its distribution function F is such that there exist some positive numbers k, A such that

$$\lim_{x \rightarrow \infty} x^k (1 - F(x)) = A \quad (13)$$

Hence, the Pareto distribution lies in the domain of attraction of the Fréchet distribution (Beirlant et al. 2004).

4 Numerical modelling tool

Here follows a description of a numerical modelling tool for the strength of glass plates in bending based on an implementation of the weakest-link principle and some concept for the surface flaws condition. The numerical method adopted in this study is based on the Monte Carlo simulation method carried out by Yankelevsky (2014). The most important difference between the present study and Yankelevsky (2014) is that the present study considers multiple flaw populations with arbitrary crack plane orientations and a mixed mode fracture criterion.

Float glass is usually produced and shipped in a standard size so-called jumbo plate with the dimensions $3.21 \times 6.00 \text{ m}^2$. Taking the standard jumbo plate as a starting point, the plate is subdivided into unit cells of 1 mm^2 . This cell size provides a reasonable compromise between resolution and computational cost. A set of flaws are randomly scattered across the cells according to a uniform distribution, although in general another spatial distribution could be adopted. It is supposed that the stochastic orientation of the crack planes is uniformly distributed. This assumption might not be conservative, however, if there is a tendency for the flaws to lie in some particular direction due to e.g. machining abrasion or contact with the rollers during manufacture. The total number of flaws on the jumbo plate is fixed and depends on the flaw density. It is assumed that the flaw density is 2 cm^{-2} yielding a total of 385,200 flaws on either face of the plate. Each flaw is independently assigned a size based on some statistical distribution function which depends on the particular flaws concept that is adopted. The random flaws are resampled in each new simulation of the jumbo plate.

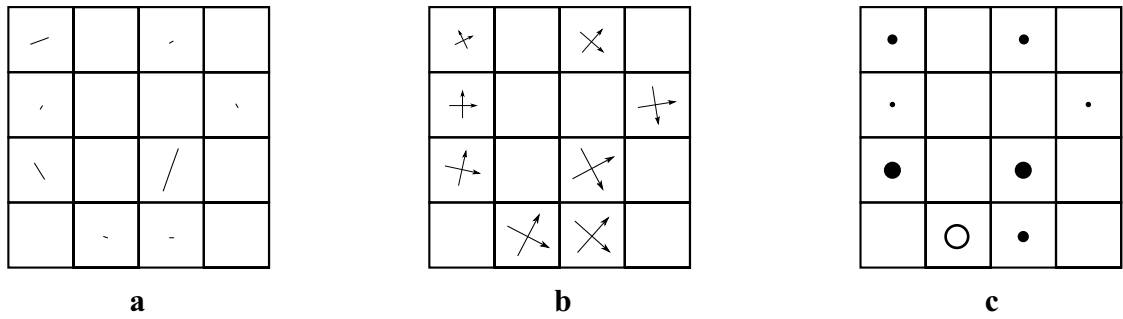


Fig. 2 Main steps leading up to the creation of the SIF envelope. **a** Random flaws are sampled and located across the unit cells. **b** The bending stresses are determined and compared with the flaws. **c** The resulting SIFs with magnitudes illustrated by discs

are calculated based on one of the fracture criteria. The large white disc represents the critical event that the SIF exceeds the fracture toughness

The stochastics of the flaws are the location, the orientation in the plane, and the size. Next, a specimen of given dimensions is extracted and separated from the jumbo plate. In the following the cut out specimen is analysed.

The cut out specimen is subjected to an arbitrary loading in increments and the stress field history at the centre of each flaw-containing unit cell determined. It is supposed that the load type is such that tensile stress actually develops on the face of the cut out specimen otherwise failure will not be detected based on fracture mechanics. In general the stress response is non-linear. The loading increment is chosen so as to produce a tensile stress increase of no more than 1 MPa per increment anywhere on the specimen. However, if the response is linear then it suffices with one increment and to scale the results. The complete stress history needs only to be calculated once for a given loading type and specimen geometry because the stochastics of the cracks do not affect the distribution of nominal bending stresses. It is assumed that the sum of load increments is sufficiently large in relation to the given flaw characteristics, i.e. flaw density, flaw size distribution, etc., to prompt fracture. Otherwise, failure might not have been detected by the end of the last load increment. There exists a SIF envelope that meets with the fracture toughness at some point in time, the smallest of which is identified as the time of failure. If the crack planes are always oriented perpendicular to the MPTS then the SIF envelope is calculated using Eqs. (2) and (3). For reference, this case is denoted MPTS mode I fracture criterion. If the crack planes are inclined at an oblique angle in

the coordinate system of the principal stresses while mode I opening displacement is considered then the SIF envelope is calculated using Eqs. (2) and (4). This case is denoted oblique angle mode I fracture criterion. If both mode I opening and mode II shearing displacements are accounted for then the SIF envelope is calculated using the left-hand side of inequality (5). This is the mixed mode fracture criterion. By token of the WLP, the fracture origin is determined from the first unit cell that contains a flaw with a SIF exceeding the fracture toughness. A search algorithm is used to detect this cell. By carrying out simulations on a whole series of cut out specimens it is possible to obtain a sample of the fracture stress which is defined as the MPTS at the failure origin. In this study the number of cut out specimens in a simulation series is 5,000. This sample size offers a reasonable compromise between precision and computational cost. Figure 2 illustrates the main steps leading up to the creation of the SIF envelope: (a) the flaw stochastics are sampled, (b) the in-plane principal stresses are determined at each load increment and (c) the SIF envelope is calculated per load increment based on either of the fracture criteria. Failure is prompted at the first instance of intersection between SIF envelope and fracture toughness (white disc). Likewise, the failure origin is determined by the first unit cell that contains a SIF which exceeds the fracture toughness. The so-called critical stress is the uniform tensile stress perpendicular to a given crack plane that would bring about failure with a pure mode I fracture criterion. The critical stress can be calculated with Eqs. (1) and (2).

5 Experimental data comparison

Double ring bending tests are frequently carried out to evaluate the strength of glass. In this testing device a glass plate is supported on a reaction ring and subjected to an applied loading through a smaller concentric ring on its opposite side. An equibiaxial state of stress is produced within the loading ring. Failures that start from edges are eliminated because tensile stress diminishes near the edges. Some experimenters discard any observation associated with a failure originating from outside the loading ring radius. Simiu et al. (1984) carried out experiments on 56 small square glass plates in double ring bending. The plates had the nominal dimensions $179 \times 179 \times 6 \text{ mm}^3$. The mean thickness was 5.4 mm. The glass was new in the as-received condition and it had been obtained from the same manufacturer and batch. The loading ring radius was 25.4 mm and the segmented reaction ring radius 60.3 mm. All specimens were subjected to ramp loads that generated an average rate of stress of 0.8 MPa/s inside the loading ring. The load-duration until failure ranged from 48 to 117 s. It is not known whether it was the tin side or air side of the glass plates that was subjected to tensile stress. The tin side is defined as the side of the glass that was in contact with the molten tin bath in the float process production method.

This experiment is selected for a number of reasons. The data report is complete with values for the fracture stress even when the failure originated from outside the loading ring. Because Simiu et al. (1984) reported the fracture locations it is possible to make comparisons with the simulated failure origin data. The data is challenging to model. A Weibull distribution for the strength can be rejected, cf. Sect. 6.1. The modelling of the surface flaws condition is simplified when edge failures are eliminated.

Using a formula for a flat circular plate of constant thickness, Simiu et al. (1984) calculated the in-plane MPTS for each fractured specimen. The stress was calculated at the centre of the plate, even when the fracture origin was not located within the loading ring radius. Twelve of the data points, however, were associated with failures originating from outside the loading ring. Those values have been readjusted by this author in order to reflect the MPTS at the actual failure location rather than the MPTS inside the loading ring. The adjustments were made based on finite element calculations with the computer software ABAQUS/CAE

(2013). The loading rings were modelled by analytic rigid surfaces. The glass part was modelled with 20-node quadratic solid elements with reduced integration, although it would also be possible to use continuum shell elements. The number of through-the-thickness elements was 5 and the number of elements in the plane was about 9500. Only a quarter of the plate was modelled for symmetry reasons. It was assumed that Young's modulus is 70 GPa and Poisson's ratio is 0.23 (Bourhis 2008). A friction coefficient of 0.1 was used in modelling the contact between loading ring and glass parts.

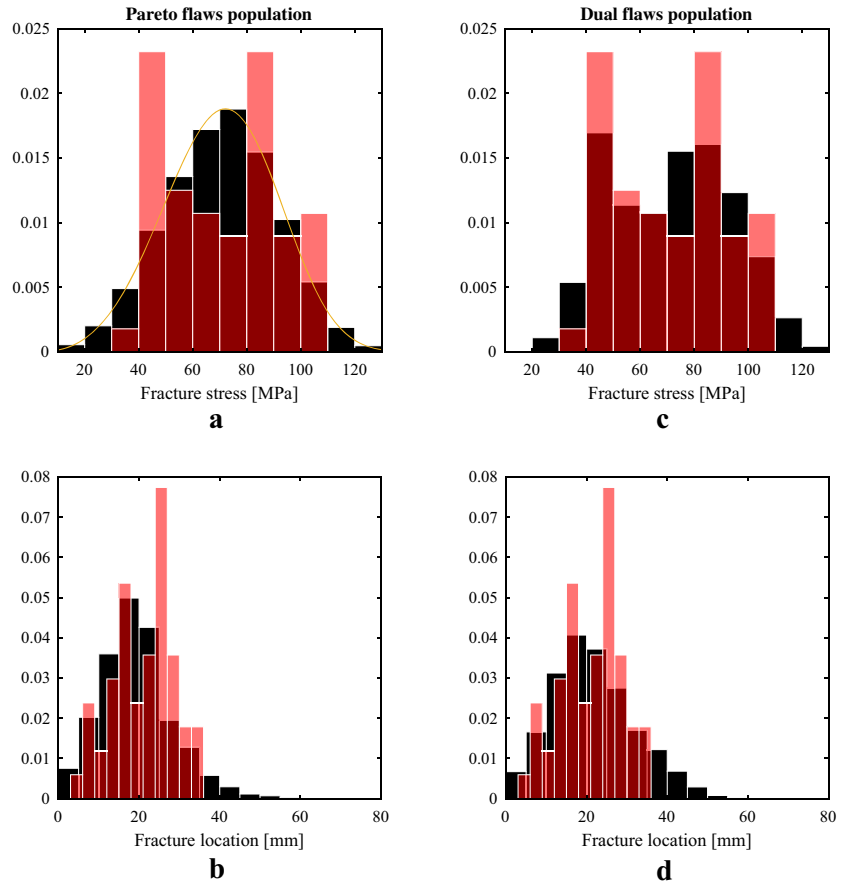
6 Results

Virtual glass specimens were tested until failure in double ring bending and the results were compared with data from the experiment conducted by Simiu et al. (1984). The analysis was carried out using the software ABAQUS/CAE (2013) and MATLAB (2016). The following cases were investigated, viz. a single population of Pareto distributed flaw sizes using either the MPTS mode I fracture criterion or oblique angle mode I criterion or the mixed mode criterion, and a two-population concept for the flaw sizes using only the MPTS mode I fracture criterion.

6.1 Single population of flaws

A fracture stress distribution was simulated based on the oblique angle mode I fracture criterion, cf. Eqs. (1), (2) and (4) while supposing that the surface condition is characterized by a single population of Pareto distributed flaw sizes. This is illustrated in Fig. 3a and the values shown are the MPTS at the failure origins. The histogram in Fig. 3a is normalized so as to reflect a probability density function. The area of each bar is the relative number of observations. The total sum of the bar areas is less than or equal to 1 depending on whether or not some of the data lies outside the bin limits. The sampled distribution was compared with a Weibull distribution and the goodness-of-fit was tested using the Anderson–Darling (AD) statistic (D'Agostino and Stephens 1986). No significance was obtained in a test at the 5% level. The simulated distribution appears to be indistinguishable from a Weibull distribution. An ordinary Weibull distribution was fit-

Fig. 3 Simulated and empirical fracture stress and failure location distributions. Semi-transparent (red) histograms represent the empirical data. Opaque (black) histograms represent the simulated data. Overlapping histograms are dark red. Sturges binning method was used for the simulated data sets



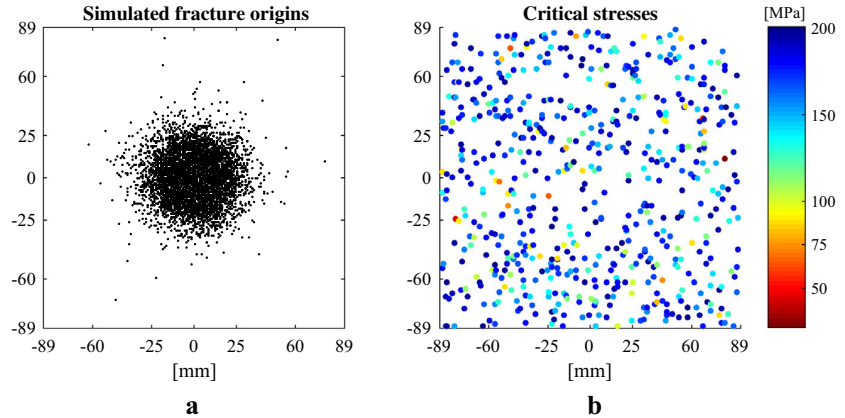
ted to the empirical data set using the maximum likelihood method and the estimated parameter values were $k = 78$ MPa and $m = 3.8$. Using the AD statistic it could be rejected at the 0.4% level that the empirical data set is Weibull distributed. The simulated distribution was optimized so as to match the ordinary Weibull model which was fitted to the empirical data. The optimization was carried out by varying the underlying Pareto distribution parameters until the simulated strength distribution was similar to the Weibull distribution that was fitted to the empirical data. The similarity was measured by fitting a Weibull distribution to the simulated sample and comparing the so fitted Weibull parameters with the parameter estimates of the Weibull model that was fitted to the empirical data set. See Fig. 3a where both the empirical data set (red bars), the fitted Weibull density function (solid line) and the simulated distribution (black bars) are illustrated.

Table 1 Pareto parameter values that generated an estimated Weibull distribution with the scale and shape parameters $k = 78$ MPa and $m = 3.8$ while using the numerical method

Fracture criterion	Scale param. (μm)	Shape param.
MPTS	8.4	2.34
Oblique angle	8.3	2.13
Mixed mode	8.8	2.26

The strength distribution was further simulated using the MPTS mode I criterion and the mixed mode criterion. The Pareto parameters were selected so that the strength distribution could be fitted by a Weibull distribution with scale and shape parameters $k = 78$ MPa and $m = 3.8$. Table 1 contains the Pareto parameter values so far discussed according to the three fracture criteria.

Fig. 4 Left: Simulated fracture locations. Right: Critical stresses in a single cut out specimen



In Fig. 3b the simulated fracture locations in the radial direction are shown together with the empirical for the oblique angle mode I case. Using a two-sample AD test (Scholz and Stephens 1987; Trujillo et al. 2007), a significant deviation between the pair of data sets could be detected. The spatial distribution of failures is further illustrated in Fig. 4a.

The critical stresses in a single cut out specimen are obtained by solving for σ_n in Eq. (2) after substituting for the fracture toughness value in Eq. (1) as illustrated in Fig. 4b.

Considering the various fracture criteria, the following was noted while using identical Pareto parameter values for generating the strength distribution. The mode I fracture criterion in the oblique angle case produced only a very small difference in the strength data sample compared with the mixed mode criterion, cf. Eqs. (1), (2), (4) and (5). The 63rd percentiles deviated by less than 3%. However, taking mode II shearing displacement into consideration increased the proportion of failures originating from outside the loading ring by 20%. Comparing the flaw-orientation independent MPTS mode I criterion, Eqs. (1), (2) and (3), with either of the two other criteria yielded a significant difference in the data samples; the 63rd percentile of the simulated strength was more than 10% lower while using the MPTS case. The proportion of failures originating from outside the loading ring increased by over 60%. The results are illustrated in Fig. 5.

6.2 Two populations of flaws

It is possible to obtain a simulated distribution like the one shown in Fig. 3c while assuming that the flaws

originate from two different populations, see Sect. 3. The flaw model parameters are given in Table 2. The resulting distribution could not be distinguished from the empirical data set with any statistical significance at the 5% level judging from the two-sample AD test statistic ($p = 0.64$). In Fig. 3d the simulated fracture locations are shown together with the empirical. It was found using the same test statistic that a significant departure exists from the hypothesis that the experimental and simulated fracture location data sets come from equal distributions.

7 Discussion

Providing for consistency in a glass failure prediction model calls for its foundation to be laid on physically sound concepts such as the WLP. The WLP captures an essential feature of brittle material failure. The existence of Griffith flaws is another physical concept to build upon. The Weibull distribution implements the WLP which makes it an attractive choice for a glass failure prediction model, at least from a theoretical point of view. All major standards including the European draft of a Eurocode of glass acknowledge Weibull's Eq. (8) in one form or another (prEN 16612:2013). A number of studies, however, have indicated that the Weibull distribution does not provide a superior fit compared with a lognormal or normal distribution (Lü 1997; Calderone et al. 2001; Veer et al. 2009; Huerta et al. 2011; Kinsella and Persson 2016). It has been noted that the estimated value of the Weibull shape parameter varies quite significantly from one sample to another in experiments (Ritter et al. 1985; Carre 1996; Huerta et al. 2011). Some researchers have called for abandoning

Fig. 5 Left: Oblique angle versus MPTS mode I fracture criterion. Right: Oblique angle mode I versus mixed mode fracture criterion. Semi-transparent (red) bars indicate the oblique angle mode I data. Overlapping histograms are dark red

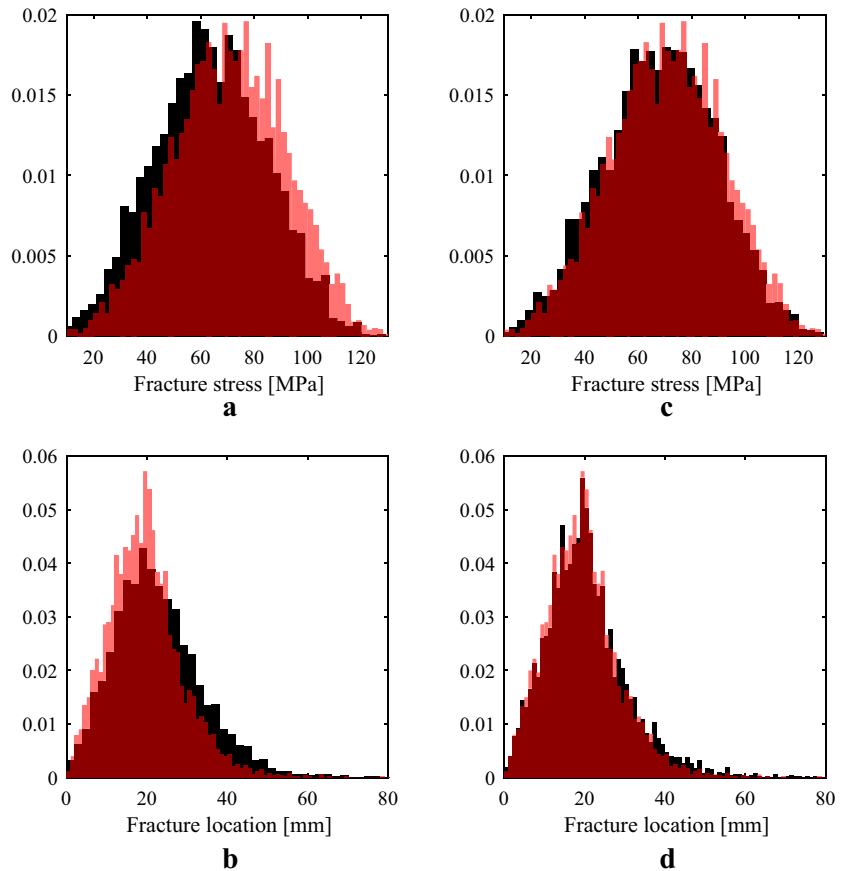


Table 2 Pareto and Fréchet parameter values used in the dual population model that was implemented with the numerical method

Pareto		Fréchet	
Scale (μm)	Shape	Scale (μm)	Shape
130	4.0	11	3.0

the Weibull model altogether in favour of a normal or lognormal distribution (Calderone et al. 2001). But to adopt a normal distribution in this case is to favour with a model lacking in failure-based physical concept. In contrast, by using the numerical method in this paper it is possible to keep intact the WLP as well as the Griffith flaws assumption while producing data fits equal or superior to the Weibull model. Figure 3a illustrates that it is possible to simulate a Weibull distribution using this numerical tool while assuming that the sur-

face flaws are sampled from one single population of Pareto distributed sizes. In keeping with recent experimental findings using optical scanning techniques, cf. Wereszczak et al. (2014), it was assumed that the flaw density is 2 cm^{-2} . From a theoretical point of view, the shape parameter of the simulated Weibull distribution should relate with the Pareto shape parameter according to Eq. (11) if the stress state is uniform uniaxial. At any rate, the Weibull distribution doesn't actually model the experimental data that was compared with.

While exploring the possibility of implementing two flaw populations, the idea is to distinguish between one large flaws population of flaws greater in depth than about 100 microns and one smaller flaws population. An idea along a similar line was proposed by Mencik (1992), cf. Sect. 3. The purpose is to model the bimodality that is frequently encountered in the strength distribution from practical experiments. Turning to Fig. 3c it is evident that an acceptable fit can be achieved with

Table 3 Weibull shape parameter estimates from 16 experiments on new annealed glass plates in double ring bending, tested in ambient conditions

Reference	Load. ring diam. (mm)	Approx. stress rate (MPa/s)	Sample size	Weib. shape param.
Peeken (1982) ^a	600	2	97	10.1
Peeken (1982) ^a	600	2	99	11.3
Simiu et al. (1984)	51	0.8	56	4.0
Simiu et al. (1984)	51	1.0	29	3.6
Mellmann and Maultzsch (1989) ^a	600	2	113	5.1
Mellmann and Maultzsch (1989) ^a	600	2	108	3.9
Fink (2000)	55	2	20	3.5
Fink (2000)	55	2	107	5.9
Overend (2002)	51	0.7	10	2.4
Overend (2002)	51	0.9	10	1.8
Overend (2002)	51	0.6	10	4.9
Haldimann (2006)	51	0.2	10	3.7
Haldimann (2006)	51	21	10	4.2
Postigo (2010) ^b	180	2.4	41	2.9
Schula (2015)	80	2	15	7.8
Muniz et al. (2016)	60	2	28	4.5

^aObtained from Sedlacek et al. (1999)

^bObtained from Huerta et al. (2011)

a two-population flaws concept. Moreover, this fit is at least as good as the fitted Weibull model in Fig. 3a as can be seen by comparing the p -values from the AD tests. Moreover, the tail of the distribution is important when calculating the design value. Therefore, when choosing between the simulated distributions as seen in Fig. 3a and c, as a matter of fact, the ordinary Weibull distribution appears to provide the most conservative approach.

With a two-parameter Weibull distribution, only two parameters are fitted to the data. With the numerical model presented in this paper, the Pareto and Fréchet distributions each require two parameters. As the number of parameters increase, it is only logical that a better fit might be produced. Therefore, the outcome while comparing Fig. 3a with c is rather predictable. However, if it were possible to estimate some of the surface flaw parameters a priori, the numerical modelling tool would gain in potential. Then, these parameter estimates would be based on the material physics. There is a need for more data on the surface flaws condition in glass. Up to date, the published data is scarce. As new techniques become available for examination and assessment of the surface condition in glass, more reliable input data will likely become available for use in this kind of numerical prediction tool.

Moreover, with this numerical tool it is possible to simulate the distribution of fracture locations. The simulations were not quite able to model the empirical distribution of fracture location. This is due to the lower mean value in the simulations as well as the longer tail, cf. Fig. 3b and d. However, it may also be due to the fact that a large number of fractures in the empirical data set occurred at the loading ring contact circle. About one in five specimens failed under the loading ring. This could have an impact not only on the failure location statistics but also on the fracture stress statistics.

The Weibull shape parameter value that was estimated based on the double ring bending experiment carried out by Simiu et al. (1984), i.e. $m = 3.8$, might indicate a high dispersion for the experimental data because the value is quite low. The data refers to an experimental campaign carried out almost 40 years ago. In order to investigate the dispersion, a table was organized, cf. Table 3, which contains the estimated Weibull shape parameter values from a range of experiments with the double ring bending device. All listed items in Table 3 refer to experiments on new, annealed glass that was tested in ambient conditions. The experiment carried out by Simiu et al. (1984) is included in Table 3 where the estimated shape parameter value was based

on the original data, unadjusted with respect to the true stress at the fracture origin, see also Sect. 5. The results found in Table 3 show clearly that there appears to be nothing unusual about the estimated Weibull shape parameter value in the experimental data of Simiu et al. (1984). However, it is possible that the estimated shape parameter values in Table 3 were affected by the following circumstances. The table comprises both the results from glass tested with the tin side in tension and glass tested with the air side in tension. It has been noted that some experiments with the double ring bending device generate a substantial number of fractures near the loading ring contact area, see e.g. Simiu et al. (1984).

Reid (2007) studied the proportion of failures occurring inside and outside the loading ring in coaxial double ring bending tests and compared the observed results with what might be expected based on theoretical considerations using Weibull statistics. He found that a series of 59 small specimens of annealed plates 6 mm in thickness produced anomalous results. The proportion of failures occurring outside the loading ring was substantially greater than expected. Reid hypothesized that this might be related to the glass having to withstand shear stresses outside the loading ring. Due to the equibiaxial state of stress within the loading ring, shear stresses are not present there. Our results show that if a uniformly distributed flaw orientation is considered in the fracture criterion, then there is a significant effect on the observed proportion of failures originating from outside the loading ring while taking mode II shearing displacement into consideration. The proportion increases by 20% with the mixed mode failure criterion. However, disregarding flaw orientation altogether in the fracture criterion, i.e. considering only the MPTS, yields the highest proportion of failures originating from outside the loading ring. Our results are therefore not conclusive with respect to Reid's hypothesis. It depends on whether or not it is assumed that flaw orientation matters. More experiments need to be carried out in order to verify or disprove this hypothesis while taking note of the fracture statistics of failures occurring outside the loading ring.

Although the simulations are more time-consuming than fitting a standard statistical distribution, significant improvements in computational efficiency can certainly be made. There is mounting evidence in the literature, see e.g. Veer (2007), that the fitted models for glass fracture data in general are lacking in potential

when using a standard distribution such as the Weibull or Normal distributions. The present study was undertaken in order to explore a novel approach towards the failure prediction of glass. In order to further validate this method, more experiments could be carried out and the surface condition of glass should be investigated further.

The effects of stress corrosion on the strength of glass were neglected in this study. In a future paper, the implementation of subcritical crack growth into the numerical method will be considered.

8 Conclusions

Using a numerical simulation tool based on the weakest-link principle and assuming the existence of Griffith flaws it is possible to simulate a Weibull distribution for the strength of glass. The incorporation of mode II shearing displacement into the fracture criterion has only a very small impact on the simulated strength distribution when the glass is subjected to double ring bending. In the case of small plates in double ring bending where edge failures can be neglected, it is feasible to model the strength based on a large-flaws and a small-flaws concept while capturing a bimodality in the data set. There is a need for more knowledge and data on the surface condition in glass.

Compliance with ethical standards

Conflict of interest On behalf of all authors, the corresponding author states that there is no conflict of interest.

Open Access This article is distributed under the terms of the Creative Commons Attribution 4.0 International License (<http://creativecommons.org/licenses/by/4.0/>), which permits unrestricted use, distribution, and reproduction in any medium, provided you give appropriate credit to the original author(s) and the source, provide a link to the Creative Commons license, and indicate if changes were made.

References

- ABAQUS/CAE Version 6.13: Dassault Systèmes (2013)
- Afferrante, L., Ciavarella, M., Valenza, E.: Is Weibull's modulus really a material constant? Example case with interacting collinear cracks. *Int. J. Solids Struct.* **43**, 5147–5157 (2006)
- Batdorf, S.B., Heinisch, H.L.: Weakest link theory reformulated for arbitrary fracture criterion. *J. Am. Ceram. Soc.* **61**(7–8), 355–8 (1978)

- Beason, W., Morgan, J.: Glass failure prediction model. *J. Struct. Eng.* **110**, 197–212 (1984)
- Beirlant, J., Goegebeur, Y., Teugels, J., Segers, J., De Waal, D., Ferro, C.: *Statistics of Extremes: Theory and Applications*. Wiley, Hoboken (2004)
- Calderone, I., MacDonald, C., Jacob, L., Jacob Associates Pty Ltd: The fallacy of the Weibull distribution for window glass design. In: *Glass Performance Days*, vol. **2001**, pp. 293–297 (2001)
- Carre, H.: *Etude du comportement à la rupture d'un matériau fragile précontraint: le verre trempé*. Ph.D. Thesis, Ecole Nationale des Ponts et Chaussées (1996)
- Charles, R.: Static fatigue of glass. I. *J. Appl. Phys.* **29**, 1549–1553 (1958a)
- Charles, R.: Static fatigue of glass. II. *J. Appl. Phys.* **29**, 1554–1560 (1958b)
- D'Agostino, R.B., Stephens, M.A. (eds.): *Goodness-of-fit Techniques*. Marcel Dekker Inc, New York (1986)
- Dalglish, W., Taylor, D.: The strength and testing of window glass. *Can. J. Civ. Eng.* **17**, 752–762 (1990)
- Danzer, R.: A general strength distribution function for brittle materials. *J. Eur. Ceram. Soc.* **10**, 461–472 (1992)
- Evans, A., Jones, R.: Evaluation of a fundamental approach for the statistical analysis of fracture. *J. Am. Ceram. Soc.* **61**, 156–160 (1978)
- Fink, A.: *Ein Beitrag zum Einsatz von Floatglas als dauerhaft tragender Konstruktionswerkstoff im Bauwesen*. Ph.D. Thesis Technische Universität Darmstadt (2000)
- Fischer-Cripps, A., Collins, R.: Architectural glazings: design standards and failure models. *Build. Environ.* **30**, 29–40 (1995)
- Forbes, C., Evans, M., Hastings, N., Peacock, B.: *Statistical Distributions*, 4th edn. Wiley, Hoboken (2010)
- Freudenthal, A.: *Statistical Approach to Brittle Fracture*, Fracture, vol. II. Academic Press, New York (1968)
- Griffith, A.: The phenomena of rupture and flow in solids. *Philos. Trans. R. Soc. A* **221**, 163 (1920)
- Haldimann, M.: *Fracture Strength of Structural Glass Elements: Analytical and Numerical Modelling, Testing and Design*. Ph.D. Thesis, Ecole Polytechnique Fédérale de Lausanne EPFL (2006)
- Hellen, T., Blackburn, W.: The calculation of stress intensity factors for combined tensile and shear loading. *Int. J. Fract.* **11**, 605 (1975)
- Horst, R.: *The Weibull Distribution: A Handbook*. Taylor & Francis Group, London (2009)
- Huerta, M.C., Pacios-Alvarez, A., Lamela-Rey, M.J., Fernandez-Canteli, A.: Influence of experimental test type on the determination of probabilistic stress distribution. In: *Glass Performance Days 2011* (2011)
- Irwin, G.: Analysis of stresses and strains near the end of a crack traversing a plate. *J. Appl. Mech.* **24**, 361 (1957)
- Jayatilaka, A., Trustrum, K.: Statistical approach to brittle fracture. *J. Mater. Sci.* **12**, 1426–1430 (1977)
- Kinsella, D., Persson, K.: On the applicability of the Weibull distribution to model annealed glass strength and future research needs. In: *Challenging Glass Conference*, vol. 5 (2016)
- Le Bourhis, E.: *Glass*. Wiley-VCH Verlag GmbH & Co KGaA, Weinheim (2008)
- Lü, B.T.: Fatigue strength prediction of soda-lime glass. *Theor. Appl. Fract. Mech.* **27**, 107–114 (1997)
- MATLAB Version 9.1 (R2016b). The MathWorks Inc (2016)
- Matthews, J., McClintock, F., Shack, W.: Statistical determination of surface flaw density in brittle materials. *J. Am. Ceram. Soc.* **59**, 304–8 (1976)
- Mellmann, G., Maultzsch, M.: *Untersuchung zur Ermittlung der Biegefestigkeit von Flachglas für bauliche Anlagen*. BAM-Forschungsbericht 161, Bundesanstalt für Materialforschung und -prüfung, Berlin (1989)
- Mencik, J.: *Strength and Fracture of Glass and Ceramics*, Glass Science and Technology, vol. 12. Elsevier, Amsterdam (1992)
- Muniz-Calvente, M., Ramos, A., Pelayo, F., Lamela, M., Fernández-Canteli, A.: Statistical joint evaluation of fracture results from distinct experimental programs: an application to annealed glass. *Theor. Appl. Fract. Mech.* **85**(Part A), 149–157 (2016)
- Newman, J., Raju, I.: An empirical stress intensity factor equation for the surface crack. *Eng. Fract. Mech.* **15**, 185–92 (1981)
- Overend, M.: *The Appraisal of Structural Glass Assemblies*. Ph.D. Thesis, University of Surrey (2002)
- Pathirana, M., Lam, N., Perera, S., Zhang, L., Ruan, D., Gad, E.: Risks of failure of annealed glass panels subject to point contact actions. *Int. J. Solids Struct.* **129**, 177–194 (2017)
- Peeken, H.: *Bruchfestigkeitsuntersuchungen an quadratischen Floatgläsern der Kantenlänge 1000 mm nach der Doppelringmethode mit überlagertem Gasdruck*. Bericht Nr. 10-82, Institut für Maschinenelemente und Maschinengestaltung der RWTH Aachen, Aachen (1982)
- Peirce, F.: Tensile tests for cotton yarns. *J. Text. Inst. Trans.* **17**, 355 (1926)
- Pisano, G., Carfagni, G.R.: A micromechanical derivation of the macroscopic strength statistics for pristine or corroded/abraded float glass. *J. Eur. Ceram. Soc.* **37**, 4197–4206 (2017)
- Poloniecki, J.: *Statistical Investigation of Surface Flaws*. Ph.D. Thesis, The University of Sussex (1974)
- Poloniecki, J., Wilshaw, T.: Determination of surface crack size densities in glass. *Nat. Phys. Sci.* **229**, 226–227 (1971)
- Postigo, S.: *Estudio teórico experimental de impactos humanos contra vidrios de acristalamientos de edificación*. Ph.D. Thesis, Universidad de Politécnica de Madrid (2010)
- prEN 16612: *Glass in building-determination of the load resistance of glass panes by calculation and testing*. CEN (2013)
- Reid, S.: Effects of spatial variability of glass strength in ring-on-ring tests. *Civ. Eng. Environ. Syst.* **24**, 139–148 (2007)
- Ritter, J., Service, T., Guillemet, C.: Strength and fatigue parameters for soda-lime glass. *Glass Technol.* **26**, 273–278 (1985)
- Scholz, F.W., Stephens, M.A.: K-sample Anderson–Darling tests. *J. Am. Stat. Assoc.* **82**(399), 918–924 (1987). <https://doi.org/10.1080/01621459.1987.10478517>
- Schula, S.: *Charakterisierung der Kratzanfälligkeit von Gläsern im Bauwesen*. Springer, Berlin (2015)
- Sedlacek, G., Blank, K., Laufs, W., Güssen, J.: *Glas im Konstruktiven Ingenieurbau*. Ernst & Sohn, Berlin (1999)
- Simiu, E., Reed, D., Yancey, C., Martin, J., Hendrickson, E., Gonzalez, A., Koike, M., Lechner, J., Batts, M.: *Ring-on-ring Tests and Load Capacity of Cladding Glass*. Technical Report, NBS Building Series 162, U.S. Department of Commerce–National Bureau of Standards (1984)

- Tandon, R., Paliwal, B., Gibson, C.: Practical aspects of using Hertzian ring crack initiation to measure surface flaw densities in glasses: influence of humidity, friction and searched areas. *Philos. Mag.* **93**, 2847–2863 (2013)
- Thiemeier, T., Brückner-Foît, A., Kölker, H.: Influence of the fracture criterion on the failure prediction of ceramics loaded in biaxial flexure. *J. Am. Ceram. Soc.* **74**(1), 48–52 (1991)
- Trujillo-Ortiz, A., Hernandez-Walls, R., Barba-Rojo, K., Cupul-Magana, L., Zavala-Garcia, R.: Andarksamtest: Anderson–Darling k-sample procedure to test the hypothesis that the populations of the drawn groups are identical. A MATLAB file. <http://www.mathworks.com/matlabcentral/fileexchange/loadFile.do?objectId=17451> (2007)
- Veer, F.: The strength of glass, a nontransparent value. *HERON* **52**, 87–104 (2007)
- Veer, F., Louter, C., Bos, F.: The strength of annealed, heat-strengthened and fully tempered float glass. *Fatigue Fract. Eng. Mater. Struct.* **32**, 18–25 (2009)
- Wachtman, J., Cannon, W., Matthewson, M.: *Mechanical Properties of Ceramics*. Wiley, Hoboken (2009)
- Weibull, W.: A statistical theory of the strength of materials. *Ingenjörsvetenskapsakademiens handlingar* 151 (1939)
- Wereszczak, A., Ferber, M., Musselwhite, W.: Method for identifying and mapping flaw size distributions on glass surfaces for predicting mechanical response. *Int. J. Appl. Glass Sci.* **5**, 16–21 (2014)
- Wiederhorn, S., Bolz, L.: Stress corrosion and static fatigue of glass. *J. Am. Ceram. Soc.* **53**, 543–548 (1970)
- Yankelevsky, D.: Strength prediction of annealed glass plates: a new model. *Eng. Struct.* **79**, 244–255 (2014)

Paper C



An Analysis of Glass Fracture Statistics

David T. Kinsella^a, Kent Persson

^aLund University, Sweden, david.kinsella@construction.lth.se

A numerical method is applied to model the fracture stress and failure location in glass panes subjected to various bending arrangements. The method assumes the weakest-link principle and the existence of surface microcracks. The fracture stress and failure origin are revealed through a search algorithm. The magnitude of strength and the location of fracture are stochastic in nature and can be predicted based on a suitable representation of the surface flaws condition. When the crack size distribution is assumed to be Pareto, the strength distribution is found to be very similar to a Weibull distribution. The stresses in large laterally supported plates which are subjected to uniform pressure are modelled and the distribution of fracture location is determined based on a single population of cracks with a Pareto distributed crack size. Two types of gasket support materials are considered, neoprene and nylon. The softer gasket material produces a greater number of fractures nearer the corners of the plate. A comparison is made with the recorded fracture locations according to various experiments. In addition, a tall vertical panel of laminated glass with a complex geometry and which is subjected to dynamic impact loading is modelled and the distribution of fracture location is determined based on a single population of cracks with a Pareto distributed crack size.

Keywords: Glass, fracture statistics, fracture mechanics, Monte Carlo

1. Introduction

Various models for predicting the fracture stress have been proposed for use on glass (Beason and Morgan 1984, Sedlacek et al. 1999). Some of the models have been implemented in national building codes (DIN 18008-1, ASTM E 1300-04). The failure models proved to have potential for prediction-making within limited domains. However, making accurate predictions of the strength remains a challenge to the general design case of a glass structure with varying boundary conditions and loading types. In fact, large safety factors are implemented in the building codes. Until recently, little attention was paid to the prediction of fracture location. In the following, a method for predicting the failure stress as well as the failure origin of a glass plate subjected to both static and dynamic loading is investigated. The method which assumes the existence of surface microcracks and the governing principle of the weakest-link is applied to different specimen geometries and loading setups. The results are compared with experimental data.

2. Background

The strength of a glass pane can be revealed by subjecting it to bending until it breaks while noting the fracture load (or pressure). The fracture stress at the origin of failure can be calculated assuming that the fracture location is known. The observed fracture stress varies generally within a large range of about 20-200 MPa and is further dependent on a number of factors including the load history, the surface condition (new or weathered or artificially scratched), the size of surface area in tension, the environmental conditions in particular the relative humidity, and the origin of failure, i.e. edge or surface (Mencik 1992).

It has been suggested to use a Weibull distribution for predicting the strength of a structural unit made from annealed float glass (Weibull 1939; prEN 16612:2017). In Eq. (1), the Weibull distribution function for the strength σ is given where k and m denote the scale and shape parameters, respectively.

$$F(\sigma) = 1 - e^{-\left(\frac{\sigma}{k}\right)^m} \quad (1)$$

It has also been suggested to make predictions of the strength based on the Glass Failure Prediction Model (GFPM) (Beason and Morgan 1984). The GFPM was calibrated with experiments in which uniform lateral pressure was applied to full-scale plates with continuous lateral support along all four edges. The American building code ASTM E 1300 implements the GFPM.

The scatter in failure stress magnitude can be explained by assuming that fracture is governed by microscopic surface flaws. Tensile stress is magnified in a localized region near the flaw tip (Griffith 1920). Flaws in glass can cause brittle failure because of the lack in capacity for plastic flow. Surface flaws arise in the production line during manufacture as well as in subsequent handling, transportation, assembly, use, and maintenance. Bulk flaws are disregarded as potential fracture sites in the following.

Variations in the surface condition of glass causes the observed strength to scatter, in general, for some given set of glass specimens, even when identical testing arrangements and specimen geometries are maintained. In fact, experiments have shown that even when the specimens are extracted from the same original standard size plate, the so-called jumbo plate, significant variations in the observed strength remain (Veer et al. 2009; Veer and Rodichev 2011; Vandebroek et al. 2014). Hence, surface flaw characteristics vary significantly not just between plates from different manufacturing batches but also between plates in the same batch.

In this paper, we consider semi-circular cracks that are uniformly distributed over the surface of some glass specimen. The corresponding mode I stress intensity factor (SIF) is determined using the following equation with a referring to the crack depth (Irwin 1957; Newman and Raju 1981)

$$K_I = 1.14 \frac{2}{\pi} \sqrt{\pi a} \sigma_n \quad (2)$$

In Eq. (2), σ_n is the tensile stress normal to the crack plane. The mode I fracture criterion is

$$K_I \leq K_{Ic} \quad (3)$$

and it is assumed that the fracture toughness K_{Ic} equals to $0.75 \text{ MPa m}^{1/2}$ (Mencik 1992). It is assumed that the individual cracks do not interact with each other. As a mixed mode criterion we take

$$\sqrt[4]{K_I^4 + 6(K_I^2 + K_{II}^2) + K_{II}^4} \leq K_{Ic} \quad (4)$$

which is based on the maximum non-coplanar energy release rate (Hellen and Blackburn 1975), see also Thiemeier et al. (1991). In Eq. (4), K_{II} can be approximated as (Thiemeier et al. 1991)

$$K_{II} = 1.14 \frac{4}{\pi} \frac{1}{2-\nu} \sqrt{\pi a} \tau \quad (5)$$

with ν referring to Poisson's ratio and τ the shear stress in the crack plane.

According to experiments with Hertzian indentation fracture in glass, flaw size can be closely fitted by a Pareto distribution (Poloniecki and Wilshaw 1971; Tandon et al. 2013). The Pareto distribution is (Forbes et al. 2010)

$$F(a) = 1 - \left(\frac{a_0}{a} \right)^c \quad (6)$$

where the scale and shape parameters are a_0 and c , respectively. It has been demonstrated that the Weibull distribution function can be derived from the WLP while assuming that the surface flaws condition is represented by a single population of cracks with a crack depth that is Pareto distributed (Jayatilaka and Trustrum 1977). It is then supposed that the stress state is uniform tensile and that the crack planes are oriented normal to the uniaxial stress. Let $f(a)$ denote the probability density function of the crack depth. Then the probability of failure at stress σ for a single crack is

$$F(\sigma) = \int_{a_c}^{\infty} f(a) da \quad (7)$$

where a_c is the critical crack depth that prompts failure for a crack subjected to tensile stress perpendicular to the crack plane. The critical crack depth is obtained through combination of Eqs. (2) and (3)

$$a_c = \frac{K_{Ic}^2}{Y^2 \pi \sigma^2} \quad (8)$$

where for the sake of convenience, the geometry factor Y has been substituted for. The geometry factor is in this case given by

$$Y = 1.14 \frac{2}{\pi} \quad (9)$$

Supposing that crack depth is Pareto distributed, we derive from Eqs. (6) and (7) while substituting for Eq. (8) that

$$F(\sigma) = \left(\frac{Y \sqrt{\pi a_0} \sigma}{K_{Ic}} \right)^{2c} \quad (10)$$

For N cracks, the probability of failure, P_f , is given by the following equation, supposing the WLP

$$P_f = 1 - (1 - F(\sigma))^N \quad (11)$$

When N is large, Eq. (11) can be approximated by the following equation which can be shown by performing a Taylor series expansion

$$P_f = 1 - \exp(-NF(\sigma)) \quad (12)$$

so that for large N , we have approximately

$$P_f = 1 - \exp \left(- \left(\frac{Y \sqrt{\pi a_0} N^{\frac{1}{2c}}}{K_{Ic}} \sigma \right)^{2c} \right) \quad (13)$$

Eq. (13) can be simplified to Eq. (1), i.e. the Weibull distribution function, with the scale parameter

$$k = \frac{K_{Ic}}{Y \sqrt{\pi a_0} N^{\frac{1}{2c}}} \quad (14)$$

and the shape parameter

$$m = 2c \quad (15)$$

Hence, it is possible to calculate the distribution of macroscopic strength of a stressed solid by starting from an analysis of the microscopic defects and applying the WLP. Others who have considered this include e.g. Matthews et al. (1976) and Batdorf and Heinisch (1978). However, the mathematics soon become intractable as various assumptions are made for the stress state, fracture criterion, crack size distribution, flaw density, crack plane orientation, and the existence of multiple flaw populations.

Stress corrosion causes subcritical crack growth when the glass is stressed in tension in an ambient atmosphere which relates, in particular, to the relative humidity being greater than zero (Charles 1958a, 1958b). However, subcritical crack growth is only observed when the mode I SIF exceeds a threshold limit value estimated at about 0.25 MPa m^{1/2} (Wiederhorn and Bolz 1970). In this paper the effect of stress corrosion is neglected.

3. Numerical method

Yankelevsky (2014) proposed a numerical solution method for calculating the strength distribution of a brittle solid that starts from an analysis of the microscopic defects. The weakest-link principle was applied in Monte Carlo simulations with Griffith flaws to model the fracture stress and fracture location of square glass plates subjected to bending. In Yankelevsky (2014), the plates were laterally supported along two opposite edges and subjected to a line-load at midspan. A Monte Carlo simulation was carried out for a large sample of 5000 virtual specimens. The method offers a tractable way to calculate the distribution of strength and fracture location for arbitrary stress states, fracture criteria, crack plane orientations, and crack size distributions, while allowing for the implementation of multiple flaw populations. The standard size so-called jumbo plate which measures 3.21x6.00 m² is taken as a starting point. The surface area is divided into unit cells and cracks are distributed over the cells according to a uniform distribution. It is supposed that the orientation of the crack plane is uniformly distributed. In this study, the

total number of cracks on the jumbo plate is fixed and depends on the flaw density. It is assumed for the model that the flaw density is 2 cm^{-2} (Wereszczak et al. 2014). The sampled crack size is based on some statistical distribution, e.g. the Pareto distribution. The random flaws are resampled each time a new jumbo plate is modelled. In summary, the stochastics of the flaws comprise the location, the crack plane orientation, and the size. A specimen is extracted from the jumbo plate and analyzed. The analysis depends on a comparison of the cracks with the time-dependent stress field using fracture mechanics. However, the stress distribution over time only needs to be calculated once for any given specimen type and bending arrangement. It is the distributed set of cracks that is resampled in each new simulation of the glass fracture. Fracture is prompted when the SIF envelope for the first time intersects with the fracture toughness. When this happens, the fracture stress and location can be determined based on the first unit cell that contains a failing crack.

In a recent paper (Kinsella and Persson 2018), this type of numerical method was applied to model the fracture stress and failure location of small glass plates subjected to double ring bending. The results allowed for making comparisons between different fracture criteria. Furthermore, a dual population concept of flaws was fitted to model the fracture stress in an empirical data set, the purpose of which was to model the apparent bimodality in the fracture stress distribution (Simiu et al. 1984). Glass fracture data tends to exhibit bimodalities (Veer et al. 2009).

This kind of numerical method was also used by Pathirana et al. (2017) who implemented a dual population concept in Monte Carlo simulations of Griffith flaws for the determination of the strength distribution in panels subjected to point contact actions.

4. Application to laterally supported plates subjected to uniform pressure

In this paper, the results from new simulations are presented that were carried out using the numerical method described in Sec. 3. The results pertain to laterally supported plates subjected to uniform pressure. As a background, the following is noted. Bending tests that record the fracture location in new full-scale plates which are laterally supported along all four edges and subjected to uniform pressure have previously been carried out by Johar (1981, 1982), Kanabolo and Norville (1985), and Calderone (1999). In Johar's and Kanabolo and Norville's experiments, the glass plates were supported between (approximately) 6 mm wide neoprene gaskets. In Calderone's experiment, 20 mm thick nylon gaskets were used. The plate nominal thickness was 6 mm in all experiments whereas the average thickness was 5.8 mm. Tab. 1 lists the sample sizes as well as the relative frequency of surface failures to edge failures. In Tab. 1, only those failures which were unambiguously identified as originating from either the surface or the edge were included in the statistics. In other words, when there was recorded multiple potential fracture origins which included a mixture of surface and edge sites, these were not counted and included in the Tab. 1 statistics. This was done for the sake of consistency because it is generally believed that the edge condition and hence the edge strength differs from the surface condition. Fig. 1 shows the recorded fracture locations and depicts the various plate dimensions that were used in the experiments.

Two square plates measuring $1200 \times 1200 \text{ mm}^2$ and with a thickness of 5.8 mm were modelled using the FEM with ABAQUS/CAE (2013). The plates were laterally supported along all four edges between continuous 6 mm wide gaskets which were 6 mm in thickness. In one case the gasket material was neoprene (Shore A55) and in the other case it was nylon. The neoprene was modelled as an incompressible Neo-Hookean hyperelastic material with shear modulus $G=1 \text{ MPa}$ (Gent 2012). The nylon was modelled as an isotropic linear elastic material with Young's modulus $E=3 \text{ GPa}$ and Poisson's ratio $\nu=0.34$. The gaskets were rigidly supported on the side opposite to the contact surface with the glass. A friction coefficient of 0.19 was adopted for the contact between gasket and glass. The glass material was assumed to have a Young's modulus $E=72 \text{ GPa}$ and a Poisson's ratio $\nu=0.23$. Solid-shell elements were used for the glass part while employing a quadrilateral mesh generator. Hybrid elements were used for the hyperelastic material parts. In the case of the neoprene material, an adaptive meshing technique was employed for the gasket parts to improve the convergence. For symmetry reasons only one quarter of the plate was modelled. The plate was subjected to uniform lateral pressure. Fig. 2 shows the deformed state of the plate as seen from one corner when the gasket material was neoprene. Figs. 3 and 4 show the maximum in-plane principal stresses on the "tension" and "compression" sides of the plate, respectively, for both plates at a pressure magnitude of 40 kPa. The maximum tensile stress at this pressure was 97 MPa (nylon) and 164 MPa (neoprene), respectively, on the "tension" side, and 165 MPa (nylon) and 48 MPa (neoprene), respectively, on the "compression" side. The "tension" side refers to the side of the plate that is in tension at the centre point. The results show that with the softer gasket material, the tensile stresses concentrated nearer towards the edges of the plate. In fact, on the "tension" side, the maximum tensile stress was also significantly greater in this case. However, with the harder gasket material, it was observed that on the "compression" side, there is a very high build-up of tensile stress near the edges.

Table 1: Sample size and relative frequency of surface to edge failure in experiments with laterally supported plates subjected to uniform pressure. Some data points were excluded in the case of multiple potential fracture locations which contained a mixture of surface and edge failure sites.

Reference	Total no. of failures	No. of surface fail's	Rel. freq. of surf. fail's
Johar (1981)	78	54	0.69
Johar (1982)	106	71	0.67
Kanabolo and Norville (1985)	206	152	0.74
Calderone (1999)	195	152	0.78

The strength and fracture locations were simulated using the numerical method that was described in Sec. 3. It was assumed that the surface condition is characterized by a single population of semi-circular cracks with a Pareto distributed crack depth. The Pareto scale and shape parameter values were chosen as $a_{\theta}=4 \mu\text{m}$ and $c=3.0$, respectively, cf. Eq. (6). The cracks were uniformly distributed over the surface area and the unit cell size was $5 \times 5 \text{ mm}^2$. The crack density was 2 cm^{-2} . The motivation behind the choice of Pareto distribution parameter values comes from assuming a Weibull distribution for the strength with the parameter values $k=74 \text{ MPa}$ and $m=6$. Eq. (14) and (15) then give (approximately) the said Pareto parameter values with $N=5655$. In fact, this Weibull distribution gives a characteristic value of the bending strength $\sigma_{b, \text{ch}}=45 \text{ MPa}$ defined as the 5% fractile, cf. Sedlacek et al. (1999). According to Haldimann (2006), this Weibull distribution represents the breakage stress of new glass plates in R400 double ring bending tests at a stress rate of 2 MPa s^{-1} the tests of which were conducted as a basis for the DIN 1249-10:1990. With an assumed flaw density of 2 cm^{-2} the number $N=5655$ is obtained because the stressed area within the loading ring is 0.2827 m^2 .

Figs. 5 and 6 show the simulated fracture locations based on a series of 5000 simulations each for the two types of gaskets, i.e. neoprene and nylon. In Fig. 5, the fracture criterion that was used assumes that the crack planes are oriented normal to the maximum principal stress, whereas in Fig. 6, the mixed mode fracture criterion, Eq. (4), was used. In this case, it was assumed that the crack plane angles were uniformly distributed in $[0, \pi)$.

Fig. 7 depicts the distribution in fracture stress for both types of gasket materials while assuming a mode I criterion with the crack planes oriented perpendicular to the maximum principal tensile stress. A two-parameter Weibull distribution was fitted to the data samples and is also shown in the diagrams. It can be noted that the mean fracture stress is slightly lower with the mixed mode fracture criterion.

5. Application to tall panels subjected to impact load

The dynamic impact load case is often relevant when performing a strength design of a glass structure. With an accurate description of the stress distribution in the impacted pane, it is possible to predict the likely fracture location. However, it is not necessarily the case that the failure location coincides with the maximum principal tensile stress (Natividad et al. 2016). By implementing the numerical method described in Sec. 3 it is possible to model the distribution of fracture location. The European standard EN-12600 details a method for testing glass to classify it in terms of impact strength.

The distribution in fracture location was studied for a tall vertical panel subjected to an impact load. The panel consists of a laminated unit with two glass plies. The panel measures approximately $1 \times 4 \text{ m}^2$ in surface area and each ply has a thickness of 10 mm. The full transient FE simulation of the panel and impactor were based on a previous model which is described in Fröling et al. (2014). The panel was supported on two sides (top and bottom edges) and it had a 6×6 array of ventilation holes near the bottom edge, cf. Fig. 8a for an illustration. The impactor consists of a weight encased in two tyres, the weight of the impactor being 50 kg according to standard (EN-12600). The tyre was swung into the panel in a pendulum motion thus generating a soft impact with a long pulse time. The glass and PVB interlayer parts were modelled by means of a hexahedral solid-shell element. The rubber supports were modelled using a solid element. The glass, interlayer and supports were modelled as linear elastic materials and the material parameters which were adopted from Persson and Doecker (2009) and prEN 16612:2017 are shown in Tab. 2. The initial velocity of the impactor was 2.97 m s^{-1} which corresponds to a fall height of 0.450 m. The central impact occurred at a height of 1.2 m.

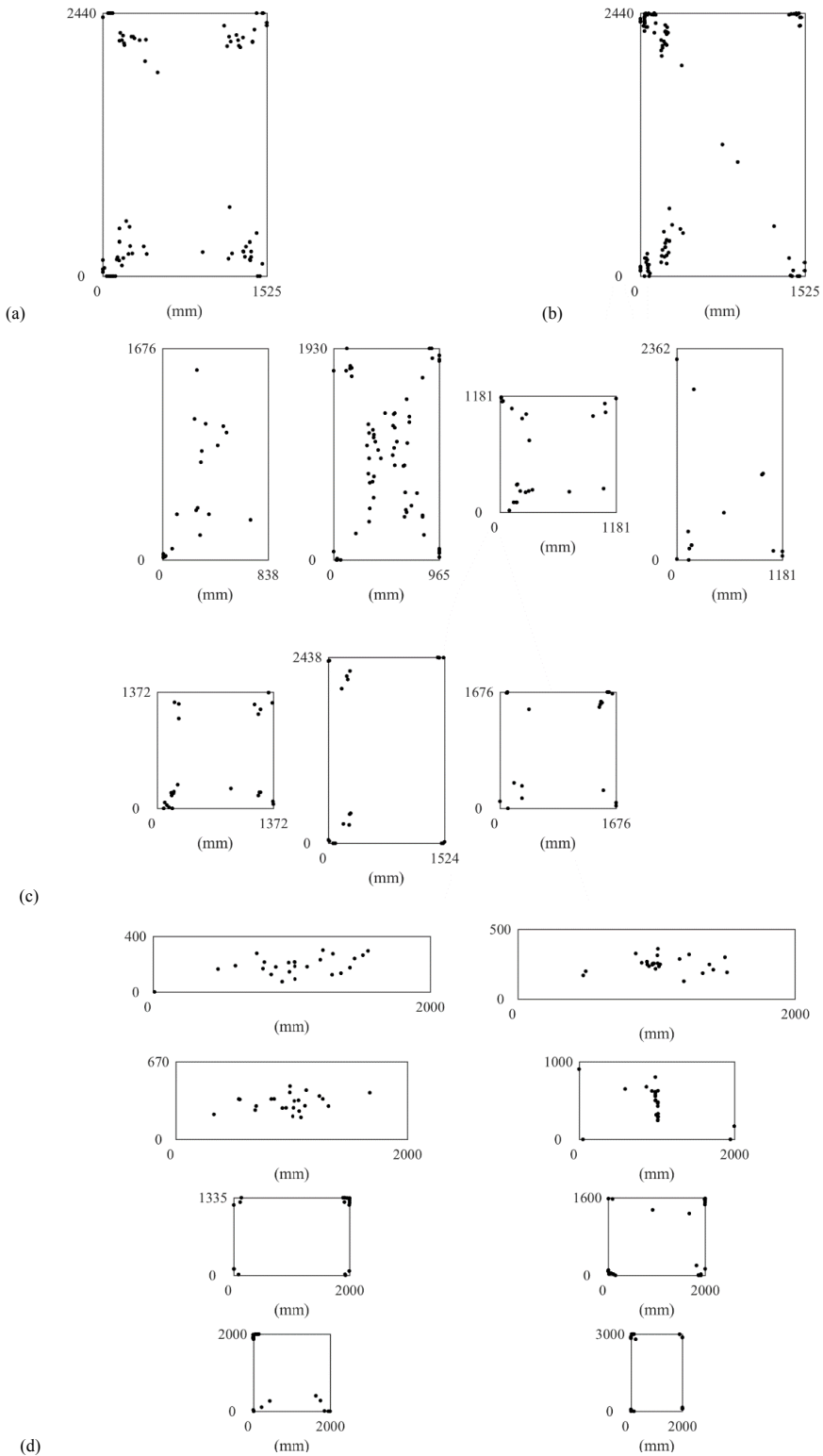


Fig. 1 Fracture origins according to four experiments (a) Johar (1981), (b) Johar (1982), (c) Kanabolo and Norville (1985), and (d) Calderone (1999).

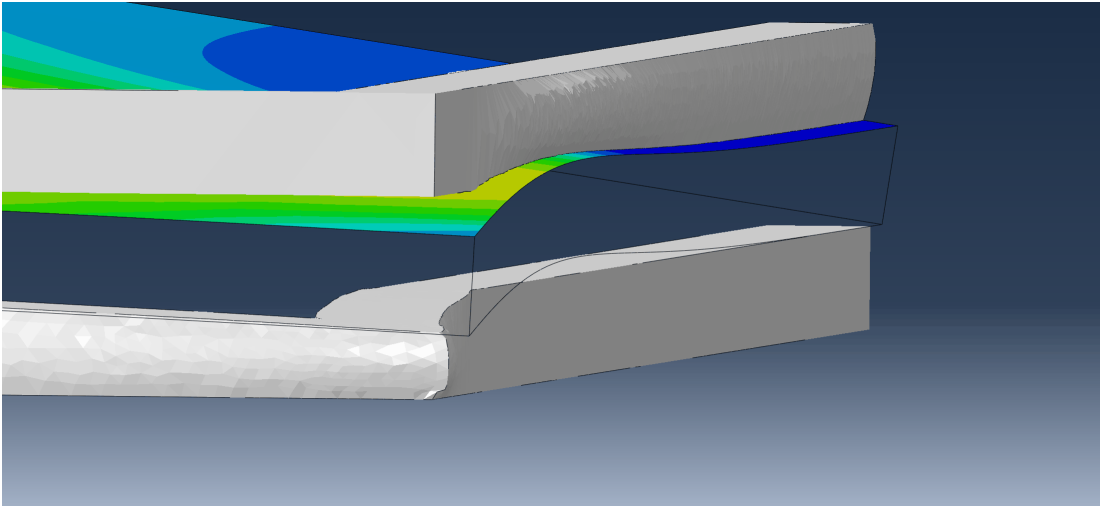


Fig. 2 Deformed state of a plate which is supported laterally between neoprene gaskets and subjected to uniform pressure. As seen from one corner. For symmetry reasons only one quarter of the plate is visible.

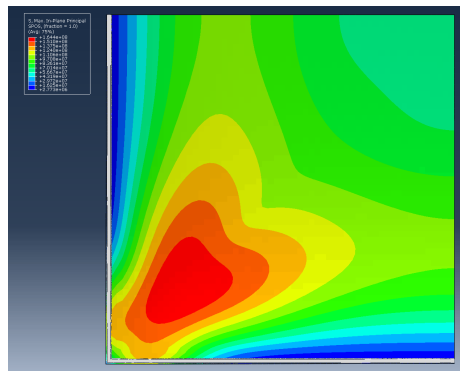
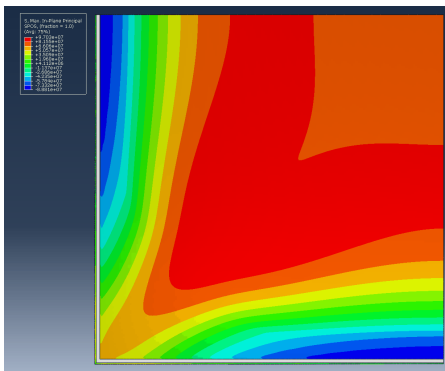


Fig. 3 Stress contours (maximum in-plane principal) on the “tension” side of the plate with (left) nylon gaskets and with (right) neoprene gaskets at the lateral pressure magnitude 40 kPa.

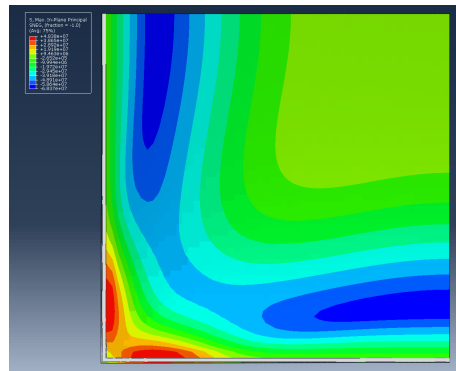
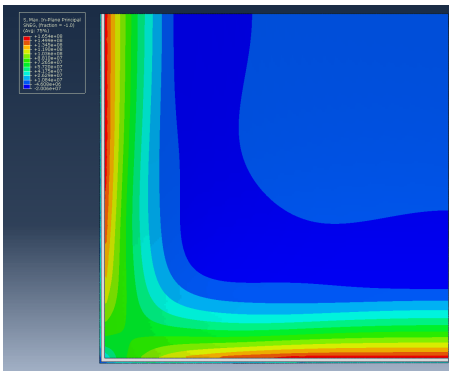


Fig. 4 Stress contours (maximum in-plane principal) on the “compression” side of the plate with (left) nylon gaskets and with (right) neoprene gaskets at the lateral pressure magnitude 40 kPa.

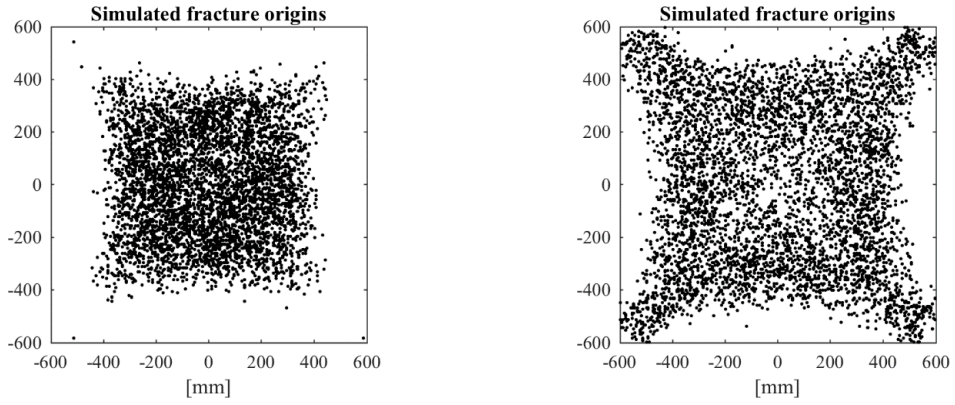


Fig. 5 Simulated fracture locations in the case of (left) nylon gaskets and (right) neoprene gaskets with a pure mode I fracture criterion assuming all crack planes to be oriented perpendicular to the max. princ. stress.

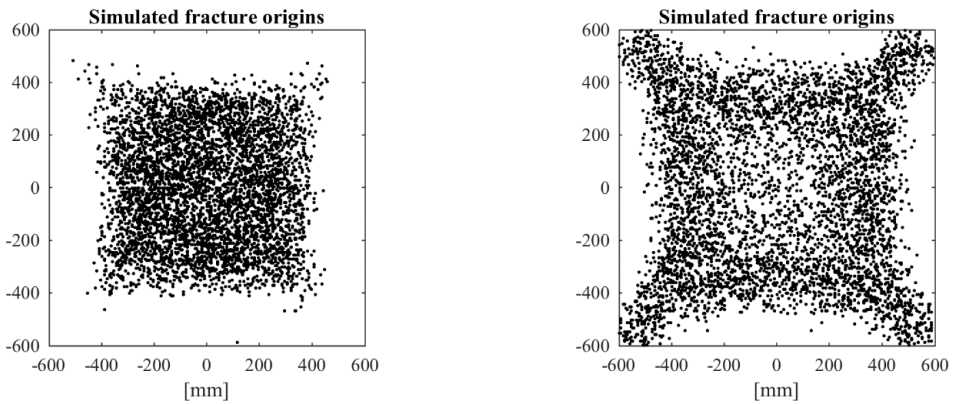


Fig. 6 Simulated fracture locations in the case of (left) nylon gaskets and (right) neoprene gaskets with a mixed mode fracture criterion.

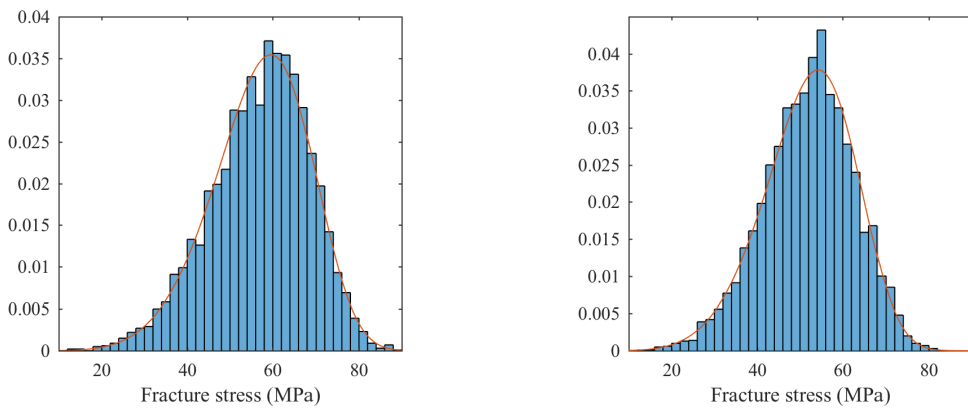


Fig. 7 Simulated fracture stress in the case of (left) nylon gaskets and (right) neoprene gaskets with the MPTS fracture criterion, i.e. assuming all crack planes to be oriented perpendicular to the max. princ. stress. Solid line corresponds to a fitted Weibull distribution. The histograms are normalized to reflect a probability density.

Fig. 8b shows the maximum in-plane principal stress contours at time equal to 15 ms when the maximum stress was about 45 MPa. Fig. 8c shows the stress contours at time equal to 30 ms when the maximum stress had reached about 82 MPa. The greatest stress (82 MPa) was located near the top row of ventilation holes. Fig. 9a shows the distribution of fracture location using a mode I fracture criterion without consideration of crack plane orientation, i.e. assuming that all crack planes are oriented normal to the maximum principal tensile stress. It was assumed that the surface condition is represented by a single population of cracks with a Pareto distributed depth with parameter values $a_0=4 \mu\text{m}$ and $c=3.0$, and that the crack density is 2 cm^{-2} . Fig. 9a depicts in total 989 fractures which occurred during the simulation of 5000 virtual panel impacts. About 40% of the failures in total occurred near one of the ventilation holes. The area near a ventilation hole was in this case defined by a bounding box around the whole 6x6 array. Fig. 9b shows the resulting strength distribution which is not necessarily in agreement with a Weibull distribution.

Table 2: Material parameters

Material	E (MPa)	ν	ρ (kg m ⁻³)
Glass	70000	0.2	2500
PVB interlayer	180	0.49	1250
Rubber support	15	0.44	1250
Impactor	2	0.3	900

Discussion

In theory, brittle fracture in glass is promoted by the existence of a large set of surface microcracks with a location and size distribution that can be described using some random variable. Because of the limited capacity for plasticity in glass, the failure mode is governed by the WLP, i.e. the first fracturing flaw prompts global breakage. A failure prediction model that is consistent with theory must therefore take into account the existence of surface microcracks including the stochastics of these, and the WLP. The Weibull model adopts the WLP and can, in theory, be associated with a single population of surface cracks having a Pareto distributed crack size. The Weibull model is preferred in major standards including the European draft prEN 16612:2017. However, the Weibull models that are fitted to empirical data are so different in scale and shape that is hard to predict the strength in general while adopting this type of distribution. A similar limitation appears to apply to the GFPM of which it has been said that it “is best suited to representing glass strength for specific test conditions.” (Reid 2007) As a matter of fact, it is not just the fracture stress magnitude that scatters, the failure location is also variable. It has been shown that the fracture origin rarely occurs at the point of MPTS in laterally supported plates subjected to uniform out-of-plane loading (Natividad et al. 2016).

The method which was investigated in this paper offers a promising alternative to the ordinary Weibull model for use in failure prediction of structural glass units. Firstly, the method is based on the physics of brittle fracture. A representation of the surface condition is implemented and fracture mechanics are combined with the WLP to reveal the breakage stress and location. By assuming that the surface condition is represented by a single population of cracks with a Pareto size distribution, it is possible to obtain a Weibull distribution for the strength. The new model differs from the Weibull model in that a greater freedom is afforded towards the representation of the surface condition in glass. Now, the available data on the surface condition is scarce. As current techniques are improved, and new methods are developed to probe the surface condition, more reliable data can be supplied as input to this kind of failure model. It is moreover possible to evaluate failure based on different fracture criteria including mixed mode criteria in a way that would be more tractable than while using the ordinary Weibull distribution. The mathematics soon become intractable when evaluating the analytical expressions necessary to implement different fracture criteria, cf. e.g. Batdorf and Heinisch (1978). With the new method, it is possible to control the crack plane orientations in a way that would not be feasible using the ordinary Weibull distribution. If one for instance assumes that the crack planes lie in some particular direction on certain parts of the surface due to, for example, mechanical abrasion, then it would be quite possible to implement this in the new model through a suitable setup of the surface condition. It is also possible to implement multiple flaw populations. The new method offers the possibility to predict the fracture location which can be useful in certain situations. For example, glass structures with more complicated geometry containing corners and holes, and glass structures subjected to more advanced loading situations such as uneven static loading and dynamic loading.

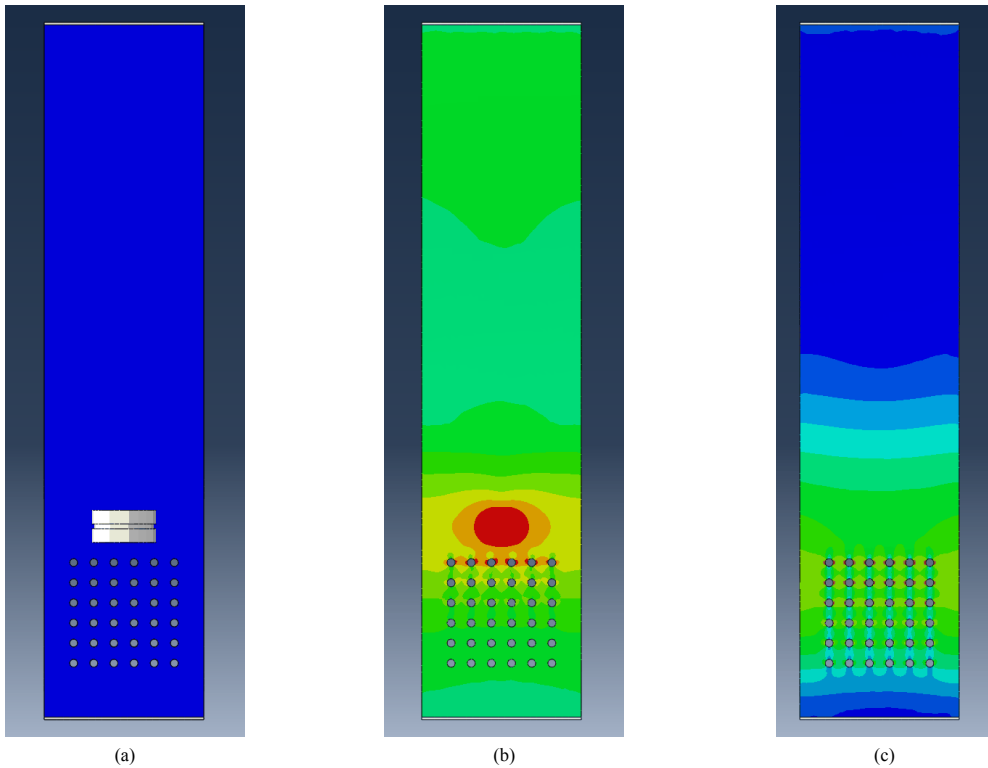


Fig. 8 (a) Tall panel and soft impactor. (b) Stress contours (max. in-plane princ.) when the max stress had reached 45 MPa at time 15 ms. (c) Stress contours when the max stress had reached 82 MPa at time 30 ms. NB, maximum stress in (c) is near the edges of the top row of ventilation holes. Red colour corresponds to tensile stress.

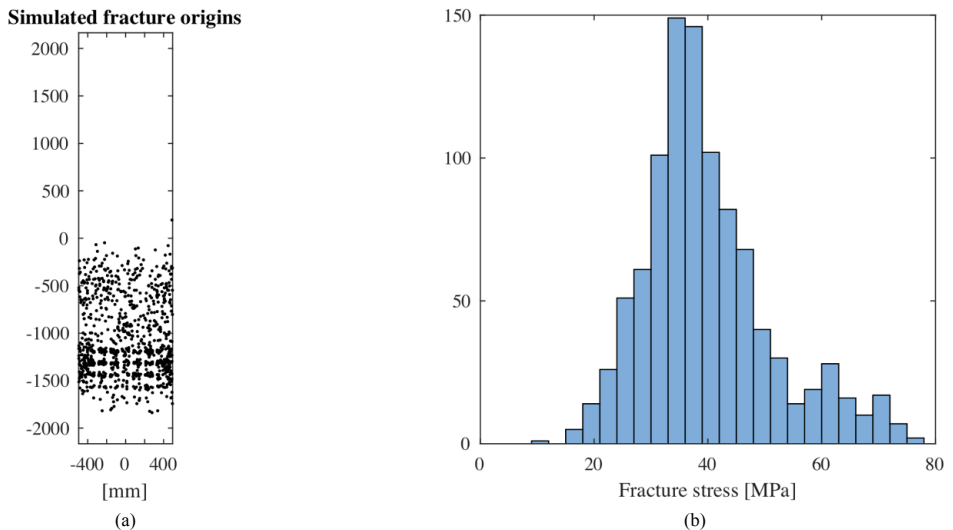


Fig. 9 (a) Simulated fracture origins. (b) Strength distribution.

In the present study, a method was applied to model the strength and fracture location of laterally supported plates subjected to uniform pressure. The comparison of the empirical data appears to indicate that a significant portion of failures in tests of large plates occur near or on the edges. This might indicate that failure is sensitive to shear stress. According to one study (Reid 2007), a series of 59 small specimens of annealed glass plates generated unexpected results when tested in a double ring bending device. The proportion of failures outside the loading ring was much

greater than expected based on Weibull statistics which do not factor shear stress into the failure criterion. There is no shear stress in the loading ring area because the stress state is equibiaxial. In the case of a large laterally supported plate subjected to uniform pressure, there emerges shear stress near the corners of the plate. In this paper, such large plates were investigated while using both a mode I fracture criterion and a shear sensitive mixed mode criterion. However, from the simulation results, it is hard to see a significant impact on the fracture location due to the presence of shear stress near the corners of the plate. Nevertheless, the fracture origin was increasingly located nearer the corners when the support gaskets were made from a softer material, i.e. neoprene. As the Figs. 3 and 4 show, the tensile stress on the “compression” side of the plates are significant, especially in the case with the nylon gaskets. At the applied pressure 40 kPa, the maximum tensile stress on the “compression” side of the nylon supported plate was in fact on par with the maximum tensile stress on the “tension” side of the neoprene supported plate. This implies that a thorough analysis of the failure of laterally supported plates subjected to uniform pressure should consider both faces of the plate. This was not done in the present study but could be conducted in a future investigation. However, according to one study on large plates subjected to uniform loading (Calderone 1999), there were only two fractures occurring from the “compression” side of 195 specimens tested in total corresponding to a relative frequency of about 1%. In that study, nylon gaskets were used and the glass was fixed firmly between the nylon supports. This indicates that failures from the “compression” side are unlikely in practical situations. However, further investigation is required in order to verify this. More important perhaps, is the fact that a significant proportion of failures occur from the edges according to experimental data, cf. Tab. 1. In the modelling that was done in connection with this paper, only the surface condition in glass was considered. The edge condition was not represented separately. This is an important issue, however, that might be considered in future research work.

The case with the vertical panel impacted by a soft body illustrates how the new method can be applied to model specimens with a more complex geometry subjected to dynamic loading. This loading leads to a time-dependent stress distribution that initially affects a relatively large portion of the glass surface to moderate tensile stress and subsequently a much smaller portion is affected, in particular at the ventilation holes, to higher tensile stress. Even if the strength distribution is known a priori, i.e. a Weibull distribution, the question remains as to how the fracture location is distributed. The simulations which were carried out show that ultimately about 40% of the failures occurred near the holes. However, the edge condition in glass is very relevant in this case and should perhaps be represented differently than the surface condition. Further research needs to be conducted in order to properly model this load case while taking the edge condition into consideration. In the simulation of the panel, stress corrosion was not considered. However, in this particular case, the dynamic impact load produces a very high stress rate. In fact, the overall maximum tensile stress was reached within about 30 ms which corresponds to an average stress rate of approximately 2700 MPa s^{-1} . Presumably, any effects of static fatigue would be limited because there would be very little time for stress corrosion to take place. It is therefore believed that stress corrosion in this case would have only a negligible effect on the results. Interestingly, Haldimann (2006) carried out experiments on glass plates which were loaded at both low and very high stress rates (0.2 MPa s^{-1} and 21 MPa s^{-1} , respectively) and compared the results. His findings seemed to indicate that the behaviour of a specimen subjected to a stress rate of as much as 21 MPa s^{-1} in ambient conditions nearly approaches that of a specimen in inert conditions.

6. Conclusions

The distribution of fracture stress and failure location in glass can be modelled using a numerical method that is based on well-established concepts including the WLP and the existence of surface microcracks. The method is applied to model the strength and fracture origin in large laterally supported plates subjected to uniform pressure and in a tall panel with a complex geometry that is subjected to impact loading. By assuming that the surface condition is represented by a single population of cracks with a Pareto distributed crack size it is possible to obtain a strength distribution that is similar to a Weibull distribution. As current methods are refined and new techniques are developed to probe the surface condition of glass, this new numerical tool has potential for greater versatility in modelling glass fracture statistics since it allows for various surface flaws conditions and fracture criterions to be used.

7. References

- ABAQUS/CAE: Version 6.13. Dassault Systèmes, (2013)
- ASTM E 1300-04: Standard Practice for Determining Load Resistance of Glass in Buildings. (2004)
- Batdorf, S.B., Heinisch, H.L.: Weakest Link Theory Reformulated for Arbitrary Fracture Criterion. *J Am Ceram Soc* **61**(7-8), 355-358 (1978)
- Beason, W.L., Morgan, J.R.: Glass Failure Prediction Model. *J Struct Eng* **110**, 197-212 (1984)
- Calderone, I.J.: The equivalent wind loading for window glass design. Monash University (1999)
- Charles, R.J.: Static Fatigue of Glass I. *J Appl Phys* **29**, 1549-1553 (1958a)
- Charles, R.J.: Static Fatigue of Glass II. *J Appl Phys* **29**, 1554-1560 (1958b)
- DIN 18008-1:2010: Glas im Bauwesen - Bemessungs- und Konstruktionsregeln - Teil 1: Begriffe und allgemeine Grundlagen. (2010)
- DIN 1249-10:1990: Flachglas im Bauwesen - Teil 10: Chemische und physikalische Eigenschaften. (1990)
- EN 12600: Glass in building - Pendulum test - Impact test method and classification for flat glass. CEN (2003)
- Forbes, C., Evans, M., Hastings, N., Peacock, B.: Statistical distributions. John Wiley and sons, Inc., (2010)
- Fröling, M., Persson, K., Austrell, P.E.: A reduced model for the design of glass structures subjected to impact loads. *Engineering Structures* **80**, 53-60 (2014)
- Gent, A.: *Engineering with Rubber*. Hanser, (2012)

- Griffith, A.A.: The Phenomena of Rupture and Flow in Solids. *Phil. Trans. R. Soc.* **A221**, 163-163 (1920)
- Haldimann, M.: Fracture strength of structural glass elements -- analytical and numerical modelling, testing and design. Ecole Polytechnique Fédérale de Lausanne EPFL (2006)
- Hellen, T.K., Blackburn, W.S.: The Calculation of Stress Intensity Factors for Combined Tensile and Shear Loading. *Int J Fract* **11**, 605-605 (1975)
- Irwin, G.R.: Analysis of Stresses and Strains Near the End of a Crack Traversing a Plate. *J. Appl. Mech.* **24**, 361-361 (1957)
- Jayatilaka, A.D., Trustrum, K.: Statistical approach to brittle fracture. *J Mater Sci* **12**, 1426-1430 (1977)
- Johar, S.: Dynamic fatigue of flat glass - Phase II. In. ORF, (1981)
- Johar, S.: Dynamic fatigue of flat glass - Phase III. In. ORF, (1982)
- Kanabolo, D.C., Norville, H.S.: The strength of new window glass using surface characteristics. Texas Tech University (1985)
- Kinsella, D.T., Persson, K.: A Numerical Method for Analysis of Fracture Statistics of Glass and Simulations of a Double Ring Bending Test. *Glass Struct & Eng* (2018). doi:10.1007/s40940-018-0063-z
- Matthews, J.R., McClintock, F.A., Shack, W.J.: Statistical determination of surface flaw density in brittle materials. *J. Am. Ceram. Soc.* **59**, 304-308 (1976)
- Mencik, J.: *Strength and Fracture of Glass and Ceramics*, vol. 12. Elsevier, (1992)
- Natividad, K., Morse, S.M., Norville, H.S.: Fracture Origins and Maximum Principal Stresses in Rectangular Glass Lites. *Journal of Architectural Engineering* **22**(2), 04015014 (2016). doi:10.1061/(ASCE)AE.1943-5568.0000197
- Newman, J.C., Raju, I.S.: An empirical stress intensity factor equation for the surface crack. *Eng. Fract. Mech.* **15**, 185-192 (1981)
- Pathirana M., Lam N., Perera S., Zhang L., Ruan D., Gad E.: Risks of failure of annealed glass panels subject to point contact actions. *Int J Solids Struct* **129**, 177-194 (2017)
- Persson, K., Doepker, B.: Glass panes subjected to dynamic impact loads. Proc. of the XXIV A.T.I.V. Conference, Parma, 9-10 July (2009)
- Poloniecki, J.D., Wilshaw, T.R.: Determination of Surface Crack Size Densities in Glass. *Nature Physical Science* **229**, 226-227 (1971)
- prEN 16612:2017: Glass in building - Determination of the lateral load resistance of glass panes by calculation. CEN, (2017)
- Reid, S.G.: Effects of spatial variability of glass strength in ring-on-ring tests. *Civ Eng Environ Syst* **24**, 139-148 (2007)
- Sedlacek, G., Blank, K., Laufs, W., GÜsgen, J.: *Glas im Konstruktiven Ingenieurbau*. Ernst & Sohn, (1999)
- Simiu, E., Reed, D.A., Yancey, C.W.C., Martin, J.W., Hendrickson, E.M., Gonzalez, A.C., Koike, M., Lechner, J.A., Batts, M.E.: Ring-on-ring tests and load capacity of cladding glass. In. (1984)
- Tandon, R., Paliwal, B., Gibson, C.: Practical aspects of using Hertzian ring crack initiation to measure surface flaw densities in glasses: influence of humidity, friction and searched areas. *Philos Mag* **93**, 2847-2863 (2013)
- Thiemeier, T., Brückner-Foit, A., Kölker, H.: Influence of the fracture criterion on the failure prediction of ceramics loaded in biaxial flexure. *J. Am. Ceram. Soc.* **74**(1), 48-52 (1991)
- Vandebroek, M., Louter, C., Caspee, R., Ensslen, F., Belis, J.: Size effect model for the edge strength of glass with cut and ground edge finishing. *Engineering Structures* **79**, 96 -105 (2014)
- Veer, F.A., Louter, C., Bos, F.P.: The strength of annealed, heat-strengthened and fully tempered float glass. *Fatigue Fract Eng M* **32**, 18-25 (2009)
- Veer, F.A., Rodichev, Y.M.: The structural strength of glass: Hidden damage. *Strength Mater+* **43**, 302-315 (2011)
- Weibull, W.: A Statistical Theory of the Strength of Materials. *Ingenjörsvetenskapsakademiens handlingar* **151** (1939)
- Wereszczak, A.A., Ferber, M.K., Musselwhite, W.: Method for Identifying and Mapping Flaw Size Distributions on Glass Surfaces for Predicting Mechanical Response. *Int J Appl Glass Sci* **5**, 16-21 (2014)
- Wiederhorn, S.M., Bolz, L.H.: Stress corrosion and static fatigue of glass. *J. Am. Ceram. Soc.* **53**, 543-548 (1970)
- Yankelevsky, D.Z.: Strength prediction of annealed glass plates -- A new model. *Eng Struct* **79**, 244-255 (2014)

Paper D





LUND
UNIVERSITY

**SURVEY OF EXPERIMENTAL DATA
ON THE STRENGTH OF ANNEALED
FLOAT GLASS PANES IN THE AS-
RECEIVED CONDITION TESTED IN
AN AMBIENT ENVIRONMENT**

DAVID KINSELLA

Structural
Mechanics

DEPARTMENT OF CONSTRUCTION SCIENCES
DIVISION OF STRUCTURAL MECHANICS
ISRN LUTVDG/TVSM--18/7166--SE (1-73) | ISSN 0281-6679

SURVEY OF EXPERIMENTAL DATA ON THE STRENGTH OF ANNEALED FLOAT GLASS PANES IN THE AS- RECEIVED CONDITION TESTED IN AN AMBIENT ENVIRONMENT

DAVID KINSELLA

Copyright © 2018 Division of Structural Mechanics,
Faculty of Engineering LTH, Lund University, Sweden.

For information, address:
Div. of Structural Mechanics,
Faculty of Engineering LTH, Lund University, Box 118, SE-221 00 Lund, Sweden.
Homepage: www.byggmek.lth.se

SURVEY OF EXPERIMENTAL DATA ON THE STRENGTH OF ANNEALED FLOAT GLASS PANES IN THE AS-RECEIVED CONDITION TESTED IN AN AMBIENT ENVIRONMENT

David Kinsella

david.kinsella@construction.lth.se

A detailed overview is provided for the strength of monolithic annealed float glass panes according to experiments carried out over the past four decades. The experiments were conducted with the coaxial double ring bending device, the three-point bending device, the four-point bending device, and the arrangement that allows for laterally supported plates to be subjected to uniform pressure. When the stress history was linear, the 2 MPa s^{-1} stress rate-equivalent strength was calculated and compared with the nominal value of the strength. The data was obtained from the open literature. Only new glass in the as-received condition was considered. Only glass that was tested in an ambient environment was included in the survey. The strength is visualized in the form of boxplots and probability plots. The three following types of probability plots were considered, viz. the Weibull, the normal, and the lognormal. The goodness-of-fit was tested numerically with the Anderson-Darling statistic.

Keywords: Glass, fracture data

Contents

1. Introduction	4
2. Environmental conditions	4
3. Bending test arrangements and strength calculations	4
Three-point bending	5
Four-point bending	5
Coaxial double ring bending	6
Uniform pressure applied to laterally supported plates	7
4. Stochastic models	7
Weibull distribution	8
Normal distribution	8
Lognormal distribution	8
5. Adjusting for static fatigue	8
6. Graphical description	9
Histogram	9
Empirical distribution function	9
Boxplot	9
Probability plot	10
7. Goodness-of-fit	10
8. Supplementary data	11
9. General overview	12
10. Experiments	12
Johar (1981)	13
Johar (1982)	15
Simiu et al. (1984)	18
Kanabolo and Norville (1985)	20
Carre (1996)	21
Calderone (1999)	23
Hess (2000)	26
Fink (2000)	27
Overend (2002)	28
Haldimann (2006)	30
Veer et al. (2006)	31
Sglavo et al. (2007)	33
Veer et al. (2009)	35
Consuelo-Huerta et al. (2011)	37
Veer and Rodichev (2011)	39

SURVEY OF EXPERIMENTAL DATA ON THE STRENGTH OF ANNEALED FLOAT GLASS

Veer and Rodichev (2012)..... 41

Vandebroek et al. (2012) 43

Lindqvist (2013)..... 45

Vandebroek et al. (2014) 52

Kozlowski (2014) 55

Kleuderlein et al. (2014)..... 56

Schula (2015) 62

Muniz-Calvente et al. (2016)..... 63

Kinsella and Persson (2016) 65

Navarrete et al. (2016)..... 66

Yankelevsky et al. (2017) 68

Osnes et al. (2018) 69

11. References70

1. Introduction

Glass in structures is commonly formed by monolithic, laminated, or insulated units of annealed, heat-strengthened or toughened float glass panes. According to the codes, e.g. DIN 18008-1:2010 and prEN 16612:2017, the strength design is based on the characteristic value of the fracture stress of a monolithic pane of annealed float glass. Hence, the distribution of strength in monolithic panes of annealed float glass is of paramount importance. In the open literature and up to date, there has been no comprehensive survey providing a detailed overview of the experimental results on the strength of monolithic panes of annealed float glass. This report was put together to provide such a detailed overview. The purpose is furthermore to enable an in-depth analysis of the most important statistics such as the characteristic value of the strength, the difference in strength between edge and surface failures, the goodness-of-fit for standard distributions, etc. The aim is moreover to enable a general assessment of phenomena such as static fatigue and the size effect. The investigation is restricted to new glass in the as-received condition that was tested in an ambient environment. The examined experiments were conducted with the following testing devices, viz. the coaxial double ring bending device, the three-point bending device, the four-point bending device, and the device that enables the application of uniform lateral pressure to plates that are continuously supported along all four edges. The empirical data was obtained from original articles, conference proceedings, reports, and dissertations from the following sources, viz. scientific publishers, societies, organizations, and universities. According to all accounts, great care was taken in the handling of the glass prior to testing and during mounting of the specimens into the respective testing rigs. The glass was always stored for some time before testing.

2. Environmental conditions

The ambient environment is somewhat represented by an indoor climate. The ambient temperature is about 20 °C and the relative humidity ranges between 40-70%. However, due to regional as well as seasonal differences and variations, the ambient temperature and relative humidity in the examined experiments was sometimes found to deviate significantly from these values. For instance, during the tests carried out in Australia (Calderone 1999), the relative humidity once reached 99%. And while tests were conducted in Canada (Johar 1982), the measured temperature dropped to 16 °C.

3. Bending test arrangements and strength calculations

The surveyed experiments were conducted using one of the following bending arrangements, viz. the three-point bending device, the four-point bending device, the coaxial double ring bending device, and the device that allows for four-sided laterally supported panes to be subjected to uniform lateral pressure. The bending strength was determined either using an analytical formula, with the use of the finite element method, or based on strain gauge measurements combined with some extrapolation method. Here follows a description of the analytical formulae used for calculating the ultimate stress at failure. The bending strength σ_f is generally determined according to

$$\sigma_f = \frac{M}{W} \quad (1)$$

where M is the maximum bending moment and W is the section modulus of the specimen. For a rectangular cross-section

$$W = \frac{hb^2}{6} \quad (2)$$

SURVEY OF EXPERIMENTAL DATA ON THE STRENGTH OF ANNEALED FLOAT GLASS

where b denotes the thickness and h the width of the specimen. In the case of the three and four-point bending setup, the terms in-plane and out-of-plane bending, respectively, refer to the orientation of the specimen in the cross-sectional plane, i.e. whether the specimen is lying down or standing up on its edge. The difference is illustrated in Fig. 1.

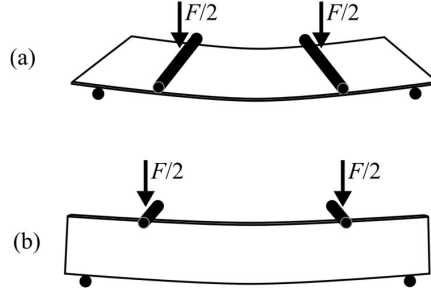


Fig. 1 (a) Out-of-plane (specimen lying down) and (b) in-plane (specimen standing on its edge) bending in a four-point setup.

Three-point bending

A schematic view of the three-point bending arrangement is given in Fig. 2. The largest bending moment is $F l / 4$ where F is the fracture load and l is the distance between the supports. With reference to Eqs. (1) and (2), the bending strength is found to be

$$\sigma_f = \frac{3 F l}{2 h b^2} \tag{3}$$

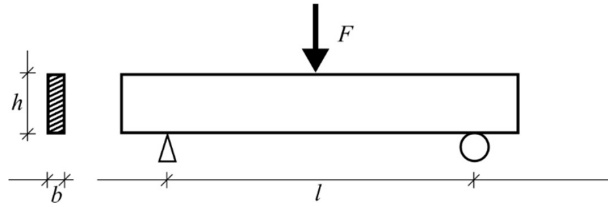


Fig. 2 The three-point bending arrangement.

Four-point bending

A schematic of the four-point bending arrangement is shown in Fig. 3. The bending strength is calculated with

$$\sigma_f = 3 \frac{F l_1}{h b^2} \tag{4}$$

where l_1 is the distance between the outer and inner supports. In the case of four-point bending tests, only the data was included that corresponds to fracture within the load span limits. In some experiments, the analytical formula, Eq. (4), was combined with finite element calculations in the calculation of the bending strength in the following way. When taking into account the stress concentration that occurs at the points where the load is introduced and supposing that fracture occurs under the loading points, the fracture stress increases by about 5%, see e.g. Vandebroek et al. (2014). As a matter of fact, it was not unusual for the fracture origin to be located at the load introduction points in four-point bending tests (Vandebroek et al. 2014).

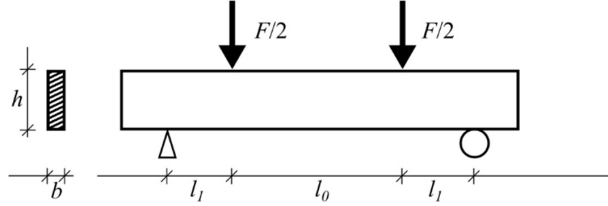


Fig. 3 The four-point bending arrangement.

Coaxial double ring bending

Fig. 4 shows a schematic of the double ring bending arrangement which uses two opposing coaxial rings of unequal diameters, one loading ring and one reaction ring. The test specimen is positioned between the rings and a load is transmitted through the smaller concentric loading ring. A uniform biaxial tensile stress is produced in the surface of the sample plate within the loading ring area. The stresses on the tensile surface of a specimen in coaxial double ring bending have radial and circumferential components and are given by a set of approximate analytical solutions (Kirstein and Woolley 1967). Geometrical nonlinearity is not accounted for by Eq. (5), (7), and (8). In the case of bending of thin plates, membrane stresses are activated and become significant when the deflection exceeds about half the plate thickness. The uniform biaxial stress within the loading ring area is

$$\sigma_r = \sigma_\theta = \frac{3F}{2\pi t^2} \left((1 + \nu) \ln \left(\frac{r_1}{r_0} \right) + (1 - \nu) \frac{r_1^2 - r_0^2}{2r_2^2} \right), r \leq r_0 \quad (5)$$

where ν is Poisson's ratio, r_0 and r_1 are the radii of the inner and outer supports, respectively. r_2 is the equivalent outer radius used for a square shaped specimen with side length $2L$ and is given by

$$r_2 = L(1 + \sqrt{2}) \quad (6)$$

The radial stress outside the loading ring area at the distance r from the plate centre point is

$$\sigma_r = \frac{3F}{2\pi t^2} \left((1 + \nu) \ln \left(\frac{r_1}{r} \right) + (1 - \nu) \frac{r_0^2(r_1^2 - r^2)}{2r^2 r_2^2} \right), r > r_0 \quad (7)$$

while the circumferential stress is

$$\sigma_\theta = \frac{3F}{2\pi t^2} \left((1 + \nu) \ln \left(\frac{r_1}{r} \right) - (1 - \nu) \frac{r_0^2(r_1^2 + r^2)}{2r^2 r_2^2} + 2(1 - \nu) \frac{r_1^2}{r_2^2} \right), r > r_0 \quad (8)$$

When the fracture occurred outside the loading ring area in coaxial double ring bending tests and provided that the fracture location was recorded, the test results were recalculated by this author with Eq. (7) to reflect the maximum principal tensile stress at the fracture location rather than the stress within the loading ring. This applies only in one case, viz. Simiu et al. (1984), and as a matter of fact, Simiu et al. (1984) used the analytical formula, Eq. (5), to calculate the fracture stress. Hence, our calculation method for the adjustment of the fracture stress harmonizes well with the original method.

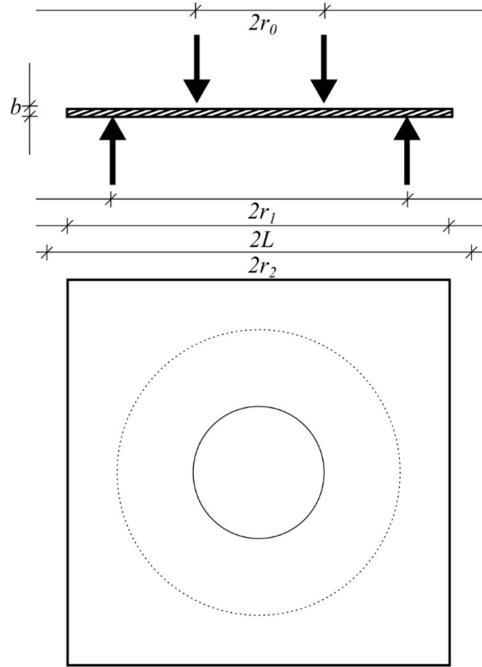


Fig. 4 The coaxial double ring bending arrangement.

Uniform pressure applied to laterally supported plates

In the case of laterally supported plates subjected to uniform pressure, analytical formulae based on plate equations were not used in any of the examined experiments. Instead, the fracture stress was determined with the finite element method or based on strain gauge measurements. Fig. 5 illustrates the general test arrangement. The boundary conditions in the experiments varied substantially. The rigidity in the supports varied depending on the gasket material in use and the clamping force applied along the edges as well as the stiffness of the surrounding frame.

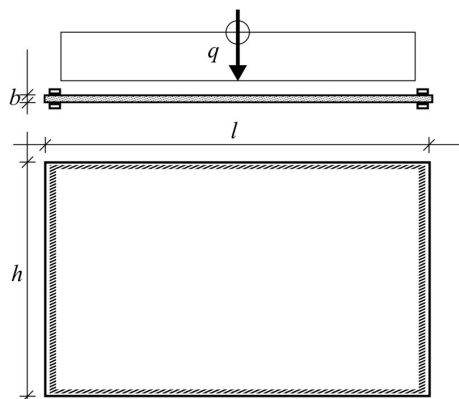


Fig. 5 The arrangement with a laterally supported plate subjected to uniform pressure.

4. Stochastic models

The following three probability distributions are considered as models for the fracture stress in glass, viz. the Weibull distribution, the normal distribution and the lognormal distribution. The

distribution parameters are estimated using the maximum likelihood method. It is supposed that the fracture stress, x , is an observation of some random variable X .

Weibull distribution

The Weibull distribution (Weibull 1939) has the cumulative distribution function

$$F(x) = 1 - \exp\left(-\left(\frac{x}{k}\right)^m\right) \quad (9)$$

where k and $m > 0$ denote the scale and shape parameters, respectively.

Normal distribution

The normal distribution has the probability density function (Forbes et al 2011)

$$f(x) = \frac{1}{\sqrt{2\pi\sigma^2}} \exp\left(-\frac{(x-\mu)^2}{2\sigma^2}\right) \quad (10)$$

where μ and σ^2 are the mean and variance, respectively.

Lognormal distribution

The lognormal distribution is related to the normal distribution in the following way. If Y denotes a normally distributed random variable, then $X = \exp(Y)$ is lognormally distributed with the probability density function (Forbes et al 2011)

$$f(x) = \frac{1}{x\sqrt{2\pi\sigma^2}} \exp\left(-\frac{(\log(x)-\mu)^2}{2\sigma^2}\right) \quad (11)$$

In Eq. (11), μ and σ^2 denote the mean and variance of the associated normal distribution, Eq. (10).

5. Adjusting for static fatigue

Following the theory of stress corrosion (Charles 1958a, 1958b) and the Load Duration Theory (Brown 1972), the nominal value of the strength can be associated with a 2 MPa s⁻¹ stress rate-equivalent strength providing that the stress history is known. In other words, the recorded value of the fracture stress is associated with an equivalent strength value that would have been, were the specimen subjected in an identical environment to a ramp stress until failure at a rate of 2 MPa s⁻¹. Supposing that the actual stress history was linear, i.e. $\dot{\sigma} = \text{constant}$, the transformation is carried out using the following equation

$$\sigma_{f,eq} = \sigma_f \cdot \sqrt[n+1]{\frac{\dot{\sigma}_{eq}}{\dot{\sigma}}} \quad (12)$$

where $\sigma_{f,eq}$ is the 2 MPa s⁻¹ stress rate-equivalent strength, σ_f is the nominal or received strength, $\dot{\sigma}_{eq}$ is 2 MPa s⁻¹, and n is the static fatigue parameter. It is assumed that $n = 16$ (Mencik 1992). In the experiments considered in this report, the stress history at the fracture location was linear in nearly all cases. Typically, the experimenter recorded the calculated rate of stress or else recorded the rate of deflection. In the latter case when the four-point bending test rig was used, the stress rate was determined by this author using the following equation

$$\dot{\sigma} = \dot{u} \frac{3E}{l_1(3l_0+2l_1)} \quad (13)$$

where \dot{u} is the rate of deformation, see also Fig. 3. The stress rate together with the fracture stress are used to adjust the value of strength for the effect of static fatigue. When Eq. (13) is

used, it is assumed that Young's modulus $E = 72$ GPa. With the 2 MPa s^{-1} stress rate-equivalent strength, Eq. (12), it is possible in theory to benchmark various measurements of the strength when the glass material was exposed to different levels of static fatigue due to different rates of stress. The word nominal is used to denote the as-received strength value which has not been adjusted with respect to static fatigue.

6. Graphical description

The histogram, the empirical cumulative distribution function (ECDF), the boxplot, and the probability plot are frequently employed in descriptive statistics to depict a data set graphically. Graphical techniques are useful because of their ease and informality while providing for powerful analyses in conjunction with formal numerical techniques (D'Agostino and Stephens 1986).

Histogram

The histogram is a bar graph that reflects the probability distribution of a continuous random variable. The range of sample values is grouped into m contiguous intervals, each interval having the length m^{-1} . The intervals are usually called bins. The number of observations falling into each bin is counted. A bar is constructed over each bin the height of which is proportional to the frequency (Sheshkin 2004). The bin width is selected to cover the data range and reveal the shape of the underlying distribution.

Empirical distribution function

The empirical cumulative distribution function (ECDF) is a step function that estimates the cumulative distribution function (CDF) that generated the observed data points. Suppose we have a random sample X_1, \dots, X_n drawn from a distribution with CDF $F(x)$. The ECDF is constructed by plotting i/n on the y -axis against the i th ordered value of the sample, i.e. $X_{(i)}$, on the x -axis (Forbes et al 2011). The ECDF $\hat{F}_n(x)$ is defined as (Wasserman 2006)

$$\hat{F}_n(x) = \frac{1}{n} \sum_{i=1}^n I(X_i \leq x) \quad (14)$$

where I is the indicator function defined by

$$I(X_i \leq x) = \begin{cases} 1 & \text{if } X_i \leq x \\ 0 & \text{if } X_i > x \end{cases} \quad (15)$$

Boxplot

The boxplot provides a visual summary of batches of data through their quartiles (McGill et al. 1978). The central mark on each box represents the second quartile, i.e. the median, while the bottom and top edges of the box represent the first and third quartiles, i.e. the 25th and 75th percentiles. The whiskers extend to 1.5 times the Interquartile Range (IQR) which is the distance between the first and third quartiles. Hence, the whiskers indicate variability outside the upper and lower quartiles. Data points that are located beyond the ends of the whiskers are indicated by a plus sign. Variability of the median value between samples is indicated by triangular markers. If the interval between the triangles in a boxplot does not overlap with the interval from another boxplot, then the samples have different medians at the 5% significance level, assuming normally distributed data. In fact, comparisons of medians are reasonably robust even for other distributions than the normal (Mathworks 2018). The interval endpoint lies at the centre of the triangle marker. The endpoints are calculated from

$$q_2 \pm \frac{1.57(q_3 - q_1)}{\sqrt{n}} \quad (16)$$

where q_2 is the second quartile, i.e. the median, and q_1 and q_3 are the first and third quartiles, respectively. n is the number of observations in the sample. The boxplot is useful for depicting a range of statistics, including the IQR, the range, the mid-range, the skewness, etc.

Probability plot

The classic form of the probability plot assumes a parameter model that can be written as

$$F(x) = F_0\left(\frac{x-a}{b}\right) \quad (17)$$

where $b > 0$ is a scale parameter, and $-\infty < a < \infty$ is a location parameter. Suppose $x_{(1)} < x_{(2)} < \dots < x_{(n)}$ are the order statistics in a random sample of size n from the distribution of X . In the probability plot, the $x_{(i)}$ are plotted against $F_0^{-1}(u_i)$ where u_i are termed the plotting positions. The most common choice of plotting position is (Lawless 2003, Mathworks 2018)

$$u_i = \frac{\left(i - \frac{1}{2}\right)}{n} \quad (18)$$

The plot of the points $\left(x_{(i)}, F_0^{-1}(u_i)\right)$ should be approximately linear if the choice of model is reasonable. In the probability plot, the scale of the y -axis is based on the values of $F_0^{-1}(u)$. A reference line that goes through the first and third quartiles is superimposed (Mathworks 2018). In the case of the Weibull distribution, Eq. (9), the distribution function can be rewritten to conform with the location-scale parameter model, Eq. (17). From Eq. (9) we deduce that

$$\ln(1 - F(x)) = -\left(\frac{x}{k}\right)^m \quad (19)$$

from which it follows that

$$\ln(-\ln(1 - F(x))) = m \ln(x) - m \ln(k) \quad (20)$$

Hence, in a Weibull probability plot, the x -axis scaling is logarithmic and the y -axis scaling is such that it maps the function $y = \ln(-\ln(1 - u))$. In the lognormal probability plot, the x -axis scaling is also logarithmic. With the normal distribution, the x -axis scaling is linear.

7. Goodness-of-fit

The experimental data was compared with standard distributions and the goodness-of-fit was evaluated in a formal numerical test using the Anderson-Darling statistic. Suppose the sample x_1, x_2, \dots, x_n contains n observations of a set of independent and identically distributed random variables X . The general test of fit is a test of the null hypothesis

$$H_0: \text{a random sample of } n \text{ observations of } X \text{ comes from } F(x; \vec{\theta}) \quad (21)$$

where $\vec{\theta}$ is a vector of parameters associated with the continuous distribution F . An empirical distribution function statistic measures the vertical difference between $\hat{F}_n(x)$ and $F(x)$. The quadratic class of EDF statistics is based on the class of measures with the following functional form (D'Agostino and Stephens 1986)

$$Q = n \int_{-\infty}^{\infty} \left(\hat{F}_n(x) - F(x)\right)^2 \psi(x) dF(x) \quad (22)$$

where $\psi(x)$ is a weighting function. The Anderson-Darling (1952) statistic is obtained by choosing

$$\psi(x) = \frac{1}{F(x)(1-F(x))} \quad (23)$$

8. Supplementary data

In a few cases, viz. Veer et al. (2006), Muniz-Calvente et al. (2016), Navarrete et al. (2016) and Osnes and Börvik (2018), supplementary information about the experiment was obtained through private correspondence with the respective author. The displacement rate that was used in the in-plane four-point bending tests as reported by Veer et al. (2006) was 1 mm s^{-1} . The fracture origin mode, i.e. edge or surface, in the out-of-plane four-point bending tests were recorded but not published by Muniz-Calvente et al. (2016). The loading ring and support ring diameters in the double ring bending tests conducted by Navarrete et al. (2016) was 51 mm and 127 mm, respectively. The data on the edge failures in the out-of-plane four-point bending tests in the experiment conducted by Osnes et al. (2018) was recorded but not published.

9. General overview

Tab. 1 contains a list of the experiments included in the survey. Also indicated in Tab. 1 are the total number of test specimens per experiment, the type of test device, the type of stress history at the fracture origin, and the edge condition of the glass as reported by the respective author.

Table 1: Summary of surveyed experiments. 4PB=Four-point bending, 3PB=Three-point bending, CDR=Coaxial double ring, ULP=Uniform lateral pressure, C=As-cut, A=Arrised, G=Ground, P=Polished, W=Water-jet cut.

Reference	No. of spec's	Testing device	Stress history	Edge proc.
Johar (1981)	78	ULP	Nonlinear	Not recorded
Johar (1982)	106	ULP	Nonlinear	Not recorded
Simiu et al. (1984)	85	CDR	Linear	Not recorded
Kanabolo and Norville (1985)	206	ULP	Nonlinear	Not recorded
Carre (1996)	81	4PB	Linear	P
Calderone (1999)	195	ULP	Nonlinear	Not recorded
Hess (2000)	15	4PB	Nonlinear	G
Fink (2000)	127	CDR	Linear	Not recorded
Overend (2002)	30	CDR	Linear	Not recorded
Haldimann (2006)	20	CDR	Linear	Not recorded
Veer et al. (2006)	32	4PB	Linear	G
Sglavo (2007)	115	3PB	Linear	CAGP
Veer et al. (2009)	54	4PB	Linear	P
Veer and Rodichev (2011)	177	4PB	Linear	C
Consuelo-Huerta et al. (2011)	66	CDR, 4PB	Linear	Not recorded
Veer and Rodichev (2012)	60	4PB	Linear	W
Vandebroek et al. (2012)	77	4PB	Linear	CP
Lindqvist (2013)	478	4PB	Linear	CAGPW
Vandebroek et al. (2014)	202	4PB	Linear	CG
Kozlowski (2014)	6	4PB	Linear	P
Kleuderlein et al. (2014)	830	4PB	Linear	CAG
Schula (2015)	15	CDR	Linear	Not recorded
Kinsella and Persson (2016)	58	4PB	Linear	P
Muniz-Calvente et al. (2016)	73	CDR, 4PB	Linear	P
Navarrete et al. (2016)	69	CDR	Linear	C
Yankelevsky et al. (2017)	56	4PB	Linear	C
Osnes et al. (2018)	93	4PB	Linear	C
Sum:	3404			

10. Experiments

Here follows a detailed summary of the experiments in the survey. The summary contains a description of the testing device employed with information about the specimen geometry and edge condition. The fracture stress data is represented graphically in the form of boxplots. Triangular markers indicate the inter-sample variation of the median only when the average sample sizes were large enough, i.e. usually greater than 7. The sample data is also visualized in the form of probability plots for the Weibull, normal, and lognormal distributions, but only when the sample size was deemed sufficiently large. Edge failures in the data are marked with a crossed circle in the probability plots. All other types of failure, i.e. surface failure or failures that were ambiguous with respect to the origin, are marked with an empty circle. When applicable, the stress rate-equivalent data is also depicted.

*SURVEY OF EXPERIMENTAL DATA ON THE STRENGTH OF ANNEALED FLOAT GLASS
Johar (1981)*

The experiment was conducted using a setup that enabled a monotonically increasing uniform lateral pressure to be applied to laterally supported plates. The glass panels were mounted vertically between continuous 12.7 mm wide neoprene gaskets in the front face of the testing rig. The front face was hinged and could be opened like a door to reveal the test chamber. Inside the chamber a negative pressure was produced. The specified loading rate was achieved by controlling the rate of movement of a hydraulically driven piston. Three different pressure rates were employed, viz. 0.15 kPa s⁻¹, 1.5 kPa s⁻¹, and 15 kPa s⁻¹. The panels were supported on two 150 mm long neoprene setting blocks at the quarter points of the bottom edge. The outside surface, i.e. the compression side, was taped with polypropylene tape. A distributed clamping force of 1 kN m⁻¹ was applied along the four edges. The lateral support was continuous along the entire perimeter. The glass plates were cut out from panes with the nominal thickness 6 mm. The mean thickness was found to be 5.8 mm. The glass was obtained from three different manufacturers denoted by M1, M2, and M3. It was not specified if the glass edges were processed in any way. Presumably, the edge condition was as-cut. The tin side was always placed in the tension side. During the experiments, the temperature was maintained at 20-25 °C and the relative humidity was 28-55%. The length of load-duration ranged from 0.2 to 53 seconds. Nondestructive tests were carried out on a strain-gauged and tempered glass panel having 41 strain gauges bound to its surface. The fracture stress, i.e. the maximum principal tensile stress at the fracture origin, was determined based on the nondestructive tests. However, the calculation method used was not detailed in the report. Dalglish and Taylor (1990) discuss the Ontario Research Foundation test results and indicate that a power law relation was fitted in order to interpolate the stresses, σ , for pressures, P , up to failure using the following equation

$$\sigma = KP^\beta \quad (24)$$

where K is a constant and β varies with the failure location. In most cases, β was in the range 0.85-0.95. In fact, β is also a function of aspect ratio and thickness. A summary of details on the experiment is given in Tab. 2. In Fig. 6, a set of boxplots depict the fracture stress characteristics for the nominal strength data. Fig. 7 shows the recorded fracture origins. NB., in some cases, there was an ambiguity as to the specific fracture origin due to the existence of multiple potential fracture sites, including, in a few cases, a mixture of potential surface and edge failures. Fig. 7 shows the primary choice of origins according to the reference in the case when the fracture origin could be uniquely determined as being either an edge failure or a surface failure.

Table 2: Details on the experiment as reported by Johar (1981). L=Low, M=Medium, H=High loading rate, ULP=Uniform lateral pressure.

Sample ID	No. of spec's	No. of unamb. edge fail's	No. of unamb. surf. fail's	Bending mode	Dimensions (mm ³)	Pressure rate (kPa s ⁻¹)
L-M1	9	3	5	ULP	6x1525x2440	0.15
L-M2	9	4	5	ULP	6x1525x2440	0.15
L-M3	10	1	9	ULP	6x1525x2440	0.15
M-M1	8	0	8	ULP	6x1525x2440	1.5
M-M2	7	4	2	ULP	6x1525x2440	1.5
M-M3	9	1	8	ULP	6x1525x2440	1.5
H-M1	9	1	6	ULP	6x1525x2440	15
H-M2	9	2	6	ULP	6x1525x2440	15
H-M3	8	0	7	ULP	6x1525x2440	15

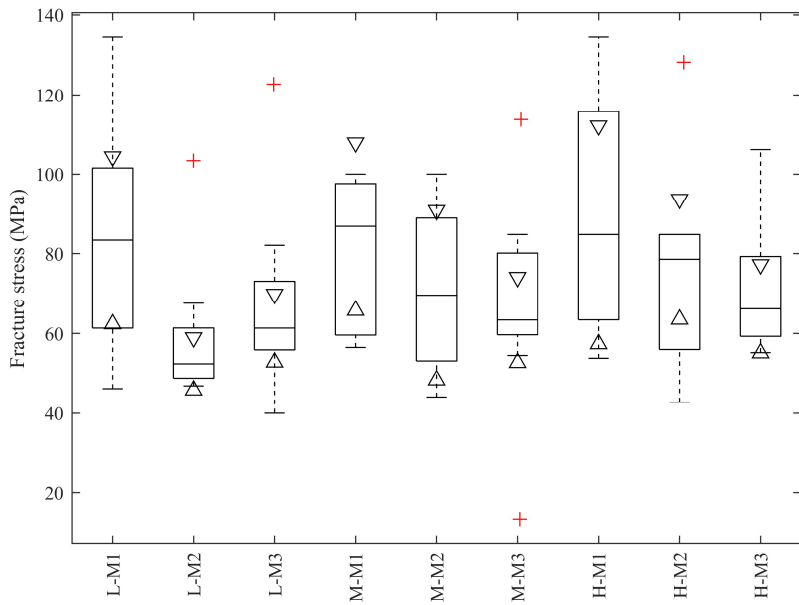


Fig. 6 Boxplots of the strength according to Johar (1981).

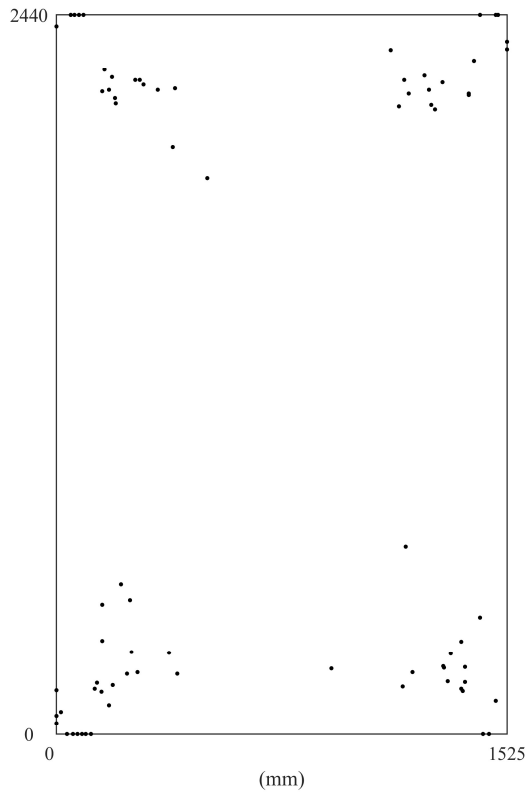


Fig. 7 Fracture locations according to Johar (1981).

SURVEY OF EXPERIMENTAL DATA ON THE STRENGTH OF ANNEALED FLOAT GLASS
Johar (1982)

The experiment was conducted with the same test rig and specimen geometry as in Johar (1981). In the following, the main differences are mentioned. The glass was obtained from one manufacturer only. During the experiments, the temperature was maintained at 16-24 °C and the relative humidity was 26-57%. A summary of details on the experiment is given in Tab. 3. In Fig. 8, a set of boxplots depict the fracture stress characteristics for the nominal strength data divided into the following categories, viz. 1) all failures irrespective of failure mode, i.e. surface or edge origin, 2) only edge failures that were unambiguously identified as such, and 3) only surface failures that were unambiguously identified as such. A set of three probability plots for each sample is shown in Fig. 10 including the respective maximum-likelihood parameter estimates and the Anderson-Darling goodness-of-fit statistic. Fig. 9 shows the recorded fracture origins.

Table 3: Details on the experiment as reported by Johar (1982).

Sample ID	No. of spec's	No. of unamb. edge fail's	No. of unamb. surf. fail's	Bending mode	Dimensions (mm ³)	Pressure rate (kPa s ⁻¹)
1	21	4	15	ULP	6x1525x2440	0.0025
2	21	7	13	ULP	6x1525x2440	0.025
3	22	5	16	ULP	6x1525x2440	0.25
4	23	5	18	ULP	6x1525x2440	2.5
5	19	2	13	ULP	6x1525x2440	25

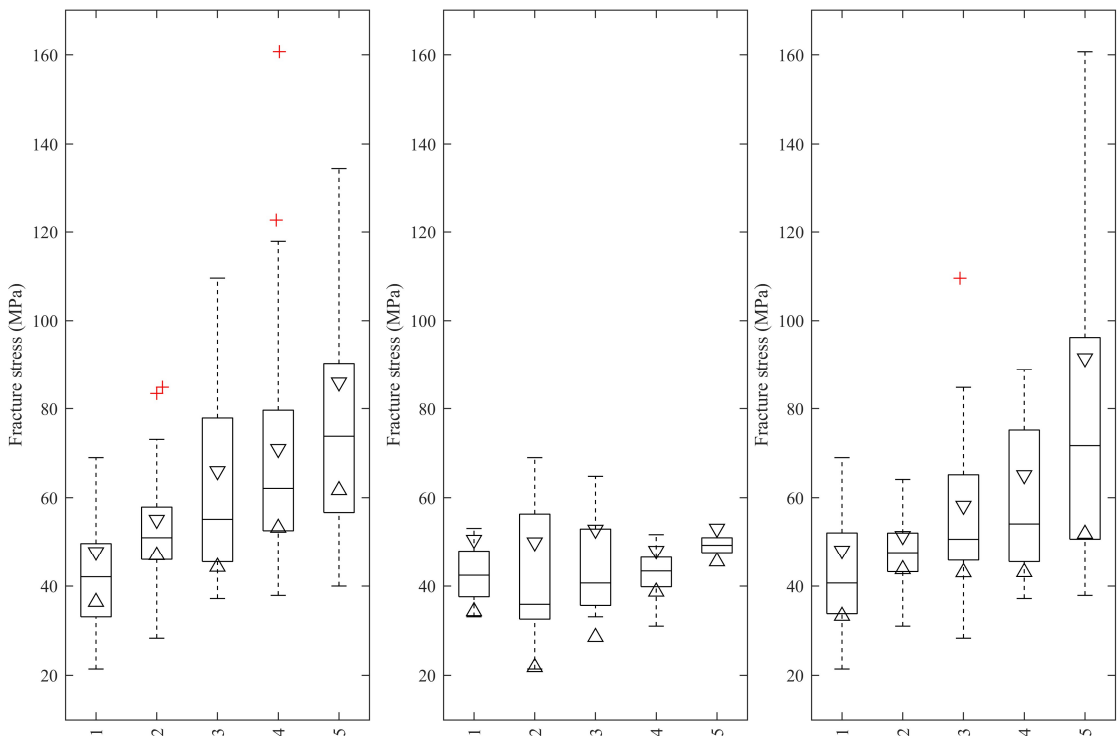


Fig. 8 Boxplots of the strength according to Johar (1982). Left: both edge and surface failures. Middle: only edge failures that were unambiguously identified as such. Right: only surface failures that were unambiguously identified as such.

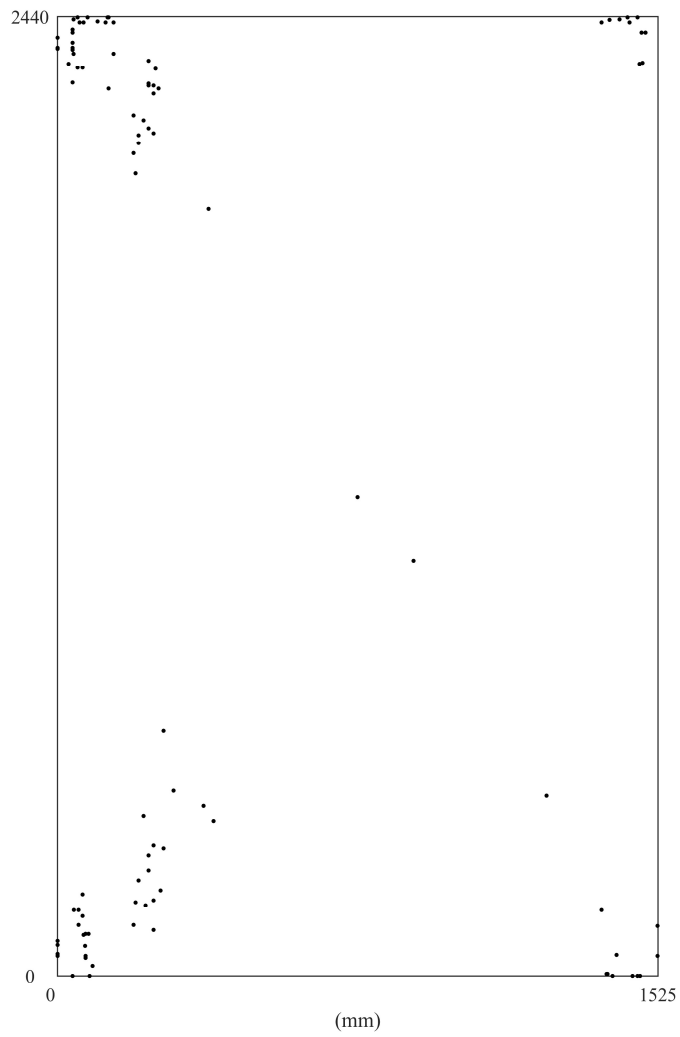


Fig. 9 Fracture locations according to Johar (1982).

SURVEY OF EXPERIMENTAL DATA ON THE STRENGTH OF ANNEALED FLOAT GLASS

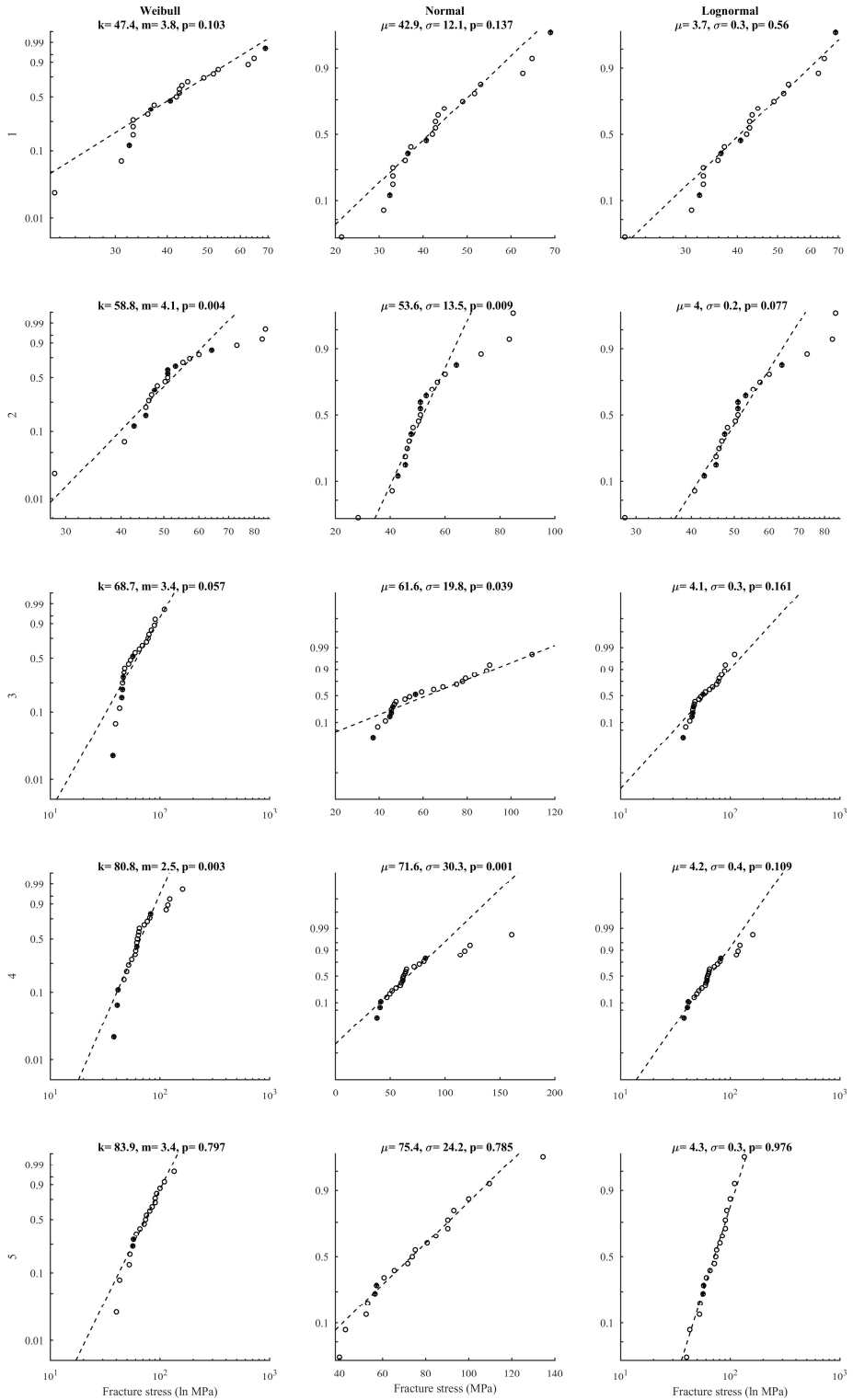


Fig. 10 Probability plots for the data samples in Johar (1982). Edge failures are marked with a crossed circle.

SURVEY OF EXPERIMENTAL DATA ON THE STRENGTH OF ANNEALED FLOAT GLASS

Simiu et al. (1984)

The experiment was conducted with a coaxial double ring bending device in combination with a Universal Testing Machine. The loading ring diameter was 51 mm and the support ring diameter was 121 mm. The support ring consisted of a segmented circular ring. The loading ring consisted of a closely wound coil. The load was transmitted to the coil by a rubber diaphragm covering a circular groove filled with water, the purpose of which was to equalize the loading along the coils. Two types of plate geometries were employed corresponding to two samples. In data sample 1, the plates were square specimens. In sample 2, the plates were circular discs. All specimens were cut out from panes with the nominal thickness 6 mm and the glass was obtained from the same manufacturer and batch. The overall mean thickness of the plates was found to be 5.44 mm. The square plate dimensions were 179x179 mm². The round plates measured 178 mm in diameter. The applied loading produced a linear stress rate with the average values 0.8 MPa s⁻¹ and 1.1 MPa s⁻¹, respectively. The load-duration until failure ranged from 31 sec to 1 min and 57 sec. It was not recorded which of the tin versus air side of the glass that was placed in the tension zone. The fracture stress was calculated using Eqs. (5) and (6). During the experiments, the temperature was maintained at room temperature and the relative humidity was 60-74%. A summary of details on the experiment is given in Tab. 4. In Fig. 11, a set of boxplots depict the fracture stress characteristics for the nominal and stress rate-equivalent strength data. A set of three probability plots for each sample is shown in Fig. 12 including the respective maximum-likelihood parameter estimates and the Anderson-Darling goodness-of-fit statistic. Fig. 13 illustrates the recorded failure origins in the radial direction from the centre point of the plate.

Table 4: Details from the experiment of Simiu et al. (1984).

Sample ID	No. of spec's	Bending mode	Dimensions (mm ² /mm ²)	Load. ring diameter (mm)	Stress rate (MPa s ⁻¹)
Square	56	CDR	6x179x179	51	0.8
Circular	29	CDR	6x178	51	1.1

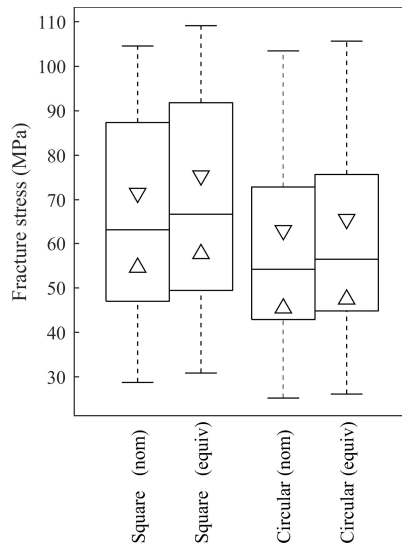


Fig. 11 Boxplots of the nominal fracture stress values and the stress rate-equivalent values for the data samples in Simiu et al. (1984).

SURVEY OF EXPERIMENTAL DATA ON THE STRENGTH OF ANNEALED FLOAT GLASS

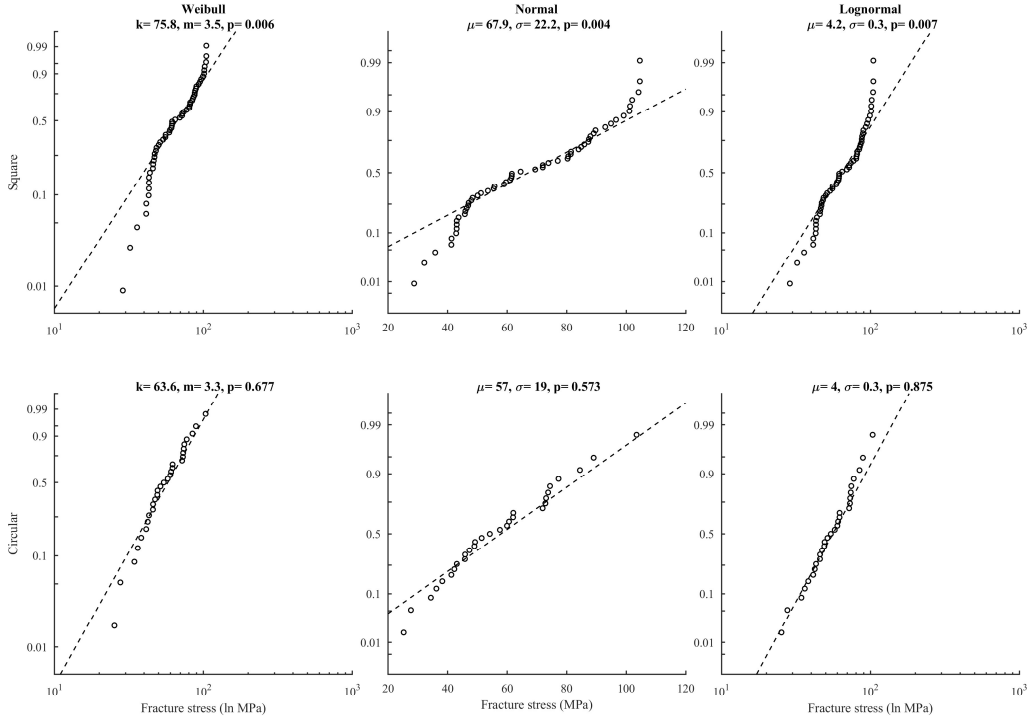


Fig. 12 Probability plots for each data sample in Simiu et al. (1984).

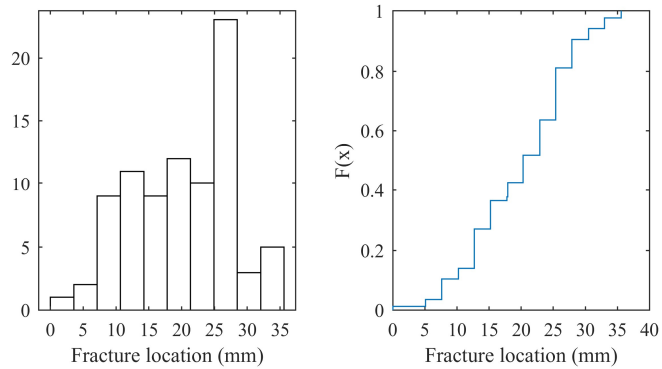


Fig. 13 Fracture locations in the radial direction from the centre point of the plate specimen, according to Simiu et al. (1984). Histogram (left) and empirical distribution function (right). NB., loading ring radius was 25.4 mm.

SURVEY OF EXPERIMENTAL DATA ON THE STRENGTH OF ANNEALED FLOAT GLASS
Kanabolo and Norville (1985)

The experiment was conducted using a setup that enabled a monotonically increasing uniform lateral pressure to be applied to laterally supported plates. The test rig consisted of a plywood deck to which a base structure of steel channels was mounted. Neoprene strips were set onto the base structure. The test specimens were mounted on the base structure and clamped between two neoprene gaskets to form an air-tight chamber. The testing procedure provided boundary conditions similar in concept to those in actual window installations. With a vacuum accumulator a negative pressure was applied to the glass surface in the test chamber. The compression surface, i.e. the surface outside the test chamber, of the specimens was taped to enable an identification of the fracture origin. The tin side of the glass was always placed in the tension side. It was not specified if the edges were processed in any way. Presumably, the edge condition was as-cut. The specimens were cut out from panes with the nominal thickness 6 mm. The overall mean thickness was 5.8 mm. The panes were obtained from two different manufacturers. A set of seven different plate dimensions were used. The various plate dimensions are detailed in Tab. 5 which also includes a summary of details on the experiment. The load-duration until failure ranged from about 0.5 sec to almost 25 min. The fracture stress was not calculated. However, Natividad (2014) calculated the MPTS at the fracture locations based on the 60 second-equivalent failure loads. Fig. 14 depicts the recorded fracture locations.

Table 5: Details on the experiment as reported by Kanabolo and Norville (1985).

Sample ID	No. of spec's	No. of edge fail's	Bending mode	Dimensions (mm ³)	Pressure rate (kPa s ⁻¹)
w-1 – w-24	20	3	ULP	6x965x1930	60.2
w-25 – w-48	18	6	ULP	6x 965x1930	17.7
w-49 – w-70	15	7	ULP	6x 965x1930	1.9
SS	19	2	ULP	6x 838x1676	87.7
SL	16	8	ULP	6x 1118x2362	33.6
Z	19	5	ULP	6x 1372x1372	50.1
SQ	18	6	ULP	6x 1181x1181	87.7
V	12	8	ULP	6x 1930x1930	37.6
H	15	9	ULP	6x 1524x2438	35.1

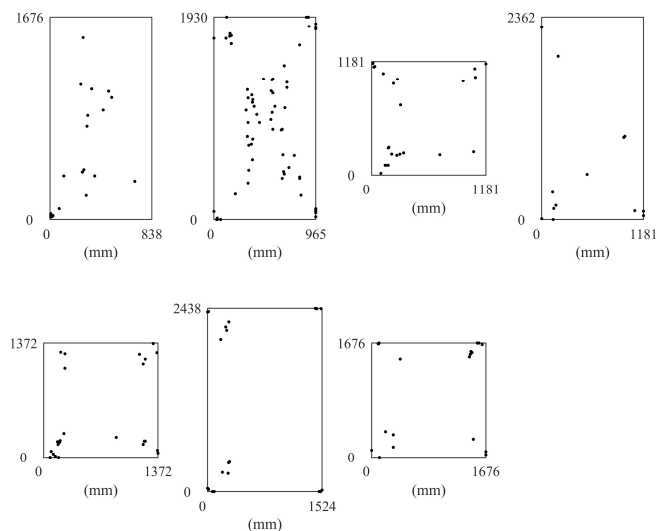


Fig. 14 Fracture locations according to Kanabolo and Norville (1985).

SURVEY OF EXPERIMENTAL DATA ON THE STRENGTH OF ANNEALED FLOAT GLASS
Carre (1996)

The experiment was conducted with the four-point bending arrangement. The load span dimension was 125 mm. The specimens were cut out from glass panes with the thickness 19 mm. Two different specimen dimensions were employed, viz. 37.5x250 mm² and 300x2000 mm². Moreover, two different edge polishing machines were utilized corresponding to the sample ID's A and B, respectively. The beams were subjected to in-plane loading generating an approximate stress rate of 0.05 MPa s⁻¹, 0.5 MPa s⁻¹, and 5.0 MPa s⁻¹, respectively. Failures that occurred outside the load span or outside the polished edge (i.e. on the surface) were excluded from the data. During the experiment, the temperature ranged between 15-20 °C while the relative humidity was 40-70%. The length of load-duration ranged from about 9 sec to over 20 min according to calculations. A summary of details on the experiment is given in Tab. 6. In Fig. 15, a set of boxplots depict the fracture stress characteristics for the nominal and stress rate-equivalent strength data. A set of three probability plots for the samples is shown in Fig. 16 including the respective maximum-likelihood parameter estimates and the Anderson-Darling goodness-of-fit statistic. The last sample was not included in the probability plot due to its limited size. The data results were extracted from the digitized graphs by this author.

Table 6: Details on the experiment as reported by Carre (1996). L=Low, M=Medium, H=High stress rate, 4PB=Four-point bending, IP=In-plane.

Sample ID	No. of spec's	Bending mode	Dimensions (mm ²)	Edge proc.	Load. span (mm)	Stress rate (MPa s ⁻¹)
M-A	28	4PB IP	19x37.5x250	Polished	125	0.5
L-A	14	4PB IP	19x37.5x250	Polished	125	0.05
H-B	9	4PB IP	19x37.5x250	Polished	125	5.0
M-B	15	4PB IP	19x37.5x250	Polished	125	0.5
L-B	12	4PB IP	19x37.5x250	Polished	125	0.05
L	3	4PB IP	19x300x2000	Polished	667	0.05

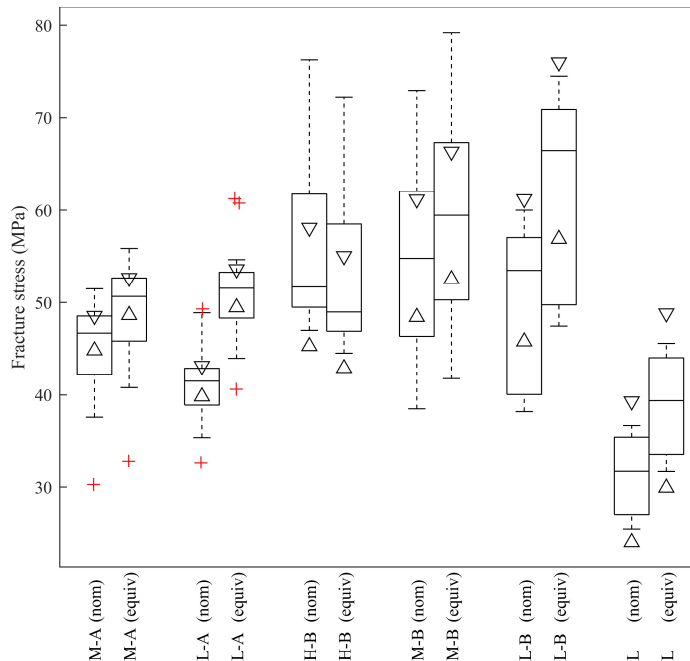


Fig. 15 Boxplots for the nominal fracture stress and the stress rate-equivalent strength according to Carre (1996).

SURVEY OF EXPERIMENTAL DATA ON THE STRENGTH OF ANNEALED FLOAT GLASS

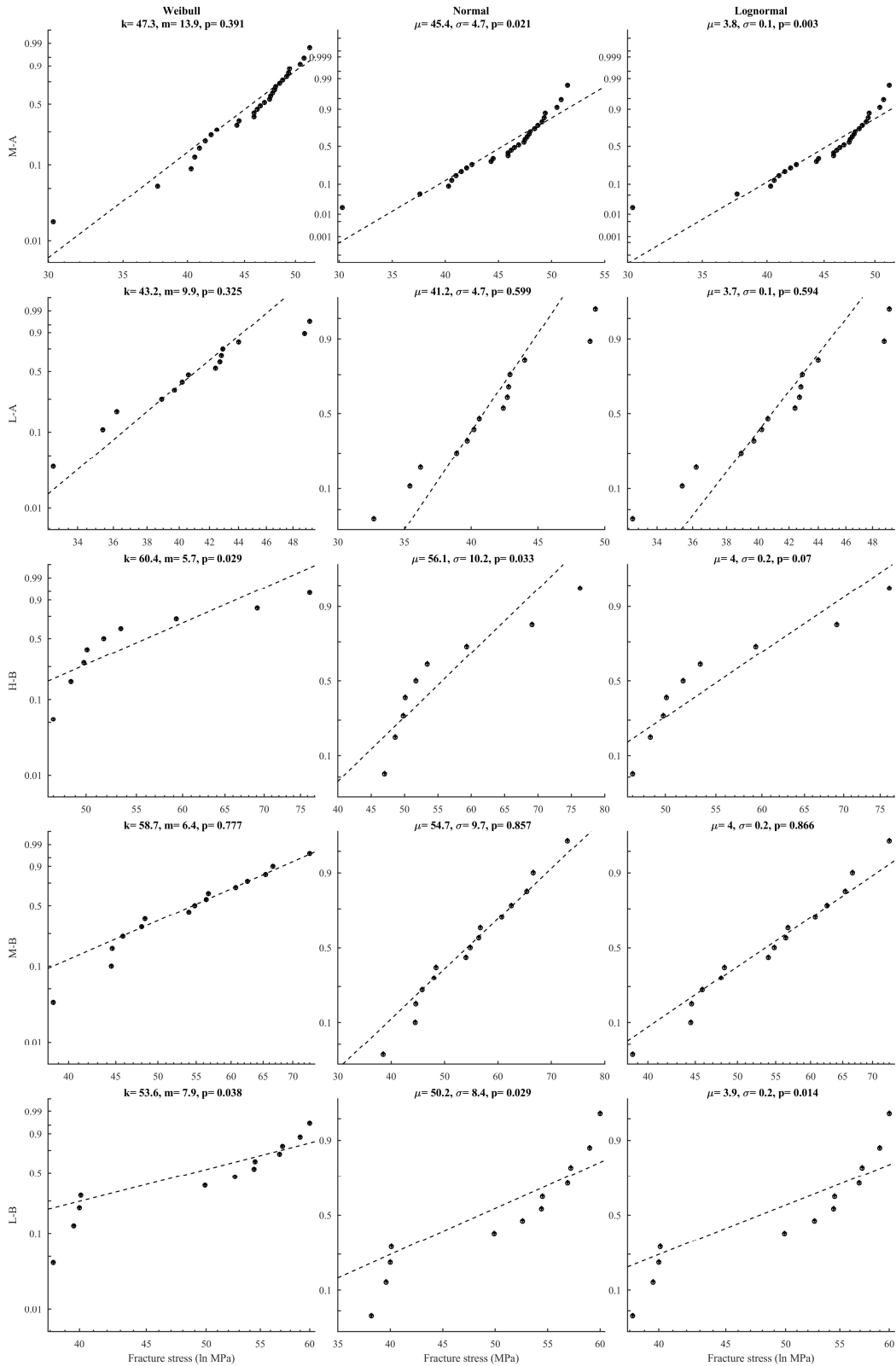


Fig. 16 Probability plots for the data sets according to Carre (1996).

*SURVEY OF EXPERIMENTAL DATA ON THE STRENGTH OF ANNEALED FLOAT GLASS
Calderone (1999)*

The experiment was conducted using a setup that enabled a uniform lateral pressure to be applied to laterally supported plates. The glass panes were mounted with their plane horizontally in the test rig. Water was used for applying the load to the glass. The test rig had the form of a horizontal table on legs. The tabletop was formed from a flat steel plate. A supporting structure was used below the table. A base frame was constructed above the tabletop and bolted to the structure below. The tabletop and the base frame formed the water reservoir. Hence, the loading was applied to the bottom surface of the glass. The specimens were mounted on continuous 20 mm thick nylon blocks which were set on the base frame. The blocks had a groove at the edge forming a support rebate. An upper frame was constructed above the base frame and bolted to it. The upper frame provided support for the glass edges from the top between a set of continuous 20 mm thick nylon in-fills. The flow of inlet and outlet water was controlled using butterfly valves. The water was supplied from a large tank which was six meters high. The water was retained within the test rig without leakage upon fracture using a soft plastic bag. The stresses at the observed fracture origins were calculated with FE software while assuming that the glass edges were restrained so that they remained in plane. However, no measurements were made on any plates using strain gauges. The specimens were cut out from panes with the nominal thickness 6 mm. The overall mean thickness was measured to be 5.9 mm. Eight different specimen dimensions were employed providing a range of different aspect ratios. The loading was applied in four different ways producing either a slow ramp pressure, a medium ramp pressure, a fast ramp pressure, or a cyclic loading. The tin surface of the glass was always placed in the tension zone, i.e. upwards. During the experiments, the temperature ranged between 12-31 °C and the relative humidity was 39-99%. The length of load-duration ranged from 48 sec to over 23 min. A summary of details on the experiment is given in Tab. 7. In Fig. 17, a set of boxplots depict the fracture stress characteristics for the nominal strength data. Fig. 18 shows the recorded fracture origins. NB. in some cases there was an ambiguity as to the specific fracture origin due to the existence of multiple potential fracture sites. Fig. 18 shows the primary choice of origins according to Calderone (1999).

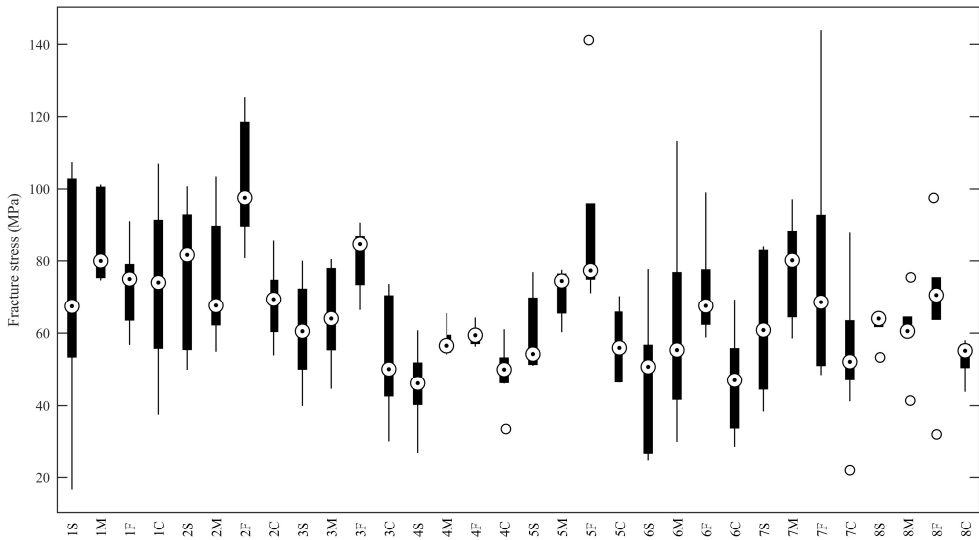


Fig. 17 Boxplots of the fracture stress according to Calderone (1999).

Table 7: Details on the experiment reported by Calderone (1999). S=Slow, M=Medium, F=Fast, C=Cyclic loading, ULP=Uniform Lateral Pressure.

SURVEY OF EXPERIMENTAL DATA ON THE STRENGTH OF ANNEALED FLOAT GLASS

Sample ID	No. of spec's	No. of unamb. edge fail's	No. of unamb. surf. fail's	Bending mode	Dimensions (mm ³)	Edge proc.	Pressure rate (kPa s ⁻¹)
1S	6	1	5	ULP	6x400x2000	Unknown	Slow ramp
1M	5	0	5	ULP	6x400x2000	Unknown	Med. ramp
1F	5	0	5	ULP	6x400x2000	Unknown	Fast ramp
1C	9	0	9	ULP	6x400x2000	Unknown	Cyclic loading
2S	6	0	6	ULP	6x500x2000	Unknown	Slow ramp
2M	7	0	7	ULP	6x500x2000	Unknown	Med. ramp
2F	5	0	5	ULP	6x500x2000	Unknown	Fast ramp
2C	7	0	7	ULP	6x500x2000	Unknown	Cyclic loading
3S	5	0	5	ULP	6x670x2000	Unknown	Slow ramp
3M	5	0	5	ULP	6x670x2000	Unknown	Med. ramp
3F	5	0	5	ULP	6x670x2000	Unknown	Fast ramp
3C	9	0	9	ULP	6x670x2000	Unknown	Cyclic loading
4S	5	1	4	ULP	6x1000x2000	Unknown	Slow ramp
4M	6	2	4	ULP	6x1000x2000	Unknown	Med. ramp
4F	5	0	5	ULP	6x1000x2000	Unknown	Fast ramp
4C	9	1	8	ULP	6x1000x2000	Unknown	Cyclic loading
5S	6	3	3	ULP	6x1335x2000	Unknown	Slow ramp
5M	5	3	2	ULP	6x1335x2000	Unknown	Med. ramp
5F	5	0	5	ULP	6x1335x2000	Unknown	Fast ramp
5C	6	3	3	ULP	6x1335x2000	Unknown	Cyclic loading
6S	6	2	4	ULP	6x1600x2000	Unknown	Slow ramp
6M	6	1	5	ULP	6x1600x2000	Unknown	Med. ramp
6F	5	2	3	ULP	6x1600x2000	Unknown	Fast ramp
6C	7	3	4	ULP	6x1600x2000	Unknown	Cyclic loading
7S	5	1	4	ULP	6x2000x2000	Unknown	Slow ramp
7M	5	1	4	ULP	6x2000x2000	Unknown	Med. ramp
7F	6	3	3	ULP	6x2000x2000	Unknown	Fast ramp
7C	9	3	5	ULP	6x2000x2000	Unknown	Cyclic loading
8S	6	1	4	ULP	6x2000x3000	Unknown	Slow ramp
8M	6	3	3	ULP	6x2000x3000	Unknown	Med. ramp
8F	6	3	3	ULP	6x2000x3000	Unknown	Fast ramp
8C	7	3	4	ULP	6x2000x3000	Unknown	Cyclic loading

SURVEY OF EXPERIMENTAL DATA ON THE STRENGTH OF ANNEALED FLOAT GLASS

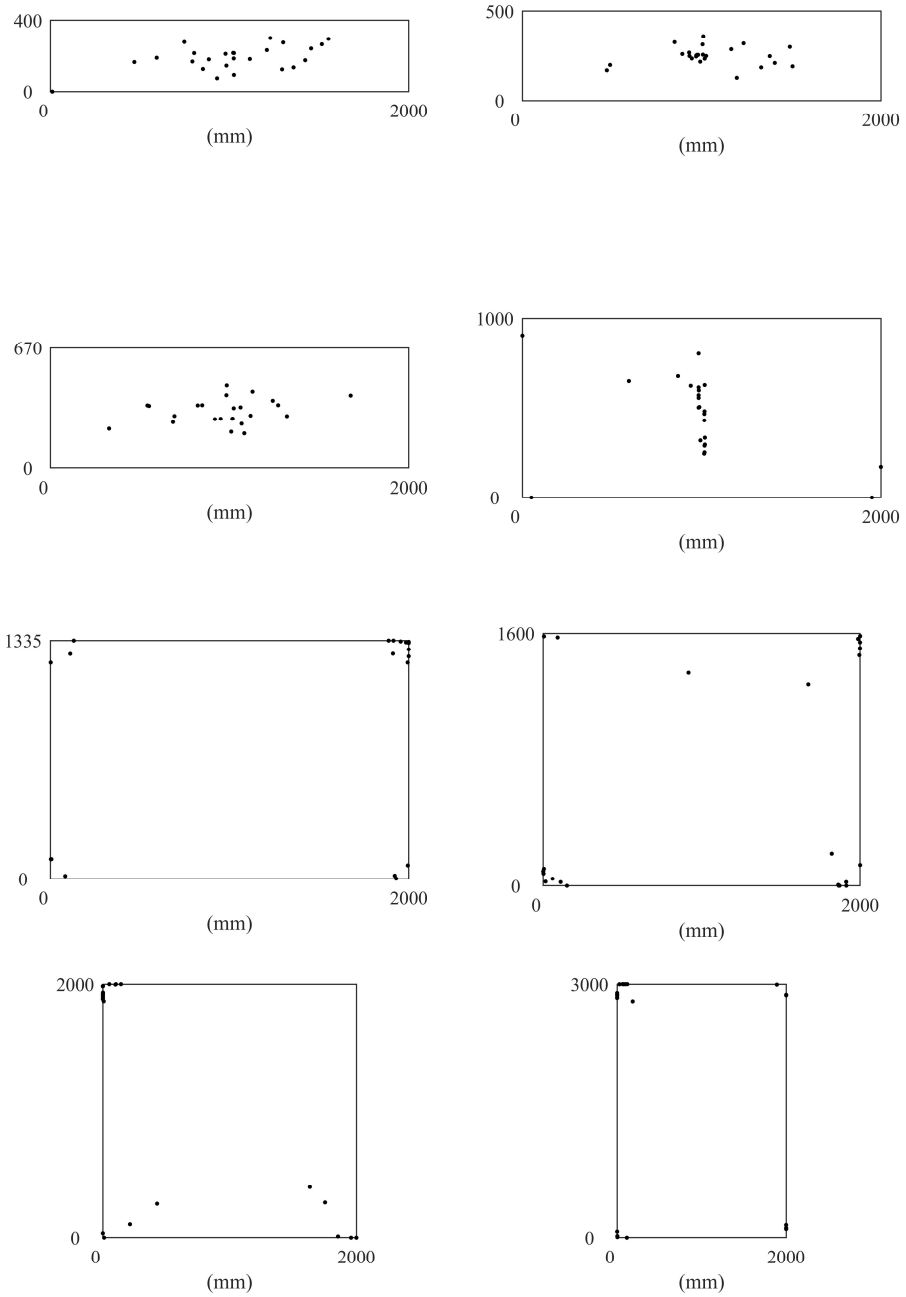


Fig. 18 Fracture locations according to Calderone (1999).

SURVEY OF EXPERIMENTAL DATA ON THE STRENGTH OF ANNEALED FLOAT GLASS
Hess (2000)

The experiment was conducted with a four-point bending device. The loading rate was controlled using a hand-driven hydraulic piston. Hence, a strictly linear stress rate could not be produced. The load span and support span were varied between 1400 mm and 4200 mm, respectively, and 200 mm and 1000 mm, respectively. All glass specimens were cut out from 10 mm thick panes except for the small set of large specimens which measured 12 mm in thickness. The glass edge was ground. Two different specimen dimensions were employed, viz. 400x4500 mm² and 360x1100 mm². Three samples of specimens were subjected to in-plane and out-of-plane loading. In one of the samples with in-plane loading, however, the stress history between the load span was nonlinear due to the high ratio of cross-sectional height to beam length. In the case of the beams which were subjected to out-of-plane loading, the type of failure, i.e. edge failure or surface failure, was not recorded. During the experiment, the temperature was maintained at 23 °C. The relative humidity was not recorded but can be assumed to be the same as in room conditions. A summary of details on the experiment is given in Tab. 8. The length of load-duration ranged from about 17 sec to 6 min and 23 sec according to calculations. Fig. 19 shows a set of boxplots for the fracture stress. Fig. 20 shows a set of probability plots for some of the data samples.

Table 8: Details on the experiment as reported by Hess (2000). 4PB=Four-point bending, IP=In-plane.

Sample ID	No. of spec's	Bending mode	Dimensions (mm ²)	Edge proc.	Load. span (mm)	Approx. stress rate (MPa s ⁻¹)
1	4	4PB IP	12x400x4500	Ground	1400	0.13
2	10	4PB IP	10x360x1100	Ground	200	N/A
3	11	4PB OP	10x360x1100	Ground	200	3.0

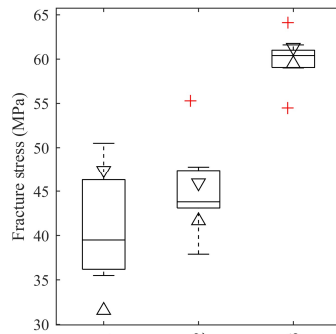


Fig. 19 Boxplots for the fracture stress according to Hess (2000).

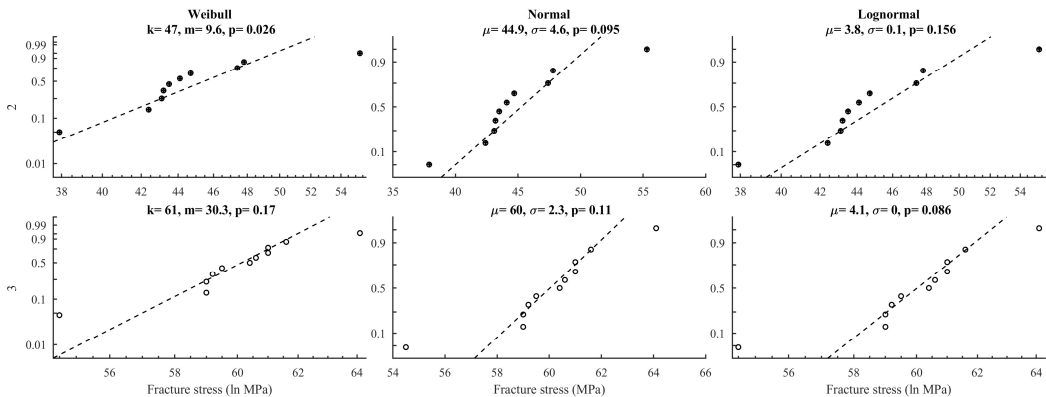


Fig. 20 Probability plots for the strength according to Hess (2000).

Fink (2000)

The experiment was conducted with the coaxial double ring bending device. The loading ring diameter was 55 mm and the support ring diameter was 145 mm. The specimens were cut out from panes with the nominal thickness 4 mm and obtained from two different suppliers in this report denoted by M1 and M2. The specimens had the dimensions 225x225 mm². The applied loading generated an approximate stress rate of 2 MPa s⁻¹. In the case of the M1 sample data, the tin side of the plates was placed in the tension zone. However, for the M2 sample, it was not recorded which of the tin versus air side that was placed in the tension zone. A piece of machine writing paper was applied to the contact surface between the glass and steel parts. The temperature during testing was 23 °C and the relative humidity was 60%. The load-duration until failure ranged from about 28 sec to 1 min and 41 sec according to calculations. A summary of details on the experiment is given in Tab. 9. In Fig. 21, a set of boxplots depict the fracture stress characteristics for the nominal strength data. A set of three probability plots for each sample is shown in Fig. 22 including the respective maximum-likelihood parameter estimates and the Anderson-Darling goodness-of-fit statistic.

Table 9: Details on the experiment as reported by Fink (2000).

Sample ID	No. of spec's	Bending mode	Dimensions (mm ³)	Load. ring diameter (mm)	Stress rate (MPa s ⁻¹)
M1	20	CDR	4x225x225	55	2
M2	107	CDR	4x225x225	55	2

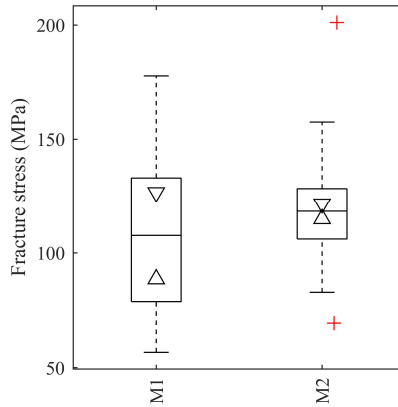


Fig. 21 Boxplots of the nominal fracture stress according to Fink (2000).

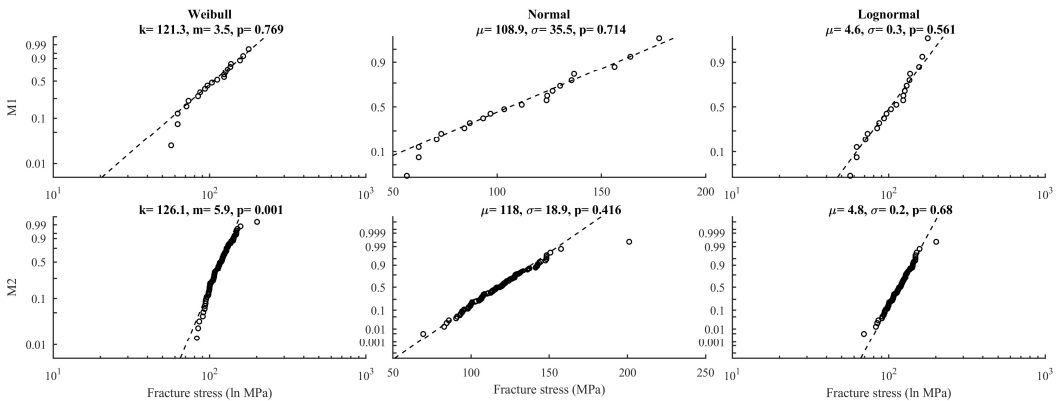


Fig. 22 Probability plots for each data sample in Fink (2000).

*SURVEY OF EXPERIMENTAL DATA ON THE STRENGTH OF ANNEALED FLOAT GLASS
Overend (2002)*

The experiment was conducted with the coaxial double ring bending setup using a Satec Universal testing machine under displacement control. The loading ring diameter was 51 mm and the support ring diameter was either 65 mm, 127 mm or 200 mm, corresponding to three samples of tests. The specimens were cut out from panes with a thickness of 6 mm. The specimen dimensions were 300x300 mm². The out-of-plane loading generated an approximate stress rate of 0.65 MPa s⁻¹, 0.90 MPa s⁻¹, and 0.64 MPa s⁻¹, respectively. Transparent adhesive tape was applied to the compression side. One specimen in each sample was strain gauged using two rosettes located at the center on the tension side of the glass and directly under the loading ring. It was not recorded which of the air versus tin side of the glass that were placed in the tension zone. The load-duration until failure ranged from about 1 min to 8 min and 43 sec. The temperature and relative humidity during testing was not specified but it can be assumed that an indoor environment represents the climatic conditions. A summary of details on the experiment is given in Tab. 10. In Fig. 23, a set of boxplots depict the fracture stress characteristics for the nominal and stress rate-equivalent strength data. The fracture stress values are the experimental values recorded by Overend (2002) which were based on strain gauge measurements and extrapolation methods. A set of three probability plots for each sample is shown in Fig. 24 including the respective maximum-likelihood parameter estimates and the Anderson-Darling goodness-of-fit statistic. The recorded fracture origins are depicted in Fig. 25.

Table 10: Details on the experiment as reported by Overend (2002). S=Small, M=Medium, L=Large reaction ring diameter, CDR=Coaxial double ring,

Sample ID	No. of spec's	Bending mode	Dimensions (mm ³)	Load. ring diameter (mm)	Stress rate (MPa s ⁻¹)
S	10	CDR	6x300x300	51	0.65
M	10	CDR	6x300x300	51	0.90
L	10	CDR	6x300x300	51	0.64

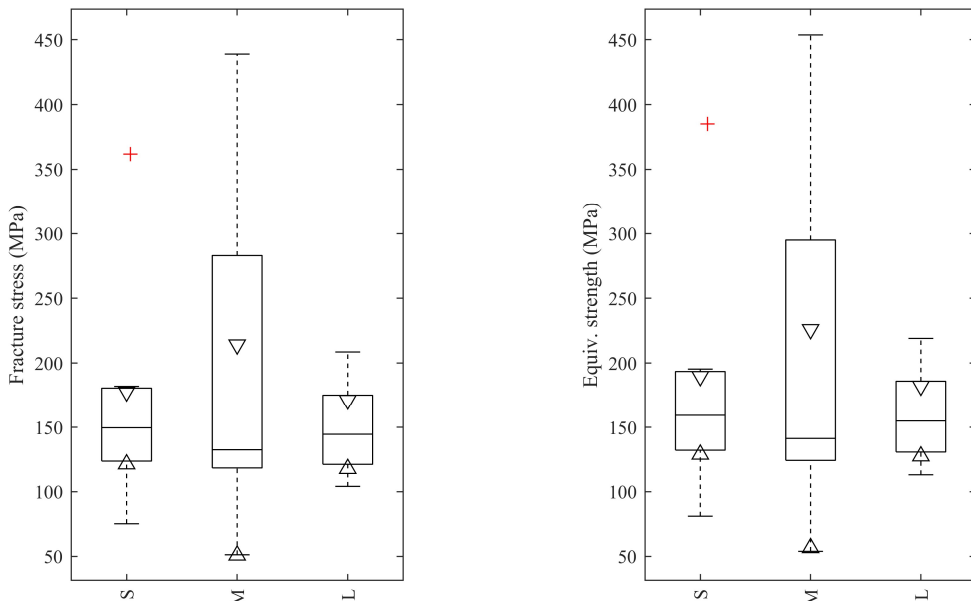


Fig. 23 Boxplots of the (left) nominal and (right) stress rate-equivalent fracture stress for the data in Overend (2002). Comb.=Combined data set.

SURVEY OF EXPERIMENTAL DATA ON THE STRENGTH OF ANNEALED FLOAT GLASS

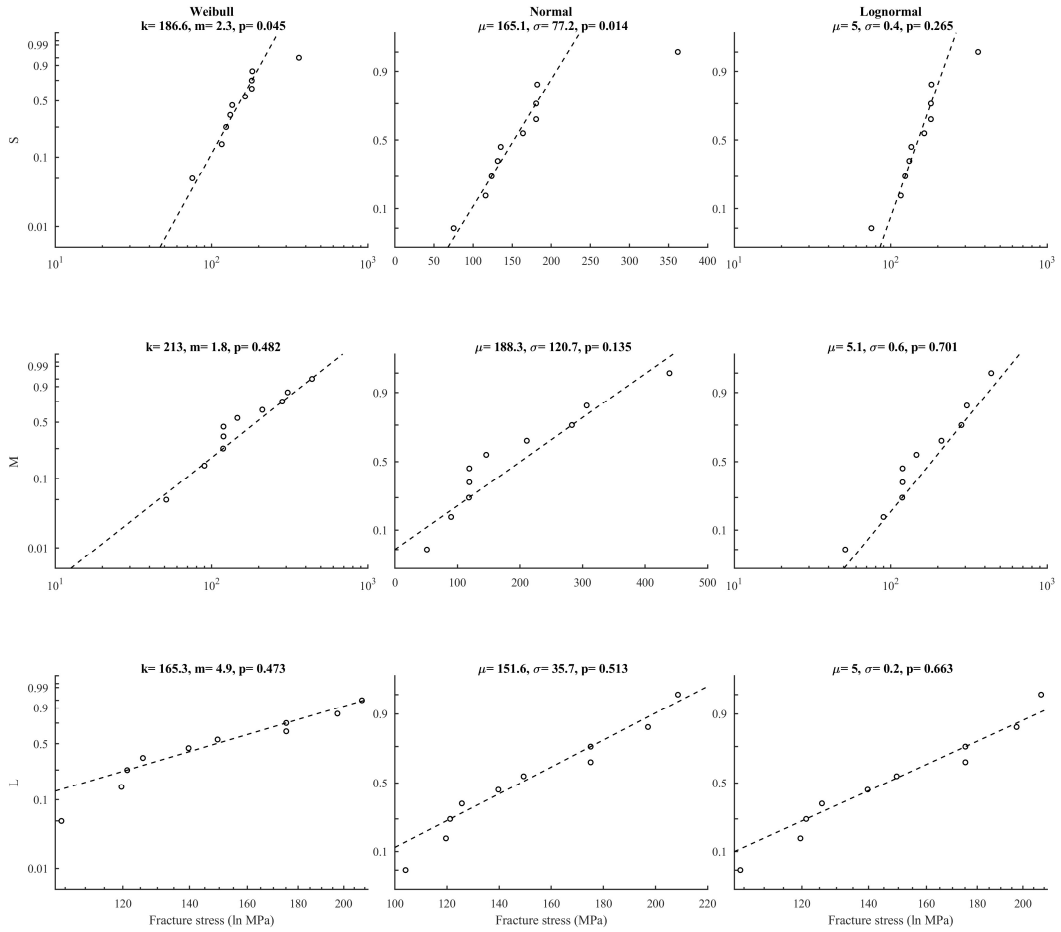


Fig. 24 Probability plots for the data samples in Overend (2002).

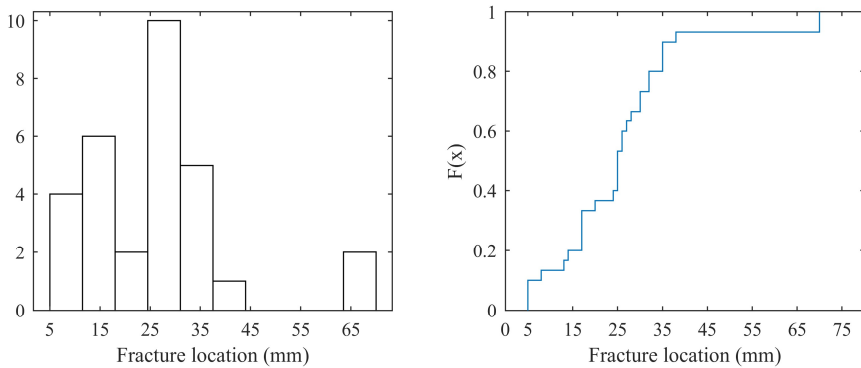


Fig. 25 Fracture locations in the radial direction from the centre point of the plate specimen, according to Overend (2002). Histogram (left) and empirical distribution function (right). NB., loading ring radius was 25.4 mm.

SURVEY OF EXPERIMENTAL DATA ON THE STRENGTH OF ANNEALED FLOAT GLASS
Haldimann (2006)

The experiment was conducted with a coaxial double ring bending setup using a universal testing machine. The loading ring diameter was 51 mm and the support ring diameter was 127 mm. The specimens were cut out from panes with the nominal thickness 6 mm. The specimen dimensions were 200x200 mm². Two different loading rates were employed which produced stress rates of approximately 0.21 MPa s⁻¹ and 21.2 MPa s⁻¹, respectively. The temperature during testing was 23-24 °C and the relative humidity varied between 51-55%. The load-duration until failure ranged from approximately 6 sec to 6 min and 59 sec. A summary of details on the experiment is given in Tab. 11. In Fig. 26, a set of boxplots depict the fracture stress characteristics for the nominal and stress rate-equivalent strength data. A set of three probability plots for each sample is shown in Fig. 27 including the respective maximum-likelihood parameter estimates and the Anderson-Darling goodness-of-fit statistic.

Table 11: Details on the experiment as reported by Haldimann (2006). L=Low stress rate, H=High stress rate, CDR=Coaxial double ring.

Sample ID	No. of spec's	Bending mode	Dimensions (mm ³)	Load. ring diameter (mm)	Stress rate (MPa s ⁻¹)
L	10	CDR	6x200x200	51	0.21
H	10	CDR	6x200x200	51	21.2

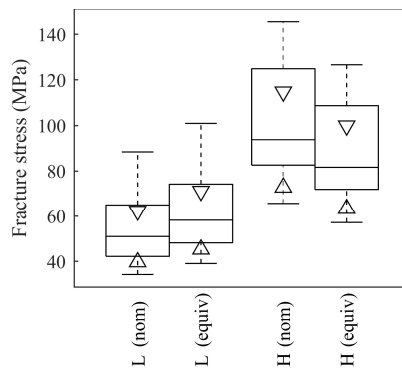


Fig. 26 Boxplots of the nominal and stress rate-equivalent fracture stress according to Haldimann (2006).

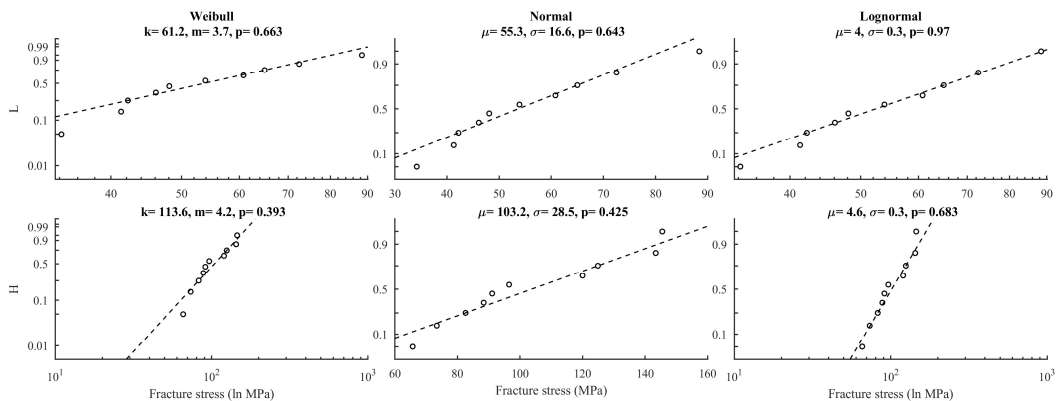


Fig. 27 Probability plots for the data samples in Haldimann (2006).

Veer et al. (2006)

The experiment was conducted with a four-point bending arrangement under displacement control using a Zwick Z100 universal testing machine. The load and support span were 230 mm and 850 mm, respectively. The specimens were cut from a single pane with the thickness 10 mm. The specimen dimensions were 125x1000 mm². The edges were machine ground on three different lines. On each line, the specimens were processed in one whole set, i.e. continuously without interruption. In fact, prior to processing the grinding lines were inspected to ensure the proper cleaning and the due replacement of grinding heads. One set of plates, Sample 1, had edges ground on a twelve years old manually controlled line. A second set, Sample 2, had edges ground on an eight year old manually controlled lone. Finally, a third set, Sample 3, had edges ground on a new computer controlled line less than three months old. The specimens were subjected to in-plane loading generating an approximate stress rate of 1.0 MPa s⁻¹. The specimens were mounted in the test rig using an anti-buckling support at the centre of the support span. The temperature and relative humidity during testing was not specified but it can be assumed that an indoor environment represents the climatic conditions. The range of load-duration was approximately 26 sec to 1 min and 4 sec. No fractures occurred from outside the load span. A summary of details on the experiment is given in Tab. 12. In Fig. 28, a set of boxplots depict the fracture stress characteristics for the nominal strength data as well as the stress rate-equivalent data. A set of three probability plots for each sample is shown in Fig. 29 including the respective maximum-likelihood parameter estimates and the Anderson-Darling goodness-of-fit statistic.

Table 12: Details on the experiment as reported by Veer et al. (2006). 4PB=Four-point bending, IP=In-plane, L=Line no.

Sample ID	No. of spec's	Bending mode	Dimensions (mm ³)	Edge proc.	Load. span (mm)	Stress rate (MPa s ⁻¹)
gro-L1	10	4PB IP	10x125x1000	Ground	230	1.1
gro-L2	11	4PB IP	10x125x1000	Ground	230	1.1
gro-L3	11	4PB IP	10x125x1000	Ground	230	1.1

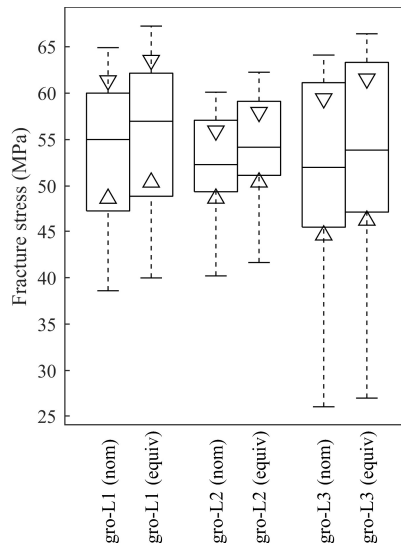


Fig. 28 Boxplots for the nominal fracture stress and the stress rate-equivalent strength according to Veer et al. (2006).

SURVEY OF EXPERIMENTAL DATA ON THE STRENGTH OF ANNEALED FLOAT GLASS

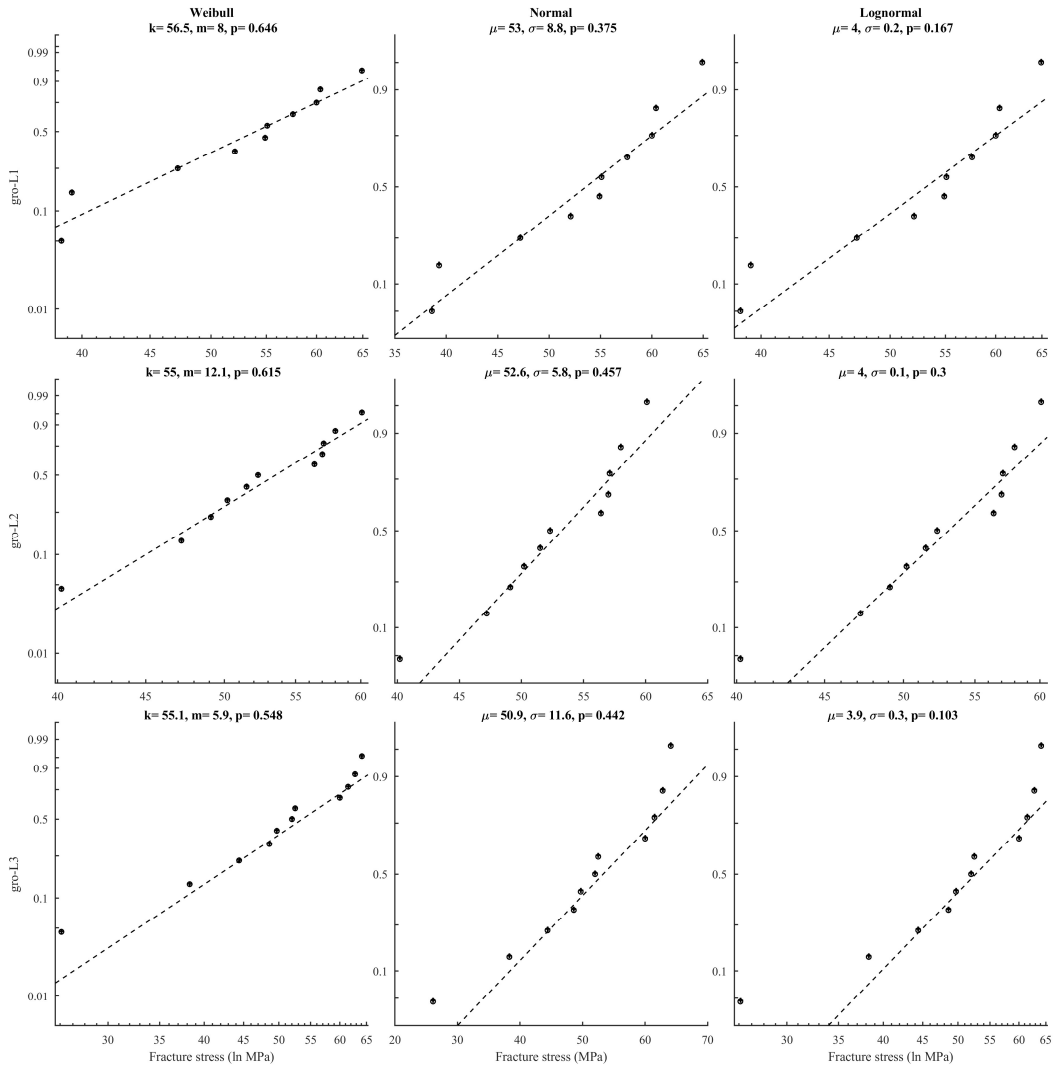


Fig. 29 Probability plots of the data sets according to Veer et al. (2006).

SURVEY OF EXPERIMENTAL DATA ON THE STRENGTH OF ANNEALED FLOAT GLASS

Sglavo et al. (2007)

The experiment was conducted with a three-point bending arrangement using displacement control. The support span was 280 mm. The specimens were cut from a set of panes with the thickness 4 mm on an industrial process line. The specimen dimensions were 200x300 mm². The edge processing types were the following, viz. as-cut, manually arrised through abrasion by traditional hand tools, machine ground, and machine polished. The specimens were subjected to out-of-plane loading producing a stress rate of approximately 3.5 MPa s⁻¹. Half of the out-of-plane loaded specimens were mounted with the mechanically scribed edge placed in the compression zone while half were positioned with the scribed edge in the tension zone. It was not recorded which of the tin side and air side that was placed in the tension zone. The compression side of the specimens were covered in adhesive transparent tape. The temperature and relative humidity during testing was estimated at about 25 °C and 40%, respectively. The range of load-duration was approximately 17 sec to 55 sec. The fracture origin mode, i.e. edge or surface, was recorded. A summary of details on the experiment is given in Tab. 13. In Fig. 30, a set of boxplots depict the fracture stress characteristics for the nominal strength data. A set of three probability plots for each sample is shown in Fig. 31 including the respective maximum-likelihood parameter estimates and the Anderson-Darling goodness-of-fit statistic.

Table 13: Details on the experiment as reported by Sglavo et al. (2007). The mechanically scribed edge was alternatively positioned Up in the compression zone and Down in the tension zone. Legend: 3PB=Three-point bending, OP=Out-of-plane.

Sample ID	No. of spec's	No. of edge fail's	Bending mode	Dimensions (mm ³)	Edge proc.	Stress rate (MPa s ⁻¹)
cut-down	12	5	3PB OP	4x200x300	Cut	3.5
cut-up	15	13	3PB OP	4x200x300	Cut	3.5
arr-down	13	4	3PB OP	4x200x300	Arrised	3.5
arr-up	14	11	3PB OP	4x200x300	Arrised	3.5
gro-down	16	7	3PB OP	4x200x300	Ground	3.5
gro-up	15	14	3PB OP	4x200x300	Ground	3.5
pol-down	15	5	3PB OP	4x200x300	Polished	3.5
pol-up	15	15	3PB OP	4x200x300	Polished	3.5

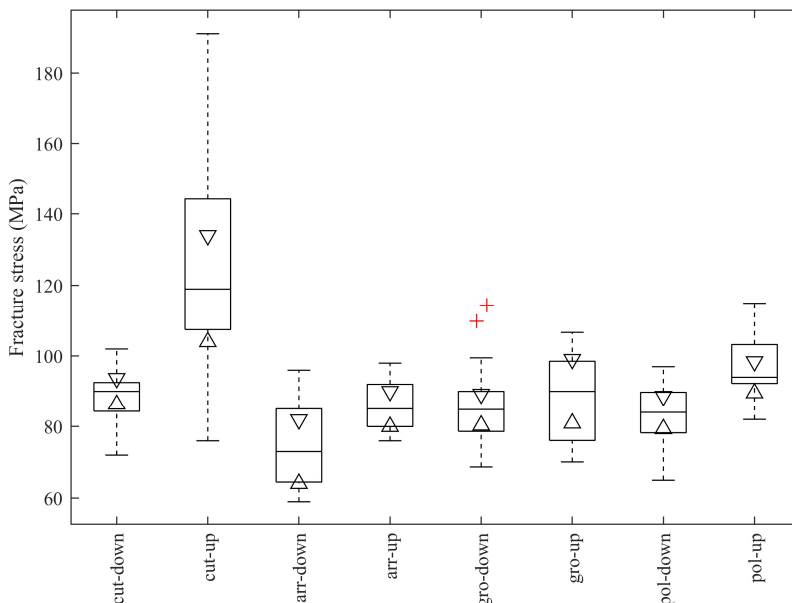


Fig. 30 Boxplots of the nominal fracture stress for each data sample in Sglavo et al. (2007). Legend: Comb=Combined data set.

SURVEY OF EXPERIMENTAL DATA ON THE STRENGTH OF ANNEALED FLOAT GLASS

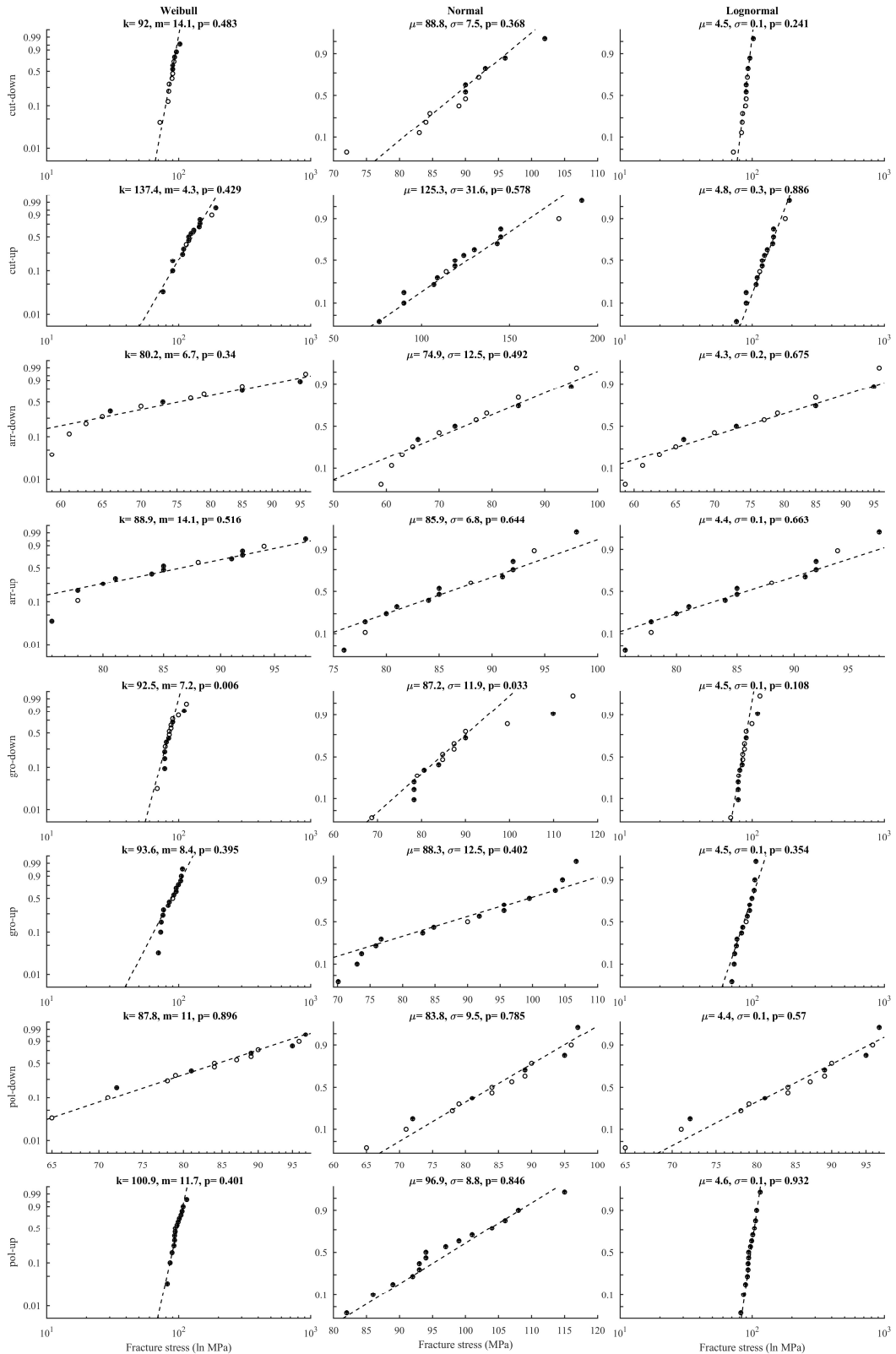


Fig. 31 Probability plots of the data samples in Sglavo et al. (2007). Edge failures are marked with a crossed circle.

Veer et al. (2009)

The experiment was conducted with a four-point bending arrangement under displacement control using a Zwick Z100 universal testing machine. The load and support span were 230 mm and 850 mm, respectively, according to private correspondence. The specimens were cut from a single pane with the thickness 10 mm using an automated cutting machine. The specimen dimensions were 100x1000 mm². The edges were processed on a single line by automated grinding and polishing. Some of the specimens were subjected to in-plane loading whereas others were subjected to out-of-plane loading generating an approximate stress rate of 0.8 MPa s⁻¹ and 0.1 MPa s⁻¹, respectively. The in-plane loaded specimens were mounted in the test rig using a 1 mm thick Teflon sheet as an intermediary at the support locations. Anti-buckling supports were employed at five locations along the length of the beam. It was not recorded which of the tin side and air side that was placed in the tension zone. The specimens were wrapped in PET foil. The temperature and relative humidity during testing was not specified but it can be assumed that an indoor environment represents the climatic conditions. The range of load-duration was approximately 26 sec to 8 min and 51 sec. The fracture origin mode, i.e. edge or surface, was not recorded in the case of the out-of-plane loaded specimens. Fractures that initiated from outside the load span were not reported so it was assumed that all fractures occurred within the load span. A summary of details on the experiment is given in Tab. 14. In Fig. 32, a set of boxplots depict the fracture stress characteristics for the nominal strength data as well as the stress rate-equivalent data. A set of three probability plots for each sample is shown in Fig. 33 including the respective maximum-likelihood parameter estimates and the Anderson-Darling goodness-of-fit statistic.

Table 14: Details on the experiment as reported by Veer et al. (2009). Legend: 4PB=Four-point bending, IP=In-plane, OP=Out-of-plane.

Sample ID	No. of spec's	Bending mode	Dimensions (mm ³)	Edge proc.	Load. span (mm)	Stress rate (MPa s ⁻¹)
pol-IP	30	4PB IP	10x100x1000	Polished	230	0.9
pol-OP	24	4PB OP	10x100x1000	Polished	230	0.1

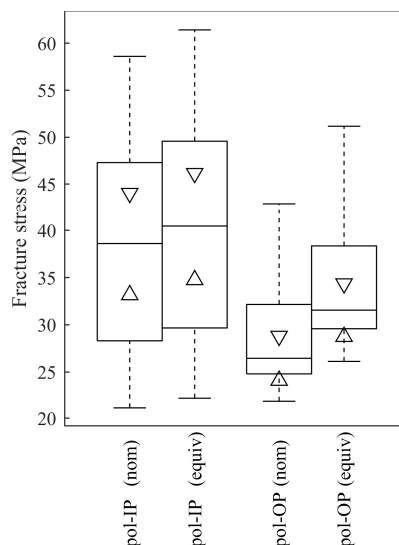


Fig. 32 Boxplots of the (left) nominal and (right) stress rate-equivalent fracture stress for each data sample in Veer et al. (2009). Legend: Comb=Combined data set.

SURVEY OF EXPERIMENTAL DATA ON THE STRENGTH OF ANNEALED FLOAT GLASS

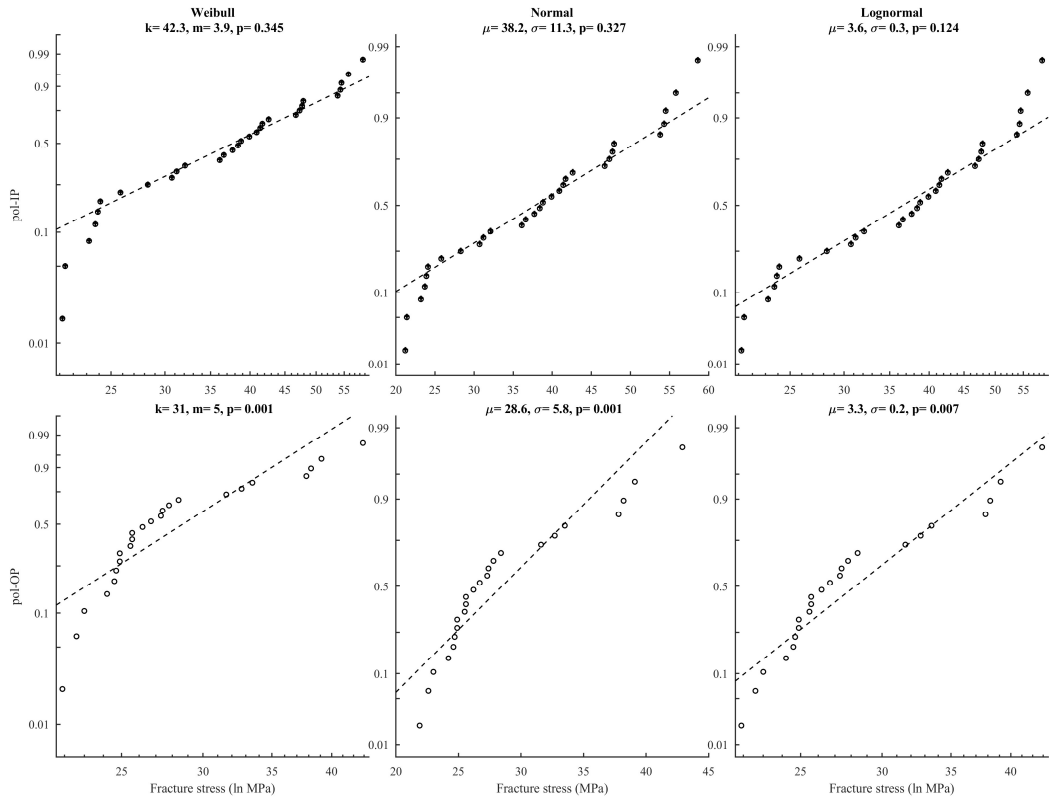


Fig. 33 Probability plots of the data sets in Veer et al. (2009).

SURVEY OF EXPERIMENTAL DATA ON THE STRENGTH OF ANNEALED FLOAT GLASS
Consuelo-Huerta et al. (2011)

In a conference article from 2011 following the proceedings of the Glass Processing Days, Maria Consuelo-Huerta and co-workers published the results from two series of tests, one of them was conducted with the four-point bending device and the other was conducted with the double ring bending device. The details regarding the specimen dimensions, loading rates, and so forth, are given in Tab. 15. Garcia-Prieto (2001) was cited as the source of the test results using the four-point bending device while Postigo (2010) was cited as the source of the results using the double ring bending device. However, upon acquiring a copy of Garcia-Prieto (2001), this author was unable to locate the original data in that reference (a PhD thesis). This author was unable to obtain a copy of Postigo (2010). Nevertheless, the experiments were detailed well enough by Consuelo-Huerta and co-workers. In the case of the specimens subjected to four-point bending, it was not recorded whether the fracture originated with the edge or the surface area of the glass. The load-durations for the two samples can be calculated to be approximately 47 secs to 1 min and 11 secs, and 15 secs to 1 min and 2 secs, respectively. Fig. 34 shows a set of boxplots for the data samples both in the case of the nominal fracture stress values and in the case of the stress rate-equivalent values. Figs. 35 and 36 show a set of probability plots for each data sample. The data results were extracted from the digitized graphs by this author.

Table 15: Details from the experiments reported of in Consuelo-Huerta et al. (2011). 4PB=Four-point bending, OP=Out-of-plane, CDR=Coaxial double ring.

Sample ID	No. of spec's	Bending mode	Dimensions (mm ³)	Edge proc.	Load. span/Load. ring diam. (mm)	Stress rate (MPa s ⁻¹)
4PB	25	4PB OP	10x100x300	Unknown	150	1
CDR	41	CDR	5x300x300	Unknown	180	2.4

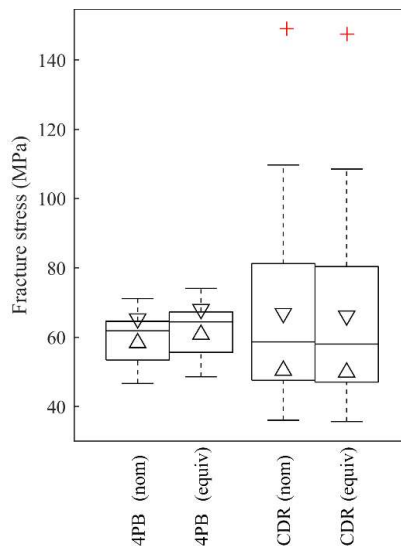


Fig. 34 Boxplot of the nominal and stress-rate equivalent fracture stress values according to the four-point bending experiment (Garcia-Prieto 2001) and the double ring bending experiment (Postigo 2010) as reported by Consuelo-Huerta et al. (2011).

SURVEY OF EXPERIMENTAL DATA ON THE STRENGTH OF ANNEALED FLOAT GLASS

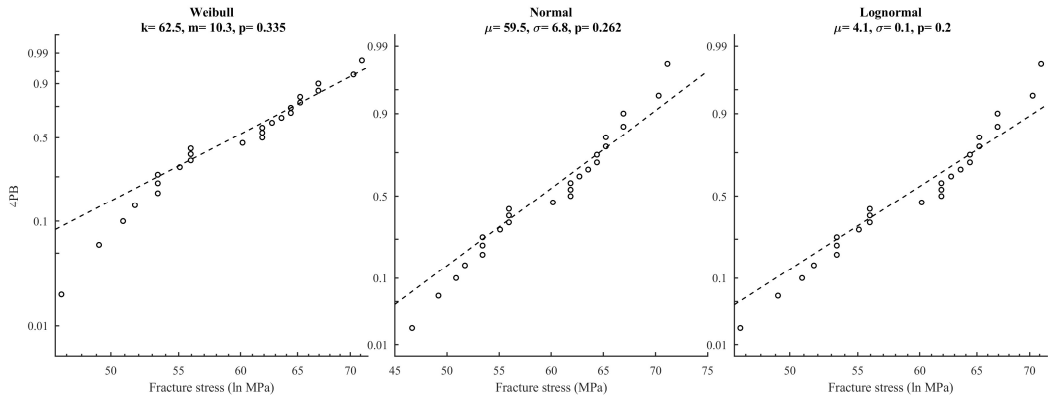


Fig. 35 Probability plots including estimated parameter values for the four-point bending experiment (Garcia-Prieto 2001) as reported by Consuelo-Huerta et al. (2011).

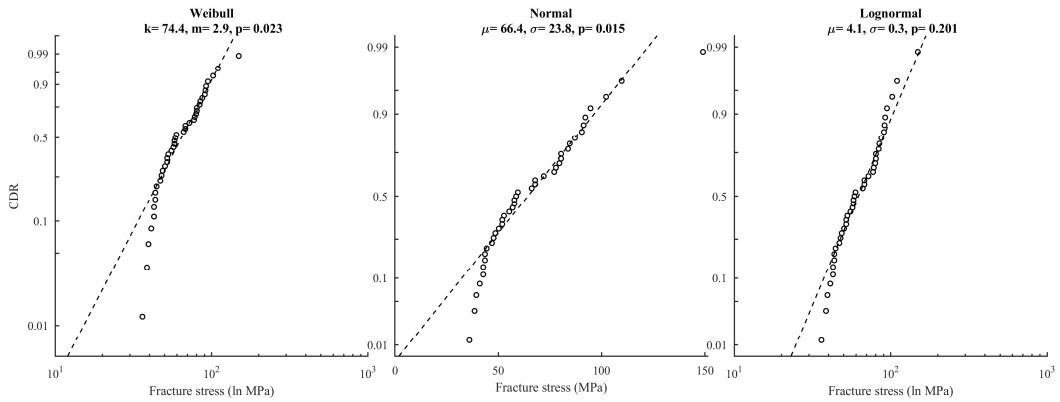


Fig. 36 Probability plots including estimated parameter values for the double ring bending experiment (Postigo 2010) as reported by Consuelo-Huerta et al. (2011).

SURVEY OF EXPERIMENTAL DATA ON THE STRENGTH OF ANNEALED FLOAT GLASS
Veer and Rodichev (2011)

The experiment was conducted with a four-point bending arrangement under displacement control using a Zwick Z100 universal testing machine. The load and support span were 175 mm and 350 mm, respectively. The specimens were cut from a single jumbo pane with the thickness 6 mm using an automated cutting table. The specimen dimensions were 50x400 mm². The edge condition was as-cut. Some of the specimens were subjected to in-plane loading whereas others were subjected to out-of-plane loading generating an approximate stress rate of 2.1 MPa s⁻¹ and 1.3 MPa s⁻¹, respectively. The in-plane loaded specimens were mounted in the test rig with frictionless anti-buckling supports. Half of the out-of-plane loaded specimens were mounted with the mechanically scribed edge placed in the compression zone and half were positioned with the scribed edge in the tension zone. It was not recorded which of the tin side and air side that was placed in the tension zone. The specimens were wrapped in self-adhesive foil. The temperature and relative humidity during testing was not specified but it can be assumed that an indoor environment represents the climatic conditions. The tests were carried out in a single week. The range of load-duration was approximately 15 sec to 1 min and 18 sec. The fracture origin mode, i.e. edge or surface, was recorded. Fractures that initiated from outside the load span were noted when occurring. A summary of details on the experiment is given in Tab. 16. In Fig. 37, a set of boxplots depict the fracture stress characteristics for the nominal strength data as well as the stress rate-equivalent data. A set of three probability plots for each sample is shown in Fig. 38 including the respective maximum-likelihood parameter estimates and the Anderson-Darling goodness-of-fit statistic.

Table 16: Details on the experiment as reported by Veer and Rodichev (2011). Legend: 4PB=Four-point bending, OP=Out-of-plane.

Sample ID	No. of spec's	Bending mode	Dimensions (mm ³)	Edge condition	Load. span (mm)	Stress rate (MPa s ⁻¹)
cut-IP.1	44	4PB IP	6x50x400	As-cut	175	2.9
cut-IP.2	44	4PB IP	6x50x400	As-cut	175	2.9
cut-OP.1	50	4PB OP	6x50x400	As-cut	175	1.8
cut-OP.2	39	4PB OP	6x50x400	As-cut	175	1.8

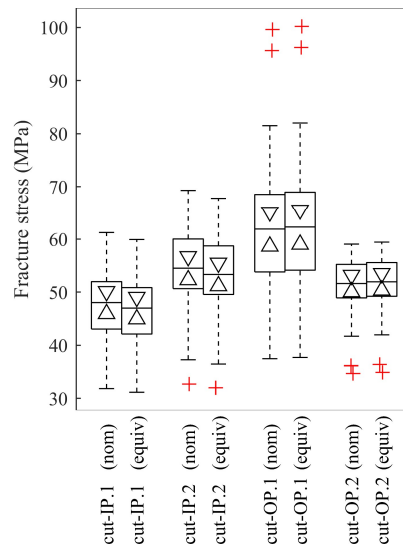


Fig. 37 Boxplots of the (left) nominal and (right) stress rate-equivalent fracture stress values for each data sample in Veer and Rodichev (2011).

SURVEY OF EXPERIMENTAL DATA ON THE STRENGTH OF ANNEALED FLOAT GLASS

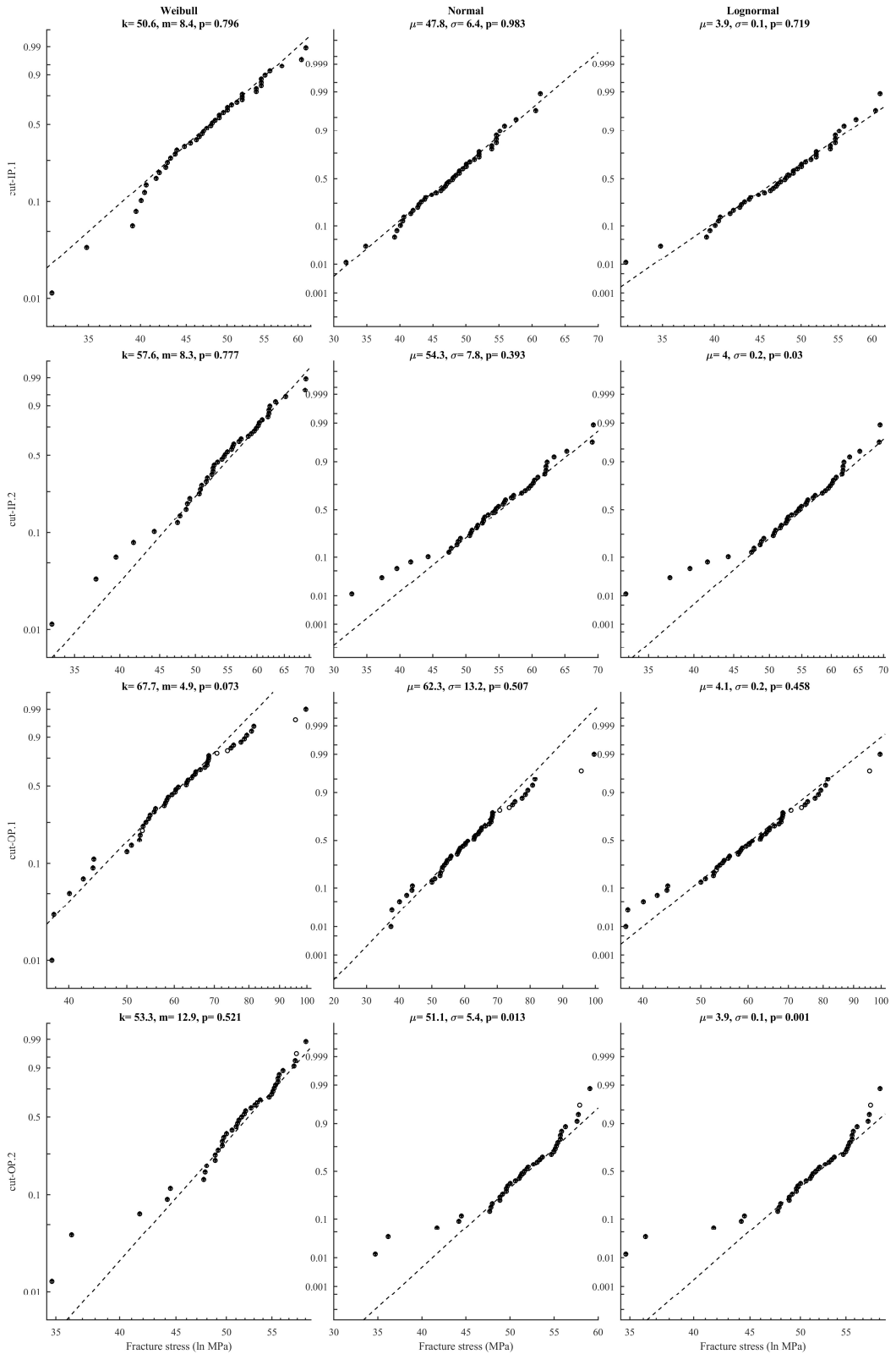


Fig. 38 Probability plots for the data samples in Veer and Rodichev (2011).

Veer and Rodichev (2012)

The experiment was conducted with a four-point bending arrangement under displacement control using a Zwick Z100 universal testing machine. The load and support span were 190 mm and 380 mm, respectively. The specimens were cut from panes with the thickness 6 mm using a water-jet cutting machine. The specimen dimensions were 40x400 mm². The water-jet cutting line was new and was optimized prior to the processing of the specimens. The specimens were subjected to out-of-plane loading generating an approximate stress rate of 1.1 MPa s⁻¹. Half of the specimens were mounted with the water-jet cut face placed in the compression zone (cut face up) and half were positioned with the cut edge in the tension zone (cut face down). It was not recorded which of the tin side and air side that was placed in the tension zone. The specimens were wrapped in self-adhesive foil. The temperature and relative humidity during testing was not specified but it can be assumed that an indoor environment represents the climatic conditions. The tests were carried out in a single day. The range of load-duration was approximately 20 sec to 33 sec according to calculations. The fracture origin mode, i.e. edge or surface, was recorded. The fractured specimens were inspected with respect to the breakage occurring between the load span. A summary of details on the experiment is given in Tab. 17. In Fig. 39, a set of boxplots depict the fracture stress characteristics for the nominal strength data as well as the stress rate-equivalent data. A set of three probability plots for each sample is shown in Fig. 40 including the respective maximum-likelihood parameter estimates and the Anderson-Darling goodness-of-fit statistic.

Table 17: Details on the experiment as reported by Veer and Rodichev (2012). Legend: 4PB=Four-point bending, OP=Out-of-plane.

Sample ID	No. of spec's	Bending mode	Dimensions (mm ³)	Edge condition	Load span (mm)	Stress rate (MPa s ⁻¹)
cut-up	30	4PB IP	6x40x400	As-cut	190	1.5
cut-down	30	4PB IP	6x40x400	As-cut	190	1.5

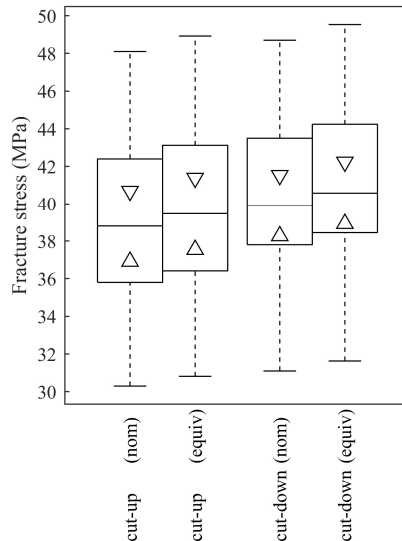


Fig. 39 Boxplots of the (left) nominal and (right) stress rate-equivalent fracture stress values for each data sample in Veer and Rodichev (2012).

SURVEY OF EXPERIMENTAL DATA ON THE STRENGTH OF ANNEALED FLOAT GLASS

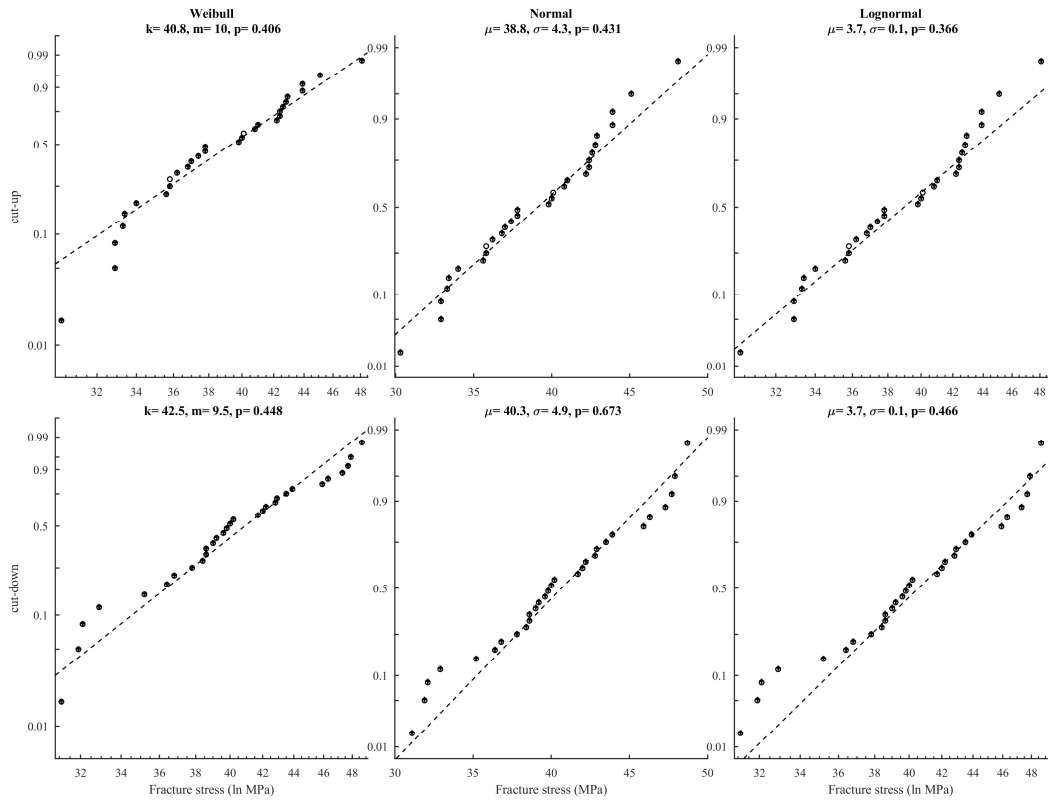


Fig. 40 Probability plots for the data samples in Veer and Rodichev (2012).

SURVEY OF EXPERIMENTAL DATA ON THE STRENGTH OF ANNEALED FLOAT GLASS
Vandebroek et al. (2012)

The experiment was conducted with a four-point bending arrangement using a universal UTS testing machine. The load and support span were 250 mm and 500 mm, respectively. The specimens were cut from panes with the thickness 4 mm. The specimen dimensions were 50x550 mm². Two types of edge condition were included, viz. the as-cut edge and the polished edge. The specimens were subjected to in-plane loading generating an approximate stress rate of 55 MPa s⁻¹ and 0.55 MPa s⁻¹, respectively. The temperature and relative humidity during testing was not specified but it can be assumed that an indoor environment represents the climatic conditions. The specimens that fractured outside the load span were identified and excluded from the analysis. The range of load-duration was approximately 1 sec to 2 min and 26 sec. A summary of details on the experiment is given in Tab. 18. In Fig. 41, a set of boxplots depict the fracture stress characteristics for the nominal strength data as well as the stress rate-equivalent data. A set of three probability plots for each sample is shown in Fig. 42 including the respective maximum-likelihood parameter estimates and the Anderson-Darling goodness-of-fit statistic.

Table 18: Details on the experiment as reported by Vandebroek et al. (2012). Legend: 4PB=Four-point bending, OP=Out-of-plane.

Sample ID	No. of spec's	Bending mode	Dimensions (mm ²)	Edge condition	Load. span (mm)	Stress rate (MPa s ⁻¹)
pol-High	20	4PB IP	4x50x550	Polished	250	55
cut-High	19	4PB IP	4x50x550	As-cut	250	55
pol-Low	19	4PB IP	4x50x550	Polished	250	0.55
cut-Low	19	4PB IP	4x50x550	As-cut	250	0.55

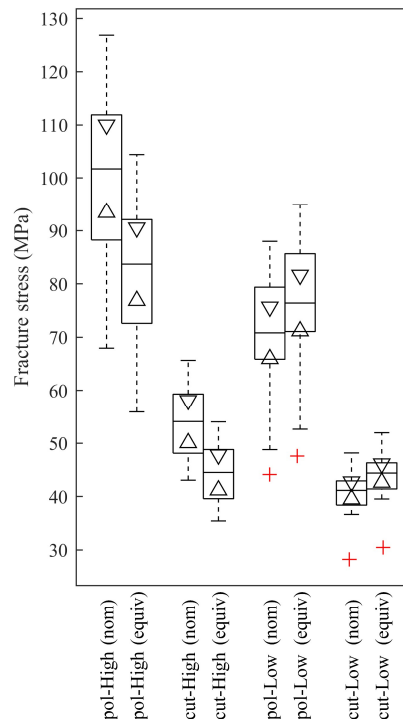


Fig. 41 Boxplots of the (left) nominal and (right) stress rate-equivalent fracture stress values for each data sample in Vandebroek et al. (2012).

SURVEY OF EXPERIMENTAL DATA ON THE STRENGTH OF ANNEALED FLOAT GLASS

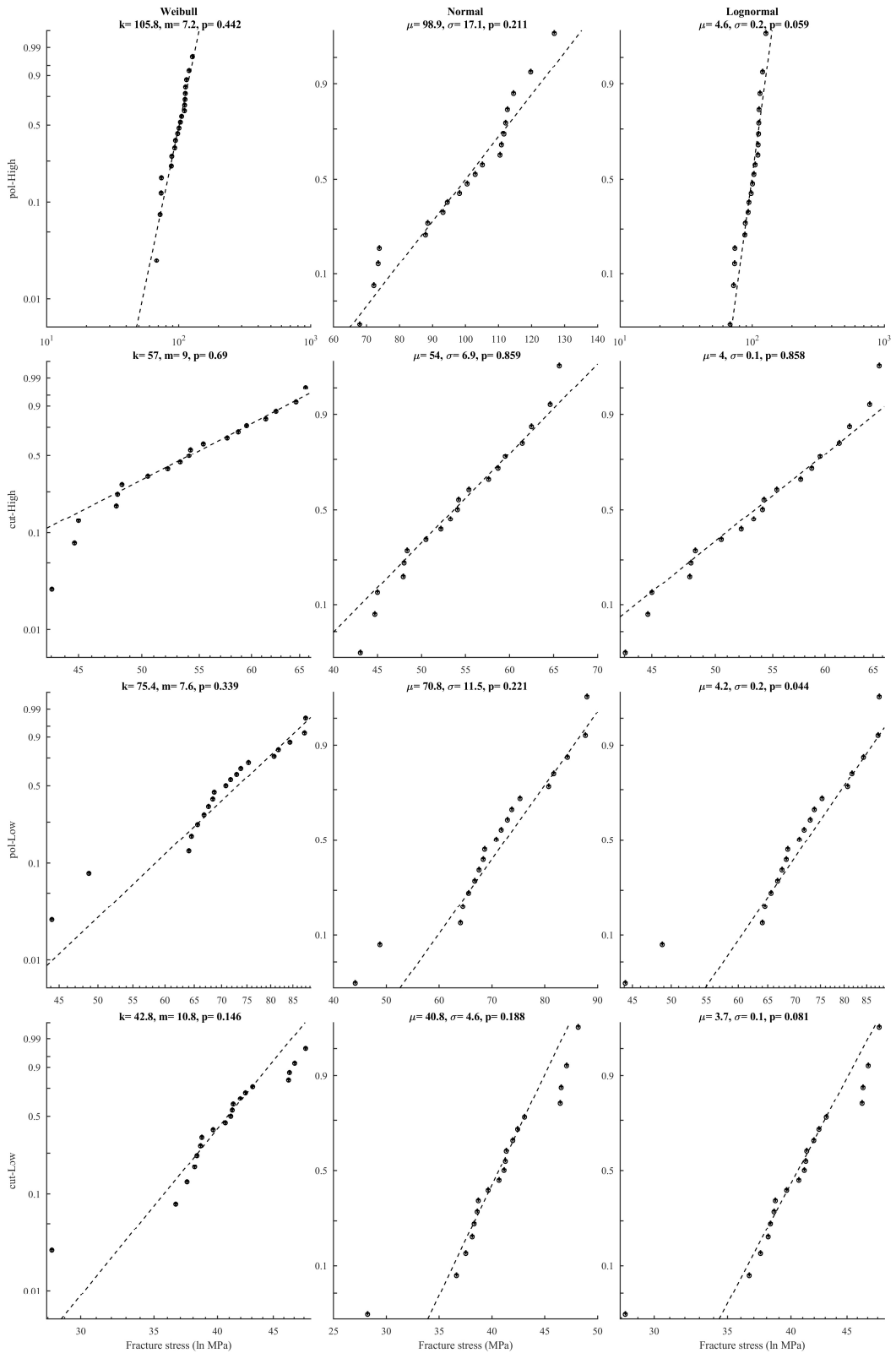


Fig. 42 Probability plots for the data samples in Vandebroek et al. (2012).

Lindqvist (2013)

The experiment was conducted with a four-point bending arrangement using a UTS test system and an Instron 5948 MicroTester. In most cases the testing was performed under displacement control or else under force control. The load span varied from 40 mm to 50 mm while the support span was maintained at 100 mm. The glass was obtained from seven different suppliers in total. The specimens were cut from panes with the nominal thickness 4 mm and 8 mm. The specimens were cut out manually or with a water-cutting machine to the approximate dimensions 10x110 mm². Five types of edge condition were included, viz. the as-cut edge, the arrised edge, the ground edge, the polished edge, and the water-jet cut edge. The specimens were subjected to in-plane loading, the generated stress rate ranging from low, i.e. 0.1 MPa s⁻¹ to 2 MPa s⁻¹, to high, i.e. 15 MPa s⁻¹ to 55 MPa s⁻¹. However, the stress rate could not be accurately determined in some cases. This is reflected in Fig. 43 below where a number of stress rate-equivalent data samples could not be computed and displayed. The surfaces of the glass (edges excluded) were covered in a transparent and highly plastic tape. The temperature ranged between 18-23 °C while the relative humidity was between 23-69%. The range of load-duration was approximately 1 sec to 8 min and 57 sec according to calculations. A summary of details on the experiment is given in Tab. 19. The dimensional measurements and stress rates given in Tab. 19 represent the mean values. In Fig. 43, a set of boxplots depict the fracture stress characteristics for the nominal strength data as well as the stress rate-equivalent data. A set of three probability plots for each sample is shown in Figs. 44 to 47 including the respective maximum-likelihood parameter estimates and the Anderson-Darling goodness-of-fit statistic.

SURVEY OF EXPERIMENTAL DATA ON THE STRENGTH OF ANNEALED FLOAT GLASS

Table 19: Details on the experiment as reported by Lindqvist (2013). Legend: 4PB=Four-point bending, IP=In-plane, H=High stress rate, L=Low stress rate.

Sample ID	No. of spec's	Bending mode	Supplier ID	Dimensions (mm ³)	Edge condition	Load. span (mm)	Stress rate (MPa s ⁻¹)
cut-M1.H:4mm	20	4PB IP	M1	3.83x10.20x110	As-cut	40	17.2
cut-M1.L:4mm	20	4PB IP	M1	3.83x10.11x110	As-cut	40	1.4
cut-M2.H:4mm	19	4PB IP	M2	3.78x10.00x110	As-cut	40	18.1
cut-M2.L:4mm	16	4PB IP	M2	3.78x9.97x110	As-cut	40	N/A
cut-M3.H:4mm	17	4PB IP	M3	3.86x12.75x110	As-cut	50	49.3
cut-M3.L:4mm	19	4PB IP	M3	3.85x12.65x110	As-cut	50	2.0
cut-M4.H:4mm	20	4PB IP	M4	3.83x12.41x110	As-cut	50	53.3
cut-M4.L:4mm	20	4PB IP	M4	3.84x12.33x110	As-cut	50	2.1
arr-M4.H:4mm	20	4PB IP	M4	3.82x12.40x110	Arrised	50	49.3
arr-M4.L:4mm	24	4PB IP	M4	3.83x12.29x110	Arrised	50	2.0
arr-M5.H:4mm	20	4PB IP	M5	3.74x12.13x110	Arrised	50	49.5
arr-M5.L:4mm	26	4PB IP	M5	3.74x12.15x110	Arrised	50	2.0
gro-M3.H:4mm	16	4PB IP	M3	3.80x12.13x110	Ground	50	50.3
gro-M3.L:4mm	21	4PB IP	M3	3.82x12.17x110	Ground	50	2.0
gro-M5.H:4mm	11	4PB IP	M5	3.80x12.24x110	Ground	50	50.0
gro-M5.L:4mm	23	4PB IP	M5	3.79x12.24x110	Ground	50	2.0
gro-M6.H:4mm	16	4PB IP	M6	3.82x12.19x110	Ground	50	48.6
gro-M6.L:4mm	23	4PB IP	M6	3.82x12.09x110	Ground	50	2.0
wat-M7.H:4mm	20	4PB IP	M7	3.82x10.44x110	Water-cut	40	20.9
wat-M7.L:4mm	19	4PB IP	M7	3.81x10.42x110	Water-cut	40	0.16
pol-M1.H:4mm	37	4PB IP	M1	3.82x9.93x110	Polished	40	20.6
pol-M1.L:4mm	33	4PB IP	M1	3.82x10.04x110	Polished	40	0.15
pol-M2.H:4mm	19	4PB IP	M2	3.78x10.80x110	Polished	40	N/A
pol-M2.L:4mm	20	4PB IP	M2	3.78x10.92x110	Polished	40	N/A
cut-M3.H:8mm	20	4PB IP	M3	7.84x12.00x110	As-cut	50	N/A
cut-M4.H:8mm	21	4PB IP	M4	7.83x12.16x110	As-cut	50	N/A
arr-M4.H:8mm	23	4PB IP	M4	7.83x12.16x110	Arrised	50	N/A
arr-M5.H:8mm	21	4PB IP	M5	7.86x12.64x110	Arrised	50	53.8
arr-M5.L:8mm	22	4PB IP	M5	7.84x12.64x110	Arrised	50	2.2
gro-M3.H:8mm	20	4PB IP	M3	7.86x12.35x110	Ground	50	N/A
gro-M5.H:8mm	18	4PB IP	M5	7.81x12.56x110	Ground	50	N/A
gro-M6.H:8mm	23	4PB IP	M6	7.71x12.32x110	Ground	50	N/A

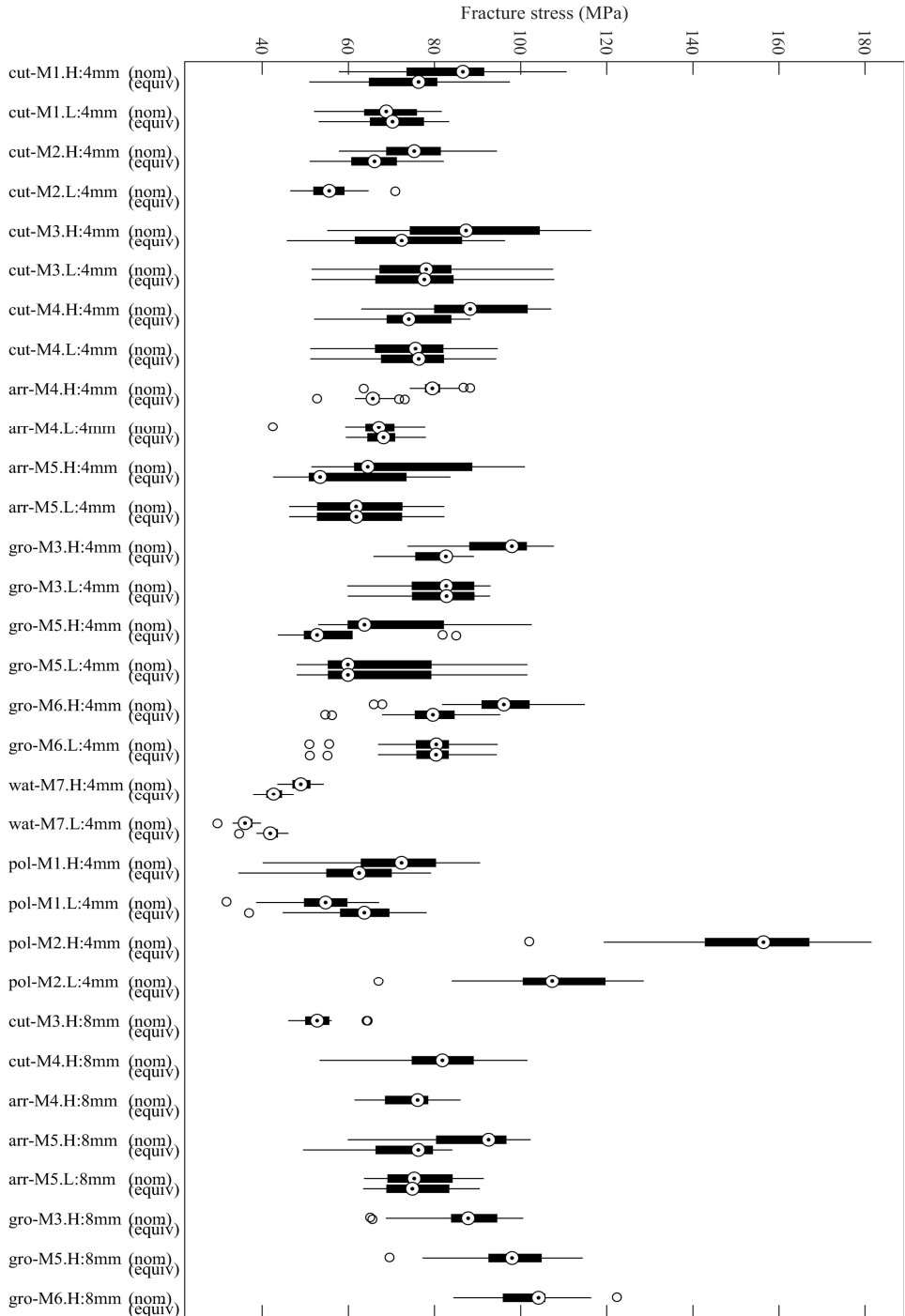


Fig. 43 Boxplots of the nominal and stress rate-equivalent fracture stress values for the data samples in Lindqvist (2013). NB. in some cases the stress rate-equivalent strength was not available in which case only the received (nominal) values are shown.

SURVEY OF EXPERIMENTAL DATA ON THE STRENGTH OF ANNEALED FLOAT GLASS

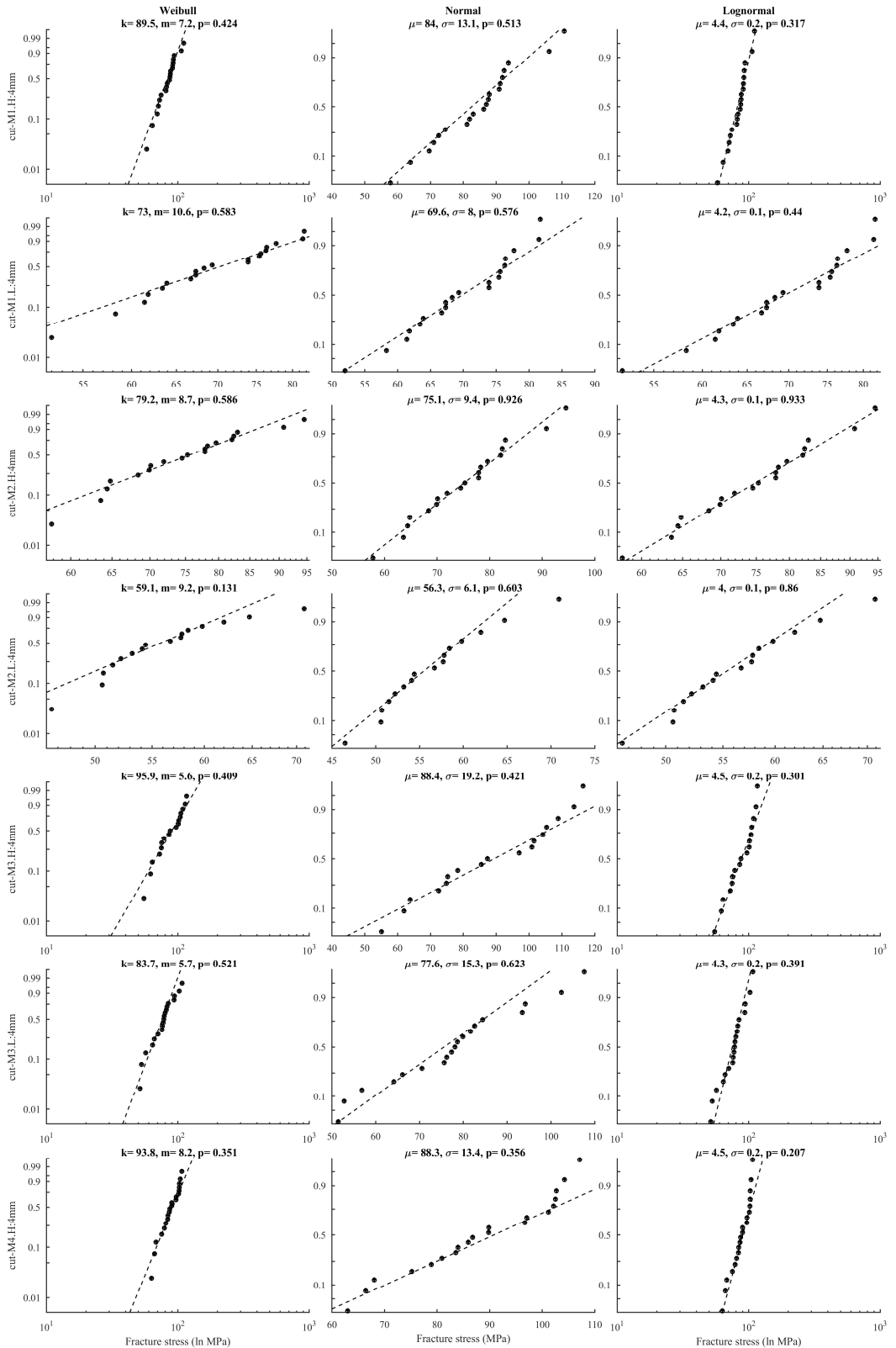


Fig. 44 Probability plots for the data samples in Lindqvist (2013).

SURVEY OF EXPERIMENTAL DATA ON THE STRENGTH OF ANNEALED FLOAT GLASS

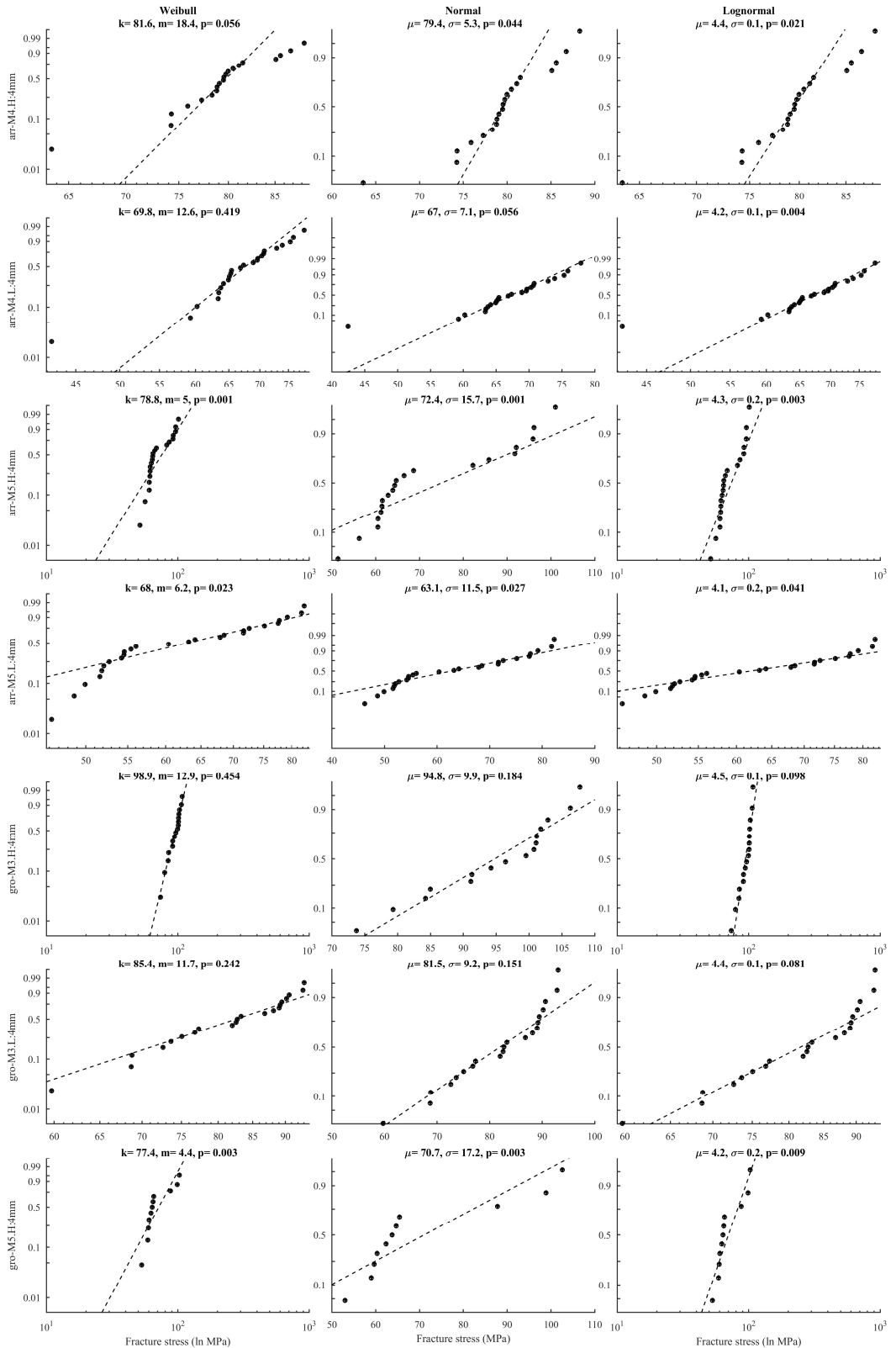


Fig. 45 Probability plots for the data samples in Lindqvist (2013).

SURVEY OF EXPERIMENTAL DATA ON THE STRENGTH OF ANNEALED FLOAT GLASS

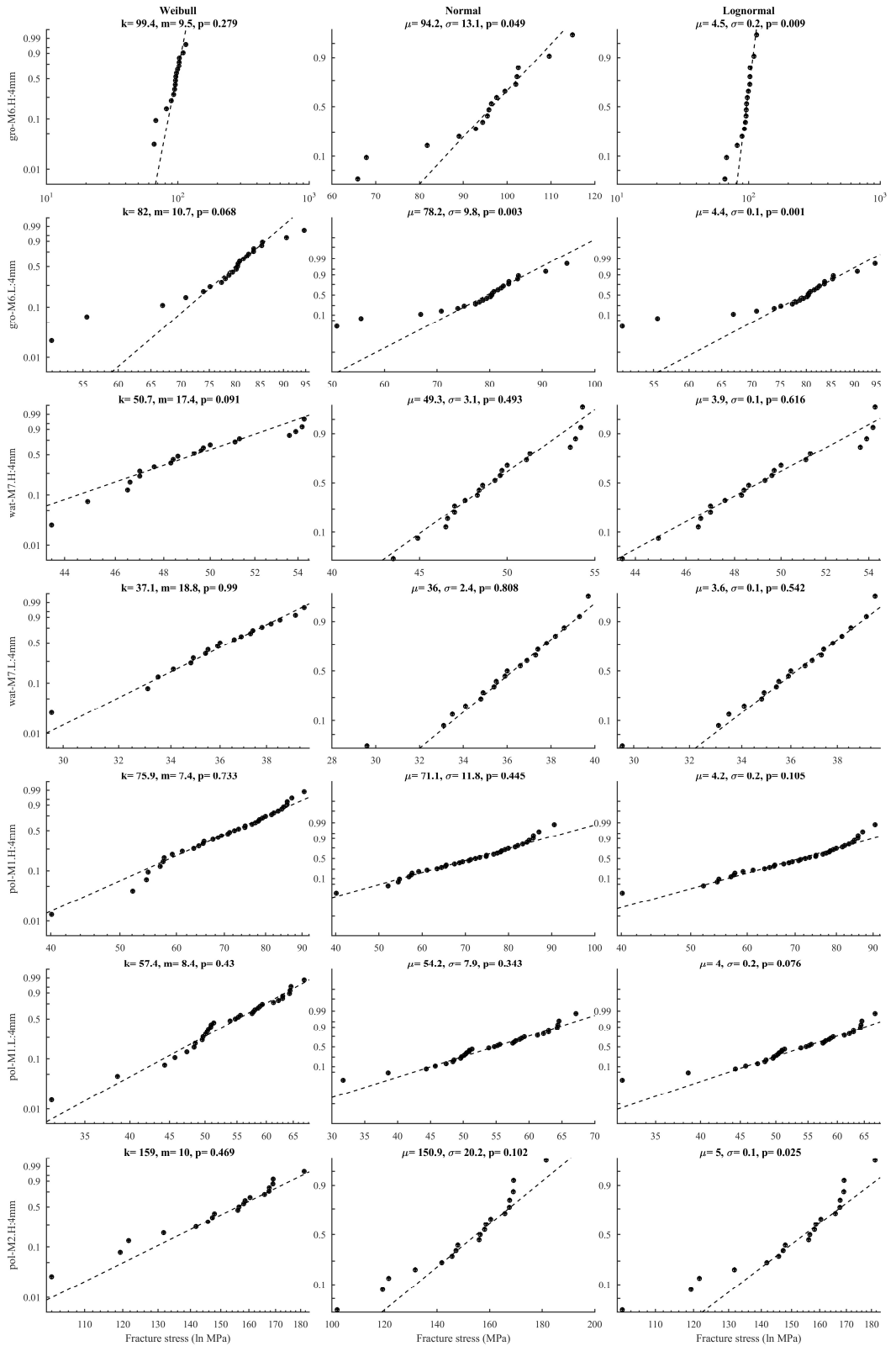


Fig. 46 Probability plots for the data samples in Lindqvist (2013).

SURVEY OF EXPERIMENTAL DATA ON THE STRENGTH OF ANNEALED FLOAT GLASS

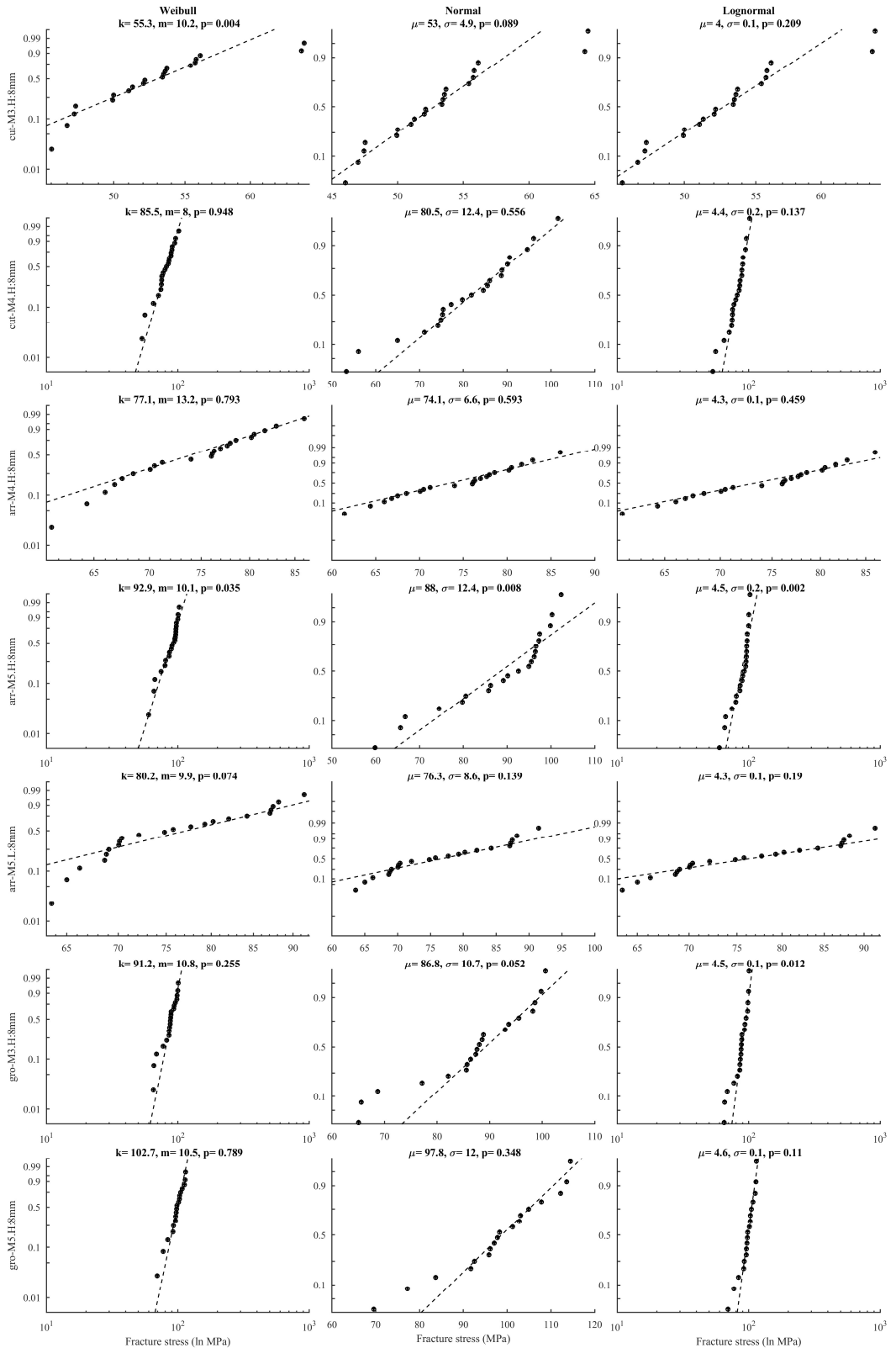


Fig. 47 Probability plots for the data samples in Lindqvist (2013).

*SURVEY OF EXPERIMENTAL DATA ON THE STRENGTH OF ANNEALED FLOAT GLASS
Vandebroek et al. (2014)*

The experiment was conducted with a four-point bending arrangement using an Instron 3369 testing machine. The load and support span were either 250 mm and 500 mm, respectively, or 500 mm and 1000 mm, respectively. The specimens were cut from panes with the thickness 4 mm and 8 mm. The specimen dimensions were 62.5x550 mm² and 125x1100 mm². The edge condition was either as-cut or ground. The machine cutting and grinding was carried out by a qualified glass processor. The scoring of the specimens was consistently performed on the air side. The edge processing took place on the same day with the same machine and with the same processing parameters for each set of glass thickness, i.e. 4 mm and 8 mm, and edge type, i.e. as-cut and ground. At least 30 days elapsed from the processing of the edge until the destructive testing. The specimens were subjected to in-plane loading generating an approximate stress rate of 2 MPa s⁻¹. The specimens were mounted using rubber intermediates at the load and support contact surfaces. Buckling supports with a Teflon interlayer were employed at mid-span. The temperature and relative humidity during testing was about 25 °C and 65%, respectively. The specimens that fractured outside the load span were identified and excluded from the analysis. The range of load-duration was approximately 14 sec to 33 sec according to calculations. A summary of details on the experiment is given in Tab. 20. In Fig. 48, a set of boxplots depict the fracture stress characteristics for the nominal strength data. A set of three probability plots for each sample is shown in Fig. 49 including the respective maximum-likelihood parameter estimates and the Anderson-Darling goodness-of-fit statistic. In the probability plots, all points have been marked as edge failures. However, according to the reference, 13% of the ground and 20% of the cut specimen failures on average were identified as originating with either of the surface sides of the glass. These specimens were not identified in the reference.

Table 20: Details on the experiment as reported by Vandebroek et al. (2014). Legend: 4PB=Four-point bending, OP=Out-of-plane.

Sample ID	No. of spec's	Bending mode	Dimensions (mm ³)	Edge condition	Load. span (mm)	Stress rate (MPa s ⁻¹)
gro-short:4mm	29	4PB IP	4x62.5x550	Ground	250	2
gro-long:4mm	26	4PB IP	4x125x1100	Ground	500	2
gro-short:8mm	27	4PB IP	8x62.5x550	Ground	250	2
gro-long:8mm	28	4PB IP	8x125x1100	Ground	500	2
cut-short:4mm	24	4PB IP	4x62.5x550	As-cut	250	2
cut-long:4mm	20	4PB IP	4x125x1100	As-cut	500	2
cut-short:8mm	27	4PB IP	8x62.5x550	As-cut	250	2
cut-long:8mm	21	4PB IP	8x125x1100	As-cut	500	2

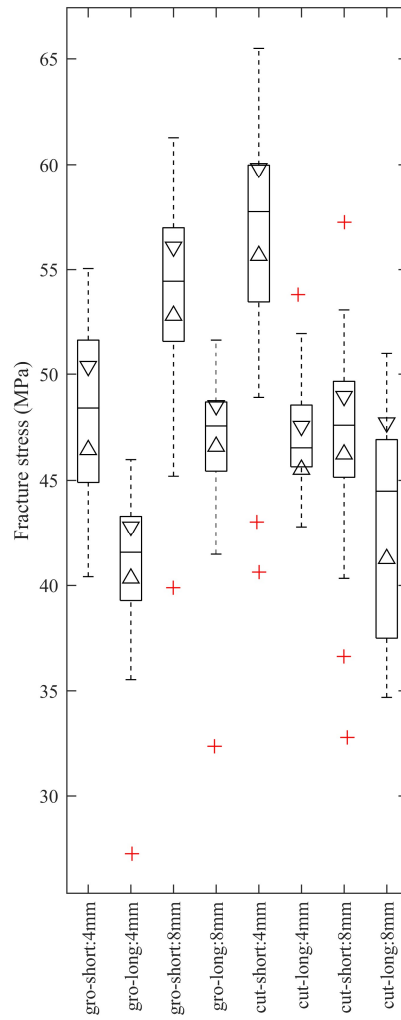


Fig. 48 Boxplots of the fracture stress values for each data sample in Vandebroek et al. (2014).

SURVEY OF EXPERIMENTAL DATA ON THE STRENGTH OF ANNEALED FLOAT GLASS

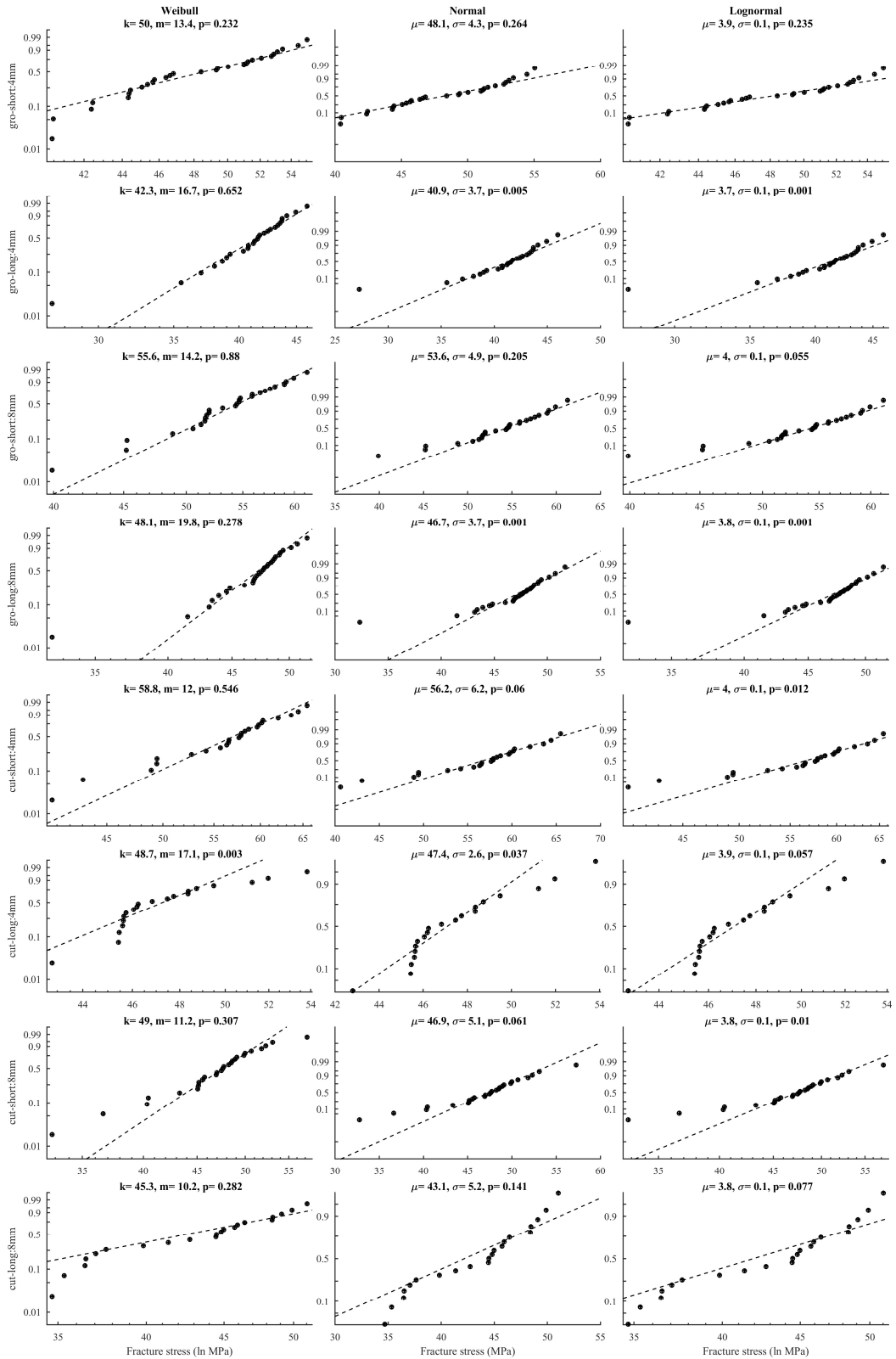


Fig. 49 Probability plots for the data samples in Vandebroek et al. (2014).

Kozłowski (2014)

The experiment was conducted with a four-point bending arrangement under displacement control. The load and support span were 500 mm and 1500 mm, respectively. The specimens were cut from panes with the thickness 8 mm. The specimen dimensions were 200x1800 mm². The edge was machine ground and polished. The specimens were subjected to in-plane loading generating an approximate stress rate of 0.3 MPa s⁻¹. The specimens were mounted into the test rig using rubber pads applied at the steel roll contact surfaces at the supports and load introduction points. Two lateral supports were employed at a distance of about 100 mm from the load introduction points. The temperature and relative humidity during testing was not specified but it can be assumed that an indoor environment represents the climatic conditions. The range of load-duration was approximately 2 min and 6 sec to 3 min and 37 sec according to calculations. A summary of details on the experiment is given in Tab. 21. In Fig. 50, a set of boxplots depict the fracture stress characteristics for the nominal strength data as well as the stress rate-equivalent data.

Table 21: Details on the experiment as reported by Kozłowski (2014). Legend: 4PB=Four-point bending, IP=In-plane.

Sample ID	No. of spec's	Bending mode	Dimensions (mm ³)	Edge condition	Load. span (mm)	Stress rate (MPa s ⁻¹)
pol:8mm	6	4PB IP	8x200x1800	Polished	500	0.3

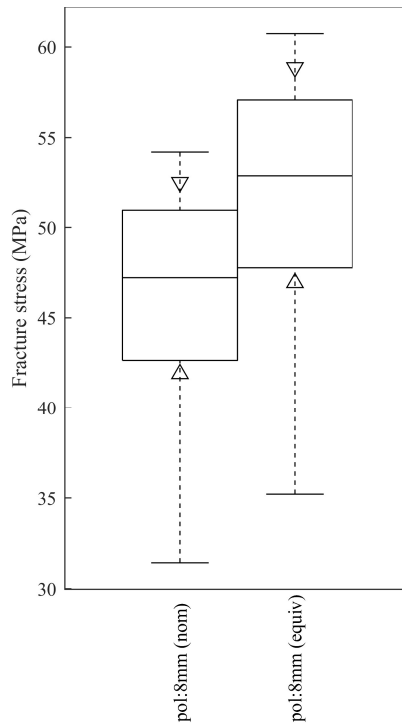


Fig. 50 Boxplots of the fracture stress values in Kozłowski (2014).

Kleuderlein et al. (2014)

The experiment was conducted with a four-point bending arrangement. The load and support span were 200 mm and 1090 mm, respectively. The specimens were cut from panes with the thickness 4 mm, 6 mm, and 8 mm. The glass was obtained from six different suppliers in total. The specimen dimensions were 125x1100 mm². The edge condition was either as-cut, arried, or ground. The glass manufacturers processed the edges with their usual settings of production parameters. All arrising, grinding, and polishing operations were done by machine. However, the production methods differed between the suppliers. For instance, edging machines with cup wheels were used by half of the manufacturers to arrise the edges while belt edging machines with manual feed were used by the others. Nevertheless, a cup wheel edging machine was used by all manufacturers for the grinding operation. The specimens were subjected to in-plane loading generating an approximate stress rate of 2 MPa s⁻¹. The specimens were mounted with four synthetic-coated lateral supports to prevent from tilting. The temperature and relative humidity during testing was not specified but it can be assumed that an indoor environment represents the climatic conditions. Only the specimens that fractured within the load span were considered. The range of load-duration was approximately 17 sec to 45 sec according to calculations. A summary of details on the experiment is given in Tab. 22. In Fig. 51, a set of boxplots depict the fracture stress characteristics for the nominal strength data. A set of three probability plots for each sample is shown in Figs. 52 to 55 including the respective maximum-likelihood parameter estimates and the Anderson-Darling goodness-of-fit statistic. The data results were extracted from the digitized graphs by this author.

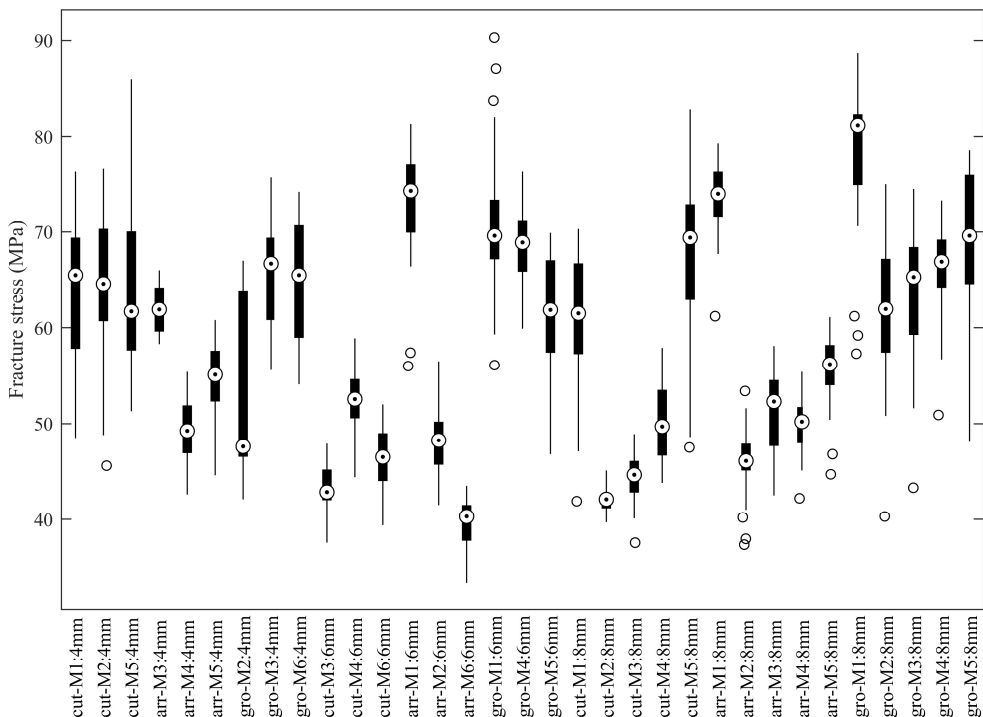


Fig. 51 Boxplots of the nominal fracture stress values for each data sample in Kleuderlein et al. (2014).

SURVEY OF EXPERIMENTAL DATA ON THE STRENGTH OF ANNEALED FLOAT GLASS

Table 22: Details on the experiment as reported by Kleuderlein et al. (2014). Legend: 4PB=Four-point bending, IP=In-plane.

Sample ID	No. of spec's	Bending mode	Supplier ID	Dimensions (mm ³)	Edge condition	Load. span (mm)	Stress rate (MPa s ⁻¹)
cut-M1:4mm	18	4PB IP	M1	4x125x1100	Cut	200	2
cut-M2:4mm	19	4PB IP	M2	4x125x1100	Cut	200	2
cut-M5:4mm	17	4PB IP	M5	4x125x1100	Cut	200	2
arr-M3:4mm	22	4PB IP	M3	4x125x1100	Arrised	200	2
arr-M4:4mm	22	4PB IP	M4	4x125x1100	Arrised	200	2
arr-M5:4mm	23	4PB IP	M5	4x125x1100	Arrised	200	2
gro-M2:4mm	23	4PB IP	M2	4x125x1100	Ground	200	2
gro-M3:4mm	26	4PB IP	M3	4x125x1100	Ground	200	2
gro-M6:4mm	24	4PB IP	M6	4x125x1100	Ground	200	2
cut-M3:6mm	28	4PB IP	M3	6x125x1100	Cut	200	2
cut-M4:6mm	20	4PB IP	M4	6x125x1100	Cut	200	2
cut-M6:6mm	22	4PB IP	M6	6x125x1100	Cut	200	2
arr-M1:6mm	19	4PB IP	M1	6x125x1100	Arrised	200	2
arr-M2:6mm	20	4PB IP	M2	6x125x1100	Arrised	200	2
arr-M6:6mm	26	4PB IP	M6	6x125x1100	Arrised	200	2
gro-M1:6mm	27	4PB IP	M1	6x125x1100	Ground	200	2
gro-M4:6mm	24	4PB IP	M4	6x125x1100	Ground	200	2
gro-M5:6mm	24	4PB IP	M5	6x125x1100	Ground	200	2
cut-M1:8mm	19	4PB IP	M1	8x125x1100	Cut	200	2
cut-M2:8mm	27	4PB IP	M2	8x125x1100	Cut	200	2
cut-M3:8mm	20	4PB IP	M3	8x125x1100	Cut	200	2
cut-M4:8mm	21	4PB IP	M4	8x125x1100	Cut	200	2
cut-M5:8mm	46	4PB IP	M5	8x125x1100	Cut	200	2
arr-M1:8mm	26	4PB IP	M1	8x125x1100	Arrised	200	2
arr-M2:8mm	48	4PB IP	M2	8x125x1100	Arrised	200	2
arr-M3:8mm	20	4PB IP	M3	8x125x1100	Arrised	200	2
arr-M4:8mm	23	4PB IP	M4	8x125x1100	Arrised	200	2
arr-M5:8mm	26	4PB IP	M5	8x125x1100	Arrised	200	2
gro-M1:8mm	22	4PB IP	M1	8x125x1100	Ground	200	2
gro-M2:8mm	26	4PB IP	M2	8x125x1100	Ground	200	2
gro-M3:8mm	53	4PB IP	M3	8x125x1100	Ground	200	2
gro-M4:8mm	28	4PB IP	M4	8x125x1100	Ground	200	2
gro-M5:8mm	21	4PB IP	M5	8x125x1100	Ground	200	2

SURVEY OF EXPERIMENTAL DATA ON THE STRENGTH OF ANNEALED FLOAT GLASS

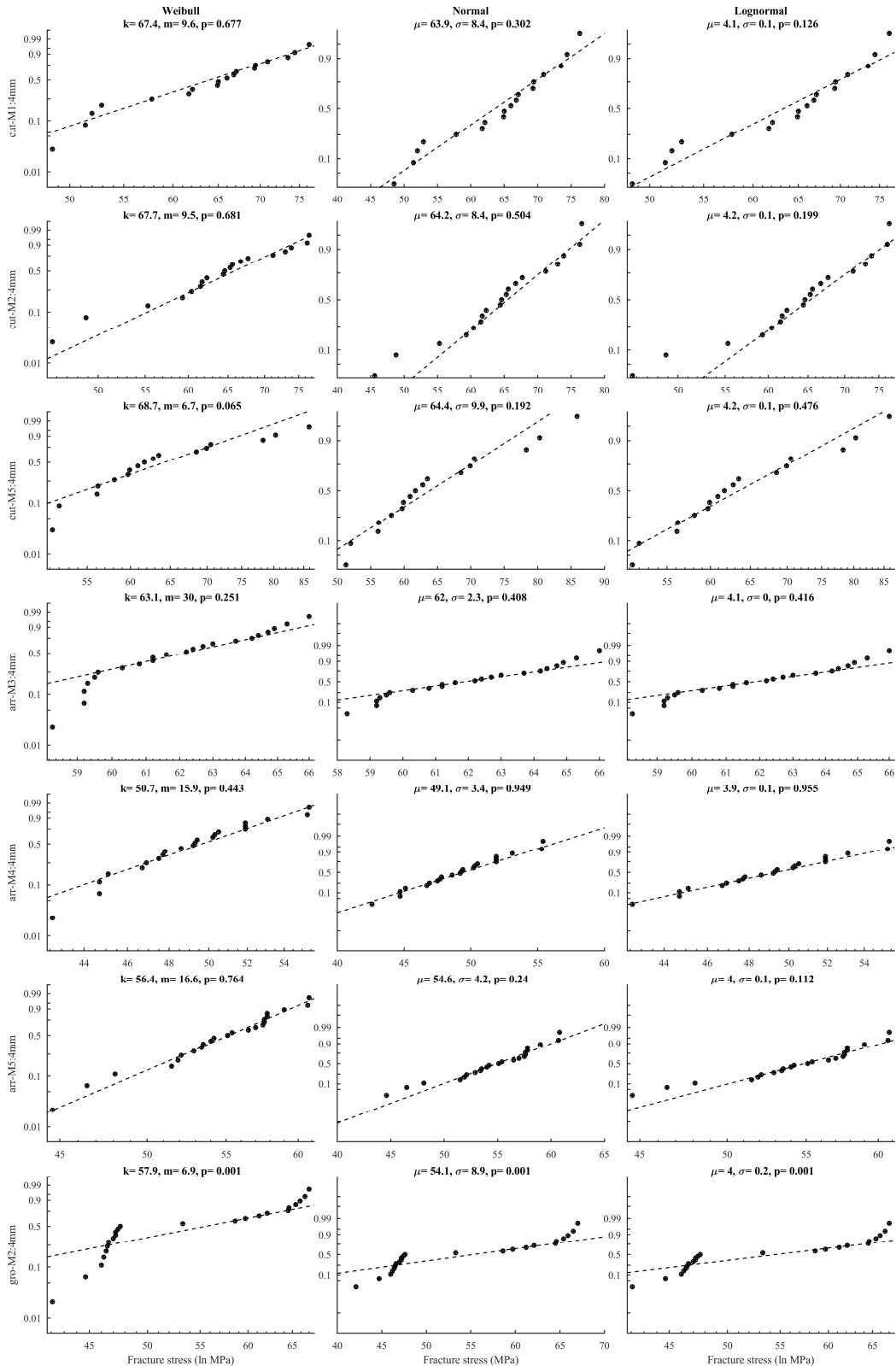


Fig. 52 Probability plots for the data samples in Kleuderlein et al. (2014).

SURVEY OF EXPERIMENTAL DATA ON THE STRENGTH OF ANNEALED FLOAT GLASS

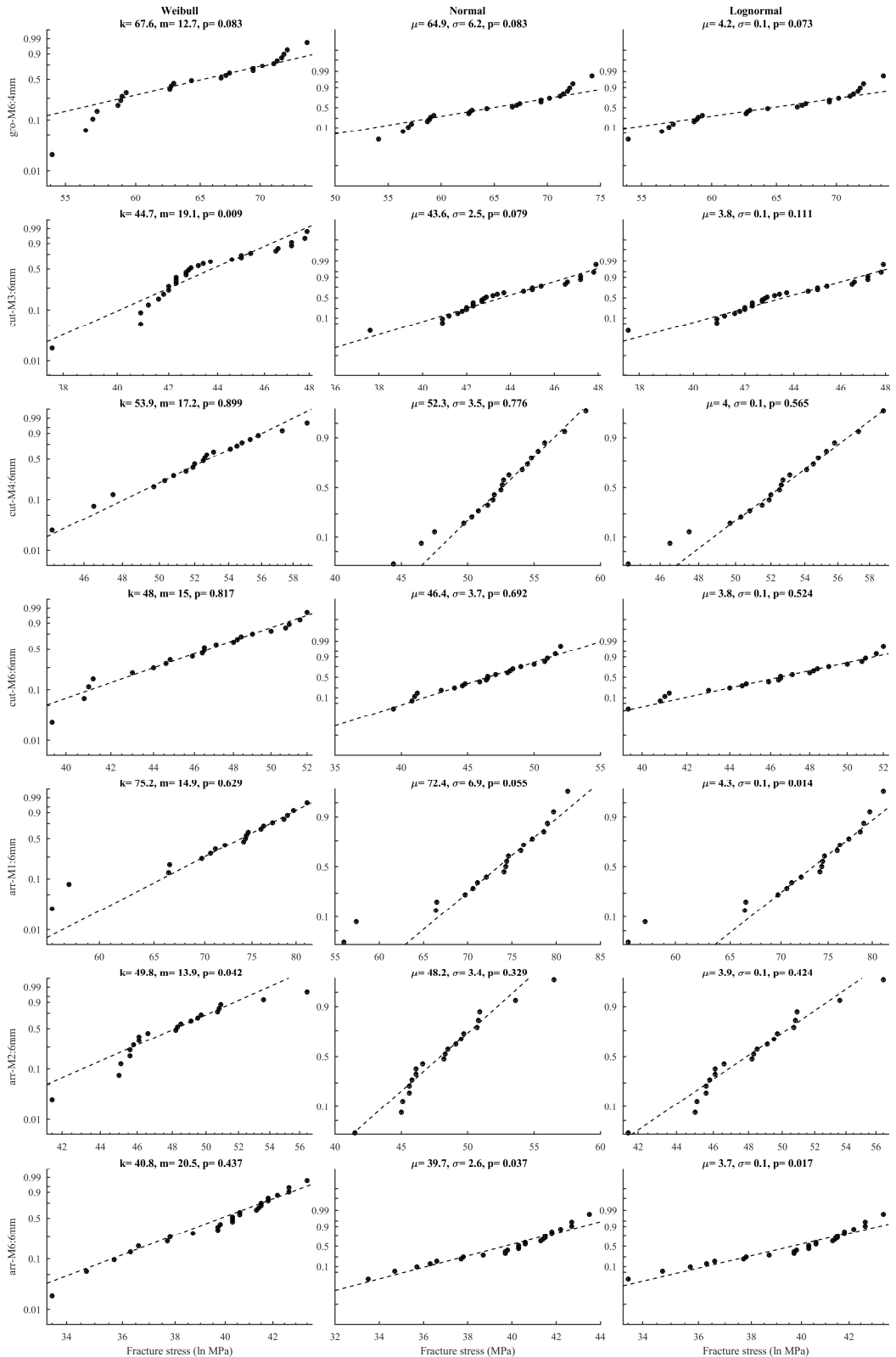


Fig. 53 Probability plots for the data samples in Kleuderlein et al. (2014).

SURVEY OF EXPERIMENTAL DATA ON THE STRENGTH OF ANNEALED FLOAT GLASS

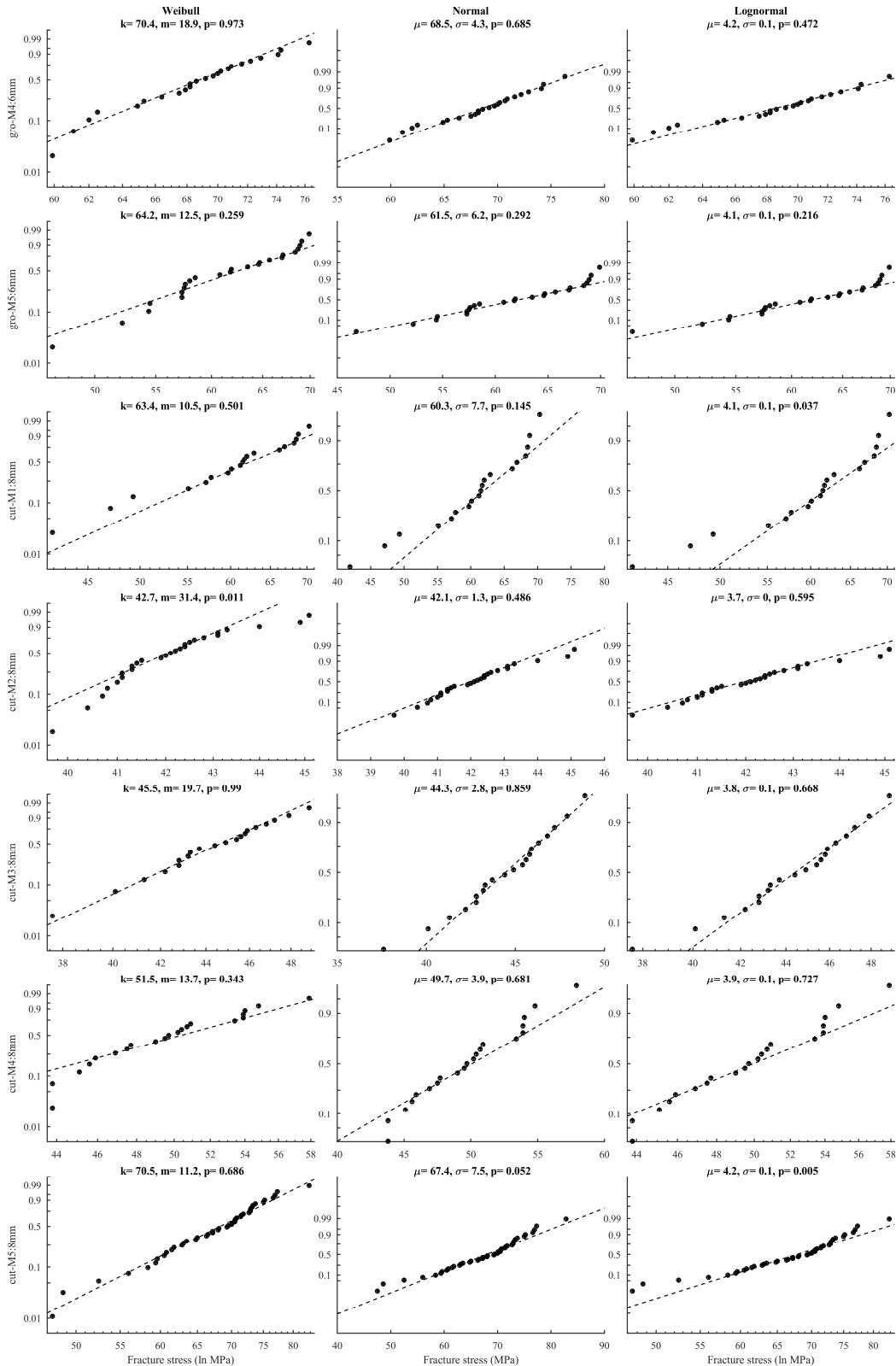


Fig. 54 Probability plots for the data samples in Kleuderlein et al. (2014).

SURVEY OF EXPERIMENTAL DATA ON THE STRENGTH OF ANNEALED FLOAT GLASS

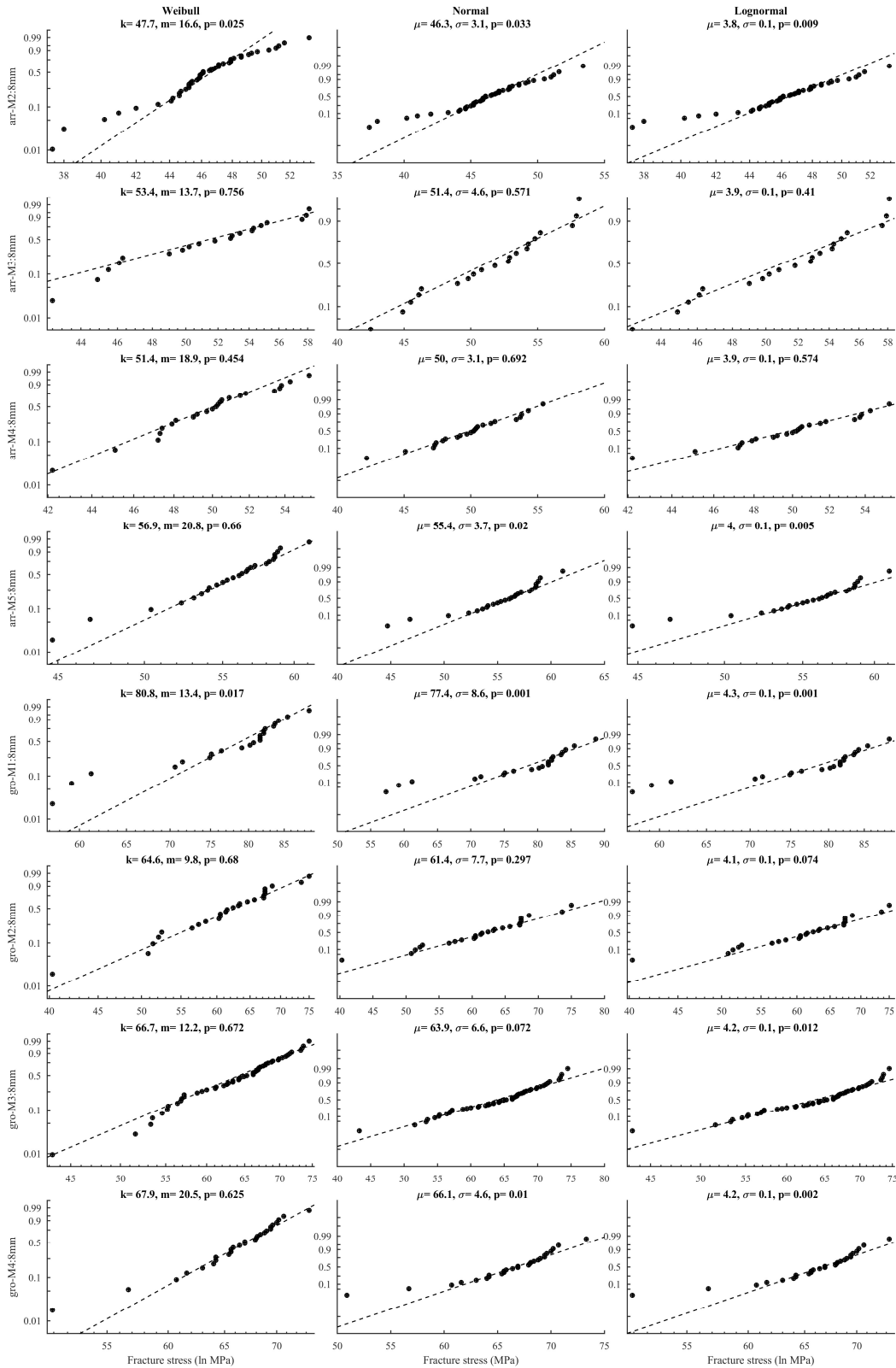


Fig. 55 Probability plots for the data samples in Kleuderlein et al. (2014).

Schula (2015)

The experiment was conducted with a coaxial double ring bending setup using a Zwick Z050 THW Allround-Line testing machine. The loading ring diameter was 80 mm and the support ring diameter was 160 mm. The specimens were cut out from panes with a thickness of 6 mm. The specimen dimensions were 250x250 mm². The specimens were subjected to out-of-plane loading generating a stress rate within the loading ring area of approximately 2 MPa s⁻¹. The tin side of the glass was positioned in the tension zone. The specimens were covered in self-adhesive foil on the compression side. The temperature during testing was 27 °C while the relative humidity was 50%. The time-duration until failure ranged from approximately 25 sec to 51 sec. A summary of details on the experiment is given in Tab. 23. In Fig. 56, a set of boxplots depict the fracture stress characteristics for the nominal strength data. A set of three probability plots for each sample is shown in Fig. 57 including the respective maximum-likelihood parameter estimates and the Anderson-Darling goodness-of-fit statistic.

Table 23: Details from the experiment of Schula (2015). CDR=Coaxial double ring bending.

Sample ID	No. of spec's	Bending mode	Dimensions (mm ³)	Load. ring diameter (mm)	Stress rate (MPa s ⁻¹)
1	15	CDR	6x250x250	80	2.0

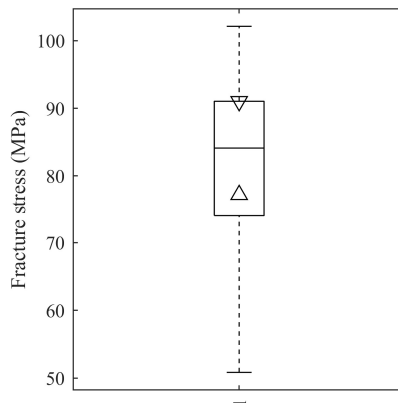


Fig. 56 Boxplots of the nominal fracture stress according to the experimental data in Schula (2015).

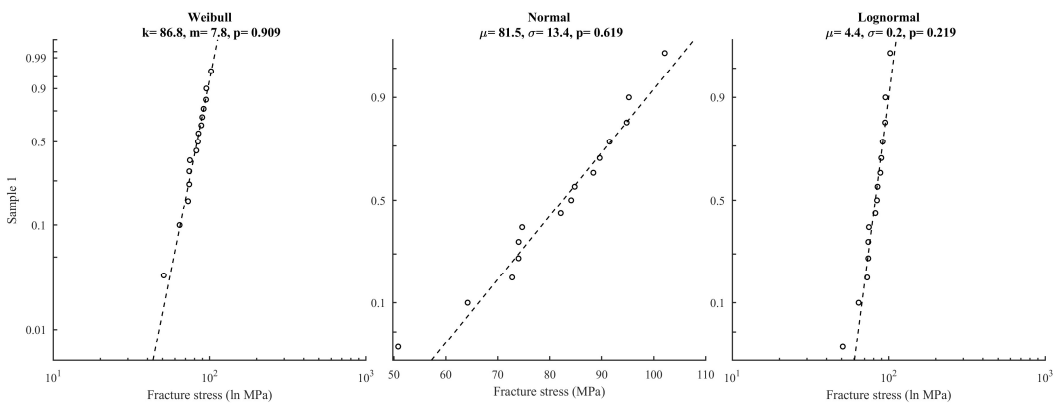


Fig. 57 Probability plots of the data sample in Schula (2015).

Muniz-Calvente et al. (2016)

The experiment was conducted with a coaxial double ring bending device and a four-point bending setup using an MTS Bionix uniaxial 100 kN testing machine. The loading and support ring diameters in the double ring bending test were 60 mm and 160 mm, respectively, whereas the load and support span dimensions in the four-point bending test were 200 mm and 1000 mm, respectively. All specimens in the double ring bending test were cut from the same glass pane with a thickness of 5 mm and all specimens in the four-point bending test were cut from the same pane with the thickness 5 mm. The plates in the double ring bending test measured 250x250 mm² in surface area while the specimens in the four-point bending test measured 360x1100 mm². The type of edge processing was polished according to personal correspondence with one of the authors. All specimens were subjected to out-of-plane loading generating an approximate stress rate of 2 MPa s⁻¹. The type of fracture origin, i.e. edge fracture or surface fracture, in the case of four-point bending was recorded but not detailed in the journal article. The time-duration of loading ranged from approximately 23 secs to 67 secs. A summary of details on the experiment is given in Tab. 24. In Fig. 58, a set of boxplots depict the fracture stress characteristics for the nominal strength data. A set of three probability plots for each sample is shown in Fig. 59 including the respective maximum-likelihood parameter estimates and the Anderson-Darling goodness-of-fit statistic.

Table 24: Details on the experiment as reported by Muniz-Calvente et al. (2016). 4PB=Four-point bending, OP=Out-of-plane, CDR=Coaxial double ring.

Sample ID	No. of spec's	Bending mode	Dimensions (mm ³)	Edge proc.	Load. span/Load. ring diam. (mm)	Stress rate (MPa s ⁻¹)
CDR	28	CDR	5x250x250	Polished	60	2
4PB	30	4PB OP	5x360x1100	Polished	200	2

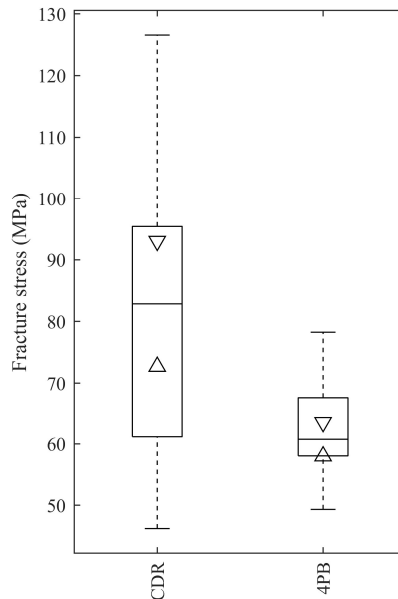


Fig. 58 Boxplots of the nominal fracture stress values in Muniz-Calvente et al. (2016).

SURVEY OF EXPERIMENTAL DATA ON THE STRENGTH OF ANNEALED FLOAT GLASS

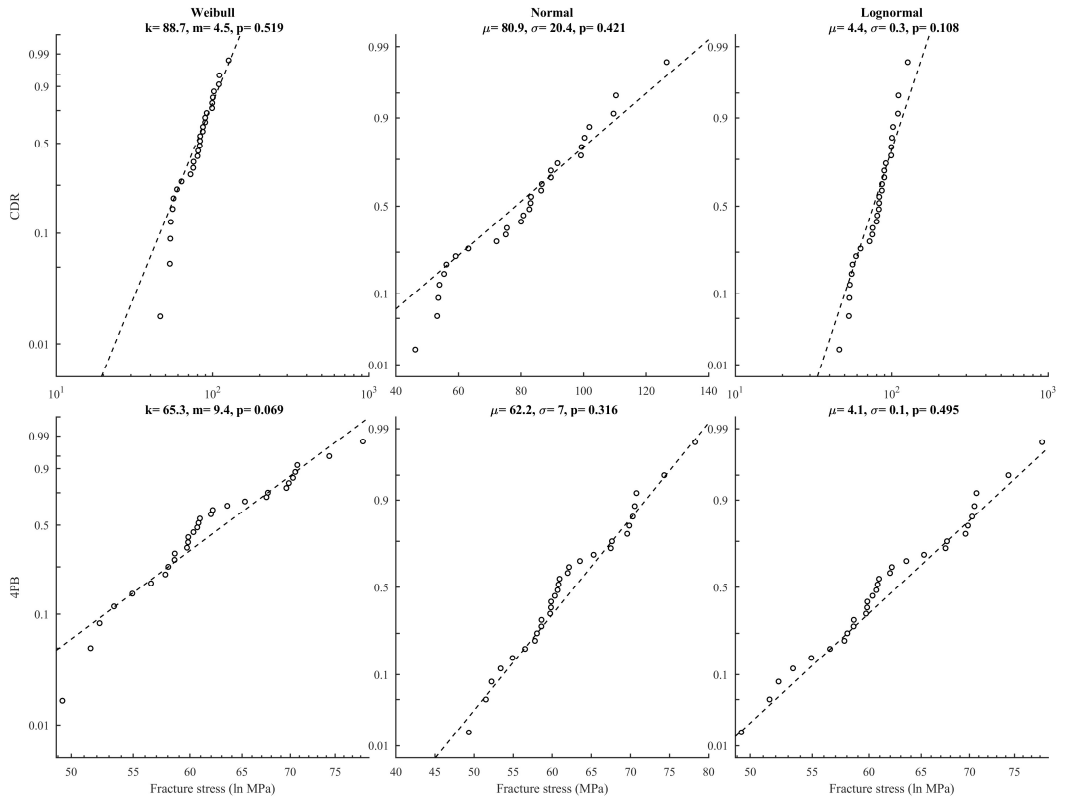


Fig. 59 Probability plots for the data samples in Muniz-Calvente et al. (2016).

SURVEY OF EXPERIMENTAL DATA ON THE STRENGTH OF ANNEALED FLOAT GLASS
Kinsella and Persson (2016)

The experiment was conducted with the four-point bending setup using an MTS 810 universal testing machine under displacement control. Two different load spans were employed, viz. 300 mm and 450 mm. The support span was 900 mm. All specimens were cut out from the same glass pane with the thickness 8 mm. The specimen dimensions were 100x1000 mm². The edges were machine ground and polished. The specimens were subjected to out-of-plane loading generating an approximate stress rate of 0.31 MPa s⁻¹. All specimens were wrapped in self-adhesive plastic foil in order to control the post-fracture behavior. The fracture origin type, i.e. edge or surface, was not recorded. The load-duration ranged from about 1 min and 24 sec to 4 min and 30 sec. The temperature and relative humidity during testing were not recorded but it can be assumed that an indoor environment represents the climatic conditions. A summary of details on the experiment is given in Tab. 25. In Fig. 60, a set of boxplots depict the fracture stress characteristics for the nominal and stress rate-equivalent strength data. A set of three probability plots for each sample is shown in Fig. 61 including the respective maximum-likelihood parameter estimates and the Anderson-Darling goodness-of-fit statistic.

Table 25: Details on the experiments as reported by Kinsella and Persson (2016). 4PB=Four-point bending, OP=Out-of-plane.

Sample ID	No. of spec's	Bending mode	Dimensions (mm ³)	Edge condition	Load. span (mm)	Stress rate (MPa s ⁻¹)
pol-short	44	4PB OP	8x100x1000	Polished	300	0.32
pol-long	29	4PB OP	8x100x1000	Polished	450	0.36

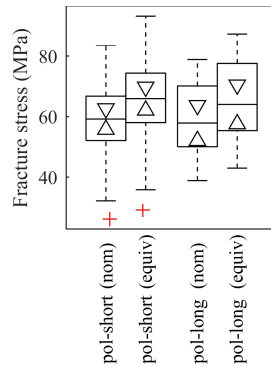


Fig. 60 Boxplots of the (left) nominal and (right) stress rate-equivalent fracture stress values for the data samples in Kinsella and Persson (2016).

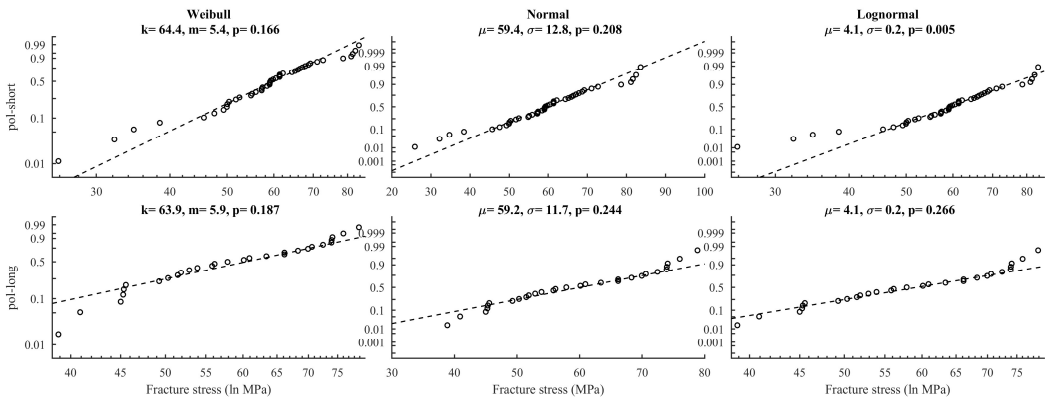


Fig. 61 Probability plots for the data samples in Kinsella and Persson (2016).

SURVEY OF EXPERIMENTAL DATA ON THE STRENGTH OF ANNEALED FLOAT GLASS

Navarrete et al. (2016)

The experiment was conducted with the double ring bending setup using an Instron 5500R universal testing machine with a constant load rate of 79 kN min⁻¹. The load and support ring diameters were 51 mm and 127 mm, respectively. All specimens were cut out from glass panes using industrial automated cutting. The pane thicknesses were 3, 4, 5, 6, 8, 10, 12, and 19 mm, respectively. The specimen dimensions were 200x200 mm². The specimens were subjected to out-of-plane loading generating an approximate stress rate according to Tab. 26. All specimens were wrapped in PET foil to control the post-fracture behavior. The load-duration ranged from about 1 sec to 55 sec according to calculations. The average temperature during testing was 20 °C. The relative humidity during testing was not recorded but it can be assumed that an indoor environment represents the climatic conditions. The specimens were tested with the tin side downwards, i.e. in the tension zone. A total number of 8 specimens were excluded from the record for reasons including the following: the fracture origin could not be determined, the fracture origin was found to lie outside the load ring, the rings were non-coaxial after the test. A summary of details on the experiment is given in Tab. 26. In Fig. 62, a set of boxplots depict the fracture stress characteristics for the nominal and stress rate-equivalent strength data. The failure stress was calculated according to ASTM C 1499-05. A set of three probability plots for each sample is shown in Fig. 63 including the respective maximum-likelihood parameter estimates and the Anderson-Darling goodness-of-fit statistic.

Table 26: Details on the experiments as reported by Navarrete et al. (2016). CDR=Co-axial double ring.

Sample ID	No. of spec's	Bending mode	Dimensions (mm ³)	Edge condition	Load. span/Load. ring diam. (mm)	Stress rate (MPa s ⁻¹)
3mm	8	CDR	3x200x200	As-cut	51	86.0
4mm	8	CDR	4x200x200	As-cut	51	48.4
5mm	8	CDR	5x200x200	As-cut	51	31.0
6mm	9	CDR	6x200x200	As-cut	51	21.5
8mm	9	CDR	8x200x200	As-cut	51	12.1
10mm	8	CDR	10x200x200	As-cut	51	7.74
12mm	9	CDR	12x200x200	As-cut	51	5.37
19mm	10	CDR	19x200x200	As-cut	51	2.14

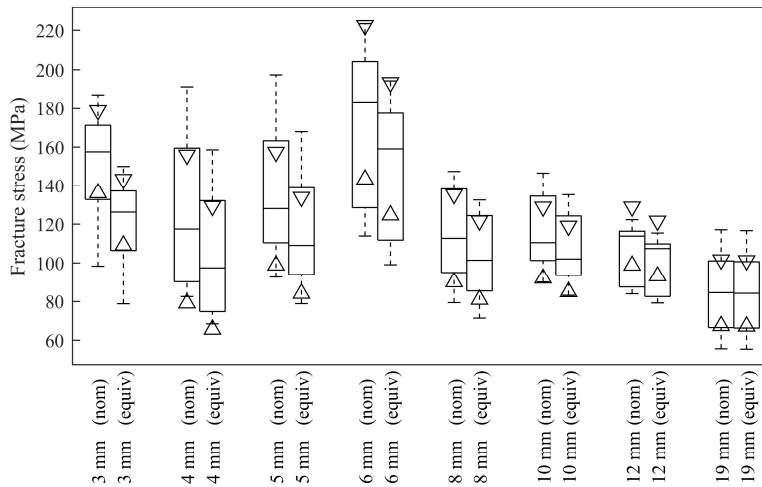


Fig. 62 Boxplots of the (left) nominal and (right) stress rate-equivalent fracture stress values for the data samples in Navarrete et al. (2016).

SURVEY OF EXPERIMENTAL DATA ON THE STRENGTH OF ANNEALED FLOAT GLASS

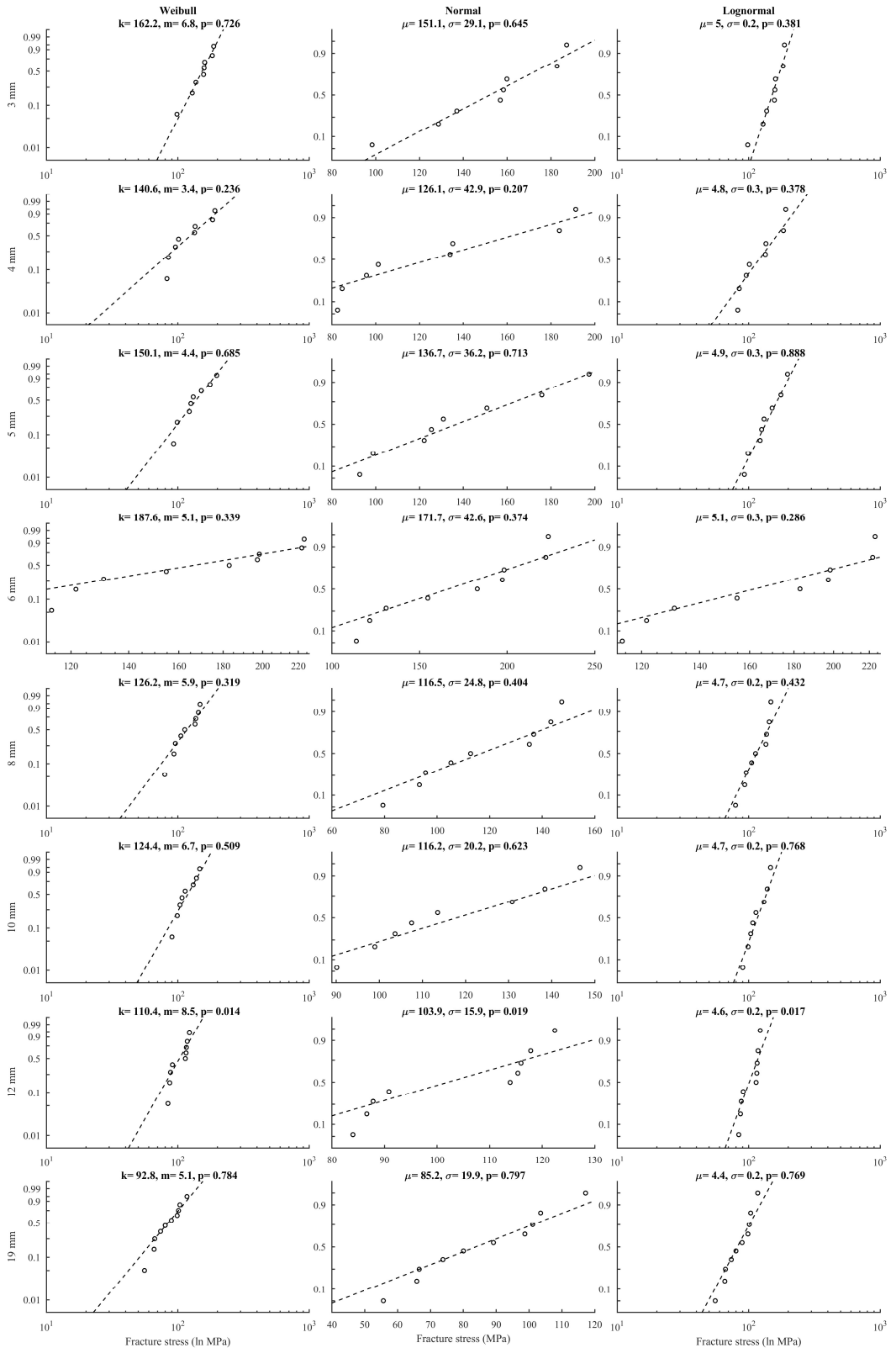


Fig. 63 Probability plots for the data samples in Navarrete et al. (2016).

SURVEY OF EXPERIMENTAL DATA ON THE STRENGTH OF ANNEALED FLOAT GLASS
Yankelevsky et al. (2017)

The experiment was conducted with the four-point bending setup under displacement control at about 0.012 mm s^{-1} . The load and support span were 100 mm and 200 mm, respectively. All specimens were cut out from glass with a thickness of about 12 mm. The specimen dimensions were $38 \times 250 \text{ mm}^2$. The specimens were subjected to out-of-plane loading generating an approximate stress rate of 1.1 MPa s^{-1} . The scored edge was placed upwards, i.e. in the compression zone. The origin of failure was identified for each specimen. The load-duration ranged from about 48 sec to 1 min and 58 sec according to calculations. The temperature and relative humidity during testing were $24 \text{ }^\circ\text{C}$ and 32%, respectively. A summary of details on the experiment is given in Tab. 27. In Fig. 64, a set of boxplots depict the fracture stress characteristics for the nominal and stress rate-equivalent strength data. A set of three probability plots for the sample is shown in Fig. 65 including the respective maximum-likelihood parameter estimates and the Anderson-Darling goodness-of-fit statistic.

Table 27: Details on the experiment as reported by Yankelevsky et al. (2017). 4PB=Four-point bending, OP=Out-of-plane.

Sample ID	No. of spec's	Bending mode	Dimensions (mm ³)	Edge condition	Load. span (mm)	Stress rate (MPa s ⁻¹)
4PB	56	4PB OP	12x38x250	As-cut	100	1.1

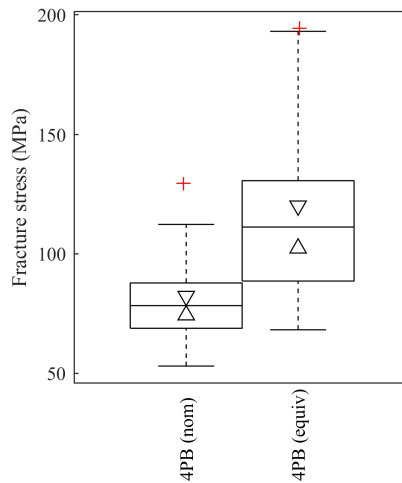


Fig. 64 Boxplots of the (left) nominal and (right) stress rate-equivalent fracture stress values for the data sample in Yankelevsky (2017).

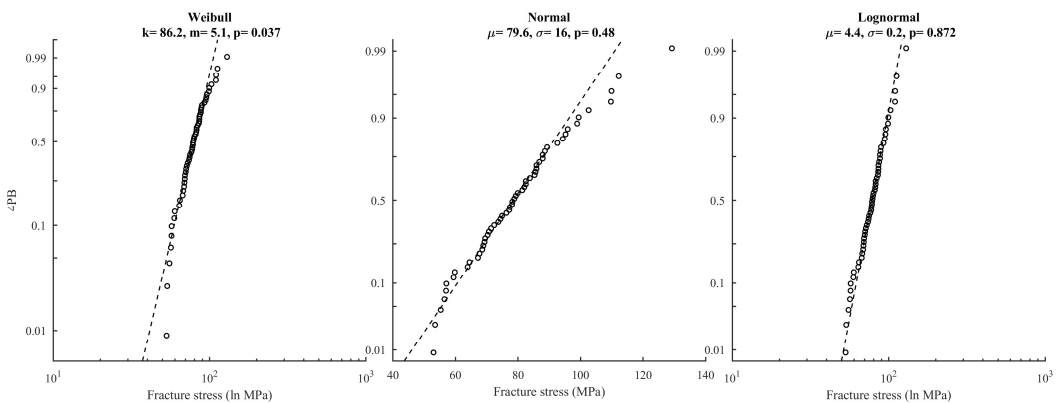


Fig. 65 Probability plots for the data sample in Yankelevsky (2017).

Osnes et al. (2018)

The experiment was conducted with a four-point bending device. The loading span varied between 40 mm, 90 mm, and 140 mm, corresponding to three different samples of specimen dimensions. The support span dimensions were 80 mm, 180 mm, and 280 mm, respectively. All specimens were cut out of panes with the nominal thickness 4 mm. The edge condition was as-cut. The specimen dimensions were 20x100 mm², 40x200 mm², and 60x300 mm². The mechanically scribed edge was always placed on the compression side. The specimens were subjected to out-of-plane loading and the loading was applied using displacement control generating an average strain rate of $10 \cdot 10^{-5} \text{ s}^{-1}$. With the estimation of Young's modulus at $E = 70 \text{ GPa}$, it follows that the stress rate was approximately 7 MPa s^{-1} . The fracture origin type, i.e. edge or surface, was recorded. It was not recorded which of the tin versus air side that was placed in the tension zone. The length of load-duration ranged from approximately 5 sec to 30 sec according to calculations. A summary of details on the experiment is given in Tab. 28. In Fig. 66, a set of boxplots is given for the nominal fracture stress values as well as the stress rate-equivalent values.

Table 28: Details on the experiments as reported by Osnes et al. (2018). Legend: 4PB=Four-point bending, OP=Out-of-plane.

Sample ID	No. of spec's	Bending mode	Dimensions (mm ²)	Edge proc. type	Load. span (mm)	Approx. stress rate (MPa s ⁻¹)
cut-short	31	4PB OP	4x20x100	As-cut	40	7
cut-medium	31	4PB OP	4x40x200	As-cut	90	7
cut-long	31	4PB OP	4x60x300	As-cut	140	7

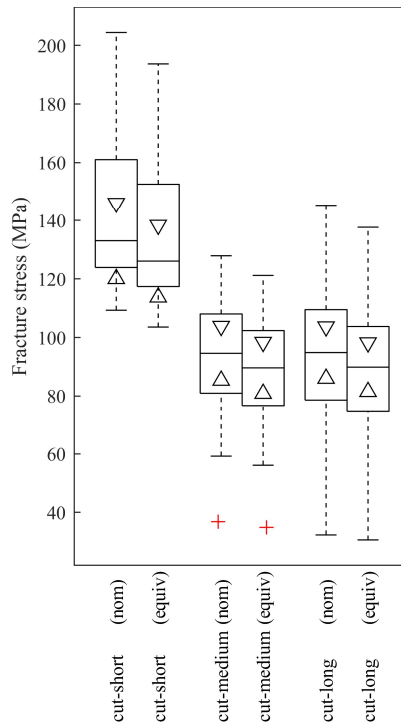


Fig. 66 Boxplots of the nominal and stress rate-equivalent fracture stress values for each data sample in Osnes et al. (2018). Surface failures only.

11. References

- Anderson, T. W. and Darling, D. A. (1952) 'Asymptotic Theory of Certain "Goodness of Fit" Criteria Based on Stochastic Processes', *Ann. Math. Statist.* The Institute of Mathematical Statistics, (2), pp. 193–212. doi: 10.1214/aoms/1177729437.
- Brown, W. G. (1974) *A practicable Formulation for the Strength of Glass and its Special Application to Large Plates.*
- Calderone, I. J. (1999) *The equivalent wind loading for window glass design.* Monash University.
- Carre, H. (1996) *Etude du comportement à la rupture d'un matériau fragile précontraint : le verre trempé.* Ecole Nationale des Ponts et Chaussées.
- Charles, R. J. (1958a) 'Static Fatigue of Glass I', *J Appl Phys*, 29, pp. 1549–1553.
- Charles, R. J. (1958b) 'Static Fatigue of Glass II', *J Appl Phys*, 29, pp. 1554–1560.
- D'Agostino, R. B. and Stephens, M. A. (eds) (1986) *Goodness-of-fit Techniques.* New York, NY, USA: Marcel Dekker, Inc.
- Dalglish, W. A. and Taylor, D. A. (1990) 'The strength and testing of window glass', *Can J Civ Eng*, 17, pp. 752–762.
- DIN 18008-1 (2010) 'Glas im Bauwesen - Bemessungs- und Konstruktionsregeln - Teil 1: Begriffe und allgemeine Grundlagen.'
- Fink, A. (2000) *Ein Beitrag zum Einsatz von Floatglas als dauerhaft tragender Konstruktionswerkstoff im Bauwesen.*
- Forbes, C. et al. (2011) *Statistical distributions.* 4th edn. John Wiley and sons, Inc.
- Garcia-Prieto, M.-A. (2001) *Dimensionamiento probabilístico y analisis experimental de vidrio en rotura.* Universidad de Oviedo.
- Haldimann, M. (2006) *Fracture strength of structural glass elements -- analytical and numerical modelling, testing and design.* Ecole Polytechnique Fédérale de Lausanne EPFL.
- Hess, R. (2000) *Glasträger.* Zürich, Switzerland.
- Huerta, M. C. et al. (2011) 'Influence of experimental test type on the determination of probabilistic stress distribution', in *Glass Performance Days 2011.*
- Johar, S. (1981) *Dynamic fatigue of flat glass - Phase II.*
- Johar, S. (1982) *Dynamic fatigue of flat glass - Phase III.*
- Kanabolo, D. C. and Norville, H. S. (1985) *The strength of new window glass using surface characteristics.* Texas Tech University.
- Kinsella, D. T. and Persson, K. (2016) 'On the applicability of the Weibull distribution to model annealed glass strength and future research needs', in *Challenging Glass Conference 5.* Ghent, Belgium.
- Kirstein, A. F. and Woolley, R. . (1967) 'Symmetrical bending of thin circular elastic plates of equally spaced point supports', *J Res Natl Bur Stds*, 71C, pp. 1–10.
- Kleuderlein, J., Ensslen, F. and Schneider, J. (2014) 'Investigation of edge strength dependent on different types of edge processing', in *Engineered Transparency. International Conference at Glasstec.* Düsseldorf, Germany.

SURVEY OF EXPERIMENTAL DATA ON THE STRENGTH OF ANNEALED FLOAT GLASS

- Kozłowski, M. (2014) *Experimental and numerical analysis of hybrid timber-glass beams*. Silesian University of Technology.
- Lawless, J. F. (2003) *Statistical models and methods for lifetime data*. 2nd edn. John Wiley and Sons, Inc.
- Lindqvist, M. (2013) *Structural Glass Strength Prediction Based on Edge Flaw Characterization*. Ecole Polytechnique Fédérale de Lausanne EPFL.
- MathWorks Inc. (2018) 'www.mathworks.com'.
- McGill, R., Tukey, J. W. and Larsen, W. A. (1978) 'Variations of Box Plots', *Am Stat*. American Statistical Association, Taylor & Francis, Ltd., 32(1), pp. 12–16.
- Mencik, J. (1992) *Strength and Fracture of Glass and Ceramics*. Elsevier (Glass Science and Technology).
- Muniz-Calvente, M. et al. (2016) 'Statistical joint evaluation of fracture results from distinct experimental programs: An application to annealed glass', *Theor Appl Fract Mec*, 85(Part A), pp. 149–157.
- Natividad, K. (2014) 'Locations of Fracture Origins and Magnitudes of Maximum Principal Stresses in Rectangular Glass Lites'. Texas Tech University.
- Navarrete, B. et al. (2016) 'Failure behavior of annealed glass for building windows', *Eng Struct*, 141, pp. 417–426.
- Nilsson, A. (1993) *Stochastic characterization of glass strength properties*.
- Osnes, K., Børvik, T. and Hopperstad, O. S. (2018) 'Testing and modelling of annealed float glass under quasi-static and dynamic loading', *Eng Fract Mech*. doi: <https://doi.org/10.1016/j.engfracmech.2018.05.031>.
- Overend, M. (2002) *The appraisal of structural glass assemblies*. University of Surrey.
- Postigo, S. (2010) *Estudio teorico experimental de impactos humanos contra vidrios de acristalamientos de edificacion*. Universidad de Politecnica de Madrid.
- prEN 16612 (2017) 'Glass in building - Determination of the lateral load resistance of glass panes by calculation'.
- Schula, S. (2015) *Charakterisierung der Kratzanfälligkeit von Gläsern im Bauwesen*. Springer.
- Sglavo, V. M., Muller, C. and Righetti, F. (2007) 'Influence of edge finishing on the resistance to thermal stresses of float glass', in *Glass Performance Days 2007*.
- Sheshkin, D. (2004) *Handbook of parametric and nonparametric statistical procedures*. 3rd edn. Chapman Hall/CRC.
- Simiu, E. et al. (1984) *Ring-on-ring tests and load capacity of cladding glass*.
- Vandebroek, M. et al. (2012) 'Experimental validation of edge strength model for glass with polished and cut edge finishing', *Eng Fract Mech*, 96, pp. 480–489.
- Vandebroek, M. et al. (2014) 'Size effect model for the edge strength of glass with cut and ground edge finishing', *Eng Struct*, 79, pp. 96–105.
- Veer, F. A., Louter, C. and Bos, F. P. (2009) 'The strength of annealed, heat-strengthened and fully tempered float glass', *Fatigue Fract Eng M*, 32, pp. 18–25.
- Veer, F. A., Louter, P. C. and Romein, T. (2006) 'Quality control and the strength of glass', in *ECF 16 conference*.

SURVEY OF EXPERIMENTAL DATA ON THE STRENGTH OF ANNEALED FLOAT GLASS

Veer, F. A. and Rodichev, Y. M. (2011) 'The structural strength of glass: Hidden damage', *Strength Mater+*, 43, pp. 302–315.

Veer, F. A. and Rodichev, Y. M. (2012) 'The strength of water jet cut glass', in *Glass Performance Days 2011*, pp. 434–438.

Wasserman, L. (2006) *All of nonparametric statistics*. Springer.

Weibull, W. (1939) 'A Statistical Theory of the Strength of Materials', *Ingenjörsvetenskapsakademiens handlingar*, 151.

Yankelevsky, D. *et al.* (2017) 'Fracture characteristics of laboratory-tested soda lime glass specimens', *Can J Civ Eng*, 44, pp. 151–160.